FACULTY
OF APPLIED SCIENCES
UNIVERSITY
OF WEST BOHEMIA

University of West Bohemia
Faculty of Applied Sciences

Application of Human Body Models in Motorcycle Passive Safety

M. Sc., Eng. Tomasz Bońkowski

A doctoral thesis submitted in fulfillment of the requirements for the degree of doctor in Applied Mechanics

Supervisor: doc. Ing. Luděk Hynčík, Ph.D.
Specialist supervisor: doc. Ing. Michal Hajžman, Ph.D.
Department of Mechanics

Pilsen 2023

FACULTY
OF APPLIED SCIENCES
UNIVERSITY
OF WEST BOHEMIA

Západočeská univerzita v Plzni
Fakulta aplikovaných véd

Použití modelů lidského těla v pasivní bezpečnosti motocyklů

Ing. Tomasz Bońkowski

Disertační práce k získaní akademického titulu doktora v oboru Aplikovaná mechanika

Školitel: doc. Ing. Luděk Hynčík, Ph.D.
Školitel specialista: doc. Ing. Michal Hajžman, Ph.D.
Katedra mechaniky

Plzeň 2023

The best instrument for measuring the tolerance of man to mechanical force is man.

Col. John P. Stapp, (1966)

All models are wrong, but some are useful.

George Box, (1976)

Contents

Declaration of Authorship

Herewith I, Tomasz Bońkowski, declare that I compose this work alone except when I clearly indicated otherwise. I have used only the literature listed in the bibliography section and in the reference section of published papers.

In Pilsen, 31.08.2023

Tomasz Bońkowski

Acknowledgments

The work presented in this dissertation thesis has been done at the Department of Mechanics, Faculty of Applied Sciences, and New Technologies – Research Center, at the University of West Bohemia, during the period September 2014 to August 2023.

The work has been performed within international and national research projects:

1. Marie Skłodowska Curie Initial Training Network MOTORIST FP7-PEOPLE-2013-ITN-608092 (years 2014-2017),
2. LTC17001 as the national link to the COST Action TU1407 “Scientific and technical innovations for safer Powered Two Wheelers (PTW)” (years 2016 – 2019)
3. AMTMI Aplikace moderních technologií v medicíně a průmyslu CZ.02.1.01/0.0/0.0/17_048/0007280 (year 2019 – 2022)

and internal University grant projects:

1. SGS-2016-059 Počítačové modelování a monitorování lidského těla s využitím v lékařství.
2. SGS-2019-002 Computer modelling and monitoring of human body used for medicine.
3. SGS-2022-008 Matematické modelovaní a numerické simulace materiálových struktur a mechanických a biomechanických systému

The financial support through these projects is gratefully acknowledged.

My supervisor Luděk Hynčík, has taught me a lot about human body models and injury biomechanics, and Pam-Crash. His tenacious support as a supervisor throughout the entire thesis duration is much appreciable.

I would like to thank my friends Jan Špička, and Jan Vychytil who helped me a lot especially during the first months after my arrival in the Czech Republic, end never left me without help even in the worst-case scenarios.

I would like to extend my heartfelt appreciation to my family and my wife for their invaluable and boundless support.

Annotation

This work is focused on the application of the scalable hybrid human body model for the improvement of the motorcyclists' passive safety. The research begins by setting the stage, elucidating the historical context, and articulating the core problem statement. It further delineates the overarching objectives that steer the entire study. The study's multifaceted approach unfolds across various interconnected domains:

Accident Statistics: A meticulous examination of accident statistics ensues, featuring a deep dive into prominent databases such as the HURT Report, CARE database, GIDAS, and MAIDS. These statistics furnish invaluable insights into real-world accident scenarios and underscore the urgency of improving motorcyclist safety.

Human Surrogate: This section delves into the realm of human surrogate models, encompassing anthropometric testing devices, post-mortem human surrogates, and human body models like HUMOS, THUMS, and GHBMC. The discussion extends to injury metrics, exploring scales such as AIS and ISS, and elucidates injury criteria for different body regions. The Virthuman model takes center stage, its geometric intricacies, structural attributes, scaling methodologies, and advanced capabilities like injury assessment and sliding simulations are comprehensively covered. Notably, this section also unveils vital enhancements to the Virthuman model, targeting specific areas for improvement.

Injury Countermeasures Testing: A profound exploration of safety testing standards ensues, encompassing helmet impact testing and motorcycle barrier testing. Advanced numerical simulations are employed to assess the efficacy of various safety measures, with a particular focus on helmet design and barrier effectiveness. The results unearth critical insights into optimizing safety countermeasures, which covers also personal protective equipment.

Accident Reconstruction: The research navigates the complex domain of accident reconstruction, unveiling sophisticated methodologies such as numerical modeling of the motorcycle and model simplification techniques. This section highlights the development and validation of models and coupling techniques. It culminates in a presentation of results for selected cases, shedding light on diverse accident scenarios and their nuances.

Full-Scale Crash Tests: The study reaches its zenith with an exploration of full-scale crash tests. Here, ISO 13232 configurations take the spotlight, with a detailed examination of kinematics and injury assessments. Of particular interest is the influence of rider stature on accident outcomes, an aspect explored in depth.

This comprehensive work, underpinned by meticulous research and analysis, holds profound implications for the realm of motorcyclist passive safety. It promises to not only enrich our understanding of motorcycle accidents but also offer tangible pathways for improving safety measures and reducing injuries and fatalities among motorcyclists. Researchers, safety engineers, and policymakers will find this study to be an invaluable resource in their mission to enhance motorcycle safety.

Keywords: human body models; passive safety; powered two-wheelers; injury countermeasures; personal protective equipment; numerical testing; traffic accident reconstruction; vulnerable road users

Anotace

Tato práce se zaměřuje na aplikaci škálovatelného hybridního modelu lidského těla pro zlepšení pasivní bezpečnosti motocyklistů. Výzkum začíná nastavením scény, objasněním historického kontextu a formulací hlavního problémového výroku. Dále rozvíjí celkové cíle, které řídí celý studijní proces. Multifaktorový přístup studie se odvíjí ve více vzájemně propojených oblastech:

Statistiky nehod: Následuje pečlivá analýza statistik nehod, zahrnující důkladný pohled do významných databází, jako jsou HURT Report, databáze CARE, GIDAS a MAIDS. Tyto statistiky poskytují nepostradatelné poznatky o reálných scénářích nehod a zdůrazňují naléhavost zlepšení bezpečnosti motocyklistů.

Lidský náhradník: Tato sekce se ponořuje do oblasti modelů lidského náhradníka, zahrnující antropometrické testovací zařízení, náhrady po smrti lidského těla a modely lidského těla, jako jsou HUMOS, THUMS a GHBMC. Diskuse se rozšiřuje na metriky zranění, zkoumá stupnice jako AIS a ISS a objasňuje kritéria zranění pro různé části těla. Model Virthuman zaujímá centrální místo, jeho geometrické nuance, strukturální atributy, metody škálování a pokročilé schopnosti, jako je hodnocení zranění a simulace jednoduchých scénářů, jsou podrobně zpracovány. Tato sekce také odhaluje klíčové vylepšení modelu Virthuman, zaměřující se na konkrétní oblasti pro zlepšení.

Testování opatření proti zranění: Následuje hluboký průzkum standardů bezpečnostního testování, zahrnujícího testování přilby oproti nárazu a testování bariér pro motocykly. Pokročilé numerické simulace jsou použity k posouzení účinnosti různých bezpečnostních opatření, s důrazem na návrh přileb a účinnost bariér. Výsledky odhalují klíčové poznatky pro optimalizaci bezpečnostních opatření kterými jsou také osobní ochranní pomůcky.

Rekonstrukce nehod: Výzkum naviguje komplexním polem rekonstrukce nehod, odhaluje sofistikované metody, jako je numerické modelování motocyklu a techniky zjednodušení modelu. Tato sekce zdůrazňuje vývoj a ověřování modelů a technik spojování. Kulminuje prezentací výsledků vybraných případů, které přinášejí světlo do různých scénářů nehod a jejich nuancí.

Nárazová zkoušky v plném měřítku: Studie dosahuje svého vrcholu průzkumem nárazových zákusek v plném meřítku. Zde přicházejí do popředí konfigurace ISO 13232 s podrobným zkoumáním kinematiky a hodnocení zranění. Zvláštní pozornost je věnována vlivu postavy jezdce na výsledky nehod, což je hlouběji prozkoumáno.

Tato komplexní práce, opřená o pečlivý výzkum a analýzu, nese hluboké implikace pro oblast pasivní bezpečnosti motocyklistů. Slibuje nejen obohatit naše porozumění nehodám motocyklů, ale také nabízí konkrétní cesty pro zlepšení bezpečnostních opatření a snížení zranění a úmrtí mezi motocyklisty. Výzkumníci, inženýři pro bezpečnost a tvůrci politiky najdou v této studii neocenitelný zdroj pro svou misi zlepšení bezpečnosti motocyklů.

Klíčová slova: modele lidského těla; pasivní bezpečnost; jednostopá motorová vozidla; opatření proti zranění; osobní ochranné pomůcky; numerické testování; rekonstrukce dopravních nehod; zranitelní účastníci silničního provozu

Anotacja

Niniejsza praca koncentruje się na zastosowaniu skalowalnego hybrydowego modelu ludzkiego ciała w celu poprawy bezpieczeństwa biernego motocyklistów. Badania rozpoczynają się od przygotowania sceny, wyjaśnienia kontekstu historycznego i sformułowania głównego problemu. Następnie określono nadrzędne cele, które kierują całym badaniem. Wieloaspektowe podejście do badania rozwija się w różnych powiązanych ze sobą domenach:

Statystyki wypadków: Następuje skrupulatne badanie statystyk wypadków, obejmujące głęboką analizę znanych baz danych, takich jak raport HURTa, baza danych CARE, GIDAS i MAIDS. Statystyki te zapewniają bezcenny wgląd w rzeczywiste scenariusze wypadków i podkreślają pilną potrzebę poprawy bezpieczeństwa motocyklistów.

Surogat człowieka: Ta sekcja zagłębia się w sferę ludzkich modeli zastępczych, obejmujących antropometryczne urządzenia testujące, pośmiertne ludzkie surogaty i modele ludzkiego ciała, takie jak HUMOS, THUMS i GHBMC. Dyskusja rozciąga się na wskaźniki obrażeń, badając skale takie jak AIS i ISS oraz wyjaśniając kryteria obrażeń dla różnych obszarów ciała. Model Virthuman zajmuje centralne miejsce, a jego zawiłości geometryczne, atrybuty strukturalne, metodologie skalowania i zaawansowane możliwości, takie jak ocena obrażeń, oraz symulacje prostych scenariuszy, są kompleksowo omówione. Co ważne, w tej sekcji przedstawiono również istotne ulepszenia modelu Virthuman, ukierunkowane na konkretne obszary wymagające poprawy.

Testowanie środków przeciwdziałania urazom: Dogłębna eksploracja standardów testowania bezpieczeństwa obejmuje testy zderzeniowe kasków i testy barier motocyklowych. Zaawansowane symulacje numeryczne są wykorzystywane do oceny skuteczności różnych środków bezpieczeństwa, ze szczególnym uwzględnieniem konstrukcji kasku i skuteczności bariery. Wyniki odkrywają krytyczne spostrzeżenia dotyczące optymalizacji środków bezpieczeństwa, które obejmują również środki ochrony osobistej.

Rekonstrukcja wypadków: Badania poruszają się po złożonej dziedzinie rekonstrukcji wypadków, odsłaniając zaawansowane metodologie, takie jak modelowanie numeryczne motocykla i techniki upraszczania modelu. Ta sekcja podkreśla rozwój i walidację modeli oraz techniki ich łączenia. Kulminacją jest prezentacja wyników dla wybranych zdarzeń drogowych, rzucająca światło na różne scenariusze wypadków i ich niuanse.

Pełnowymiarowe testy zderzeniowe: Badanie osiąga swój zenit wraz z eksploracją testów zderzeniowych w pełnej skali. Tutaj w centrum uwagi znajdują się konfiguracje ISO 13232, ze szczegółowym badaniem kinematyki i oceny obrażeń. Szczególnie interesujący jest wpływ antropometrii kierowcy na wyniki wypadków, który to aspekt został dogłębnie zbadany.

Ta kompleksowa praca, oparta na skrupulatnych badaniach i analizach, ma głębokie implikacje dla sfery bezpieczeństwa biernego motocyklistów. Obiecuje nie tylko wzbogacić nasze rozumienie wypadków motocyklowych, ale także oferuje konkretne ścieżki poprawy środków bezpieczeństwa i zmniejszenia liczby obrażeń i ofiar śmiertelnych wśród motocyklistów. Naukowcy, inżynierowie bezpieczeństwa i decydenci uznają to badanie za nieocenione źródło informacji w ich misji poprawy bezpieczeństwa motocyklistów.

Słowa kluczowe: modele ludzkiego ciała; bezpieczeństwo bierne; pojazdy jednośladowe; środki zapobiegania urazom; środki ochrony indywidualnej; badania numeryczne; rekonstrukcja wypadków; szczególnie narażeni użytkownicy dróg

List of Figures

List of Tables

Glossary

ACEM	Association of European Motorcycle Manufacturers
AIS	Abbreviated Injury Scale
ARB	Articulated Rigid Body
ATD	anthropometric testing device
CC	Cubic Centimeters
CFC	Cannel Frequency Class
COG	Centre of Gravity
CRI	configuration risk index
CVT	Continuously Variable Transmission
DOF	degree of freedom
ECE 22.05	the standard for testing motorcycle helmets in Europe
ECE R	ECE Regulation
EES	Energy Equivalent Speed
EMS	Emergency Medical Service
EPS	Expanded Polystyrene
FE	Finite Element
FEM	finite element method
FHWA	Federal Highway Association
GHBMS	Global Human Body Models Consortium
HBM	Human Body Model
HIC	Head Injury Criterion
ISO	International Organization for Standardization
ISO 13232	the standard for testing motorcycle-installed safety devices
L.I.E.R	French road-side barrier testing protocol
L3	Legal Category of the Motorcycle
LM	lumped mass
LNL	Lower Neck Load Index
MAIDS	Motorcycle Accidents In-depth Study
MATD	Motorcycle Anthropometric Testing Device
MBS	multi-body system
MDB	moving deformable barrier
MYMOSA	MotorcYcle and MOtorcyclist Safety Project
NCAC	George Washington University's National Crash Analysis Center
NCAP	New Car Assessment Programme
NHTSA	National Highway Traffic Safety Administration
NIC	Neck Injury Criterion
Nij	Normalized Neck Injury Criterion
OV	Opposite Vehicle
PB350	Piaggio Beverly 350
POI	Point of Impact
POR	Point of Rest
PPE	Personal Protective Equipment
PTW	Powered Two Wheeler

RB	Rigid Body
REV	Revolute Joint
RP	Reference Point
SAE	Society of Automotive Engineers
SNR	Signal-to-Noise Ratio
THUMS	Total Human Model for Safety
TRA	Translation Joint
VPS	Virtual Performance Solution
WHO	World Health Organization

1 Introduction

Motorcycles are a popular and efficient means of transportation, offering a sense of freedom and agility unmatched by conventional vehicles. However, motorcyclists are disproportionately vulnerable to severe injuries and fatalities in the event of a crash, making motorcycle safety a critical concern for both riders and the general public. The development of passive safety systems, such as protective gear and vehicle design improvements, has become a fundamental aspect of minimizing injury severity and fatality rates among motorcyclists. In recent years, human body models (HBMs) have emerged as powerful tools for understanding the biomechanics of human injury during accidents and assessing the effectiveness of safety measures. HBMs are computerized representations of the human body that simulate various tissues, bones, and organs' interactions in response to external forces, making them indispensable for analyzing injury mechanisms and guiding the design of effective passive safety systems.

This work aims to explore the application of human body models in motorcycle passive safety, shedding light on their significance in advancing rider protection. By combining state-of-the-art research and comprehensive analysis, the author endeavors to provide valuable insights into the potential of HBMs in enhancing the safety of motorcyclists. The introduction of sophisticated computer simulations and virtual testing environments has revolutionized the field of motorcycle safety research. Traditional physical testing using crash test dummies and real-world experiments, while essential, can be costly, time-consuming, and sometimes ethically challenging. HBMs offer a non-invasive, cost-effective, and repeatable approach, allowing researchers to evaluate a wide range of injury scenarios, explore different crash scenarios, and assess the efficacy of safety equipment under various conditions.

As we delve into the core of this work, we will examine the biomechanical aspects of motorcycle crashes, considering factors such as impact speed, crash angle, and rider positioning. Utilizing human body models, we can study how these variables influence injury severity and determine the most vulnerable body regions during different crash scenarios. Such insights can then inform the development of targeted safety measures and optimized motorcycle designs to mitigate injury risks effectively. Moreover, we will discuss the latest advancements in human body modeling technology and how they have enabled more accurate representations of human physiology and injury response taking motorcycles' riding into account. These improvements have not only increased the reliability of HBM predictions but have also expanded their applications in assessing the impact of various protective gear and vehicle safety systems on motorcyclist protection.

In conclusion, the integration of human body models into motorcycle passive safety research represents a promising avenue for promoting rider protection and reducing the tragic consequences of motorcycle accidents. As we work towards creating a safer riding environment, the application of HBMs will undoubtedly play a pivotal role in shaping future safety standards and innovations in the motorcycle industry. Through this work, the author aspires to contribute to the growing body of knowledge in this field and advocate for the continued adoption of cutting-edge technologies to safeguard the lives and well-being of motorcyclists worldwide.

1.1 Background

The road transportation system is an example of the Human-Environment System (HES). This system is established to cover the needs of the individual person and society. To fulfill its function, the system must generate interactions between the components of the system: a human being, technology, and the environment. Interactions may cause the occurrence of risks. Those risks could be considered with the long-, and/or short- term view. In the short-term view, the human being is the most pliant entity in this system. Due to its pliability human is exposed to the risk of injury. In order to maintain the operation of the system, additional steps must be taken. One of the steps could be to feed the system with the appropriate injury countermeasures or in other words safety measures. Each of the system's components could be equipped with safety measures, for example, a pliant bumper (for technology - vehicles), a roadside barrier (for the environment), and finally personal protective equipment for a man. None of the safety measures are appropriate or useful by a-priori assumption. Their performance needs to be proven in well-established test procedures. The test procedures need to be relevant and repeatable. To design relevant test procedures appropriate and common conditions of injury occurrence must be found. Those conditions can be called: realistic impact conditions.

The powered two-wheeler (PTW) riders are among the group of vulnerable road users (VRU). That means that they are the users who are exposed to the highest risk of injury in road transportation. The PTW's drivers often travel with a speed considerably higher than a bicyclist, but they had only a little better protection against potential injuries. A helmet is the only one required and forced by the law as personal protective equipment (PPE), which is expected to protect a rider's body against impact. The PPE market provides a wide spectrum of protectors (gloves, garments, boots, joint protectors), but for daily use, none of them are required to be worn by the rider. Another safety measure in the road transportation system is a road barrier, which for the PTW should meet different testing protocols than the car/truck barrier. Due to the complicated kinematics of the rider-PTW-opposite vehicle (OV) system in the crash conditions, the current tools for accident simulation and reconstruction, in the PTW crash cases, expose problems of simulation stability and computational cost (finite element method- based tools), or problems of insufficient models' bio-fidelity and/or over-simplification (multibody system based tools). This thesis will present a hybrid approach, which joins the advantages of both methods and could be used for the PTW passive safety. The manifestation and the center point of this method is a scalable, hybrid human body model (HBM) Virthuman, which could cover wide spectra of the population. This HBM has already proven its applicability as the pedestrian and car occupant surrogate. This work deals with the application of the Virthuman to the field of PTW accident reconstruction and development of the future PPE testing standards.

The safety of road transportation can be divided into two groups: active safety and passive safety. This division is time-dependent (Fig. 1.1) Centre point for this dependency is the moment of the crash (accident). Where the crash could be defined as a collision of two or more objects, each object could be part of the following groups: traffic participants, road infrastructure, road-side infrastructure, undesired road intrudes (breeding cattle, wild animals, etc.). To assess the road safety for certain regions and transportation modes, an in-deep statistical analysis is often made. However, such a deep study must take into account many dependent and independent variables (up to 2000 for each crash) to create a significant insight. Such a wide analysis due to economic issues is often limited to some finite area (one city, district, etc.), and finite time-period (maximum few years). This in-deep analysis is often made by research teams that are looking for new insights about road safety. On the other hand, basic road safety indicators are often monitored yearly for areas of bigger organization units (e.g.: countries, unions). Those basic parameters (number of accidents, fatalities) give an overall view

of the efficiency of legislation-based road safety measures enforcement (seat belt usage enforcement, motorcycle helmet usage enforcement). The basic statistics are collected and monitored by police authorities. Between these two exist the insurance company's statistical records. This statistical data contains often more variables than the police reports (e.g. length of the treatment), but still less than in-deep analysis.

The most recent statistical research by K. Santos [1], which covered the topic of increasing injury severity of powered-two wheelers accidents by performing a retrospective analysis of 37769 PTW accidents that happened between 2010 and 2015 in Portugal, found that male riders who did not wear helmets are more prone to the risk of severe injury during the accident.

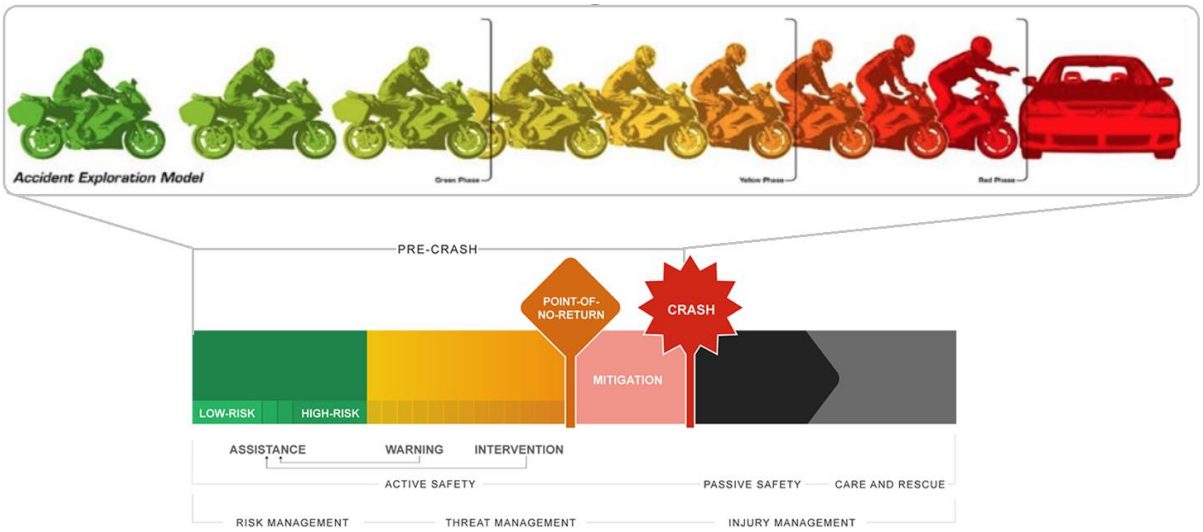

Figure 1.1 The time-dependent description of the accident [2]**.**

1.2 Problem Statement

In 1998 the research team from DEKRA under the guidance of F. Berg [3] published a paper, in which conclusions aimed to assess the actual situation with the passive safety of the motorcycles. They used an accident investigation and crash tests as their tool. Firstly, the evaluation of the powered-two-wheeler types has been done in accordance with the regulations of the Federal Republic of Germany. Where the six types of PTW were distinguished (Kleinkraftrad, Mofa 25, Leichtkraftrad, Kraftrad, Kraftroller, and Motorrad), every further conclusion was associated with one of the types of PTW. The accident investigation was done on the DEKRA database of accidents with 302 accidents from 1989 to 1996. It was found that some of the PTW driver body regions have higher exposure to the risk of injury "head and the lower extremities (foot/ankle, lower leg, knee, upper leg) are at particular risk" [3]. The crash test part of this research is discussed in the chapter about the full-scale crash tests page. 132.

One of the most current methods for the assessment and enchantment of vulnerable road users (VRU) safety during the crash phase was disseminated by M. Ptak [4]. The research paper specifies the following six steps: norms and regulations, experimental tests, criteria, numerical simulations, numerical-based criteria, and technical countermeasures, where the three first are already well established in the industry and the next three (especially the establishment of the numerical simulation standards for the VRU) are still in the phase of research group interest. The simulation (or

overly CAx[1]) part is depicted in Figure 1.2. This approach could be also implemented for the PTW safety approach by putting particular emphasis on the proper human body models.

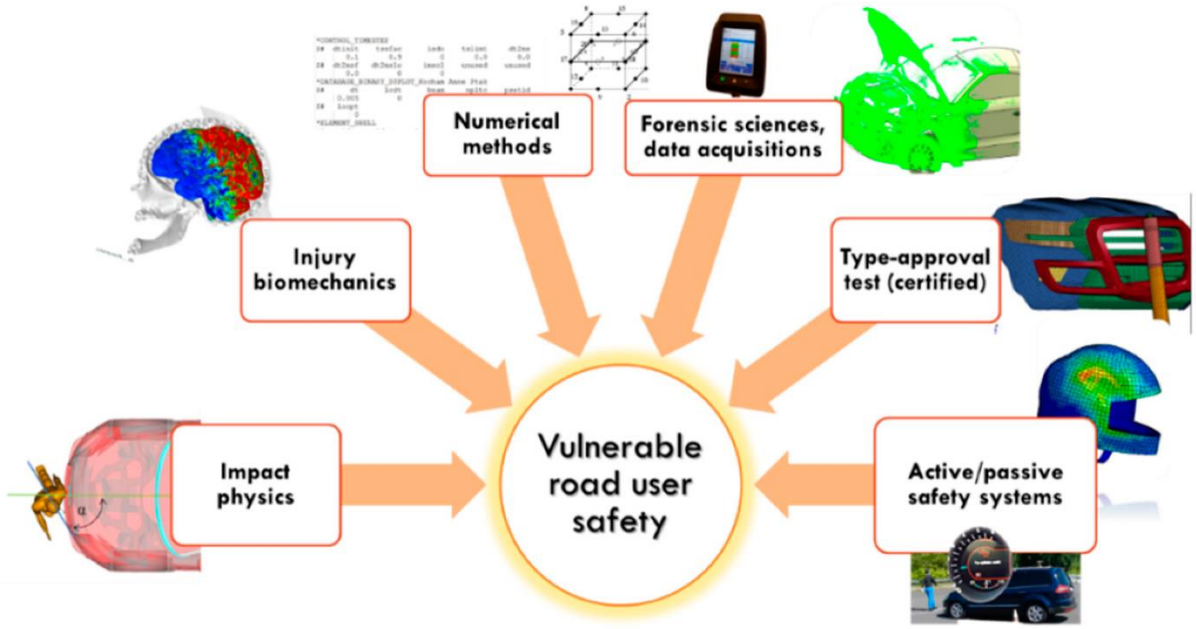

Figure 1.2 M. Ptak [4] **approach to CAx safety enchantment for VRU.**

The statement is: how to incorporate the virtual human body model into the motorcycle passive safety to receive an added value without big investments and non-cost effective experimental research. To answer this question this work needs to follow the entire way of formulation of the framework of the virtual arena of motorcycle passive safety, which starts from the finding of the realistic impact scenarios with parallel numerical modeling of simplified law-enforced personal protective equipment (helmet) to establish the full-scale multi-scenario PTW accident model (this point expect also simplified opposite OV). To evaluate the robustness of the accident model a validation versus the real accident needs to be conducted. Finally, the working framework will be used to simulate the most common PTW – OV accidents with the assessment of the injury criterion on the human body model. The benefit and the added value of the developed framework would be the cost-effective virtual tool for the testing of personal protective equipment.

1.3 Objectives of the thesis

The dissertation work deals with the problematics of impact biomechanics, human body modeling (with a particular emphasis on parametric anthropometric modeling), and passive safety of the PTW drivers. Based on the foregoing work and conclusion, the following scope of the dissertation was determined. The ultimate goal of the research work is to establish a solid scientific framework on the basics of injury biomechanics, which could be used for rigorous evaluation of the PTW passive safety measures. This aims express the steps from the problem statement.

[1] CAx stands for Computer Aided Design/ Computer Aided Manufacturing / Computer Aided Engineering

- Statistical analysis of the accident database to obtain macroscopic realistic impact conditions and most common accident configurations;
- Modeling of a simplified helmet and coupling with HBM;
  - Standard-based helmet validation;
- Creation of full-scale multi-scenario PTW numerical accident model;
  - Creation and validation of the numerical PTW model;
  - Coupling of HBM, MC, and PPE;
  - Simplification of the OV model;
- Reconstruction of real cases involving PTW, OV, and driver;
- Simulation of most common PTW - OV accidents with injury criteria assessment

Taking into account the steps defined above**, the major contribution of the thesis to the scientific field is a framework for the virtual testing methodology for improving motorcyclists' safety.**

2 Accident statistics

2.1 State of the Art

Conducting a thorough statistical analysis of PTW accident databases demands an understanding of their scope and limitations. Variability exists among European crash databases, with some containing only basic accident information. Additionally, there are specialized databases that provide an opportunity to uncover relationships between accidents and resulting injuries.

2.1.1 HURT Report

One of the first wide motorcycle safety studies was conducted in the USA from 1976- 1977, the findings were published in 1981 in the report **Motorcycle Accident Cause Factors and Identification of Countermeasures** which was named HURT Report [5] after its main contributor and author professor Harry Hurt. The key components and objectives of the Hurt Report encompassed:

Data Collection: Researchers embarked on in-depth investigations of motorcycle accidents, involving on-scene examinations, rider interviews, and the scrutiny of accident reports. This meticulous approach aimed to accumulate comprehensive insights into the root causes of accidents.

Factors of Influence: The study delved into a diverse array of elements that played a role in motorcycle accidents. These encompass rider behavior, vehicle attributes, road conditions, weather variables, and the prevailing traffic environment. The intent was to pinpoint primary causative factors and identify potential measures to mitigate risks.

Analysis of Injuries: A significant aspect of the Hurt Report involved comprehending the nature and severity of injuries sustained by motorcyclists in accidents. The objective was to gain a nuanced understanding of the prevalent and severe injuries, thereby informing the development of safety measures and improvements in equipment design.

Recommendations: Drawing from its comprehensive findings, the Hurt Report put forth a series of recommendations aimed at enhancing motorcycle safety. These recommendations spanned domains

like rider training, the utilization of helmets, road infrastructure enhancement, vehicle specifications, and revisions to traffic regulations.

Impact and Significance: The findings of the Hurt Report left a lasting imprint on motorcycle safety policies and practices within the United States. Its insights guided the establishment of legislation mandating helmet usage contributed to advancements in road design, and influenced the formulation of educational programs for motorcyclists.

In essence, the Hurt Report stands as a seminal and foundational work in the realm of motorcycle safety. Its contributions through deciphering accident causation and understanding injury mechanisms have profoundly influenced motorcycle safety regulations and initiatives. The study's legacy persists in shaping accident databases that aim to curtail the frequency and severity of motorcycle accidents.

2.1.2 CARE database

The CARE database, formally known as the Community database on Accidents on the Roads in Europe, functions as an inclusive and centralized compilation of data pertinent to road traffic incidents within European nations. Administered by the European Commission, CARE stands as a valuable asset for comprehending and scrutinizing trends and statistics concerning road safety across Europe. Central features encompass Accident Data Compilation: CARE assembles data encompassing a wide spectrum of factors intertwined with road accidents. This includes specifics like accident locales, time, weather conditions, road classifications, and collision particulars. Vehicle and Road User Insight: The database synthesizes insights about involved vehicles, encompassing types, manufacturers, models, and technical specifications. Also, details about road users—such as drivers, passengers, pedestrians, and cyclists—are meticulously recorded. Injury and Fatality Statistics: CARE meticulously furnishes data regarding injuries sustained by individuals involved in accidents. It categorizes these injuries based on type and severity, facilitating a deeper understanding of the human impact of accidents. Contributory Elements: The database meticulously documents elements contributing to accidents, spanning human conduct (like speeding and distracted driving), environmental contexts (such as road conditions and weather), and vehicle-related factors (including technical malfunctions). Geographical and Temporal Analysis: CARE's capabilities extend to the analysis of accident patterns across diverse regions, countries, and temporal intervals. This analytical prowess aids in spotting trends and disparities in road safety. Research and Policy Implications: CARE is harnessed by researchers, policymakers, and road safety experts for diverse objectives: conducting studies, gauging intervention effectiveness, crafting policies, and conceiving strategies to enhance road safety. Comparative Studies: CARE facilitates cross-country comparisons, thereby fostering insights into discrepancies in road safety measures, regulations, and eventual outcomes. Data Fidelity and Precision: A strong emphasis is placed on data fidelity and accuracy within the database, ensuring that the provided information is dependable and useful for decision-making processes.

The CARE database stands as a cornerstone in the progression of road safety research throughout Europe. By offering a repository rich with insights into road accidents and the factors correlated with them, it bolsters the foundation of evidence-based policy formulation, encourages the adoption of optimal road safety practices, and significantly contributes to the reduction of accidents, injuries, and fatalities on European roadways. [6],

2.1.3 GIDAS

The GIDAS database (German In-Depth Accident Study) is an extensive and meticulously maintained collection of data concerning road traffic accidents. Managed by the Federal Highway Research Institute (BASt) in Germany, GIDAS offers a comprehensive and in-depth view of various aspects of accidents. This includes vital information such as accident location, timing, weather conditions, road characteristics, and collision types [7].

Moreover, GIDAS compiles detailed data on the vehicles involved, encompassing details like make, model, manufacturing year, technical specifications, and vehicle types. This information is pivotal for understanding how vehicle design and technological features influence the outcomes of accidents. Injury data within GIDAS is equally thorough, spotlighting specific injuries sustained, their severity, and the parties affected. This aspect of the database facilitates thorough analyses of safety measures and vehicle design efficacy in preventing and mitigating injuries. Human factors contributing to accidents are meticulously documented within GIDAS. These encompass a broad spectrum of variables, from driver behavior and distractions to the utilization of safety equipment such as seat belts and helmets. By considering these factors, researchers can develop comprehensive insights into accident causes. The database also delves into vehicle dynamics, recording data about speed, braking, steering, and impact angles. This aspect offers a comprehensive view of the movements and interactions of the vehicles involved. Photographic documentation accompanies many entries in the GIDAS database, providing visual context and supporting detailed analyses. As a versatile resource, GIDAS is utilized by researchers, policymakers, and vehicle manufacturers for a range of objectives. These include understanding accident causation, assessing safety measures, refining vehicle design, and identifying trends in road safety over time. The longitudinal nature of the GIDAS database is particularly noteworthy. By collecting data over extended periods, it facilitates analyses of evolving accident patterns, shifts in road safety policies, and advancements in technology. In essence, the GIDAS database plays a pivotal role in enhancing road safety. By providing comprehensive insights into accident causation and consequences, it aids in shaping effective strategies for accident prevention, fostering safer vehicle design, and developing more secure road infrastructure.

2.1.4 MAIDS

The MAIDS database (Motorcycle Accidents In-Depth Study) is highly suitable for analyzing motorcycle accidents due to its comprehensive and meticulous approach to data collection, encompassing various critical factors specific to motorcycle incidents. This depth of information provides unique advantages for understanding and addressing motorcycle safety concerns.

In-Depth Data Collection: MAIDS gathers extensive and detailed data from real-world motorcycle accidents, capturing a wide array of variables including road conditions, vehicle dynamics, human behavior, environmental factors, and injury outcomes. This comprehensive dataset allows for a thorough analysis of the complex interactions leading to motorcycle accidents.

Motorcycle-Specific Factors: Unlike general accident databases, MAIDS focuses exclusively on motorcycle accidents. This specialized approach enables the collection of factors specific to motorcycles, such as rider posture, visibility challenges, and the interaction of two-wheeled vehicles with other road users.

Biomechanical Insights: MAIDS includes information about injury mechanisms and injury severity for both riders and passengers. This enables researchers to gain insights into the unique biomechanical

responses of motorcyclists during accidents, aiding in the development of effective safety measures and protective gear.

Human Factors: MAIDS records detailed information about human factors, including rider behavior, skill level, and decision-making. This information is crucial for understanding how rider actions contribute to accidents and for devising targeted interventions to improve rider safety.

Vehicle Dynamics: The database captures data related to motorcycle dynamics, such as speed, braking, and collision angles. This allows for a nuanced examination of how motorcycle handling and maneuverability impact accident outcomes.

Crash Scenarios: MAIDS analyses various crash scenarios, encompassing different collision types, road environments, and traffic situations. This diversity of scenarios provides a comprehensive view of motorcycle accident patterns.

Policy and Design Implications: The insights derived from MAIDS can inform the development of policies, regulations, and design modifications that specifically address motorcycle safety, ultimately leading to safer road environments for motorcyclists.

Evidence-Based Interventions: By providing detailed information about the causes and consequences of motorcycle accidents, MAIDS supports the development and implementation of evidence-based interventions aimed at reducing motorcycle accidents and improving rider protection.

In essence, the MAIDS database's tailored focus on motorcycle accidents, coupled with its in-depth data collection and analysis, positions it as a highly suitable resource for understanding the complexities of motorcycle accidents and formulating effective strategies to enhance motorcycle safety. [8, 9],

2.1.5 Summary

The MAIDS, Hurt Report, CARE database, and GIDAS are all significant projects in the realm of road safety research, each contributing valuable insights into different aspects of accident analysis and prevention.

Table 2.1 Comparison of the PTW accident studies

	MAIDS	Hurt Report	CARE Database	GIDAS
Focus	In-depth investigation of motorcycle accidents in Europe.	Study of motorcycle accident causes and countermeasures in the United States.	Compilation of road traffic accident data across European countries.	In-depth investigation of road traffic accidents in Germany.
Scope	Comprehensive data collection on accident circumstances, contributing factors, injury mechanisms, and rider behavior.	Detailed examination of contributing factors, rider behavior, vehicle dynamics, injuries, and recommendations	Comprehensive collection of accident details, vehicle and road user information, injury statistics, and contributing factors.	Comprehensive data collection on accident circumstances, vehicle dynamics, injury mechanisms, and

		for safety improvements.		contributing factors.
Contribution	Provides detailed insights into motorcycle accident causation, injury patterns, and potential preventive measures.	Influential in shaping motorcycle safety policies, helmet regulations, and road design in the United States.	Offers a holistic view of road safety trends, aiding evidence-based policymaking and road safety strategies.	Offers detailed insights into accident causation, injury patterns, and the effectiveness of safety measures.
Uniqueness	Offers motorcycle-specific data, making it a pivotal resource for understanding the complexities of motorcycle accidents.	Pioneering efforts in understanding motorcycle accidents and their prevention, with a focus on the U.S.	Provides a centralized and extensive dataset for cross-country comparisons and geographical analyses.	Focuses on accidents in Germany, allowing for analyses specific to the country's road conditions and traffic environment.

In summary, these projects/databases contribute significantly to road safety research by offering distinct perspectives on accident analysis and prevention. MAIDS and GIDAS provide specialized insights into motorcycle and general accidents, respectively, while the Hurt Report shaped motorcycle safety in the U.S. The CARE database offers a European-wide view of accidents, aiding policymaking, and the implementation of road safety measures. Each of these efforts plays a vital role in advancing road safety practices and reducing accidents, injuries, and fatalities on the road.

2.2 MAIDS analysis

Particularly MAIDS database was selected to analyze because it provides the highest number of parameters (discussed further) for every accident case, by design is tailored-made for the motorcycle cases (PPE utilization by rider, strong emphasis on rides mass, etc.), last but not least this database was the most convenient for the author as the owner (ACEM) was a partner in the MOTORIST research project in which the author of this thesis was also involved.

MAIDS (Motorcycle Accidents In Depth Study) can be described as an exhaustive in-depth database, which contains PTW accident data from Europe. Using the support of the European Commission, ACEM with a group of 9 partners started the process of MAIDS creation in 1999. It was built using the OECD common research methodology. Data was collected during 3 years from 5 EU countries, and 921 PTW accidents have been investigated. A questionnaire used to describe the accidents contains 2000 variables. Accident patterns were identified for 5 particular EU countries (France, Germany, Netherlands, Spain and Italy).

One of the key objectives of the study is to investigate injury mechanisms involved in motorcycle accidents and assess the severity of injuries sustained by riders and passengers. It evaluates the effectiveness of existing motorcycle safety measures, such as protective gear, helmets, anti-lock braking systems (ABS), and other active and passive safety technologies. The MAIDS study has

revealed that human factors, such as inadequate training, speeding, and failure to perceive hazards, play a significant role in motorcycle accidents. Motorcyclists' vulnerability on the road due to their smaller size and visibility also contributes to a considerable number of collisions with other vehicles. Intersection accidents have been identified as a common occurrence, emphasizing the need for improved intersection design and awareness among road users. Findings from the study highlight the effectiveness of helmets in reducing the risk of severe head injuries and fatalities in motorcycle accidents. Additionally, speeding and alcohol consumption are major risk factors that lead to higher chances of severe injuries and fatalities. The study emphasizes the importance of properly worn protective gear, such as helmets, jackets, gloves, and boots, in significantly reducing the risk of injury during accidents. Overall, the MAIDS study has played a crucial role in enhancing our understanding of motorcycle accidents, offering valuable insights that inform the development of new safety measures, improved road infrastructure, and increased awareness among motorcyclists and other road users. By promoting evidence-based policies and interventions, the MAIDS study aims to make motorcycling safer and reduce the number of motorcycle accidents worldwide.

The MAIDS-generated database has been re-evaluated by the author to obtain the input parameters for the most common impact scenarios. These parameters are the crash configuration, and the impact speed, all with respect to the legal category (L1 or L3) and motorcycle style (body geometry). Additionally, the human factor as rider age and statue was evaluated with respect to the frequency of the PTW accidents.

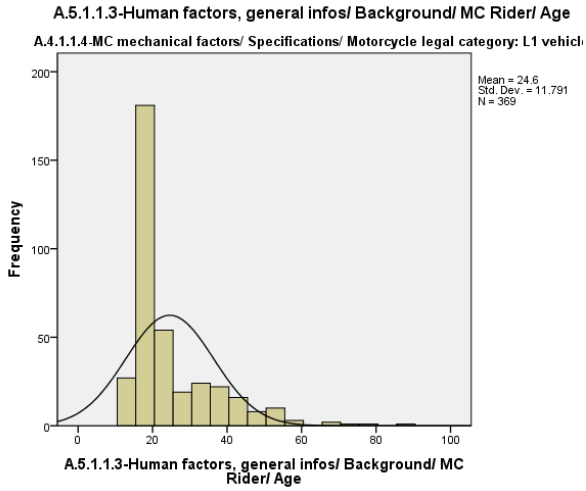

Figure 2.1 L1 Vehicle rider age. (author own work)

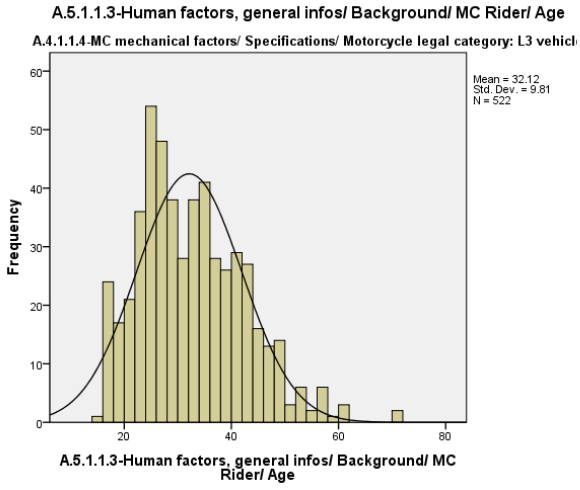

Figure 2.2 L3 vehicle rider age. (author own work)

It can be found from the conducted analysis that:

- The mean value of the L1 riders' age is lower than for the L3 riders.
- In the group of drivers under 20 years of age, there were more accidents among the L1 vehicles (56 % of the L1 accidents involved drivers < 20 years).
- The L3 vehicle share of accidents with drivers < 20 years of age was only 10 %.

The MAIDS database also contains information about the style of PTW which had an accident The motorcycle style can show the initial position of a driver during an accident. Mechanical specifications of each "style" influence the driver body kinematics as well. One of those mechanical specifications of

the style is the location size and shape of the fuel tank. According to the evaluation of the MAIDS data, the scooter style express more than 38% of all L1 and L3 vehicles which had an accident.

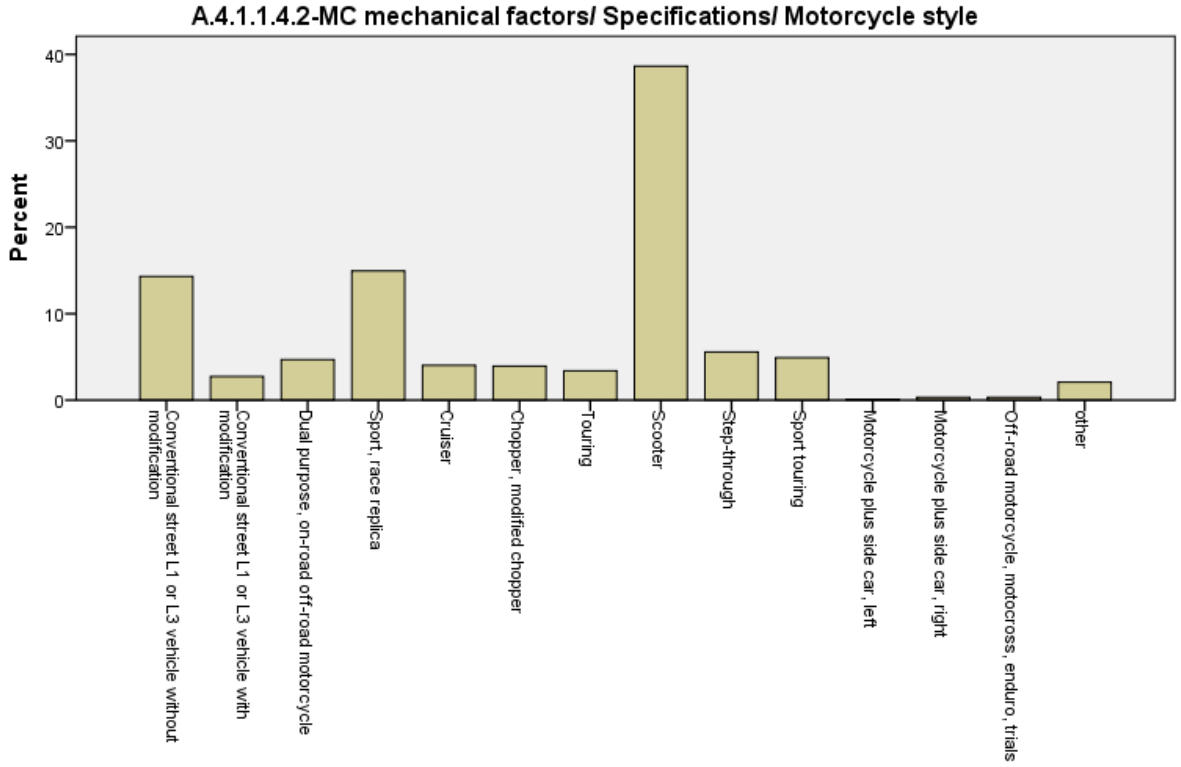

Figure 2.3 Motorcycle style frequency analysis. (author's work)

The analysis concentrated on the mass of PTWs involved in accidents, categorized according to legal definitions within the database. By considering the vehicle's gross mass alongside the crash speed, insights were gained into the kinetic energy that needed to be dissipated to safeguard the rider during the accident. Within the entire vehicle population, those PTWs with a gross mass under 100 kg accounted for approximately 42%. Specifically, in the L1 category (as depicted in Figure 2.4), the majority of vehicles possessed a mass below 100 kg (about 91%). The mass distribution of L3 vehicles was more diverse, revealing notable clusters around 125 kg and 200 kg (as depicted in Figure 2.5).

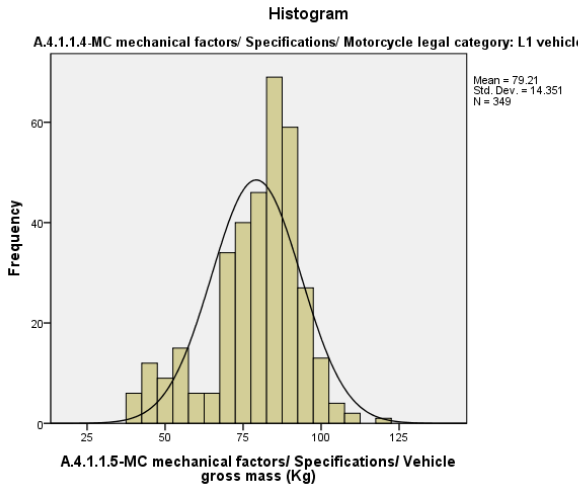

Figure 2.4 L1 Vehicle gross mass. (author's work)

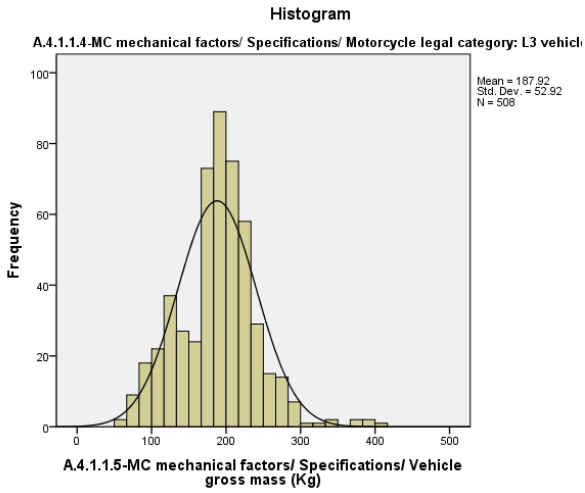

Figure 2.5 L3 Vehicle gross mass. (author's work)

Accident configuration and its probability are the most important information for future simulations of accidents. Vital input for virtual simulations can be obtained using in-depth analysis of pre-crash data.

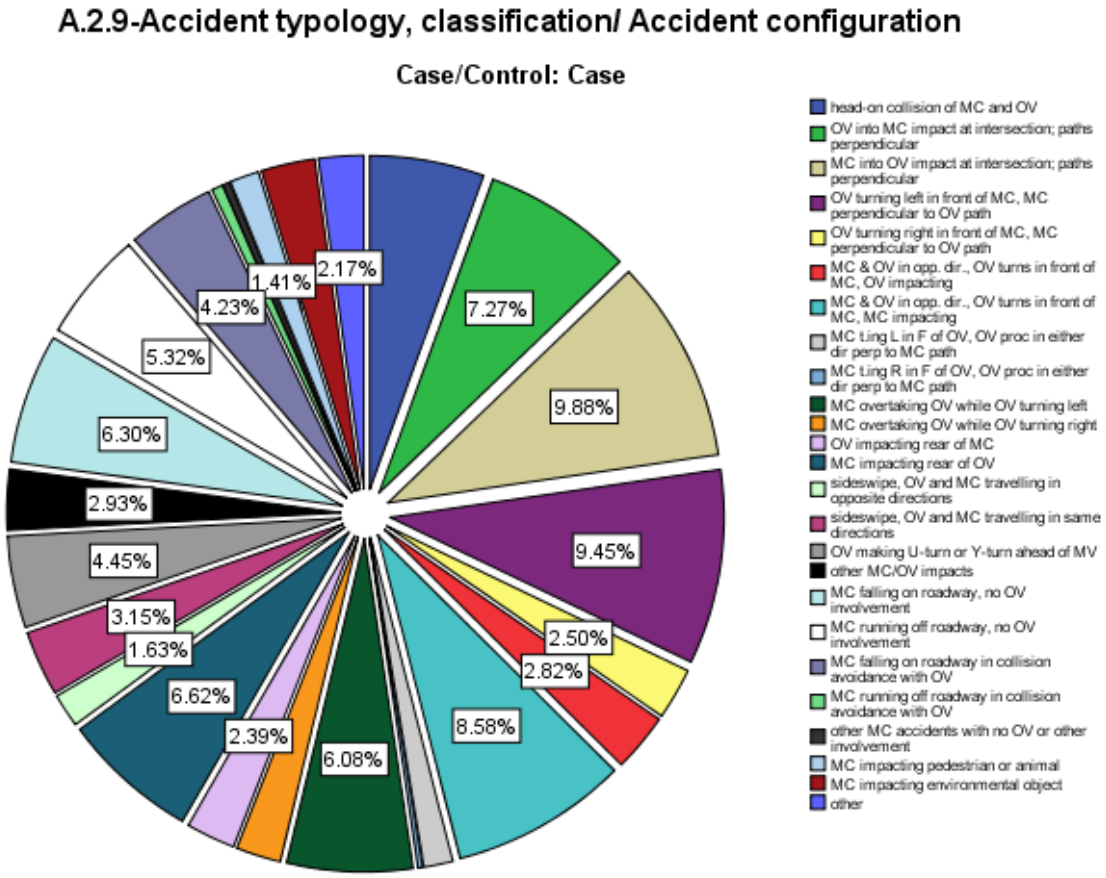

Figure 2.6 Accident typology - configuration. (author's work)

The analysis undertaken (as depicted in Figure 2.6) reveals that PTW to OV impacts manifest in 43.2% of all instances. Accidents devoid of interaction between PTW and OV arise in 16.6% of cases, attributed to either the absence of an OV involvement or the adept evasion of collision by the PTW operator. The configurations primed for simulation within the virtual realm encompass:

- Motorcycle colliding with OV along a perpendicular trajectory – ISO 413
- OV colliding with a motorcycle along a perpendicular trajectory – ISO 143
- Motorcycle colliding with OV from the rear – ISO 711
- Motorcycle colliding with the side of OV (at approximately +/- 45 degrees from the PTW's side axis) – ISO 412, ISO 414
- OV colliding with the motorcycle via the bumper edge (at 45-60 degrees from the PTW's side axis) – ISO 226, ISO 242, ISO 243

The analysis of motorcycle crash speed (as illustrated in Figure 2.7 and Figure 2.8) necessitates a contextual examination of the legal classification of vehicles, given the divergent mechanical attributes exhibited by PTWs within each category.

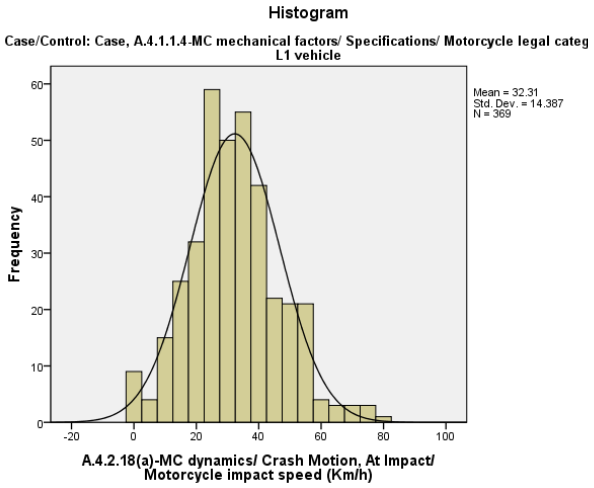

Figure 2.7 L1 vehicle impact speed distribution. (author's work)

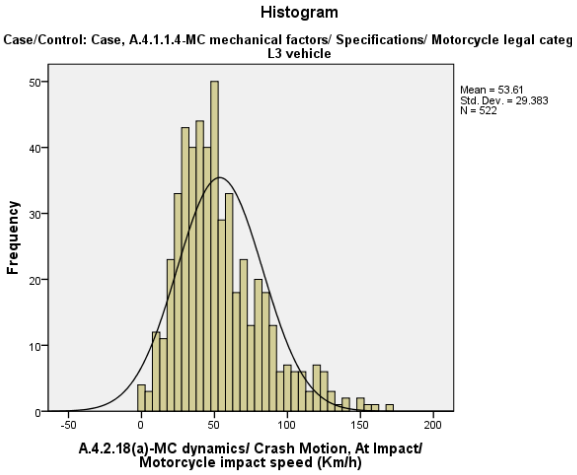

Figure 2.8 L3 vehicle impact speed distribution. (author's work)

The analysis established the fulfillment of a one-sigma confidence level regarding PTW crash speed as a prerequisite for numerical simulations. Adhering to this criterion mandates the simulation of PTW accidents at the ensuing velocities:

- L1: (32 ± 11) km/h => 21 km/h, 32 km/h, 43 km/h
- L3: (53 ± 18) km/h => 35 km/h, 53 km/h, 71 km/h

These assumptions are formulated, taking into account the distribution of accident speeds, which exhibit proximity to a Gaussian distribution. Furthermore, simulations of PTWs across all categories should include a stationary position (0 km/h).

3 Human Surrogate

Biomechanics of injury applies mechanical principles to analyze human injury and response. The field's key objectives include quantifying tissue reactions, identifying injury mechanisms, and gauging tolerance to irreversible tissue damage. Enhanced comprehension of injury mechanisms and their associated thresholds empowers engineers in devising effective trauma prevention measures. Five distinct agents, each with inherent strengths and limitations, are commonly utilized in research and development endeavors: cadavers, volunteers, anthropometric testing devices (ATDs), animals, and computer models [10]. Ethical considerations play a pivotal role in both volunteer and animal testing within the context of passive safety research. Striking the balance between advancing our understanding of safety measures and ensuring the well-being of individuals, be they human volunteers or animals, is a moral imperative. Consequently, rigorous ethical protocols and safeguards must be in place to safeguard the dignity, rights, and safety of all participants [11], whether human or animal [12], in these crucial studies.

Biological reliability pertains to a surrogate's capacity to emulate human behavior under similar loading conditions. This assessment involves engineering measurements encompassing kinetic elements such as force, moment, displacement, and acceleration. In light of modern high-speed transportation, surrogate studies have been pivotal in understanding the impacts of vehicle and aircraft collisions. This chapter evaluates the respective merits of these substitutes, acknowledging their indispensability while recognizing that each alone is insufficient to comprehensively enhance our grasp of injury mechanisms and tolerances.

3.1 State of the Art

3.1.1 Anthropometric Testing Devices

Across the globe, highway safety agencies rely on crashworthiness tests, involving the controlled collision of automobiles into barriers to assess damage and gather performance data. These tests utilize specialized crash test dummies, technically referred to as ATDs, designed to replicate human body appearance and response. These dummies are equipped with advanced instrumentation that records data like acceleration, speed, impact deceleration, impact force, and the nuanced movements and distortions of their limbs and torsos. Safety engineers analyses this data, comparing it to human biomechanical behavior and potential injuries. Despite its widespread use, the experimental crash test method has notable drawbacks. It often results in partial or complete vehicle damage, depending on the test goals. While one of the expectations from the dummies is that they must allow the user to be reused multiple times (with a reasonable level of repetitiveness). That’s why achieving a level of response matching the complexities of human bodies with the robustness and endurance of mechanical systems remains an ongoing refinement process.

In 1949, the Sierra Sam (Figure 3.1) dummy was developed by Sierra Engineering Co. under a contract with the United States Air Force for evaluating aircraft ejection seats (depicted in Figure 3.2) on rocket sled tests. It later found application as a lap shoulder harness test device. Despite being durable and serviceable, Sierra Sam had poor repeatability, and its biofidellity was limited to human-like exterior shape, body weight, and ranges of motion of articulated limb joints. Its mechanical lumbar spine and neck design bore little resemblance to its human counterparts, but at the time, it represented state-of-the-art technology. Sierra Engineering became the first company to manufacture anthropometric testing devices.

Figure 3.1 Sierra Sam [13]**.**

Figure 3.2 Sierra Sam application – parachute [14]**.**

Figure 3.3 VIP Series [15]**.**

Figure 3.4 Sierra Susie (bald head) [16]**.**

Figure 3.5 Sierra Toddler [17]**.**

In 1952 Sam Alderson developed the Mark 1 dummy in his freshly established Alderson Research Laboratories. It was a 95th percentile general-purpose dummy for use by the U.S. and European Air Forces. Its segmentation was determined by making cuts through estimated joint centers on a life subject, resulting in a full plaster cast. The dummy featured a two-piece cast aluminum skull with a cranial cavity for housing accelerometers and pressure transducers. It had a neck with precision investment cast semi-spherical ball-and-socket joints connected by a tensioned steel cable. The limbs had precision torque adjustable joints, but the one-piece limb design made some articulations too stiff. Though resembling its human counterpart in shape, size, and total weight, only a few prototypes were made.

The year 1956 resulted in the new family of ATDs, when Alderson Research Laboratories (ARL) introduced a modular series of general-purpose dummies (Models F, B & P) for various applications, offering fuller motion capabilities than needed in ejection-seat testing. These modular dummies were used in diverse programs, including automotive and aircraft testing with specialized modifications. The dummies came in eight sizes, ranging from 3rd to 98th percentiles (Air Force Anthropometry-AFA), with additional custom motion ranges supplied to meet specific test requirements. The models utilized ball-and-socket joints for lumbar spine motion, but their capability for dynamic simulation was

limited. This year can be considered as the beginning of the construction of dummies providing a better description of the wider population (in this case related to the AFA). Four years later cooperation between ARL and Grumman resulted in the development of the Gard dummy, the application was similar: the testing phases of aircraft ejection seats with rocket catapults. The dummy was integrated with sensors and telemetry instrumentation to ensure the correct center of gravity and moment of inertia alignment. The Gard Dummy was designed to measure critical parameters of ejection-seat performance, rotational stability, acceleration histories, and man-seat interface stresses.

In 1966, the Model VIP Series (Very Important People) was introduced, signifying a shift in dummy development. Previous iterations of test dummies were primarily tailored to the needs of the aircraft industry, serving the purpose of testing pilot escape systems. However, it became increasingly evident that these dummies did not adequately meet the demands of the automotive sector (Figure 3.3). Notably, they lacked a pelvic structure and the necessary spinal articulation, which undermined their effectiveness in evaluating automotive restraint systems. This was particularly crucial for accurately simulating events like jack-knifing and submarining during crashes. To address these limitations, a collaborative effort involving Ford Motor Co. and General Motors Corp. was initiated. This program aimed to create more sophisticated test dummies that closely mimicked human responses to crash decelerations, generating more accurate and reliable data than previously available. Achieving a comprehensive simulation of all relevant human characteristics for crash research necessitated a long-term, evolutionary approach founded on two distinct objectives: immediate and long-term goals. The immediate objectives encompassed replicating the motions observed in human subjects during crash decelerations, ensuring the reproducibility of motion responses, and matching the impact response of the human rib cage.

The years 1967 and 1968 were the years of competition between two manufacturers of dummies, which wanted to apply their ATDs to the automotive safety market. Namely in 1967 it was Sierra Stan, an adult male dummy representing the 50th percentile, was meticulously designed based on H.E.W. (Health and Education Welfare) anthropometric data by Sierra Engineering Co. This dummy, akin to the VIP50 model, was tailor-made to fulfill the rigorous demands of the automotive industry for testing purposes. It was crafted in a semi-seated posture, allowing it to replicate both an upright stance and a seated position ideal for automotive evaluations. The structural framework of Sierra Stan was enveloped in a layer of vinyl skin and polyurethane foam flesh, facilitating easy access through zipper closures. Noteworthy features included a chest design incorporating a potentiometer for measuring force deflection, offering valuable insights into the impacts experienced. The shoulder structure was characterized by a distinct linkage mechanism, utilizing telescoping rods that connected the shoulders to the sternum via ball joint rod ends. To emulate lifelike motions, a "ball-and-socket" design was applied to the neck and lumbar spine. The abdominal region incorporated a viscera sac, simulating the behavior of the dummy's human counterpart during seat belt testing. Ample space was allocated in the head, chest, and thighs to accommodate instrumentation needs. On the second side the VIP50 after a series of extensive tests based on comparison with a similarly upgraded Sierra Engineering Dummy "Sierra Stan" and air force volunteers at the Holloman Air Force Base in New Mexico the VIP5O dummy was modified and became VIP-50A, "The first standard automotive crash test dummies. The first production dummies were delivered to Ford Motor Co., General Motors, and the National Bureau of Standards in Washington D.C. in early 1968.

Figure 3.6 Sierra Susie and realistic wig [18]**.**

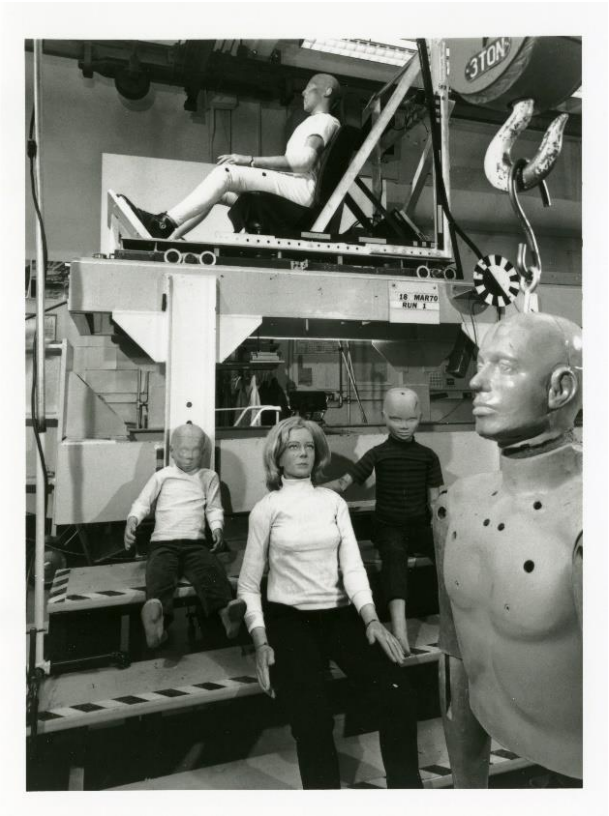

Figure 3.7 "Sierra Dummy Family"[19]**.**

The 1970s brought the focus of dummy manufacturers to the lack of female representation among crash dummies. This resulted in the creation of VIPF5 and Sierra Susie. The VIP95 and VIPF5, both developed in 1970, consist of an adult large male and a small female test dummy respectively. They share similarities in terms of their relative scale factors compared to the VIP-50A Test Dummy. In relation to key anthropometry and joint motion, they adhere to the 50th percentile standards established by SAE J-963. Their joint load adjustability and instrumentation provisions align with the requirements specified in NHTSA's standard 208. However, their level of biofidellity is limited primarily to their humanlike external appearance. These dummies continue to be utilized by certain automobile manufacturers for fitting lap shoulder harnesses. On the other hand, the Sierra Susie, developed in the same year, is an adult female dummy representing the 5th percentile. Structurally, her interior design resembles that of Sierra Stan. Despite her petite size with a weight of 104 lbs. and a seated height of 30.9 inches, her torso area incorporates a design akin to that of Sierra Stan. Notably, Susie is designed with meticulous attention to aesthetic appearance, even featuring a realistic wig (depicted in Figure 3.6).

The next development phase of the vehicle safety assessment in the 1970s was the development of child anthropomorphic testing devices aimed to simulate the responses of young passengers. Sierra Sammy and Sierra Toddler, representing six and three-year-old children respectively, were designed with the guidance of anthropometric data from the Institute of Transportation and Traffic Engineering, University of California, Los Angeles. Although distinct in appearance, these dummies did not accurately replicate weight distribution. The toddler dummy featured an articulated neck and lumbar spine, a flexible rib cage, and a movable mandible. They were part of the broader "Sierra Dummy Family," which included other adult dummies like Sam, Stan, Saul, Susie, and Sue (depicted in Figure 3.7.)

In 1971, General Motors integrated aspects of the VIP series and components from Sierra Engineering into Hybrid I, resulting in enhanced biofidellity and improved result repeatability. Subsequently, sponsored by NHTSA, the Hybrid II series underwent further enhancements, debuting in 1973 as the inaugural dummy to be formally included in the 49 CFR Part 572 standards for anthropomorphic test devices [20].

The HYBRID II (Part 572 Dummy), introduced in 1972, is an adult male dummy representing the 50th percentile size as specified by Part 572 of the Code of Federal Regulations. It is designed for compliance testing of vehicles equipped with passive restraints. The development of the HYBRID II was based on the VIP-SO dummy initially created by Alderson Research and later refined by General Motors for enhanced repeatability in lap/shoulder harness testing. While used for limited qualification testing of air cushion restraint systems, the main attributes of the HYBRID II include its commendable repeatability, durability, and serviceability. However, its biofidellity is constrained to its humanlike external appearance, body weight, and partial range of motion in specific articulated joints. Notably, the measurements of its response are somewhat restricted, focusing solely on orthogonal linear head and chest acceleration components as well as axial femoral shaft loads. Consequently, due to its limitations in biofidellity and response measurements, the dummy's efficacy as a predictive surrogate for injuries is confined. Nonetheless, the HYBRID II serves as a benchmark for evaluating the acceptability of repeatability and reproducibility in the responses of other dummies. In essence, the Part 572 dummy embodies the forefront of dummy technology in the early 1970s.

Figure 3.8 Hybrid III ATD [21]**.**

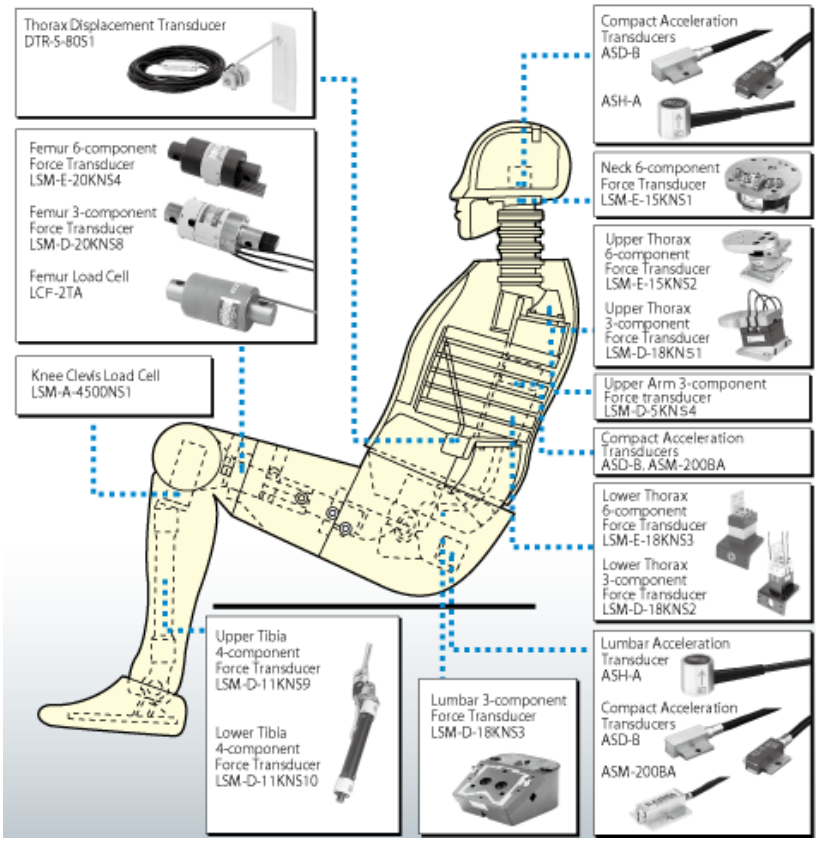

Figure 3.9 Hybrid III sensors placement [22]**.**

The HYBRID III (Part 571 Dummy), established in 1976, is an adult male dummy embodying the specifications outlined by Part 571 of the Code of Federal Regulation for compliance testing of

vehicles. Rooted in the ATD 502, a sophisticated test dummy developed by General Motors in 1973 under the auspices of the National Highway Traffic Safety Administration, the HYBRID III boasts advanced features. The ATD 502 incorporated a head with humanlike impact response qualities for rigid-surface forehead impacts. Further innovations encompassed a curved lumbar spine to emulate realistic automotive seating postures, and constant torque joints were integrated into the knee, elbow, and shoulder joints to enhance consistency and minimize joint torque setup times. The shoulder structure was redesigned to improve alignment with seat belts, addressing a concern with the previous HYBRID II (Part 572) model. The HYBRID III retained these advancements while introducing modifications to enhance the impact response biofidellity of the neck, chest, and knees. Additionally, the dummy featured transducers for measuring various factors such as orthogonal linear acceleration components of the head and chest, reactions between the head and neck, sternum displacement relative to the thoracic spine, and axial femoral shaft loads (Figure 3.9, Table 3.1). The fully instrumented HYBRID III dummy surpasses the 50th percentile adult male median weight by approximately 7.3 lbs. (3.3 kg) primarily due to the inclusion of fully equipped lower legs with ball joint ankles. These enhancements prevent lower leg and ankle breakage during crash tests, particularly in scenarios involving severe rearward displacements of vehicle floors or firewalls. Although the added weight is offset by the augmented measurement capabilities, compensating for any potential drawbacks, the increased capabilities of the HYBRID III underscore its significance in the realm of safety testing.

Table 3.1 Measurement Capacity of Fully Instrumented Hybrid III

Measurement	Data Channels
Head	
Tri-axial acceleration	3
Angular acceleration	1
Facial Laceration	
Neck	
Axial load	1
Shear load	1
Bending moment	1
Chest	
Tri-axial acceleration	3
Sternum acceleration	2
Deflection	1
Pelvis	
Tri-axial acceleration	3
Anterior/superior iliac spine load	6
Upper Extremities	
Lower arm bending moments	4
Lower extremities	
Femur load	2
Femur/tibia translation	2
Tibia bending moments	4
Tibia axial load	2
Medial/lateral tibia plateau load	4
Lateral or fore/aft ankle bending moment and shear load	4
Knee laceration	
Total Data Channels	44

As this work is concerned with the PTW's safety, a dummy designed or utilized for motorcycle accident reconstruction should be mentioned. The Motorcycle Anthropometric Test Device (MATD) emerged as a product of international collaboration during the 1990s. The efforts of ISO TC22/SC22/WG22 culminated in the establishment of a test protocol for assessing motorcycle-automobile collisions, along with corresponding tool specifications for conducting these crash tests. Enshrined in part 3 of the ISO 13232 document, the MATD dummy draws inspiration from the long-standing standard for frontal impacts, the Hybrid-III frontal impact dummy. However, ISO 13232 necessitated several adaptations to render the dummy suitable for motorcycle crash scenarios.

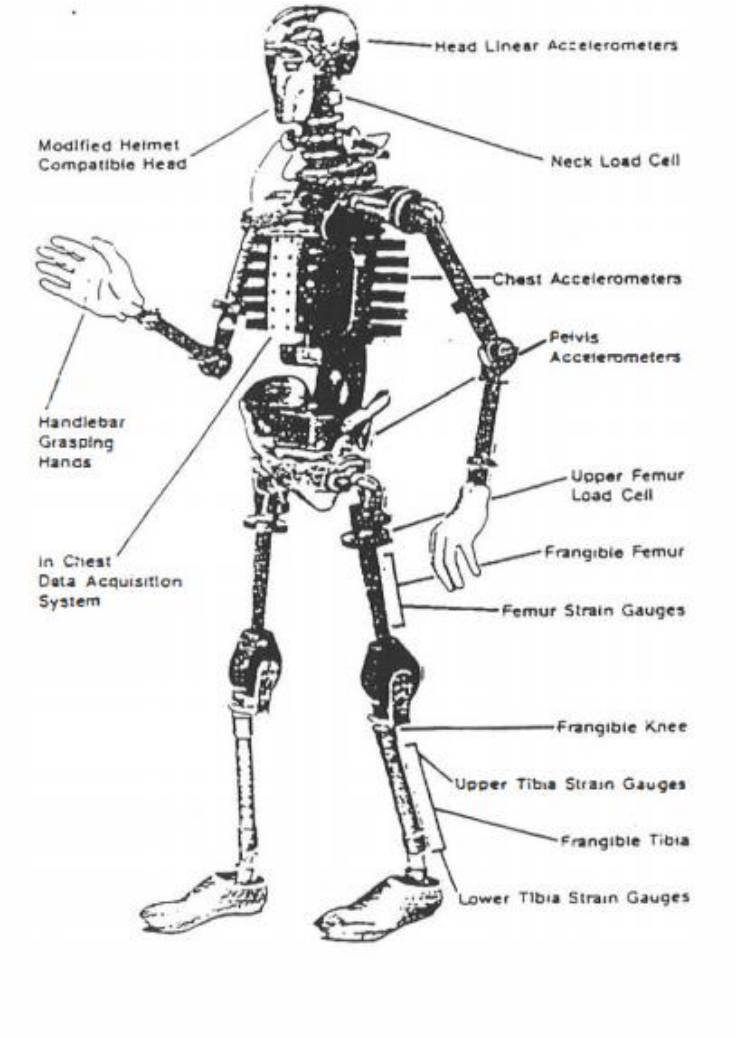

Figure 3.10 MATD improvements over the pedestrian Hybrid III [23]**.**

Key features of the MATD dummy include:

- A customized head compatible with motorcycle helmets (depicted in Figure 3.12),
- A freshly devised neck affording versatile motorcycle positioning while maintaining an upright head orientation (depicted in Figure 3.11-3.12),
- Incorporation of the Hybrid-III sit-stand pelvis for positioning on motorcycles (third image in Figure 3.15),
- Dummy hands facilitating grasp around handlebars (Figure 3.10),
- Incorporation of frangible upper legs, lower legs, knees, and abdomen (first image in Figure 3.15),
- On-board dummy data acquisition system situated in an adapted spine box (Figure 3.15),

- Expanded range of motion in upper and lower neck to accommodate riding posture,
- Integration of a torsional module at the upper neck to achieve biofidelic neck twist response (Figure 3.14),

of particular significance are the last two points. The dummy's neck has been subjected to thorough scrutiny to explore the potential compatibility of airbag systems with motorcycles. As inflatable restraint systems have gained prominence in automobiles, a new category of accidents, referred to as "out-of-position," has emerged. The feasibility of extending airbag protection to motorcyclists in crash scenarios must be balanced against challenges similar to those faced by "out-of-position" situations in cars.

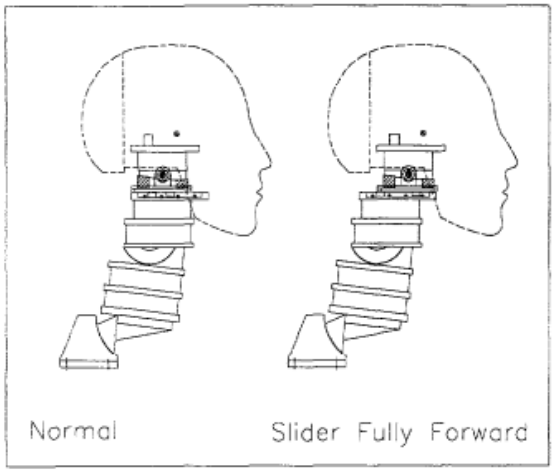

Figure 3.11 MATD neck forward sliding capabilities [24]**.**

Figure 3.12 MATD head with the neck - frontal view [25]**.**

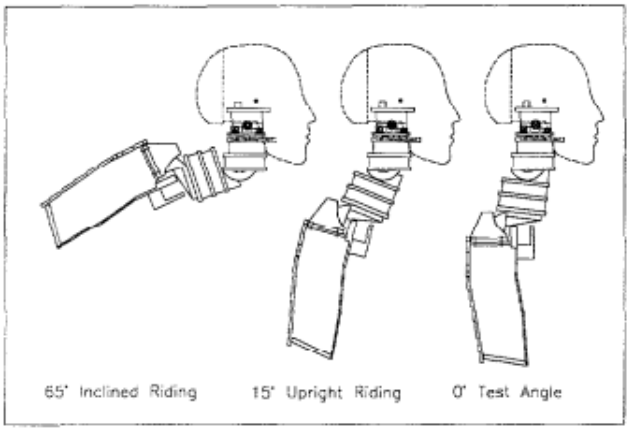

Figure 3.13 MATD neck inclining capabilities [24]**.**

Figure 3.14 MATD head with the neck - side view [25]**.**

Given the absence of seat belts and predefined seating arrangements for motorcyclists, the likelihood of riders assuming out-of-position postures during crashes is substantial. Coupled with the presence of helmets, this could heighten the risk of neck injuries for motorcyclists. Endeavors to enhance the biofidellity and efficacy of the MATD neck have primarily relied on the standard Hybrid III neck platform 641. However, it has been recognized that further advancements in the MATD neck would necessitate a more revolutionary approach, potentially entailing the introduction of an entirely new

neck design. This article delineates the conception and performance of such a ground-breaking prototype neck for the MATD [26].

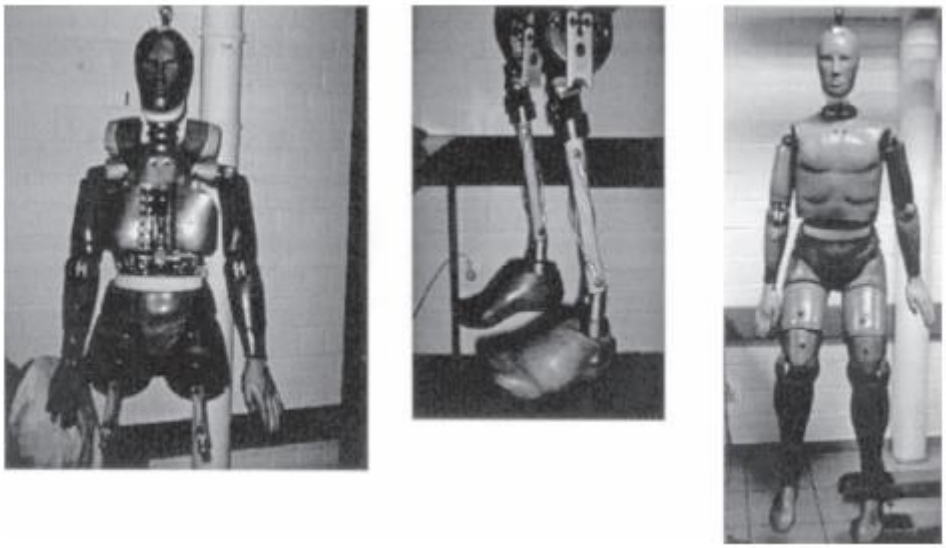

Figure 3.15. Photography of the inside structure of MATD [27]**.**

For more than 20 years the development of the physical motorcyclist ATD has been stopped. However, in 2022 Autoliv proposed a new PTW crash dummy [28] whose main part is based on the Hybrid III 50th percentile ATD with pedestrian-type pelvis (allows to change the position from siting to standing). The new dummy head and neck are adapted from the WorldSID with an additional tilt mechanism (Figure 3.16). Since then the dummy has been validated only versus the impact of the motorcycle with the speed of 50 km/h versus the side of the car driving 20km/h with the assessment of the peak head acceleration and HIC_{15} criteria.

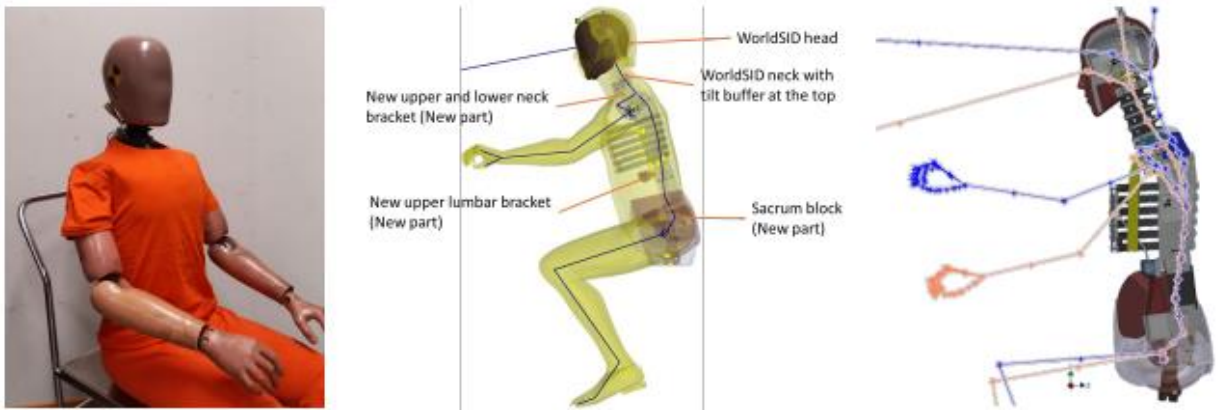

Figure 3.16. Autoliv PTW dummy Version 1.0.

The European Side Impact Dummy, known as Euro-SID, and its latest iterations - ES-2 and ES-2re dummies, serve as integral components in both regulatory and consumer test procedures aimed at evaluating injuries resulting from side impact collisions. These dummies are designed to represent the anthropometric characteristics of an average-sized (50th percentile) adult male occupant. The finalized design of the ES-2 (depicted in Figure 3.17) dummy gained official acceptance within Europe for utilization in the EuroNCAP and ECE R95 testing protocols during 2003 and 2004, respectively.

Subsequently, in 2006, the US regulatory body NHTSA sanctioned the ES-2re variant (an ES-2 version with a modified rib structure) for use in American occupant safety test protocols such as FMVSS 214 and eventually USNCAPMY 2011. This widespread approval led to the global replacement of its forerunners, namely the EUROSID-1 and US-SID dummies. [29, 30].

Figure 3.17 ES-2 dummy [31]**.**

Figure 3.18 WorldSID dummy [31]**.**

In September 2007, the Federal Motor Vehicle Safety Standard (FMVSS) No. 214, focusing on "Side Impact Protection," underwent significant enhancements. These upgrades encompassed the integration of an updated anthropometric test device (ATD) - the ES-2re, representing a 50th percentile male, and the inclusion of a 5th percentile female dummy (SID-IIs) within the testing procedures. Additionally, FMVSS No. 214 underwent modifications to introduce a new testing scenario - the oblique pole impact. In the final rule, the National Highway Traffic Safety Administration (NHTSA) expressed its intention to assess the potential inclusion of the WorldSID dummies into the standard. Subsequently, in 2011, the NHTSA's New Car Assessment Program (NCAP) test protocols were updated to encompass these novel dummies and to integrate the oblique pole impact evaluation.

The development and design of the WorldSID 50th percentile male dummy (WSID-50M - Figure 3.18) commenced in June 1997, under the auspices of the International Organization for Standardization (ISO), specifically within the working group on anthropomorphic test devices (TC22/SC12/WG5). The WSID-50M was conceived to replace the prevailing ATD employed for assessing vehicles in side impact testing. Its primary objective was to establish harmonization across various countries by introducing a standardized 50th percentile male dummy for side impact evaluations. Crafted to serve as a universally acknowledged model for side impact evaluations, the WorldSID dummy at the 50th percentile embodies a commitment to robust biofidellity and comprehensive injury tracking capabilities [32].

In 1985 J. Melvin in his paper on the ESV conference [33] summarized the research contract which has been established between the NHTSA and the Highway Safety Research Institute at the University of Michigan. The main idea behind this contract was to develop a new advanced ATD. Finally, after 35 years in 2020, EuroNCAP proposed the 50% Male THOR Dummy in some of their tests for Safety

Ratings. The main advantages of the THOR over the HIII lie not only in biofidelic kinematics but also in the overall improvement of dynamic response, which is closer to the experimental corridors (depicted on the left part of Figure 3.19). The main biofidelic improvements are:

- Neck that bends, twists, and stretches for realistic head motion,
- Torso with anatomically correct ribcage and shoulder,
- Flexible spine to allow proper upper body motion,
- Abdomen and pelvis that mimic human seat belt interaction,
- Legs that respond to the impact of the dashboard and pedal.

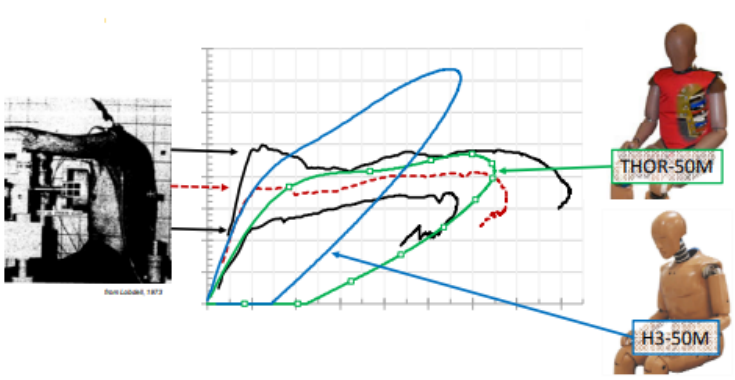

Body Region	THOR-50M	H3-50M
Head	Excellent	Poor
Neck	Good	Poor
Thorax	Excellent	Good
Abdomen	Marginal	Marginal
Knee/Thigh/Hip	Good	Poor
Lower Extremity	Good	Excellent
Whole-body	Good	Good

Figure 3.19 Biofidellity comparison of particular body parts between Hybrid III 50th percentile male and THOR 50th percentile male [34]**.**

Figure 3.20 THOR-50M with exposed biofidelic ribcage [35]**.**

The design objective of the Humanities BioRID-II was to facilitate the advancement of superior head and neck safeguarding mechanisms in the context of rear impact collisions. Preceding iterations of anthropomorphic test dummies had underscored a conspicuous deficiency in replicating biological authenticity. Consequently, the BioRID was meticulously engineered to showcase a biomechanical veracity that aligns with the inherent neck kinetics ensuing from the forces associated with rear impact-induced whiplash. The validation of the BioRID-II entails meticulous comparisons against low-

velocity volunteer data. This anatomical test device was a collaborative endeavor involving Chalmers University and Denton ATD [36].

Figure 3.21 Side view of BioRID-II with the state-of-the-art neck for the rear impact scenarios purposes [36]**.**

Properties of the BioRID-II body parts [37]:

- Head: The BioRID-II incorporates modifications from the Hybrid III model, resulting in a refined configuration that ensures clearance of the cervical vertebrae. This adaptation facilitates the precise placement of a leveling tool for mounting.
- Neck, Thorax, and Abdomen: The salient innovation of the BioRID-II resides in its vertebral column, a comprehensive assembly encompassing 24 distinct vertebrae, comprising seven cervical, 12 thoracic, and five lumbar segments. This intricate architecture is meticulously emulated using a combination of washers, urethane bumpers, and springs that emulate muscular responses. Within a silicone sheath, the vertebral column features pin linkages to the vertebrae and includes a water-filled bladder in the abdominal region, thus achieving a remarkably authentic physiological representation.
- Pelvis: The fusion between the spine assembly and the adapted Hybrid III pelvis is realized through the Sacrum-to-L5 Interface Plate. This amalgamation incorporates a modified pelvic structure featuring a lower cut iliac and an expanded leg opening to ensure an anatomically faithful integration.

- Legs and Arms: The extremities of the dummy remain consistent with the standard Hybrid III 50th model, with the option of integrating a spectrum of available sensors tailored to these appendages.

3.1.2 Post Mortem Human Surrogates

The Post Mortem Human Surrogate (PMHS) application often raises the hands of ethical committee members. However, if utilized properly (according to the law, with the handling not detached from respect to the donor) they became an irreplaceable source of valuable data. The appearance of PMHS in biomechanics evolved from the medical autopsies of corpses.

The most common usages of Post Mortem Human Surrogates (PMHS), often also called Cadavers, in the field of biomechanical research, firstly lie in the validation of the response for other artificial surrogates, secondly, their particular body parts can be investigated (for example brain) for the development of injury criteria (IC). The first application allows the parts of the ATD to have the physical response as the biological tissues. An example could be the response of the HIII neck in the frontal crash, where the kinematics of the ATD head must be in the prescribed corridor. This corridor came from the range of the tests with PMHS in prescribed conditions and expressed the behavior of the spine-neck-head system for the population. These full-body biomechanical experiments are conducted by very few laboratories in the world (for example by the Centre of Applied Biomechanics at the University of Virginia, Wayne State University). The property of the ATD which expresses the goodness of fit of a particular response to the corridor is called biofidellity. The Sled-test in which the kinematical response for the head and the T1 vertebrae is depicted in Figure 3.22. With the set of tests in the same setup but with different stature and corridor of responses can be acquired (as shown in Figure 3.23). The second application is connected with the development of the criteria for tissue injury. Those criteria are made by the biomechanical research teams to correlate the physical values such as force, acceleration, velocity, and deformation with the injury of a particular organ or body part. Above mentioned correlation allows to implementation of the criteria in different typed of surrogates (ATDs, HBMs, freefall head forms).

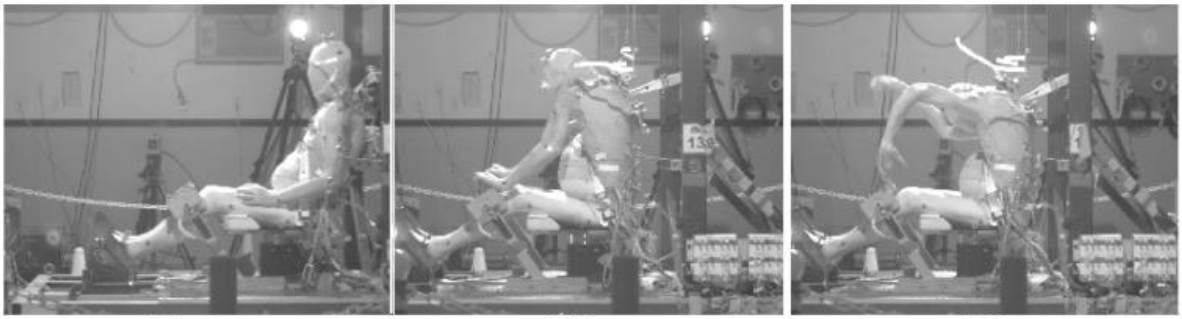

Figure 3.22. The sled test with the PMHS [38]**.**

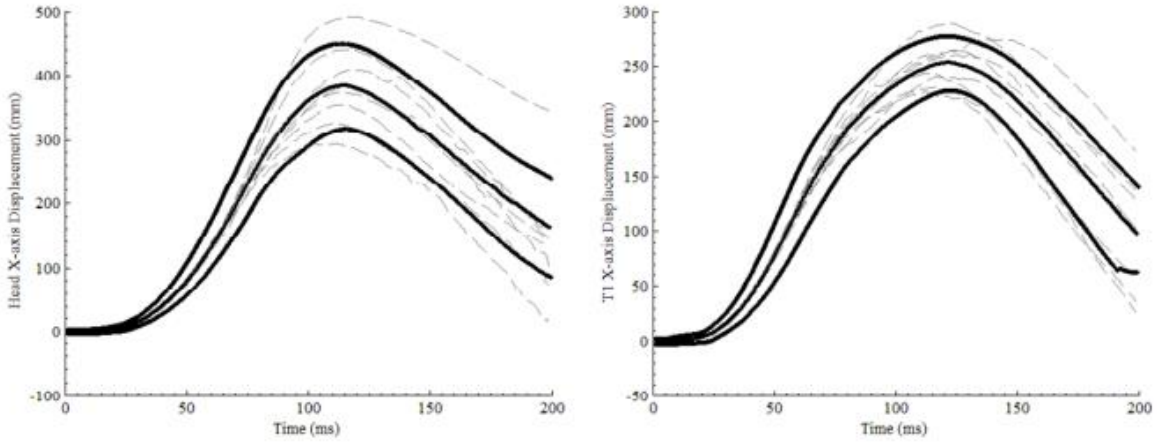

Figure 3.23. Head and T1 X-dir. Displacement (frontal) from the obtained from the PMHS experimental study [38]**.**

There are no known studies that applied the PMHS as a motorcycle driver for full-scale crash tests or similar sled-like tests. However, for the sake of the motorcycle accidents analysis improvement, the C.R. Brass team re-evaluated the one of neck injury criteria used in the standard ISO 13232 (related to the motorcycle mounted protective devices) by using 36 head-neck PMHS system with attached mass, which was acting as a helmet dummy [39].

It should be noted that the PMHS application does not only come with advantages. Firstly the acquisition of desirable surrogates is often problematic. Even the well-established laboratories with the know-how in this field and with the agreements, signed with hospitals, are limited to the anthropometries' and the age of the donor bodies. Secondly, the handling of the cadavers is problematic due to the need to keep them cold before the planned test. The body of the donor must be thawed and re-articulated in the joints before the test. Thirdly the cadavers represent only the response of the dead/unconscious body. There is no active muscle response [10].

3.1.3 Volunteers

From the tissue response and anthropometry point of view, the volunteers are perfect surrogates for biomechanical research. Basically in this situation, the human being is surrogated by itself, and the kinematic, kinetic, and dynamical behavior of the test subject is the same (without the view on the differences in anthropometry and other body parameters that differentiate one person from another) as the occupant of the vehicle or different user of the transportation system (pedestrian, motorcycle driver, etc.). As stated by J. R. Crandall [10] volunteer testing has one main disadvantage – it needs to be planned with a high margin of safety coefficient related to the volunteer loading. Directly speaking, no volunteer testing is allowed beyond the well-defined limit for the human capabilities of bearing the load (the volunteer cannot be injured during the test). One of the most severe volunteer tests were conducted in the 70's by the Naval Biodynamic Laboratory (NBDL) with a group of male participants at a young age. The purpose of the tests was to assess the head and neck (T1 vertebrae) motion. The NBDL tests [40] are depicted in Figure 3.24 on the left side along with the numerical model which utilized the results to achieve the outer biofidellity (right) [41].

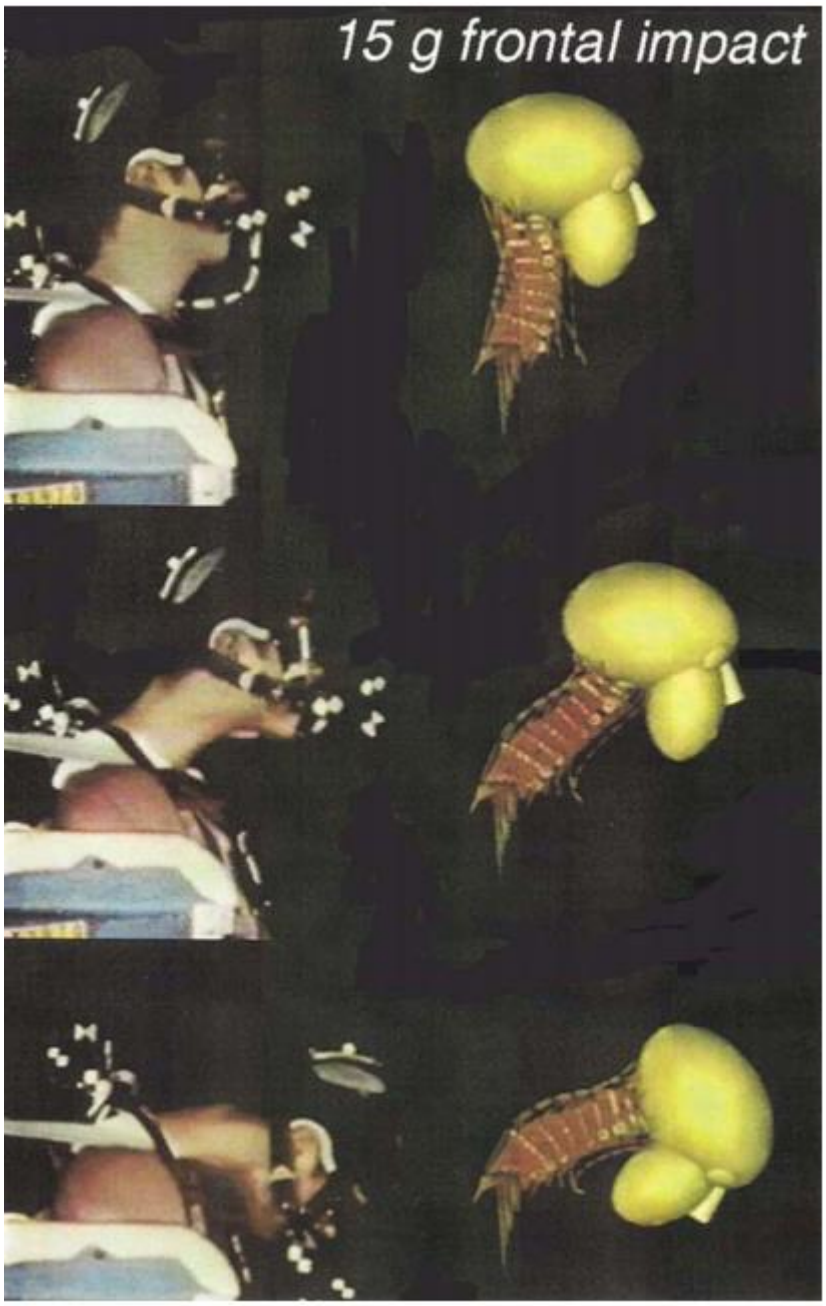

Figure 3.24. The high-speed volunteer tests done in Naval Biodynamic Laboratory (NBDL) [40, 41]**.**

Above mentioned limit of the volunteer testing was not well established in the early days of the occupant safety research. Partially because the human injury limits haven't been yet known. The best-known volunteer testing experiments are the rocket sled-tests done by John Stapp, It should be noted that Col. Stapp wasn't the only volunteer in those tests (there was a group of 11 volunteers), and nonetheless before each volunteer, he was testing himself on the planned setup. The fastest experiment on the rocket sled conducted and participated by him set a record of the ground speed of the man (1017 km/h in six seconds) and gave him the title of "Fastest Man on Earth." Intentionally or not, the deceleration (from 1017 km/h to 0 in 2 seconds) of the test made him black out, but after the examination by the doctors, it appeared that he did not suffer major injuries [42]. The six phases of the Stapp rocked-sled test can be seen in Figure 3.25. (phase 1 to 3 was the acceleration with the 12 g and the phase 4-6 was the deceleration with 22g) [43].

Figure 3.25. Col. Stapp during the sled test [43]**.**

3.1.4 Human Body Models

Human body models (HBM) or numerical models of the human body are idealized by particular numerical approaches (lumped-mass, multi-body system, finite element method) representations of an entire human body or its parts. By utilizing one of the above-mentioned formulations the equation of motion could be solved to gain the model behavior under prescribed loading. The increasing complexity of formulation brings not only a more detailed description of the problem but also comes with a higher computational cost and a bigger burden on obtaining the model parameters, also detailed models are often expecting wider validation of response. Where the one- or two–dimensional lumped-mass models, in which the system is built from a couple of rigid parts described by its mass/inertia, and are coupled by the springs with prescribed stiffness (often without their own mass) expect the user just to provide as a input this small number of parameters (topology of

connection, masses of parts, stiffness of springs) and the excitation description (acceleration, force, deflection), the full 3 dimensional models of entire human body (FEM) are often described by the hundreds if not thousands constitutive materials describing each modelled body part. The modeling approach should be used concerning the problem that the engineer/researcher wants to solve. As was shown by the early research of R. Willinger even the simple lumped-mass models (depicted in Figure 3.26) could be efficiently used for predicting the resonances oh the head-brain system [44, 45].

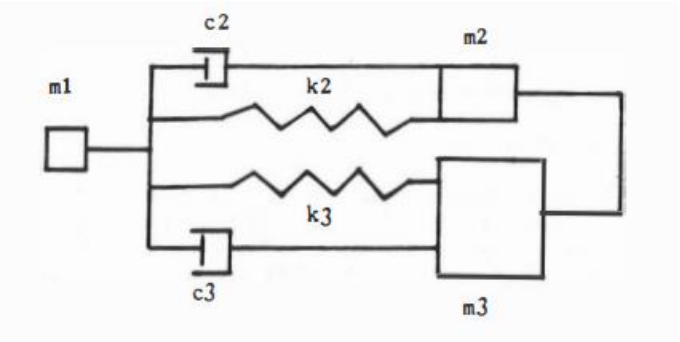

Figure 3.26. One dimensional (1D) Lumped-mass model of the head (where the distribution of head mass is as follows m1 = 10%, m2 = 35%, m3 = 55%) [44]**.**

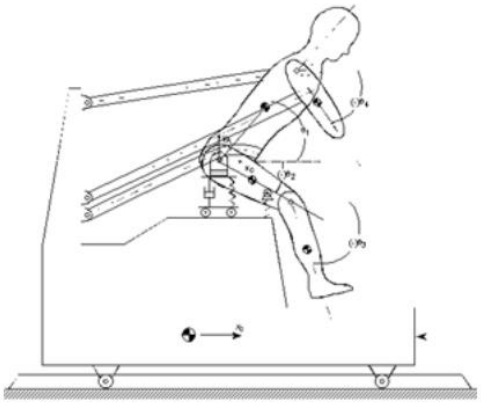

Figure 3.27. A two-dimensional (2D) multi-body system model referred as Crash Victim Simulation (CVS) [46]**.**

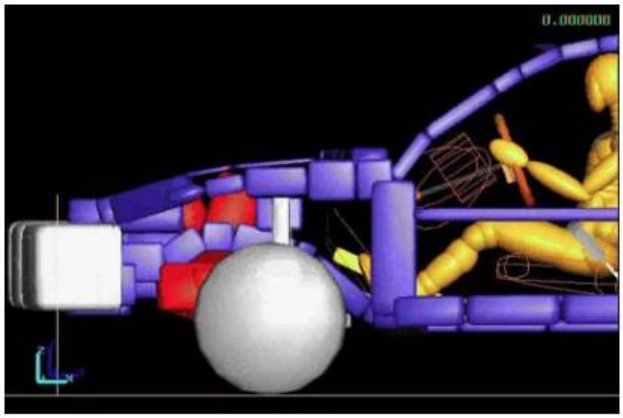

Figure 3.28. The 3-dimensional (3D) model for frontal collisions with the multi-body system model of the driver [47]**.**

One of the first two-dimensional (2D) multi-body system model with 7 degrees of freedom was developed on the 60 by R.R. McHenry to assess the correlation of the restrained human body model with the experiment [48, 46].

3.1.4.1 HUMOS, HUMOS2

Presently, automotive engineers rely on anthropometric crash dummies, which exhibit notable constraints in terms of biofidellity and the scope of their application (frontal, lateral, and side impacts). As a result, these dummies exhibit significant deficiencies that prevent them from replicating real-world crash scenarios with accuracy, displaying biofidelic behavior only within a limited application range. With the advancement of computational capabilities, engineers have embraced simulation techniques as an integral part of their prototype design process. This integration extends to numerical dummy models, which are now seamlessly incorporated into crash simulation procedures. Nonetheless, these numerical models inherit the shortcomings of their physical counterparts, such as limitations in biofidellity.

The subsequent phase of simulation naturally involves the development of occupant models that more faithfully represent the complexities of the human body. This advancement holds the promise of enhanced insights and predictive capabilities concerning injury risks, benefiting both vehicle occupants and pedestrians alike. Crafting such a model necessitates a profound understanding of human body geometry, material properties, and an extensive experimental dataset for validation purposes. While some relevant data exists in the literature, its utility is constrained by experimental heterogeneity. The HUMOS project seeks to gather and complement existing data, overcoming this limitation [49].

The project's primary goals encompass three key facets:

- Formulating human body models and tools optimized for application within design offices, thereby augmenting the safety dimensions of road transportation. This analytical capacity is also poised to mitigate the environmental costs of accidents. Notably, other transportation sectors (aviation, railways) and design considerations like ergonomics and comfort, not exclusively linked to safety, could likewise gain from the outcomes of the HUMOS project.
- Embedding human variability aspects (including geometry, behavior, and tolerance) within the design cycle, thereby achieving a holistic approach.
- Serving as a collaborative initiative on a European scale, addressing shared concerns (production, prevention, regulation) of the European community by providing a reliable mathematical tool that could replace the reliance on Post Mortem Human Subjects (PMHS) and Anthropomorphic Test Devices (ATDs) [50].

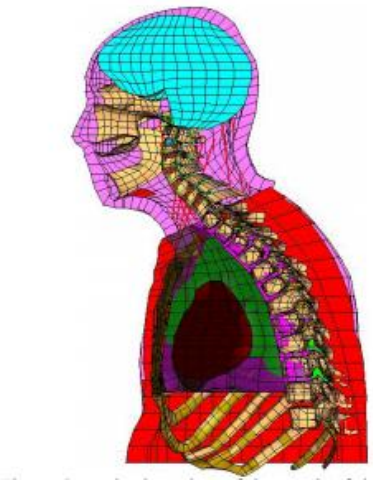

Figure 3.29 The mesh of the upper body of HUMOS (sagittal plane section).

The HUMOS2 project, funded by the European Commission (EC), aimed to develop Finite Element (FE) human models that encompass a broad spectrum of the European population. These models are intended to accurately predict injury risks for individuals involved in road accidents. In a previous iteration, the HUMOS project introduced the HUMOS model, representing a male in a driving position close to the 50th percentile.

Firstly, the HUMOS2 project has devised methods for personalizing numerical human models, encompassing anthropometry, geometry, and positioning. This includes a scaling tool that can generate individualized models from the original one using mesh control points and statistical relationships derived from external and internal dimensions. These relationships were established through geometric data collected from standing and sitting human volunteers, employing a low-dose bi-plane X-ray system, as well as directly measured data from isolated bone parts. Additionally, a positioning tool has been created, based on a set of reference postures ranging from seated car occupants and out-of-position (OOP) scenarios to pedestrian postures. This tool allows for model adjustments and testing across various sitting and standing poses.

Secondly, the consortium under the HUMOS2 has conducted experimental studies on human volunteers to determine the influence of muscular tension on body response to moderate impacts. This effort has led to the establishment of a comprehensive biomechanical test database, tailored for model validation. The database incorporates new biomaterial laws for ligaments and skeletal muscles, along with existing cadaver test results from previous EC projects and Heidelberg University [51].

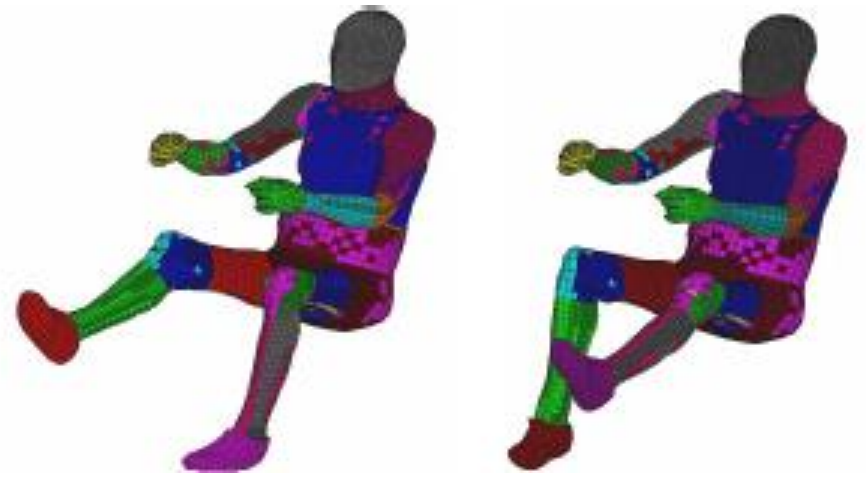

Figure 3.30 HUMOS2 model showing the leg positioning capabilities [51]**.**

The HUMOS in its second version: HUMOS2, was used by S. Peldschus [52] in the APROSYS project for the development of a test standard for the impacts of powered two-wheelers on roadside barriers. It was possible as his validation of the PAM-Crash implementation of the HUMOS2 model has encompassed lateral thorax loading, as evidenced by Merten in 2006. Furthermore, the model's capabilities extend to portraying injury mechanisms resulting from motorcyclists' collisions with roadside barriers, as demonstrated by S. Peldschus and E. Schuller in 2006. The results of this research are depicted in Figure 3.31 and were summarized by the authors: “The deflections of the affected part of the thorax were assessed in this simulation using the approach described in [53]. The highest deflections at 50% of the thorax's half circumference at the height of ribs 4 and 8 were 51mm and 48mm, respectively. These findings point to the possibility of serious thoracic injuries as a result of lateral stress in such an incident.”

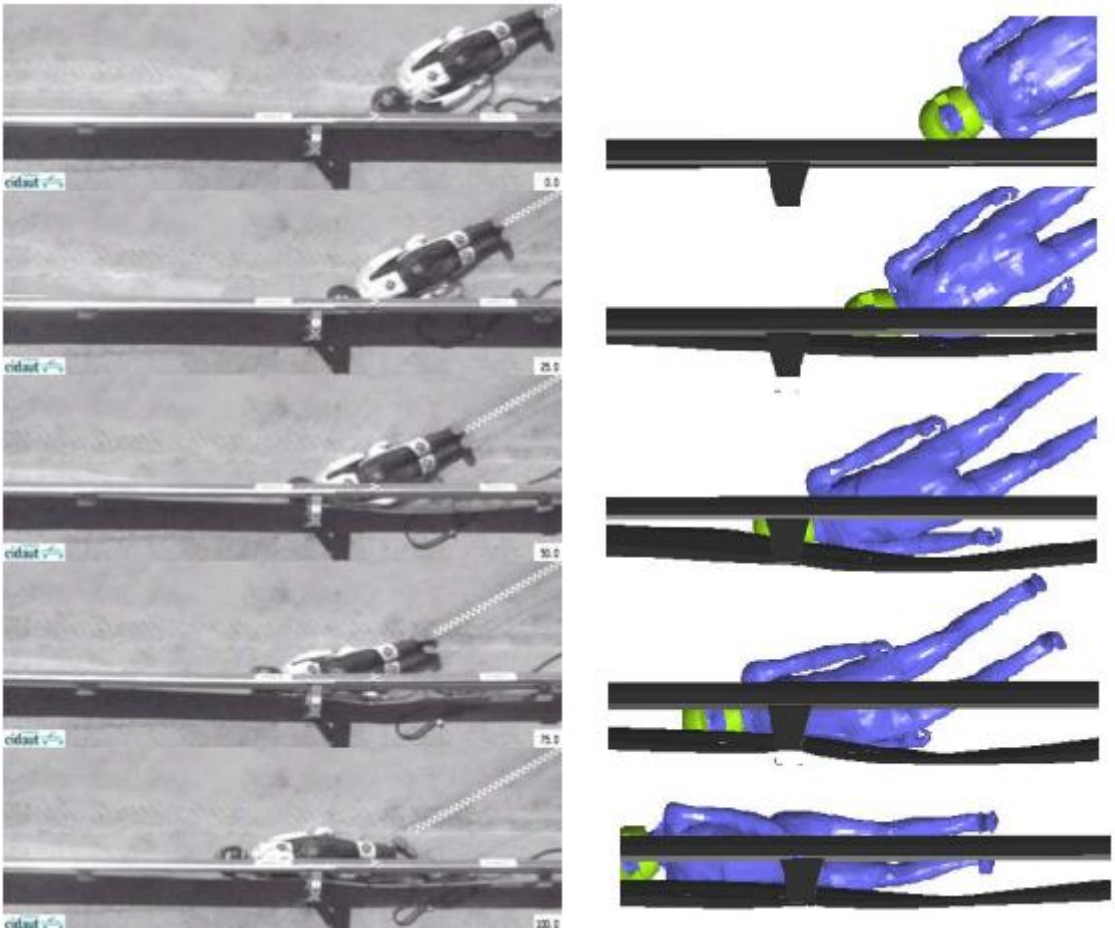

Figure 3.31 Virtual barrier test with HUMOS2 model.

In 2010 the HUMOS car driver model was used by L. Thelon, [54] to evaluate the thoracic airbag for motorcyclists as depicted in Figure 3.32. In his research two configurations were evaluated: lower sternum impact and upper sternum impact, with and without the analyzed airbag concept. The impactor has the shape of an 80mm solid cylinder with 12 kg of mass. Lower sternum impacts were conducted with the impactor perpendicular to the body part with three impact speeds: 3.33, 4.33, and 5.33 m/s. In the upper sternum configuration, the impactor was set parallel to the body (similar to the orientation of the hypothetic straight handlebar), with impact speeds: of 2.78, 5.56, 8.33, and 11.11 m/s. The scenarios were evaluated in terms of the chest compression criterion and transcoded to the AIS by the following expression:

$$AIS = -3.78 + 19.56 * C, \tag{3.1}$$

where: AIS is the thoracic injury in the AIS scale (discussed in chapter 3.2.1.1), and C is the compression of the chest in %.

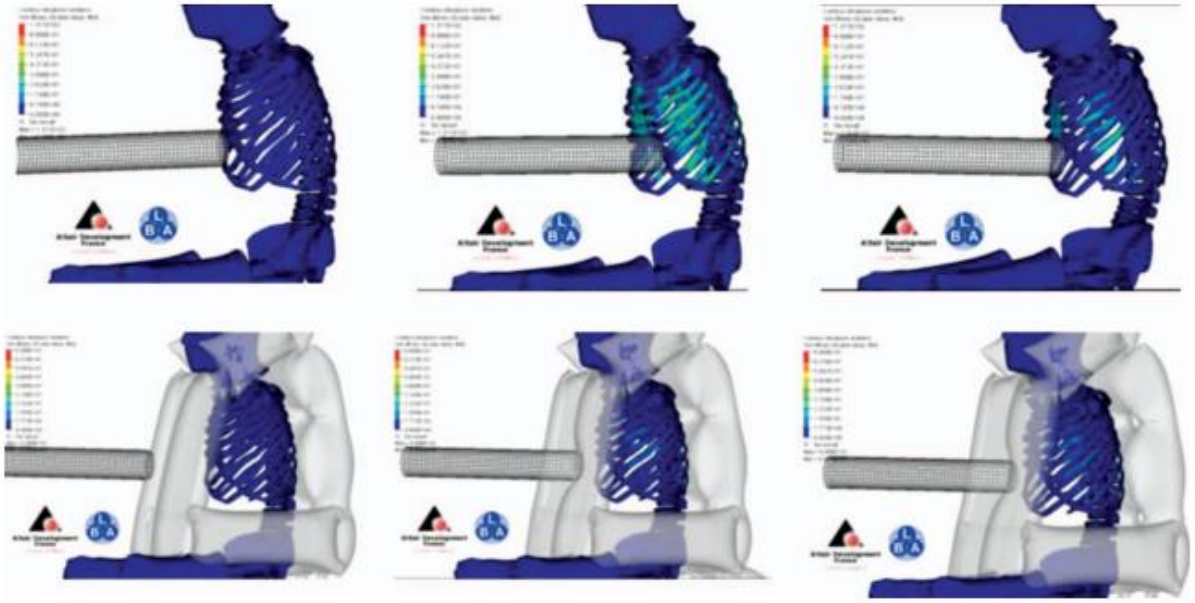

Figure 3.32. The stress in the HUMOS ribs for configuration with airbag and without.[54]

The research paper summarized the main outcome of the research: “The benefits of using of an airbag jacket as a new protection system were also assessed, as it could significantly reduce the sternum deflection and the injury gravity (from AIS = 5 without airbag to AIS = 2 with the airbag jacket).”[54]

3.1.4.2 THUMS

THUMS (Total HUman Model for Safety) is an advanced crash test human body FE model developed by Toyota Motor Corporation (TMC). In its most stable 4.0 version, this male dummy builds upon the previous generation, which introduced bone-like structures and a brain model, by incorporating detailed models of internal organs. This enhancement is particularly significant due to real-world instances where seat belts and airbags failed to prevent internal organs from retaining inertia during car crashes, resulting in hemorrhages. Toyota's THUMS 4 enables researchers and engineers to assess the extent of damage to torso regions and internal organs in collisions, providing valuable insights into crash safety and improving safety measures. Whereas version 5 offers the muscle-tendon complexes which were modeled by truss elements with Hill-type muscle material and seat belt elements with tension-only material [55]. The development process of the model is depicted in Figure 3.33. It is worth mentioning that since 2020 the THUMS model has been released as free software accessible for anyone who wants to use it for safety improvement purposes. The newest version offers both: detailed FE models of the organs with the active muscles (Table 3.2).

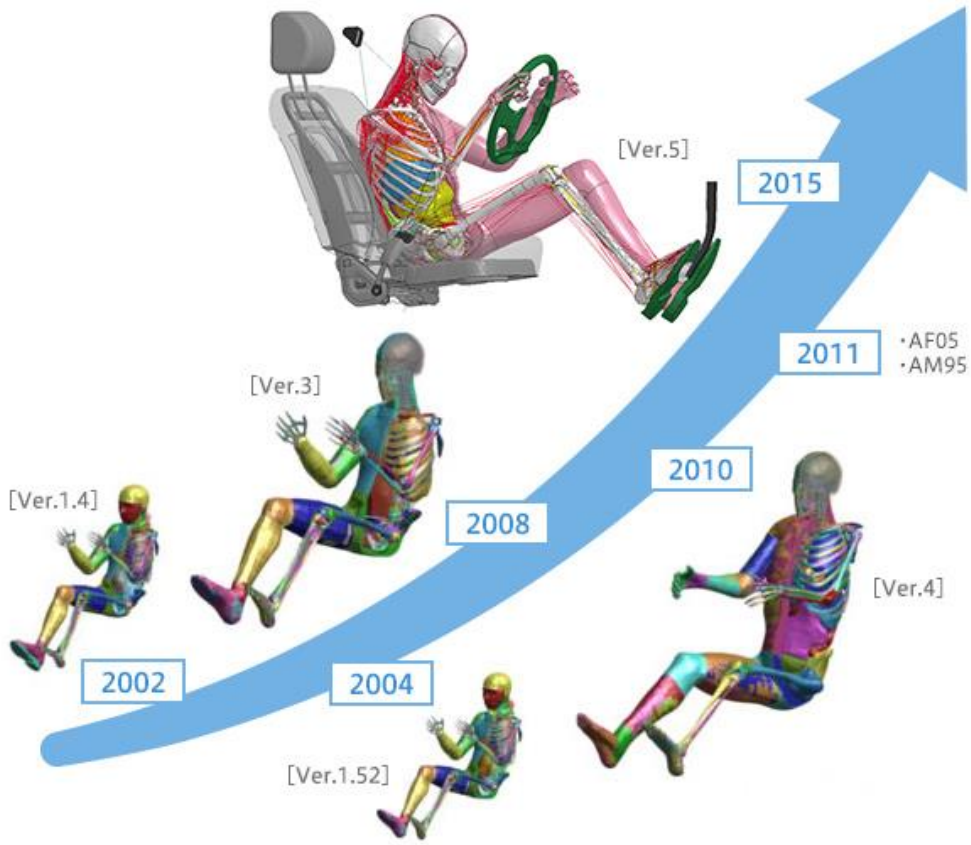

Figure 3.33 THUMS development timeline [56]**.**

Table 3.2 THUMS versions improvements [56]**.**

YEAR	PROGRESS	DETAILS
1997	Toyota begins developing THUMS together with Toyota Central R&D Labs, Inc.	
2000	Version 1 released	Detailed modeling of bones added
2005	Version 2 released	Detailed modeling of faces added
2008	Version 3 released	Detailed modeling of the brain added
2010	Version 4 released	Detailed modeling of internal organs added
2011	A variety of different physiques added to Version 4	Small female, and large male models added
2015	Version 5 released	Modeling of all body muscles added
2016	Child models added to Version 4	Child models aged 3, 6, and 10 years old added
2019	Version 6 released	Modeling of muscles added to modeling of internal organs
2020	Free access will be offered	Current release

The application of the THUMS is not limited to automotive safety. In 2016 W. Wang [57] utilized THUMS 50th percentile model as a surrogate for the train driver which allow him to assess the loading of the driver's chest during an event (Figure 3.34-3.35). The detailed FE HBM in this case allowed not only to evaluate the safety by the injury criteria means but also by direct assessment of the organ deformation (for example chest strain).

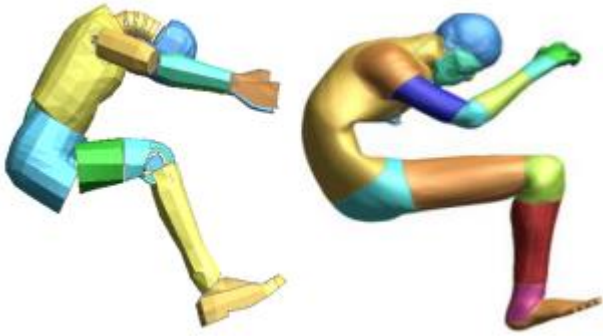

Figure 3.34 THUMS vs HIII numerical model [57]**.**

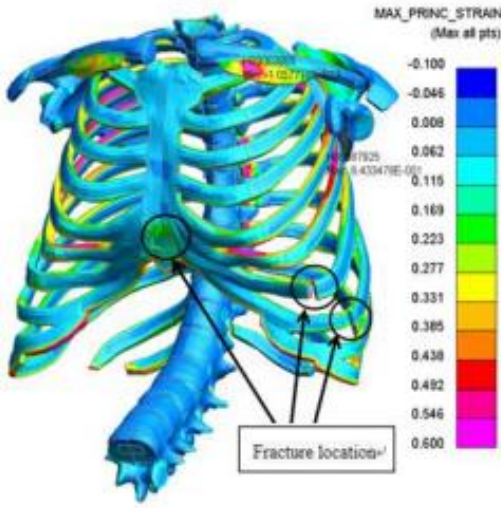

Figure 3.35 Chest assessment during rail event [57]**.**

3.1.4.3 GHBMC

Established in April 2006, the Global Human Body Models Consortium (GHBMC) emerged with the overarching goal of amalgamating global research and developmental endeavors in human body modeling, unifying these initiatives into a cohesive international endeavor aimed at propelling the advancement of crash safety technology. The primary mission of the GHBMC revolves around the creation and maintenance of Finite Element human body models of exceptional fidelity, expressly tailored for employment in automotive crash simulations.

Membership within the GHBMC currently encompasses prominent entities such as General Motors Holdings LLC, Honda R&D Co., Hyundai Motor Co., Nissan Motor Corp. Ltd., Renault S.A., and Stellantis N.V. The National Highway Traffic Safety Administration (NHTSA) holds the position of Sponsor, while Autoliv Inc., Ford Motor Co., and Faurecia SE serve as Participants, contributing substantively to the technical evolution of the consortium's initiatives.

Distinguished by its endeavors, the GHBMC has successfully conceived a comprehensive suite of virtual human models, spanning male and female seated occupants of diverse statures, as well as pedestrians, encompassing even a representation of a six-year-old child. The meticulously designed models and Computer-Aided Design (CAD) constructs developed by the GHBMC are available for licensing purposes. Furthermore, an academic license, provided at no cost, is extended to qualified academic institutions, facilitating broader dissemination and exploration of the consortium's contributions [58].

Figure 3.36 The GHBMC base model (left - organs, middle - muscles and skeletal system, right - soft organs and skeleton).

3.1.5 Summary

Surrogates for the human body encompass a range of tools and methodologies used in biomechanical research to simulate human responses in various scenarios. These surrogates play a crucial role in assessing injury risks, evaluating safety measures, and advancing our understanding of human biomechanics. They include numerical human body models, anthropometric testing devices, volunteer testing, and cadaver testing.

Human Body Models (HBM):

Numerical human body models are computer simulations that replicate the anatomical structure and biomechanical behavior of the human body. These models use computational methods, such as finite element analysis, to predict how tissues, bones, and organs respond to mechanical forces in different situations, like crashes. NHBMs provide insights into injury mechanisms, allow virtual testing of safety systems, and offer cost-effective ways to study a wide range of scenarios.

Anthropometric Testing Devices (ATDs):

ATDs, commonly known as crash test dummies, are physical replicas of the human body used to simulate the response of a human in vehicle crashes. These devices are designed with various sensors to measure forces, accelerations, and deformations during impacts. ATDs provide valuable data for evaluating the effectiveness of safety features like seat belts, airbags, and restraint systems. They come in different sizes and types to represent diverse demographics, such as adults, children, and pedestrians.

Volunteer Testing:

Volunteer testing involves using human volunteers to participate in controlled experiments that replicate real-world scenarios. This approach allows researchers to collect data on human responses to impacts, falls, and other mechanical forces. While volunteer testing provides valuable data on

human behavior and tolerances, it's limited in terms of ethical considerations, sample size, and the range of impact severities that can be tested.

Cadaver Testing:

Cadaver testing involves using post-mortem human bodies to study biomechanical responses under controlled conditions. This method helps researchers understand injury mechanisms, assess injury thresholds, and develop safety measures. Cadaver tests provide insights into the actual physical behavior of human tissues, bones, and organs during impacts. However, ethical concerns, specimen availability, and limitations in reproducing living conditions are challenges associated with cadaver testing.

These surrogate methods collectively contribute to a comprehensive understanding of human biomechanics, injury patterns, and the effectiveness of safety interventions. While each approach has its advantages and limitations, combining data from numerical models, ATDs, volunteer testing, and cadaver tests helps researchers refine safety measures, design more effective vehicles, and develop strategies to mitigate injuries in various scenarios.

Table 3.3 Important properties of human surrogates in injury biomechanics [10]**.**

	ATD	Models (HBM's)	Human volunteers	Cadavers
Human anthropometry	Yes	Yes	Yes	Yes
Human anatomy	Partial	Yes	Yes	Yes
Physiologic response	No	Potential	Yes	No
Testing to injurious Levels	Yes	Yes	No	Yes
Direct Observation of Injury	No	Potential	No	Yes

3.2 Injury metrics

The injury metrics are the quantitative tools to describe the injury of the human body. These tools are designed ad evaluated to be useful for the comparison of the injury between different crash cases. This feature allows accident statisticians to use them in the accident databases, which gives them a way to see the bigger picture of road safety. An example could be the assessment of the helmet enforcement policy introduction: the statistician checks the database cases before and after the date of policy introduction for the head injury metrics; if the number of cases with the head injury dropped it means the policy has some effect on the road safety. The injury metrics could be divided into two types: injury scales and injury criteria, one is used to code the injury of the crash participants in a numerical way, whereas the second correlate the dynamical parameters of the accident with the injury of the part of the road user body.

3.2.1 Injury scales

Injury scales are standardized systems used to assess and classify the severity of injuries sustained by individuals in various types of accidents, such as vehicle crashes, falls, and other traumatic events. These scales provide a consistent and objective way to quantify and communicate the extent of injuries.

3.2.1.1 AIS

One of the most used anatomic scales for traumatic injuries is the AIS. The Society for the Advancement of Automotive Medicine developed the Abbreviated Injury Scale (AIS) to define and explain the severity of injuries. It depicts the injury's threat to life rather than a full assessment of the severity of the damage. The scale was initially published in 1969, with substantial modifications in 1976, 1980, 1985, 1990, 1998, 2005, 2008, and 2015. The score codes three characteristics (type, location, and severity) of the injury using seven numbers inscribed as 12(34) (56).7. The meaning of the number is as follows (1- body region, 2- type of anatomical structure, 3,4- specific anatomical structure, 5,6- level, 7- severity code (depicted on Figure 3.37)) [59].

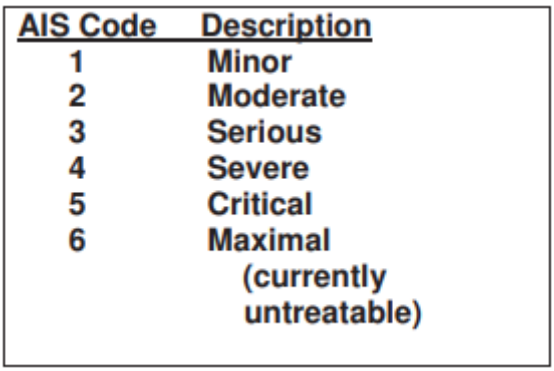

AIS Code	Description
1	Minor
2	Moderate
3	Serious
4	Severe
5	Critical
6	Maximal (currently untreatable)

Figure 3.37. The general format of AIS severity coding [59]**.**

Easily it can by defined by one phrase: “The AIS is an anatomically-based, consensus-derived, global severity scoring system that classifies each injury by body region according to its relative importance on a 6- 6-point ordinal scale.” [59] [60].

3.2.1.2 ISS

A different situation appears when the patient has multiple injuries and for some reason (for example statistical, archiving, etc.) his case needs to have assigned one injury level. One easy solution to this problem could be just using the Maximum AIS number, but such a shortcut does not give a wider view of the case. Fortunately, in 1974 one metric that solves this problem was developed. It is called the Injury Severity Score (ISS), and over the years it has been adopted as the most widely used scoring system in trauma literature. The ISS can characterize the trauma of a patient with multiple injuries of multiple body parts by just one number. The input for the formula is the three highest injuries by body region described in the AIS scale:

$$ISS = \left(AIS_{bodyregion\ A}\right)^2 + \left(AIS_{bodyregion\ B}\right)^2 + \left(AIS_{bodyregion\ C}\right)^2, \quad (3.2)$$

where: A, consists of the head, neck, and face; B, the thorax and abdomen, and C, the extremities.

Table 3.4. example calculation of ISS based on AIS codes [61]**.**

ISS Body Region*	Injury	AIS Code	Highest AIS	AIS²
HEAD/NECK	Cerebral contusion NFS	140602	4	16
	Internal carotid artery transection (neck)	320212		
FACE	Closed fractured nose	251000	1	
CHEST	Rib fractures on left side, ribs 3 – 4	450202	2	
ABDOMEN	Retroperitoneal Hematoma	543800	2	4
EXTREMITIES	Fractured femur (NFS)	853000	3	9
EXTERNAL	Abrasions (NFS)	910200	1	
				ISS = 29

It can be seen based on Table 3.4., that the maximum score of ISS cannot exceed 75 (three regions with an AIS of 5). An additional constraint is that: any AIS6 (unsurvivable) makes the maximum ISS of 75 [62].

3.2.2 Injury Criteria

3.2.2.1 Injury criteria for the head

The Head Injury Criterion (HIC) criterion is often referred in the literature as the evolution of the Wane State Tolerance Curve [63]. This initial segment of the WSTC (Figure 3.38) curve (2 < t < 6 ms) was deduced from cadaver experiments, focusing on skull fracture as the basis for injury assessment. The intermediate pulse durations (6 < t < 10 ms) were informed by cadaver tests utilizing intracranial pressure as the injury indicator, as well as animal tests using concussion as the injury parameter. The extended portion of the curve (t > 10 ms) was established through volunteer trials. The Head Injury Criterion has its origins in the work of Gadd, who developed the so-called severity index using the WSTC (SI) [64]. Versace (1971) presented a version of the HIC as an average acceleration metric that corresponds with the WSTC in 1971. The US National Highway Traffic Safety Agency (NHTSA) then recommended the current form of HIC, which is incorporated in FMVSS 208. HIC is calculated using the following formula:

$$HIC = max\left[\frac{1}{t_2 - t_1}\int_{t_1}^{t_2} a(t)dt\right]^{2.5} (t_2 - t_1), \quad (3.3)$$

t_2 and t_1 can be any two arbitrary time points throughout the acceleration pulse. Time is recorded in seconds and acceleration is measured in multiples of gravity's acceleration [g]. For the computation, the resulting acceleration is employed. FMVSS 208 mandates t2 and t1 to be no more than 36 ms apart (referred to as HIC36), with the maximum HIC36 not exceeding 1000 for the 50th percentile. NHTSA also developed the HIC15 in 1998, which is the HIC assessed over a maximum time interval of 15 ms [65].

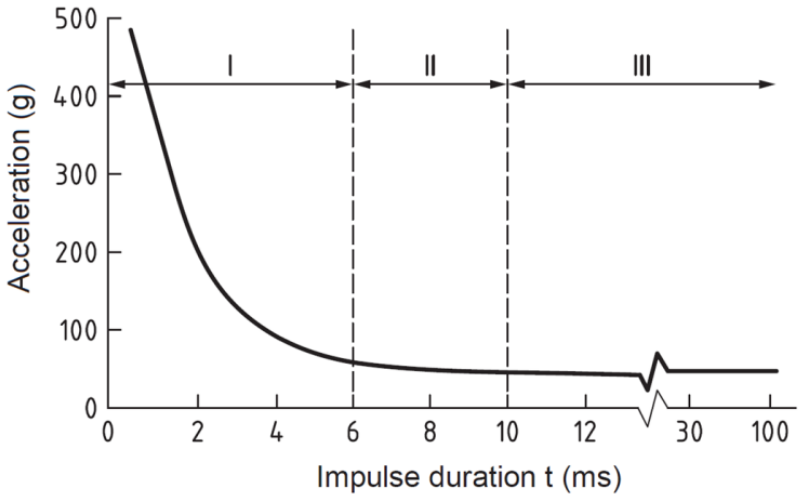

Figure 3.38 Wayne State Tolerance Curve [63]**.**

A maximum of 700 was indicated for the 50th percentile man for the corresponding threshold value. The above-mentioned threshold is valid for the full-scale frontal crash test of motor vehicle, for the case of motorcycle helmet testing the HIC should not exceed the value of 2400 according to the ECE 22.05 for the impact with the higher velocity: 7.5 m/s [66]. Besides the most established HIC criterion in the literature, we can find at least another nine head/ brain injury criteria with different definitions and a wide range of applications (GAMBIT [67], HIP [68], WPCS [69], PRHIC [70], RIC [70], BRIC [71], BrIC [72], BITS [73] and RVCI [74] - Table 3.5).

Table 3.5 List of advanced head/bran criteria.

Criterion	Equation	Missing parameter
GAMBIT	$GAMBIT = \left[\left(\frac{a(t)}{a_c}\right)^n + \left(\frac{\alpha(t)^m}{\alpha_c}\right)\right]^{\frac{1}{k}}$	- unknown critical values - no duration - no direction dependency
HIP	$HIP = \sum m a_i \int a_i\, dt + \sum I_{ii} \cdot \alpha \cdot \int \alpha_i\, dt$	- missing I_{ij} - no direction sensitivity for a
WPCS	$PCS = 10 \cdot ((0.4718 \cdot sGSI + 0.4742 \cdot sHIC + 0.4336 \cdot sLin + 0.2164 \cdot sROT) + 2)$	- no physical model - no time history for rotation

PRHIC	$PRHIC = (t_2 - t_1) \cdot max\left[\frac{1}{(t_2 - t_1)}\int_{t_1}^{t_2} HIP_{rot}dt\right]^{2.5}$	- missing I_{ij}
RIC	$RIC = (t_2 - t_1) \cdot max\left[\frac{1}{(t_2 - t_1)}\int_{t_1}^{t_2} \alpha(t)dt\right]^{2.5}$	- No direction-sensitivity
BRIC	$BRIC = \frac{\omega_{max}}{\omega_{cr}} + \frac{\alpha_{max}}{\alpha_{cr}}$	- no duration - no direction dependency - no linear accelerations
BrIC	$BrIC = \sqrt{\left(\frac{\omega_x}{\omega_{xC}}\right)^2 + \left(\frac{\omega_y}{\omega_{yC}}\right)^2 + \left(\frac{\omega_z}{\omega_{zC}}\right)^2}$	- no duration - no linear accelerations - impact duration not considered
BITS (Brain Injury Threshold Surface)	$BITS = \left(\frac{\omega_{max}}{\omega_{cr}}\right)^2 + \left(\frac{\alpha_{max}}{\alpha_{cr}}\right)^2 - \left(\frac{\Delta t_{crit}}{\Delta t}\right)^2$	- no direction dependency - cannot be applied for humans now
RVCI (Rotational Velocity Change Index)	$RVCI = R_x\left(\int_{t_1}^{t_2}\alpha_x dt\right)^2 + R_y\left(\int_{t_1}^{t_2}\alpha_x dt\right)^2 + R_z\left(\int_{t_1}^{t_2}\alpha_x dt\right)^2$	- no linear accelerations - determination of Δt

The evaluation of the head and brain injury criterion should be done with a view on the entire head motion and possible interactions with other objects (ground, helmet, and vehicle interior). An example of such evaluation is depicted in Figure 3.39. We can imagine a fast-moving head hitting something that's not moving. The front of the head is at the top of each picture. When the back of the skull hits and moves downward (shown by the big arrow), it makes the skull temporarily change its shape (small arrows; A). But then, the skull stops quickly (in less than a second, about 50 milliseconds). The brain, though, still has momentum and wants to keep moving, so it moves relative to the skull (B). This brain movement creates pressure where the hit happened (we call it "coup") and opposite that point, there's lower pressure (we call it "counter-coup") (C). The hatched areas in the front of the skull show where the brain moved away from the skull [75]. In this case, the criterion which takes into account just the linear accelerations could be sufficient for the scull injury evaluation.

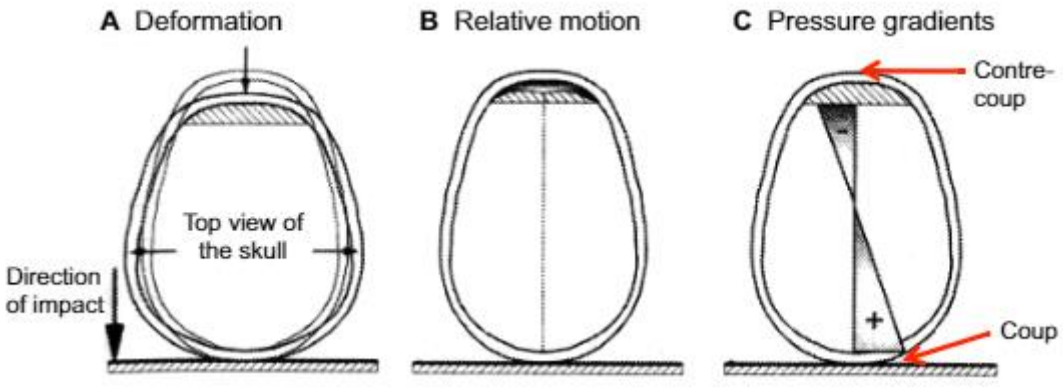

Figure 3.39 Deformation types of scull and brain in case of the impact [76]**.**

3.2.2.2 Injury criteria for the neck

When the **Nij** criterion was created, crash test data from dummies were analyzed along with its importance. In these tests, a standard 6-axis upper neck load cell recorded the forces and moments in all three directions at the top of the neck when the dummy experienced a certain force. In frontal crashes, the main movements and measured neck reactions occur in the up-and-down plane. Other sideways movements and reactions are usually not as important. Because of this, only the measurements related to the up-and-down movement are used for the current Nij neck injury criteria. These measurements include the force along the neck (Fz) and the bending force that makes the neck bend forward or backward at the base of the skull (My). The sideways force (Fx) is only used to figure out the effective bending force at the base of the skull. To do this, the sideways force is multiplied by how far the load cell is from the base of the skull and then subtracted from the up-and-down twisting force recorded by the load cell, following the rules set by SAE [77].

$$N_{ij} = \frac{F_Z}{F_{int}} + \frac{M_y}{M_{int}}, \tag{3.4}$$

Boström et al. in 1996 [78] introduced the neck injury criterion **NIC** by assuming that abrupt changes in fluid flow within the fluid compartments of the cervical spine are connected to neck injuries. To define NIC over time, they validated it through experiments on animals. They established a relationship (Equation 3.5) that predicts injuries due to pressure gradients. This relationship connects the acceleration in the front-back direction (referred to as the x-direction when using SAE J211/2) of the head's center of gravity in relation to the first thoracic vertebra (T1) with the resulting velocity:

$$NIC = 0.2a_{rel}(t) + v_{rel}(t)^2, \tag{3.5}$$

The established threshold value indicating a considerable likelihood of experiencing minor (AIS1) neck injury was determined as 15 m^2/s^2. This value has proven effective in accident analysis and remains in use. Nonetheless, it has become evident that accurate values are only applicable during the retraction phase of a rear-end collision, wherein both acceleration and velocity are directed backward within a fixed vehicle reference system [76].

The Lower Neck Load Index (**LNL)** serves as an assessment tool for the potential risk of neck injury, relying on the load experienced by the T1 thoracic vertebra. This indicator is particularly responsive to the safety seat's design factors and aligns with the facet joint injury mechanism endorsed by Yoganandan [79]. The formula for its calculation is as follows:

$$LNL(t) = \left|\frac{\sqrt{(My_{lower}(t))^2+(Mx_{lower}(t))^2}}{C_{moment}}\right| + \left|\frac{\sqrt{(Fy_{lower}(t))^2+(FX_{lower}(t))^2}}{C_{shear}}\right| + \left|\frac{Fz_{lowet}(t)}{C_{tension}}\right|, \tag{3.6}$$

where Fi(t) and Mi(t) are the force and moment components, respectively.

The $\mathbf{N_{km}}$ metric was introduced by Schmitt [80]. It is derived from a linear combination of shear forces occurring in the sagittal plane and extension/flexion bending moments, both recorded at the occipital condyles. This methodology is akin to the formulation of the Nij criterion used for frontal impact assessment, making the newly introduced N_{km} a variation of the prior approach. The N_{km} criterion is expressed by the following equation:

$$N_{km}(t) = \frac{F_X(t)}{F_{int}} + \frac{M_y(t)}{M_{int}}. \quad (3.7)$$

In this equation, $F_x(t)$ and $M_y(t)$ stand for the shear force and flexion/extension bending moment, respectively. These measurements are acquired from the upper neck's load cell. F_{int} and M_{int} are the critical intercept values utilized for normalization purposes.

The **UNE 135900** [81, 82] requirements are not in line with the direct definition of injury criterion, however, in the context of motorcyclist protection they could be treated as so. Besides the intercept value of the HIC, the protocol defines the intercept values for the neck forces and moments (Table 3.6). Acceptable ATD response for the neck shear, tension, and compression must remain under the solid lines. The blue line corresponds to Level I certification; the orange line to Level II (Figure 3.4-3.42).

Table 3.6 UNE 135900/2008 intercept values.

Body region	Parameter	Severity Level	Limit
Head	HIC_{36}	I	650
		II	1000
Neck			
	Neck Shear	I	Figure 3.40
		II	
	Neck Tension	I	Figure 3.41
		II	
	Neck Compression	I	Figure 3.42
		II	
	Neck Lateral Flexion	I	134 Nm
		II	134 Nm
	Neck Extension	I	42 Nm
		II	57 Nm
	Neck Flexion	I	190 Nm
		II	190 Nm

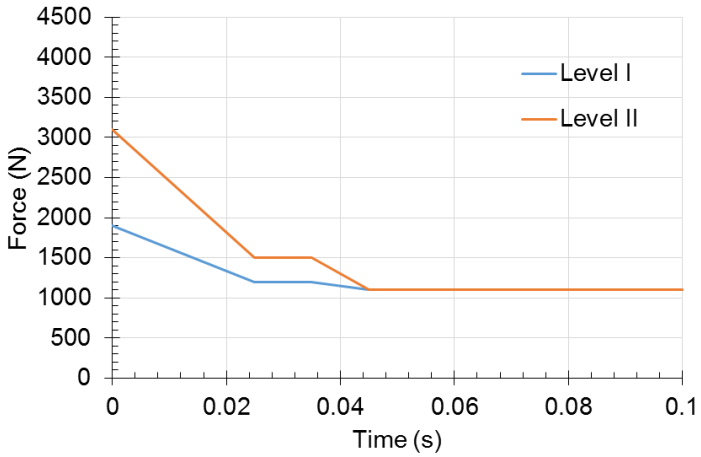

Figure 3.40 Neck shear force vs. Time risk curve [82]**.**

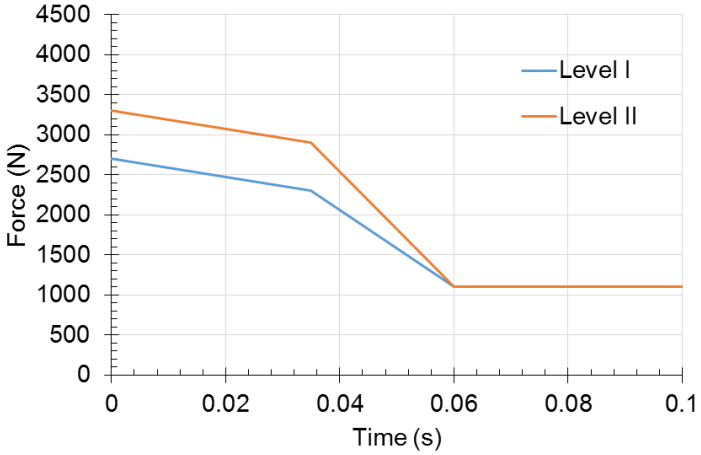

Figure 3.41 - Neck axial tension force vs. Time risk curve [82]**.**

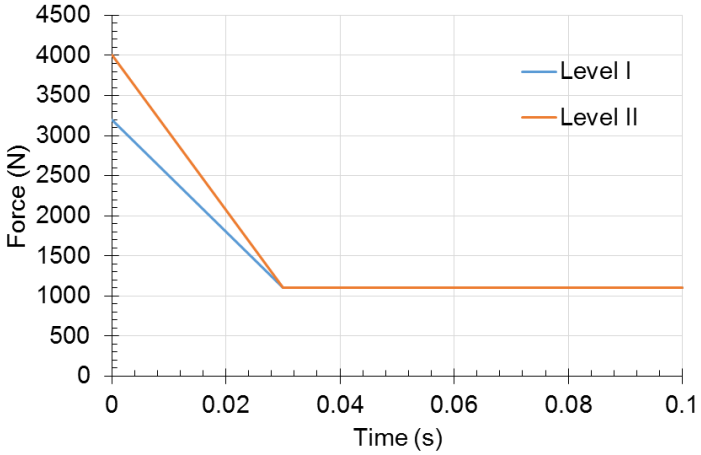

Figure 3.42 Neck compression force vs. Time risk curve [82]**.**

3.2.2.3 Injury criteria for the extremities

Lower extremity injuries in motorcycle accidents are a significant concern, often involving the legs and feet. These injuries can range from fractures and dislocations to soft tissue damage. Common lower extremity injuries include tibia and fibula fractures, ankle fractures, knee injuries, and foot injuries. These injuries can occur due to direct impact, crushing, or twisting forces during collisions. Protective gear such as sturdy boots and pants with reinforced padding can help reduce the severity of these injuries. The injury criteria for the extremities have been designed to help with the assessment of these body parts.

Compression Force of the femur is one of the basic criterion accepted by the FMVSS 208. This standard states that to protect the hip-thigh-knee complex the loading in the longitudinal axis of the femur should not exceed 10 kN.

A similar threshold but for the tibia (**TCFC**) is defined by the UN R94 [83], where the European standard states that "the force axially transmitted to each tibia of a test dummy" should not go beyond 8 kN.

In the UN R94, the femur safety assessment criterion is a little more complicated and defined as the Femur Force Criterion (**FFC**). In this case the criterion not only checks the compression force working on the femur but also the duration (as depicted in Figure 3.43).

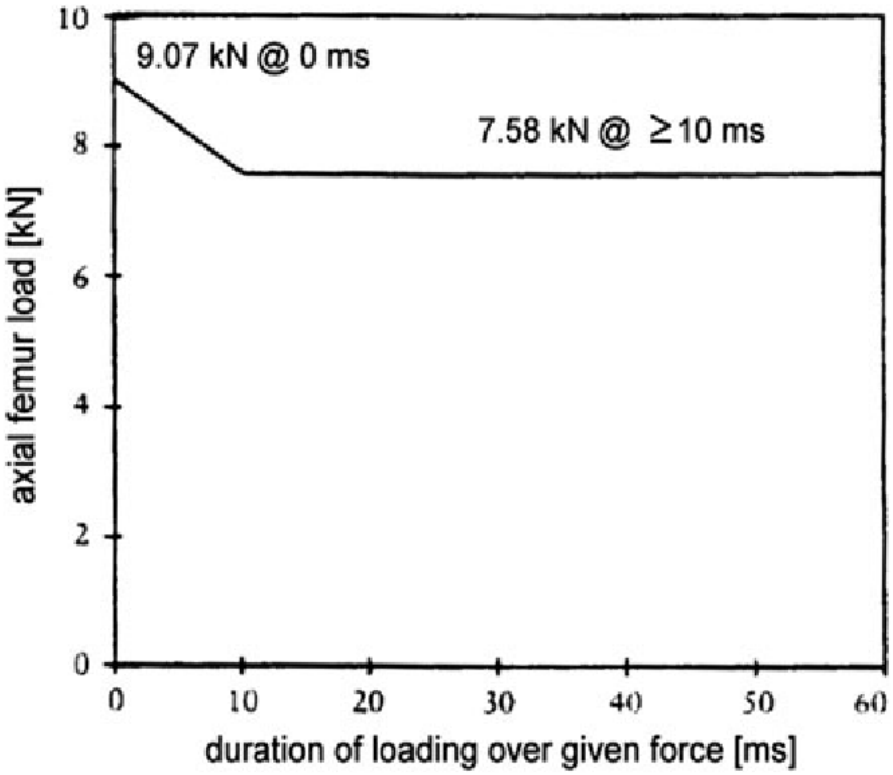

Figure 3.43 The FFC threshold definition in UN R94 [83]**.**

The Tibia Index (**TI**) encompasses both bending moments and axial force acting on the tibia. The fundamental concept of the TI is to mitigate tibia shaft fractures. The calculation of the TI is defined by the following equation:

$$TI = \left|\frac{\sqrt{(Mx)^2+(My)^2}}{(Mc)_r}\right| + \left|\frac{Fz}{(Fc)_z}\right|, \quad (3.8)$$

where Mx and My are the bending moments at the tibia ends, and the Fz is the compressive force. The critical values (Mc and Fc) are different for specific percentiles of the HIII dummy and can be seen in Table 3.7.

Table 3.7 The TI critical values for HIII anthropometries [84]**.**

Dummy Type	***Mc*: Critical Bending Moment (Nm)**	***Fc*: Critical Compression Force (N)**
Hybrid III 5th percentile female	307	44.2
Hybrid III 50th percentile male	225	35.9
Hybrid III 95th percentile male	115	22.9

3.3 Virthuman

The Virthuman model [85] which is a scalable hybrid human body model has been developed over the years by the team of researchers gathered around L. Hynčík. The main idea which was standing behind the creation of this HBM was the possibility to easily scale and position the model without losing the outer biofidellity. It was possible by building up the model from scratch with the MBS structure supported by the fine-tuned system of springs and dumpers which connects the outer so-called super-elements with the non-deformable MBS skeleton. The first attempts that resulted in a working scaling algorithm could be dated back to 2007 [86]. Whereas the name Virthuman first time appears in the year 2012 with the presentation of a working and partially validated (against the Kroell chest deflection corridors) model [87]. This stage of model development couldn't be done without the cooperation with the MECAS ESI s.r.o, Plzen, the Czech branch of ESI Corporation (currently ESI Eastern Europe), and the financial support from the Technology Agency of the Czech Republic (grant number TA01031628). The next step of the model improvement was to extend its validity for different body parts by performing the extended biofidellity tuning and validation against the experimental tests. This stage of development was in its current state in 2014 by publishing the SAE Tech paper [88]. Meanwhile, the scaling algorithm has also reached its adulthood and was presented to a wider audience at the SAE World Congress in 2013 [89]. The improvements of the Virthuman biofidellity and its application (as pedestrian [90, 91], pedestrian impacted by tram [92], autonomous car occupant [93], and finally motorcycle driver [94]). It is worth mentioning that the Virthuman was even used for the evaluation of possible death scenarios of J. Masaryk [95].

3.3.1 Geometry

The selection of reference surface geometry is based on the European CAESAR database. The CAESAR database aimed to update and broaden the existing body measurement database by gathering new body measurements from approximately 2,500 individuals in the United States and 2,500 in Europe. These individuals encompassed diverse weight categories and included both males and females within the age range of 18 to 65. The collected data was carefully analyzed and presented in a format that proved valuable to scientists and engineers worldwide [96]. It allows to close match the body dimensions of Hybrid III 50% and EuroSID II ATDs [87].

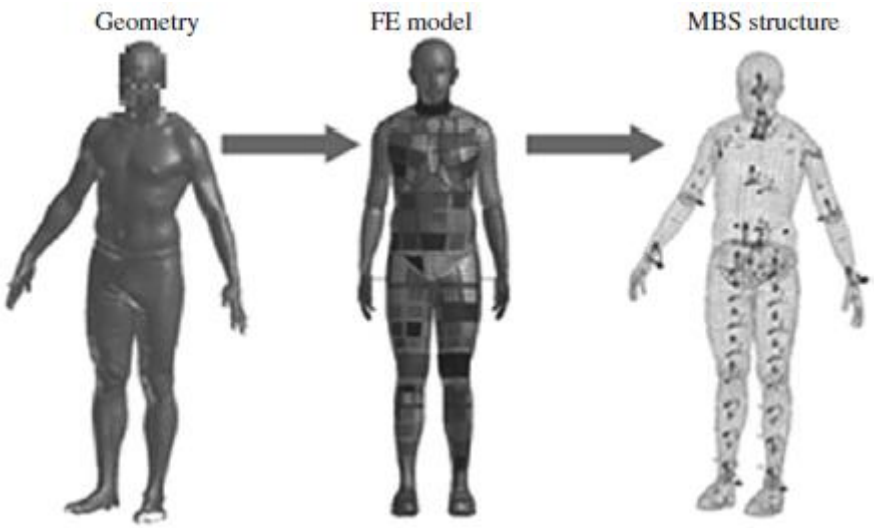

Figure 3.44. The Virthuman geometry creation process [87]**.**

3.3.2 Structure

The entire model was constructed using the Multi-Body System (MBS) approach. The MBS method offers notable advantages, such as reducing computation time and accommodating the deformation of individual components [97, 98]. MBS employs rigid bodies linked by specific types of joints or springs and dumpers.

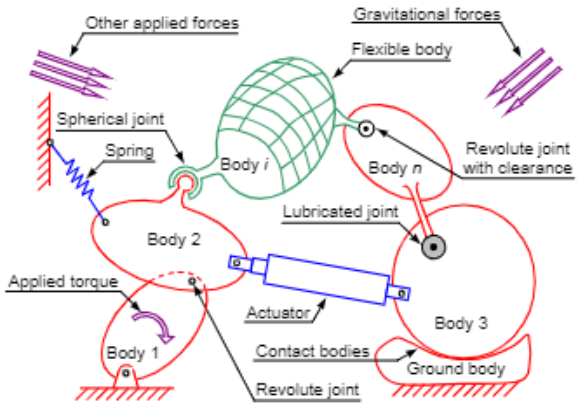

Figure 3.45 The MBS system open tree concept [99]**.**

This structure follows an open tree arrangement (depicted in Figure 3.45), commencing from the base body. The external shape was meshed utilizing a specialized approach (depicted in Figure 3.46), considering that the model can be positioned in various configurations, such as a seated position for frontal or side crash tests, a standing position for pedestrian tests, or other general orientations. Specific segments of the Virthuman model were developed with attention to incorporating sensors and complying with measured injury criteria, aligning with methodologies commonly used in the automotive industry. These properties of the Virthuman are especially useful for PTW-related scenarios, where the positioning of the model itself for the FEM models (THUMS, GHBMC) could be a demanding task.

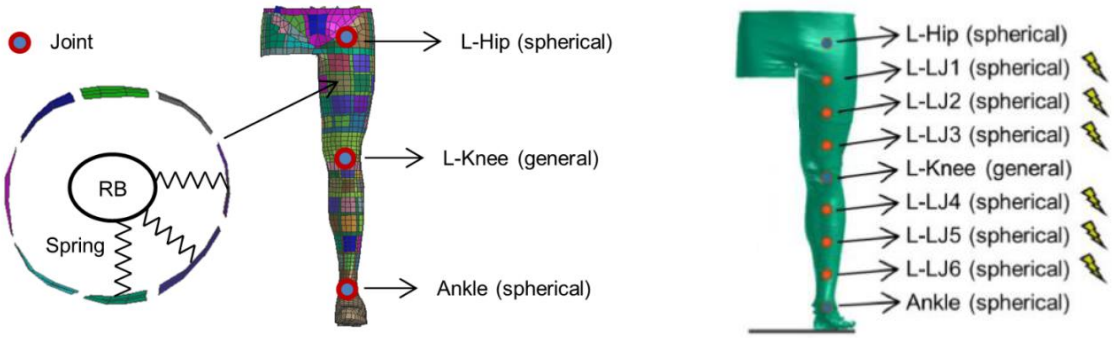

Figure 3.46 The structure of the Virthuman model [89]**.**

3.3.3 Scaling

The scaling algorithm, developed by L. Hynčík [89], operates on height and age parameters for body dimensions. Specifically, given a certain age, the corresponding height percentile is selected, determining the required set of measurements. Notably, age influences body flexibility. While the CAESAR database was used to establish the reference model size, the scaling algorithm draws from Bláha's measurements [100], supplemented by additional data. This compilation forms a distinctive database due to its comprehensive measurements from a significant number of individuals, statistically analyzed across different age groups. The database encompasses age-related percentiles linked to anthropometric dimensions for all major body segments, delineated by distinct landmarks.

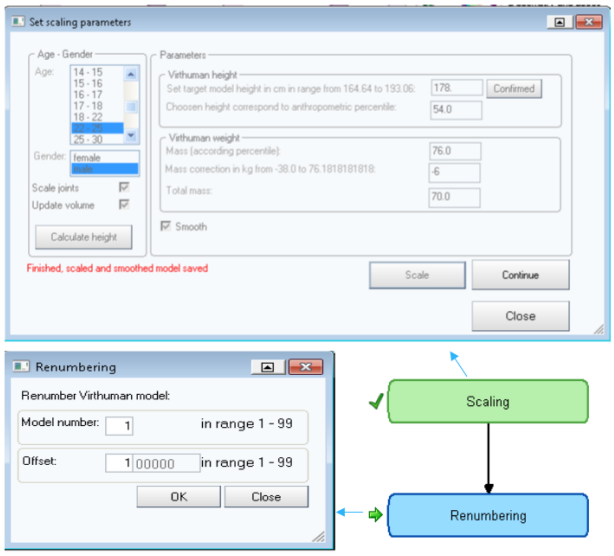

Figure 3.47 Implementation of the VH scaling algorithm in the VPS add-on [101]**.**

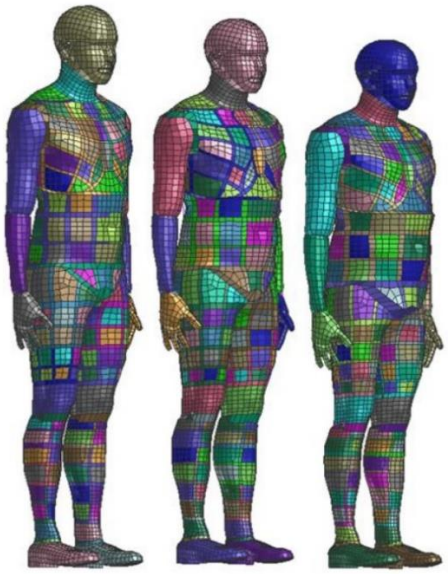

Figure 3.48 Models generated by the scaling tool [101]**.**

3.3.4 Injury assessment

Injury values within the models exhibit variations based on age. Notably, injuries tend to be more pronounced in children as compared to adults under identical load conditions. Consequently, the depiction of injury contours is segmented into distinct age categories, primarily encompassing 6 years, 20 years (Table 3.8), and 100 years. For intermediate age groups, values are derived through linear interpolation. Evaluation of injury severity involves a color-coded scheme classified into four fundamental levels (depicted in Figure 3.49). The color spectrum is stratified as follows: green signifies either no injury or a minor degree of injury, yellow indicates an acceptable level of injury, orange denotes a marginal degree of injury, and red signifies injuries that are either fatal or gravely serious. Besides this simple assessment, a detailed evaluation by analyzing the time series of the loads is possible [102].

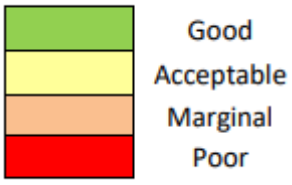

Figure 3.49 Color coding for different thresholds [102]**.**

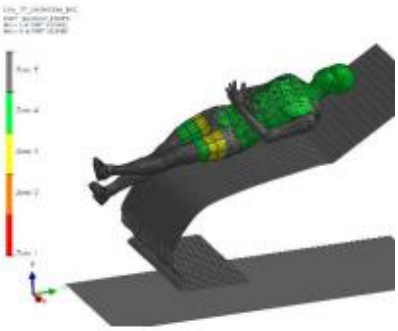

Figure 3.50 Example of injury of simple color injury evaluation [102]**.**

Table 3.8 Virthuman injury criteria color coding for age category 20 years [102]**.**

	Criterion	20Y Injury Criteria			
		<	<	>=	>=
Head	HIC36	650	825	825	1000
Neck	Upper neck MY EXTENSION [Nm]	-42	-49.5	-49.5	-57
	Upper neck MY FLEXION [Nm]	88	139	139	190
	Upper neck FZ TENSION [kN]	2.7	3	3	3.3
	Upper neck FZ COMPRESSION [kN]	-2.7	-3.35	-3.35	-4
	Upper neck SHEAR [kN]	1.9	2.5	2.5	3.1
Thorax	Front DEFLECTION [mm]	22	36	36	50
	Front VC [m/s]	0.5	0.75	0.75	1
	Side DEFLECTION [mm]	22	32	32	42
	Side VC [m/s]	0.32	0.66	0.66	1
Abdomen	Compression FORCE [kN]	1	1.75	1.75	2,5
Pelvis	Pubic FORCE [kN]	3	4,5	4.5	6
Legs	Femur compression FORCE [kN]	3.8	6.435	6.435	9.07
	Femur MOMENT [Nm]	300	340	340	380
	Knee MOMENTS [Nm]	100	120	120	140
	Tibia compression FORCE [kN]	2	5	5	8
	Tibia MOMENT [Nm]	200	240	240	280

The Virthuman lower extremities are equipped with 12 breakable joints (Figure 3.52). The following naming convention is used to identify these joints:

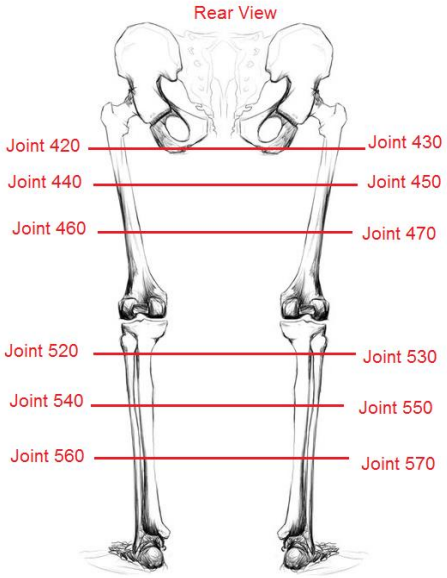

Figure 3.51 Breakable joints naming convention[2].

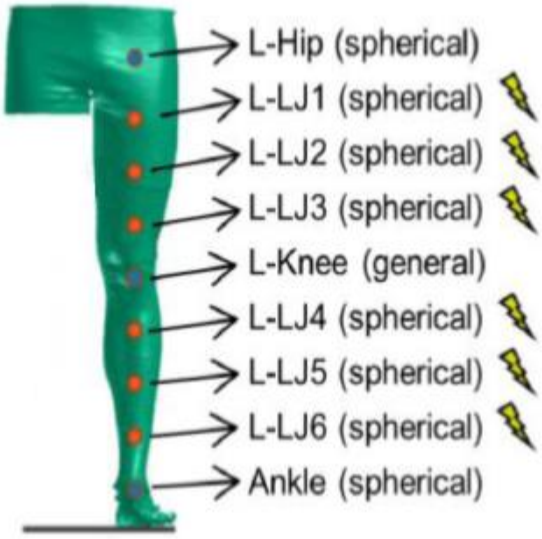

Figure 3.52 Breakable VH leg joints [101]**.**

[2] Image adapted from http://hippie.nu/~nocte/tutorial-currentchapter/img/basics/humananatomy/leg-bones.jpeg

3.3.5 Sliding simulation

As reported by the MAIDS study [8], single-vehicle accidents constitute approximately 16% of the overall motorcycle crash incidents. Among these, the "low side" scenario stands out as a particular type of single motorcycle accident characterized by a loss of traction. Particularly at elevated speeds, this form of accident can lead to the rider being forcefully ejected from the seat. It is essential to note that during such low-side events, the only safeguard shielding the rider's body against the abrasive forces of the road is appropriate protective attire. Thus, the significance of wearing proper protective clothing cannot be overstated as it offers a critical layer of defense in mitigating potential injuries [103].

3.3.5.1 Real accident and simulation setup

The instance involving the sliding of a motorcycle rider transpired during a riveting Moto GP racing event in the year 2011, which unfolded on the iconic TT Circuit Assen. It was on the 17th turn of the circuit that Karel Abraham, the skilled Czech rider, found himself sliding along the asphalt surface following a low-side crash incident (depicted in Figure 3.53). This particular occurrence served as a pivotal case study for the research team, affording them a prime opportunity to develop a high-speed low-side accident simulation. The foremost objective of this simulation endeavor was to derive accurate and lifelike estimations of the contact forces that manifest between the rider's body and the road surface during such events. By closely examining this real-world occurrence and effectively translating it into a simulated scenario, the research team aimed to capture the intricate dynamics and physical interactions that unfold in these types of high-speed sliding accidents.

Figure 3.53. The image[3] of the first contact of the rider's body with the ground, and the numerical representation.

[3] Provided by PSi Hubík, s.r.o., Daimlerova 3, 301 00 Plzeň, Czech Republic

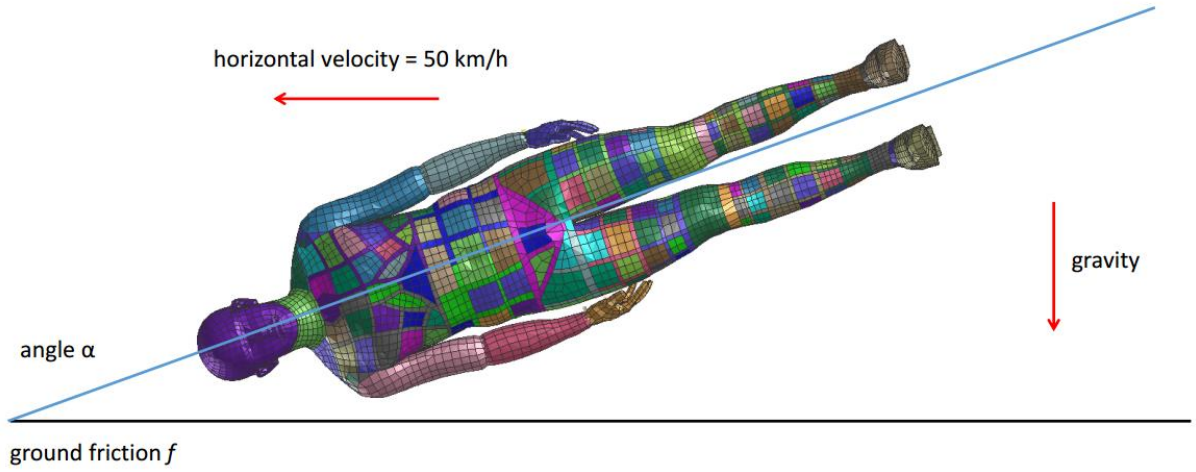

Figure 3.54 Sliding setup simplification.

To assess the genuine human body response during the accident scenario, the author employed the VPS Explicit Virthuman model, meticulously tailored to match Karel Abraham's body mass and dimensions by the Virthuman scaling algorithm. In light of the unavailability of experimental data concerning the friction coefficient, a thorough sensitivity analysis was conducted. The positioning of the Virthuman model closely followed the configuration illustrated in Figure 3.52. Our simulation was executed nine times, encompassing three distinct values of the friction coefficient (f. = 0.1, 0.5, and 0.9) combined with three varying alpha angles. Each of the alpha angles corresponded to a distinct scenario of initial contact points: 110° representing the shoulder impact first, 115° signifying simultaneous head and shoulder impact, and 135° indicating the head impact as the initial contact.

3.3.5.2 Sliding simulation results

Throughout the simulation, two primary parameters were meticulously observed and recorded as outputs: the head injury criteria and the contact force experienced by the right arm. The computed head injury criteria exhibited a variation spanning from 710 to 14,417 (Table 3.9), encompassing the lowest value for a f of 0.1 and an angle of 135°, and the highest for an f of 0.9 and an angle of 110°. In tandem, the contact force exerted on the right arm exhibited a range of 2 to 4.2 kN (depicted in Figure 3.55). Notably, it's important to acknowledge the limitation of this study, which pertains to the absence of a helmet model integrated with the motorcycle rider. In light of this, future work was planned to address this limitation by incorporating a comprehensive helmet model into the simulation framework. Furthermore, the investigation brought to light a significant observation regarding the behavior of the model's neck when subjected to a direct impact of the head against the ground. This realization underscored the need for improvements in this specific aspect of the model to ensure a more accurate and biofidelic response.

Table 3.9 The HIC dependency on f. and alpha.

	alpha [deg.]		
f [-]	135	115	110
0.1	**HIC15 = 710** t_1 = 273; t_2 = 279	**HIC15 = 1 738** t_1 = 346; t_2 = 348	**HIC15 = 3 189** t_1 = 364; t_2 = 366
0.5	**HIC15 = 2 514** t_1 = 273; t_2 = 280	**HIC15 = 3308** t_1 = 346; t_2 = 351	**HIC15 = 3 030** t_1 = 364; t_2 = 366
0.9	**HIC15 = 5 425** t_1 = 273; t_2 = 278	**HIC15 = 5425** t_1 = 273; t_2 = 278	**HIC15= 14 417** t_1 = 364; t_2 = 369

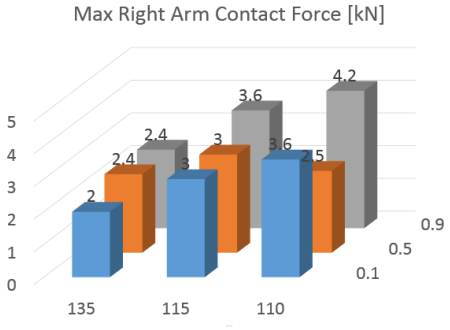

Figure 3.55 Right arm contact force [kN].

3.3.6 Improvements of VH

In the context of PTW impact scenarios, the head, neck, and extremities are subjected to intricate multi-directional forces. This arises from the body's near-unrestricted motion in space due to inertia. This section outlines the efforts aimed at refining the model to better accommodate pedestrian testing, involving updates to the neck and shoulder components specifically tailored for PTW riders.

3.3.6.1 Neck improvement for direct impacts

The Virthuman neck model comprises seven vertebrae connected by six joints, with an additional two joints facilitating the connection between the neck and the head, as well as the torso. These joints possess six degrees of freedom, each characterized by nonlinear stiffness and damping attributes. The endeavor to achieve authentic and biologically faithful kinematics of the head-neck complex led the author to establish a range of motion (ROM) for individual joints based on physiological data [94]. The problem of the neck non-biofidelic behavior was found by the author during his first attempts to establish the working simulation [104]. We could call it “0”-iteration of the framework, where the Virthuman positioned in the driving position (without any other model) was impacting the rigid wall (Figure 3.56).

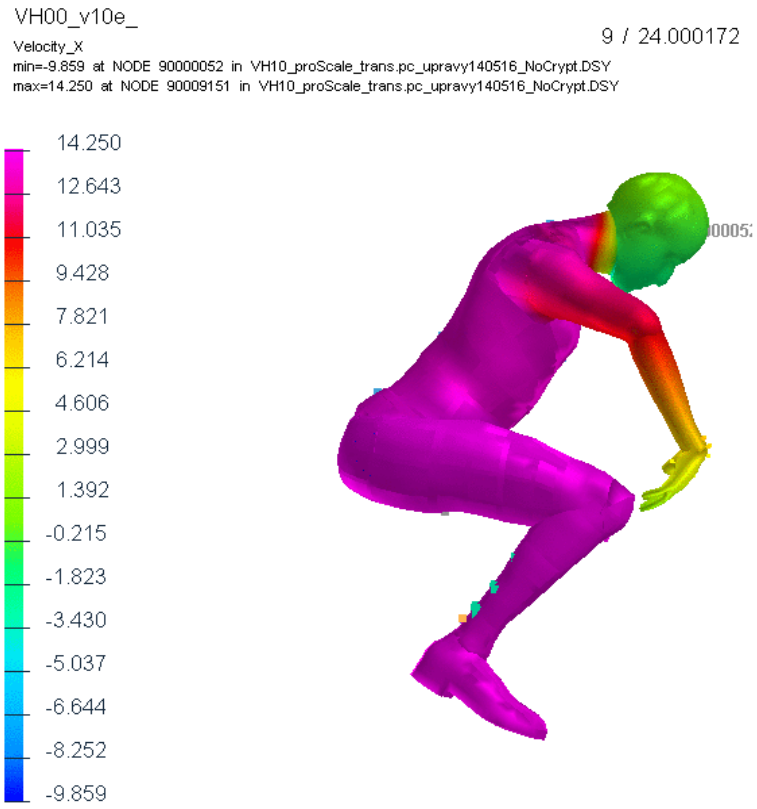

Figure 3.56 Iteration "0" framework - neck problem in direct impact identified.

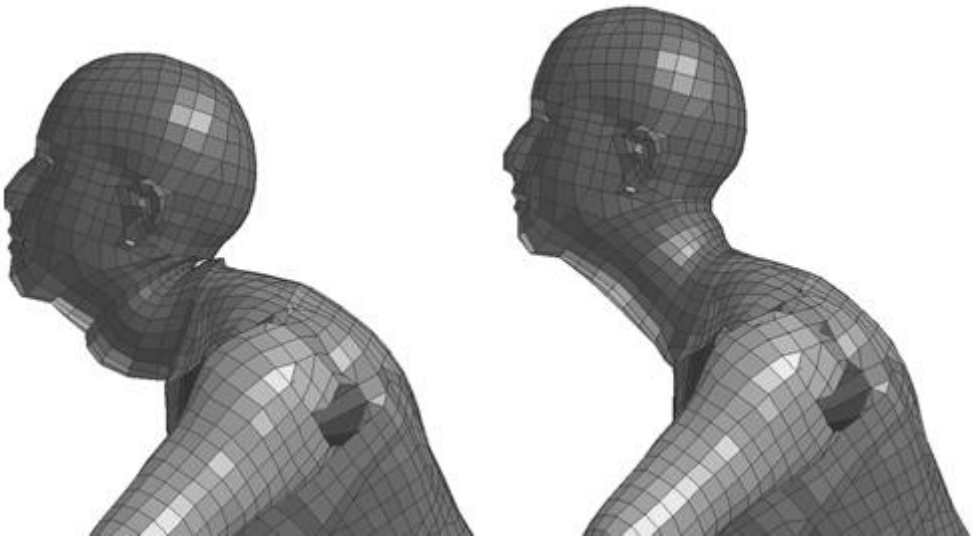

Figure 3.57. The behavior of the neck during direct 50km/h impact to rigid wall (left: original neck, right: improved neck).

Given that scenarios involving VRUs, such as collisions between pedestrians and vehicles or the PTWs accidents, often entail substantial neck deformations, the stiffness parameters of specific joints around their ROM were adjusted. Importantly, these adjustments were carefully made without compromising the validation against 15 g frontal and 7 g lateral sled tests. The validation process

centers on sled tests, wherein the head and neck are isolated from the model, encompassing all neck vertebrae and even the first thoracic vertebra, T1. These isolated components are subjected to a frontal load of 15 g and a lateral load of 7 g.

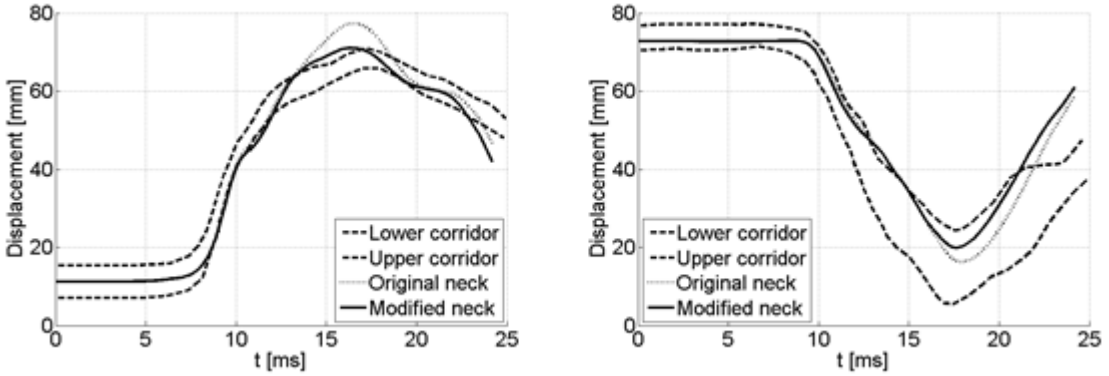

Figure 3.58 Head movement observed during the 15 g frontal impact test (left: in the frontal direction, right: in the vertical direction).

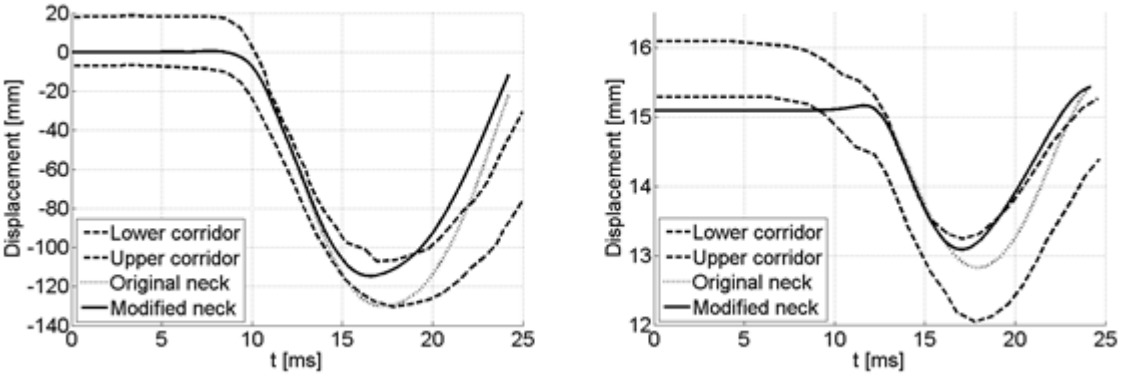

Figure 3.59 Head movement observed during the 7 g lateral impact test (left: in the lateral direction, right: in the vertical direction).

The model featuring the enhanced range of motion (ROM) in the neck joints demonstrates accurate biofidelic behavior. While the improved neck model's kinematic behavior is depicted in Figure 3.57 during the frontal rigid wall impact at 50 km/h, its responses to both 7 g and 15 g impacts remain within acceptable limits, as illustrated in Figure 3.58 and Figure 3.59.

3.3.6.2 Shoulder structure improvement

In standard sled test setups, where upper extremities have limited influence, the shoulder complex can be simplified to a single joint with a well-validated ROM. However, for accident scenarios involving VRUs including the PTW drivers, where the body experiences intricate motions, an accurate shoulder response is essential [94].

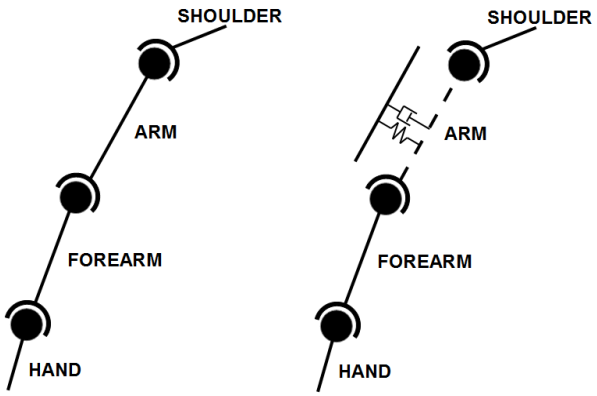

Figure 3.60 The configuration of the upper arm MBS structure (left: original, right: enhanced).

Figure 3.61 The cylinder impacting shoulder at 4.5 m/s – validation setup.

To capture the intricate shoulder motion resulting from the impact on the upper arm, a two-part rigid structure was employed for the upper arm (as shown in Figure 3.60). The first part forms the framework of the entire MBS, while the second part is connected to the first, allowing for compressibility of the upper arm complex and realistic behavior of the shoulder under impact conditions. The parameters governing compression were adjusted to align with experimental benchmarks.

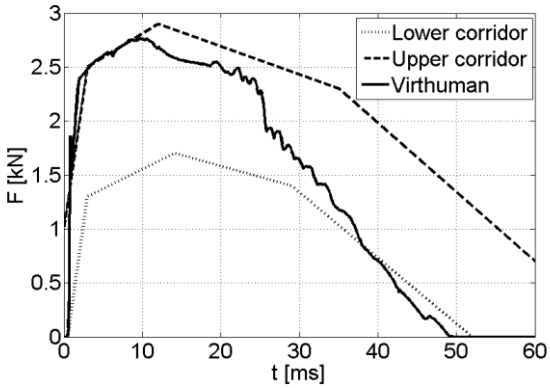

Figure 3.62. Force response from validation.

The time-series of the contact force is illustrated in Figure 3.62. Overall, the projected curve falls within the designated range, indicating a favorable alignment with the experimental data. Towards the conclusion of the impact, the force slightly descends below the expected corridor. This could potentially be attributed to the reduction in the contact area between the impactor and the shoulder, implying that the contact area simulated in the model (rigid impactor on rigid segment) is smaller compared to the contact area observed in the actual experiment (soft tissues of the shoulder adapting to the flat surface of the rigid impactor).

3.3.7 Ground impact with the helmet

In the majority of motorcycle accidents, the body angle towards the ground is typically 30 degrees or less, as indicated by the findings of COST327 [105]. Thus, an oblique impact scenario is chosen for evaluation, following the methodology proposed by Ghajari et al. in 2013 [106]. This analysis involves a comprehensive investigation using the fully validated FE model THUMS for benchmarking against the hybrid model Virthuman. The loading conditions encompass the effects of gravity and variable impact normal (v_n) and tangential (v_t) velocities. The experimental configuration is depicted in Figure 3.63.

3.3.7.1 Methods

The Virthuman model scaled to the THUMS (175 cm, 77 kg). Since the scaling algorithm desires age, the age group chosen was 30 – 35 years, because the average height (50 percentile) equals 176 cm and average mass equals 78 kg, which are the closest values for scaling.

The medium size FE helmet model developed within the MYMOSA project [106, 107] is coupled to the human head. Due to the head and helmet geometry, minor mesh corrections on the head are done to avoid penetrations to position the helmet with a small constant gap between the helmet liner and the head. This gap is usually filled by the comfort foam in reality. The helmet chin strap is passed under the chin and tightened by the pretension force of 5 N and there is defined a sliding contact between the liner and the head with friction coefficient equal (f.) to 0.2 [106].

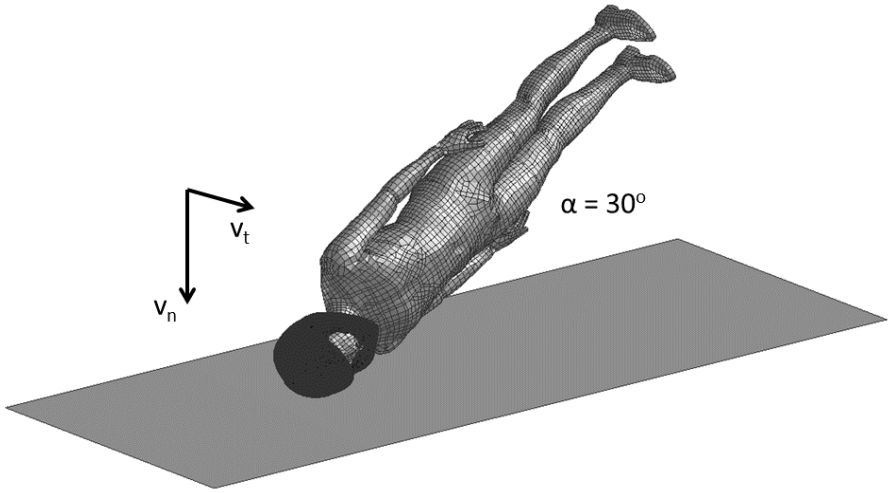

Figure 3.63. Ground impact simulation setup.

3.3.7.2 Results on helmeted VH ground impact

The interplay of normal and tangential velocities introduces intricate head and neck kinematics following ground impact. The efficacy of the scaled virtual human body model Virthuman is assessed in an oblique impact scenario, with a comparison against the THUMS model. The evaluation is based on parameters including the maximum tangential and normal contact forces ($F_{t,max}$ and $F_{n,max}$ respectively), their ratio $F_{t,max}$ / $F_{n,max}$, and the maximum head acceleration (a_{max}) as outlined in Ghajari's work [106], presented in Table 3.10.

Table 3.10. Response comparison between VH and THUMS.

Impact velocity		Contact force						*Head acceleration*	
v_n *[m/s]*	v_t *[m/s]*	$F_{n,max}$ *[kN]*		$F_{t,max}$ *[kN]*		$F_{t,max}$ / $F_{n,max}$ *[-]*		a_{max} *[g]*	
		VH	THUMS	VH	THUMS	VH	THUMS	VH	THUMS
2.5	5	4.27	3.82	1.59	1.31	0.37	0.33	67	73
	10	4.40	3.85	1.75	1.54	0.40	0.40	68	73
5	5	9.93	7.90	3.01	2.21	0.30	0.22	132	144
	10	9.97	7.68	3.96	3.08	0.40	0.38	136	143
7.5	5	12.88	11.54	4.09	3.32	0.32	0.18	190	199
	10	12.52	11.72	4.72	3.50	0.38	0.31	190	191

The simulation results indicate consistent outcomes across various normal and tangential velocities. As the normal velocity increases, the impact of the MBS approach used in the development of the Virthuman model becomes evident, leading to a stiffer response and higher contact forces. However, when assessing head acceleration and potential injury, the maximum head acceleration values align closely with those obtained using the FE model THUMS.

The chapter's comprehensive coverage creates a robust foundation for understanding the landscape of human surrogates, injury assessment methodologies, and the applications of the Virthuman model within the context of PTW safety.

4 Injury countermeasures testing

In the realm of PTW passive safety, ensuring the well-being of riders is of paramount importance. As opposite to other modes of transport, the PTW does not protect the rider well by energy absorption, because the size of the PTW is comparable to the rider. As riders are more exposed and vulnerable to potential accidents compared to occupants of enclosed vehicles, the development and testing of effective injury countermeasures become essential. This pursuit involves a multifaceted approach, encompassing Personal Protective Equipment (PPE) and Roadside Barriers. This introduction sheds light on the critical endeavor to test and validate these countermeasures, with a focus on their significance in enhancing PTW rider safety.

Personal Protective Equipment (PPE): A Shield of Passive Safety

The rider's last line of defense against potential injuries, PPE plays a pivotal role in minimizing the outcomes of accidents. Helmets, body suits, gloves, and specialized footwear constitute the ensemble of PPE designed to mitigate injury risks. Rigorous testing of these protective gears involves evaluating their ability to absorb and distribute impact forces, reduce the risk of head and limb injuries, and offer crucial safeguards against abrasions and fractures.

Roadside Barriers: Safeguarding Beyond the Vehicle

The physical environment in which PTW riders operate presents its own set of challenges. Roadside barriers, while designed to enhance road safety, need to be carefully engineered to minimize harm to riders in the event of a collision. Testing the effectiveness of these barriers involves analyzing their ability to redirect, absorb, or dissipate impact forces, thereby preventing riders from being thrown into more dangerous terrain or colliding with rigid structures.

The Intersection of Numerical Simulation Technology and PTW Passive Safety

Advances in technology have paved the way for sophisticated testing methodologies. Crash simulations, virtual scenarios, and biomechanical models offer insights into how injury countermeasures perform under various conditions. These tools allow researchers and engineers to iterate, optimize, and tailor countermeasures to the unique dynamics of PTW accidents. The pursuit of safer PTW riding experiences hinges on meticulous testing and validation of injury countermeasures. By rigorously assessing the effectiveness of PPE and engineering Roadside Barriers that prioritize rider safety, we can establish a robust foundation for reducing injury risks and safeguarding the lives of PTW riders. As we navigate the intricacies of PTW safety, the collaborative efforts of researchers, engineers, and stakeholders pave the path towards a future where every rider embarks on their journey with greater confidence and security.

4.1 State of the Art

This chapter delves into the prevalent helmet standards governing both European and US markets. Specifically, it focuses on ECE 22.05 [108], DOT FMVSS 218 [109], and Snell M2015 [110] for motorcycle helmets. The primary objectives of these helmet standards are twofold: Firstly, they serve as a robust mechanism for assessing helmet performance, ensuring their efficacy in real-world scenarios. Secondly, they provide valuable guidelines for the development of new helmet designs that meet stringent safety requirements. As these standards gain mandatory status, they necessitate that every helmet available in the respective market adheres to their stipulated regulations. This interplay between standardization and safety profoundly impacts the design, manufacturing, and sale of helmets, ultimately safeguarding users by promoting the highest levels of protection.

4.1.1 Helmet impact testing standards

During testing, a headform equipped with a helmet is released from a predetermined height and directed toward a rigid anvil. In nearly all of these tests, the peak linear acceleration (PLA) experienced during impact is measured and recorded.

To achieve the appropriate testing speed, the drop towers are utilized. Broadly speaking, test drop towers can be categorized into two primary types: guided and unguided freefall systems (depicted in Figure 4.1). Guided freefall drop towers typically adopt either a twin wire or monorail arrangement. Within the guided freefall setup, there is a constraint that prevents any rotation of the headform during impact. On the other hand, unguided freefall systems do not have this restriction, allowing for rotational motion of the headform upon impact. The most used impact surfaces are the flat, hemispherical, and curbstone anvils, all of which are made of steel.

Figure 4.1 Two types of drop towers (left -guided, right- unguided).

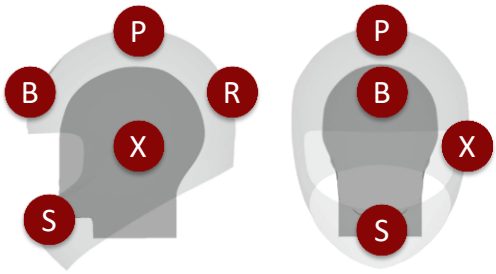

Figure 4.2 ECE R22.05 helmet impact points [111]**.**

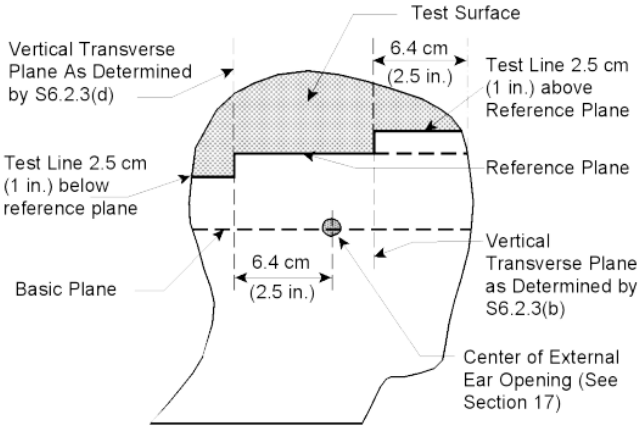

Figure 4.3 Test surface definition for DOT standard [109]**.**

The comparison of the headform sizes and their masses (in kg) for the different testing standards looks as follows:

DOT Standard:

The DOT standard employs three headform sizes. The small headform weighs between 3.4 to 3.6 kg. The medium-sized headform has a weight range of 4.9 to 5.1 kg. Lastly, the large headform falls within a weight range of 6.0 to 6.2 kg.

ECE Standard:

The ECE standard utilizes five different headform sizes. The headform with a circumference of 50 cm weighs 3.1 kg. For the headform with a circumference of 54 cm, the weight is 4.1 kg. The headform measuring 57 cm in circumference weighs 4.7 kg. Moving up to a headform of 60 cm circumference, the weight is 5.6 kg. Finally, the largest headform with a circumference of 62 cm weights 6.1 kg.

SNELL Standard:

The SNELL standard incorporates six headform sizes. The headform with a circumference of 50 cm weighs 3.1 kg. For the 52 cm headform, the weight is 3.6 kg. The headform with a circumference of 54 cm weighs 4.1 kg. The headform measuring 57 cm in circumference weights 4.7 kg. As the circumference increases to 60 cm, the weight becomes 5.6 kg. Lastly, the largest headform with a circumference of 62 cm weighs 6.1 kg.

It's important to note that each size includes a variation of ±100 g in weight. The DOT standard comprises three sizes, the ECE standard features five sizes, and the SNELL standard employs six sizes for their respective headforms. 60 cm: Weighing 5.6 kg

All existing standards utilize pass/fail criteria that are based on translational measurements. These criteria can be categorized into two main types: Peak Linear Acceleration (PLA) criteria and those linked to impact duration, such as Dwell time and HIC. To pass the ECE test the helmet should not exceed $g_{max} \leq 275g$, $HIC_{15} \leq 2400$ from the 7.5 m/s impact (at points B, P, R, X, and S depicted in Figure 4.2). The DOT FMVSS 218 standard passing means to have $g_{max} \leq 400g$, Dwell time≤2ms@200g and Dwell time≤4ms@150g. Dwell time is defined as the duration or time interval during which a specific level of force or acceleration is sustained on a human body or an object. The SNELL standard evaluates only the peak acceleration and has different thresholds for particular sizes of headforms $g_{max} \leq 275g$ for A, C, E, J, $g_{max} \leq 264g$ for M, and $g_{max} \leq 243g$ for O. It should be noted that for SNELL the impact velocity is higher than the ECEs (7.75 m/s), where for DOT standard impact velocity is lower and related to the headform size (6.0 m/s for small and 5.2 m/s for large headform). An illustrative instance of a pass/fail criterion and its application to a specific acceleration pulse is demonstrated in the following example (Figure 4.4, Figure 4.5, Figure 4.6) time-series of head COG acceleration [112]:

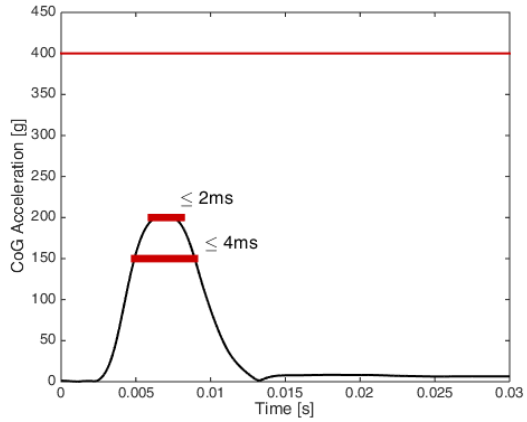

Figure 4.4 DOT standard PLA and Dwell time thresholds [66]**.**

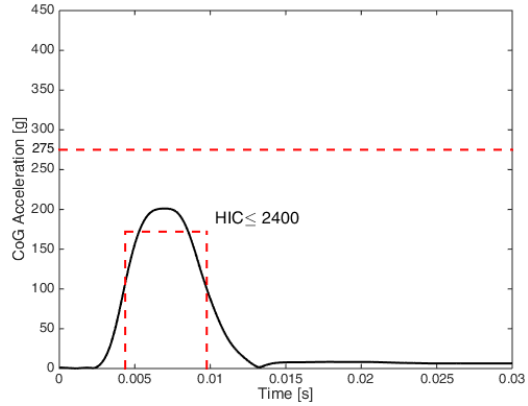

Figure 4.5 ECE standard PLA and HIC thresholds [66]**.**

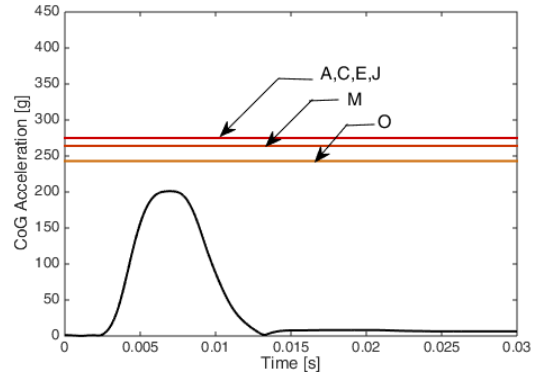

Figure 4.6 SNELL PLA thresholds for different headform sizes [66]**.**

4.1.2 Motorcycle barrier testing standards

Presently, a variety of national standards and testing procedures are in place to evaluate the effectiveness of barriers in safeguarding motorcyclists across Europe (Figure 4.7). In addition to these standards, the CEN (Centre Européen de Normalisation), in partnership with the Technical Committee (TC) 226, has developed a Technical Specification aimed at enhancing infrastructure design concerning motorcyclists. This segment provides an overview of the prevailing national standards and introduces the proposal originating from the European Union.

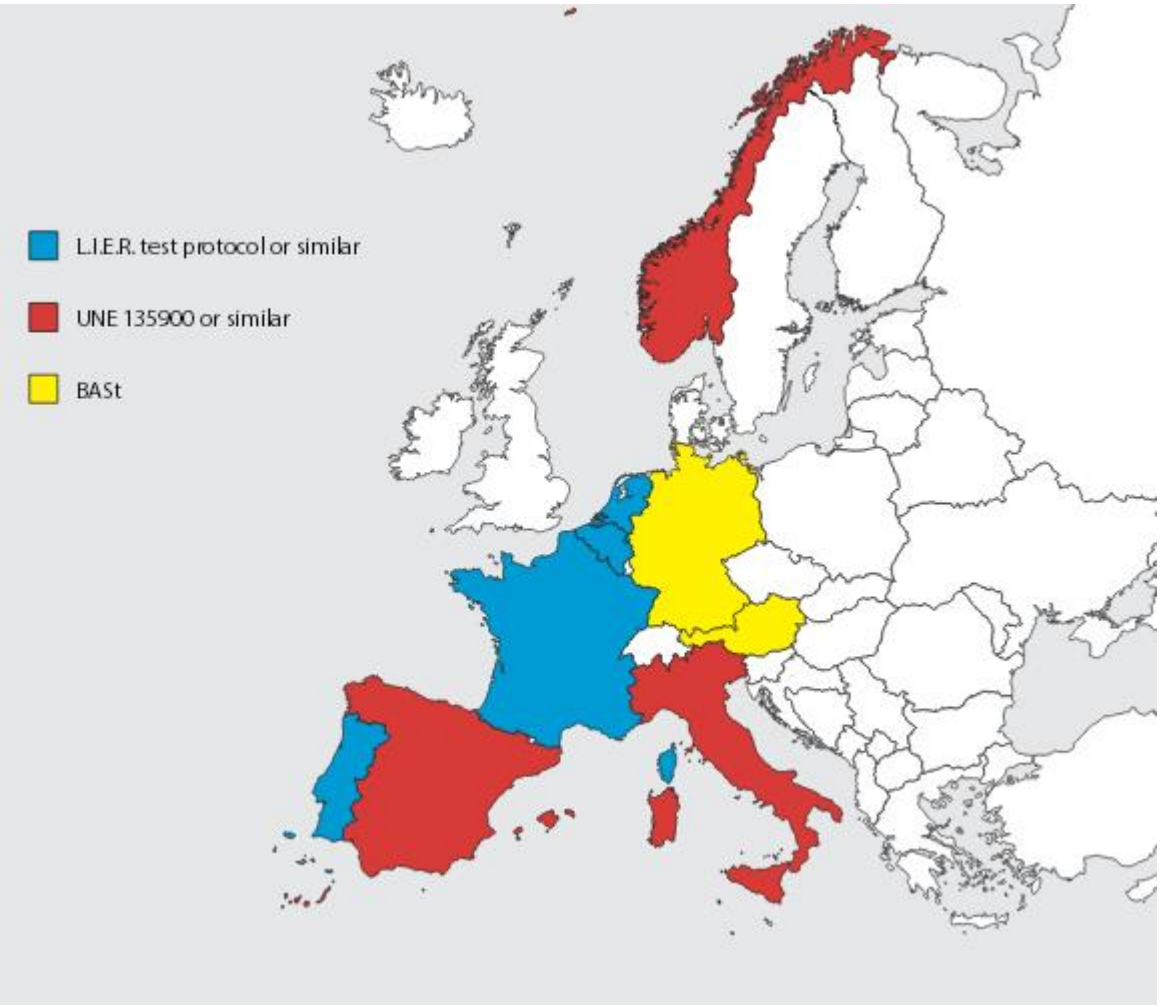

Figure 4.7 Barrier testing standards in Europe [113]**.**

The French authorities approached **L.I.E.R.** [4] with a request for a test protocol aimed at mitigating the severity of motorcycle crashes involving collisions with road barriers. Formulated in 1998, the protocol encompasses two distinct tests. Each test involves the use of an anthropomorphic test device (ATD) or crash test dummy, equipped with sensors, propelled from a sled to impact the barrier. The sole variation between the two tests lies in the relative angle between the ATD and the barrier, illustrated in Figure 4.8. Both scenarios entail a velocity vector positioned at a 30-degree angle in relation to the

[4] Currently the LIER laboratory is registered as a TRANSPOLIS, 340 Rue de Hongrie 69125 LYON SAINT-EXUPERY AEROPORT, France

barrier, with a magnitude of 60 km/h, while the dummy skids on its back. Notably, the ATD consistently impacts the barrier post in this protocol. The employed ATD is a hybrid combination of components from different dummies: the Hybrid II thorax coupled with the head/neck assembly of the Hybrid III, complemented by a pedestrian kit. The dummy is attired in protective motorcyclist clothing and a helmet.

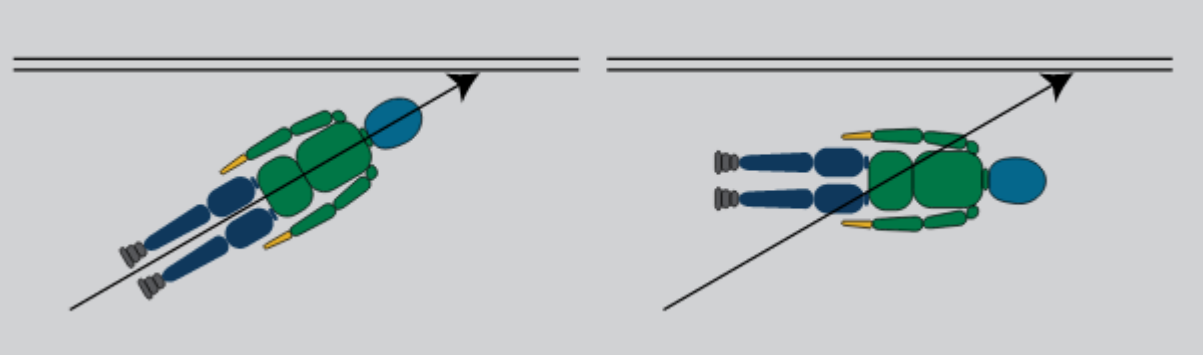

Figure 4.8 L.I.E.R test protocol [113]**.**

Under this testing standard, the evaluation focuses on two specific anatomical areas, namely the head and the neck (Table 4.1). The aim is to determine the safety barrier's capacity to safeguard a motorcyclist who is sliding along the ground and subsequently colliding with the system.

Table 4.1 L.I.E.R. thresholds and criteria for the barriers.

Body region	**Parameter**	**Limit**
Head	HIC_{36}	1000
Neck		
	Neck Shear	3300 N
	Neck Tension	3300 N
	Neck Compression	4000 N

The Spanish **UNE 135900** standard exhibits a notable distinction from the French L.I.E.R program in its approach. It introduces the division of testing protocols into two distinct categories: "discontinuous systems" (those encircling barrier poles) and "continuous systems" (lower rails extending between barrier poles). For both these categories, the standard mandates two distinct impact scenarios: a central impact where the displacement vector aligns with the barrier pole, and either an off-center (for punctual systems) or central (for continuous systems) impact. In the former case, the ATD is directed 20 cm away from the center of the discontinuous system, and in the latter case, the ATD is aimed at the midpoint between two barrier posts. Schematic representations of these three impact configurations can be seen in Figure 4.9, Figure 4.10, and Figure 4.11.

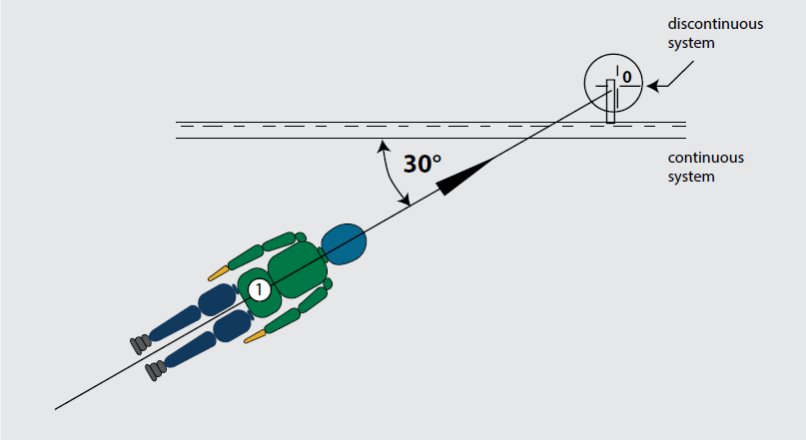

Figure 4.9 First test (continuous and discontinuous barriers) – centered [113]**.**

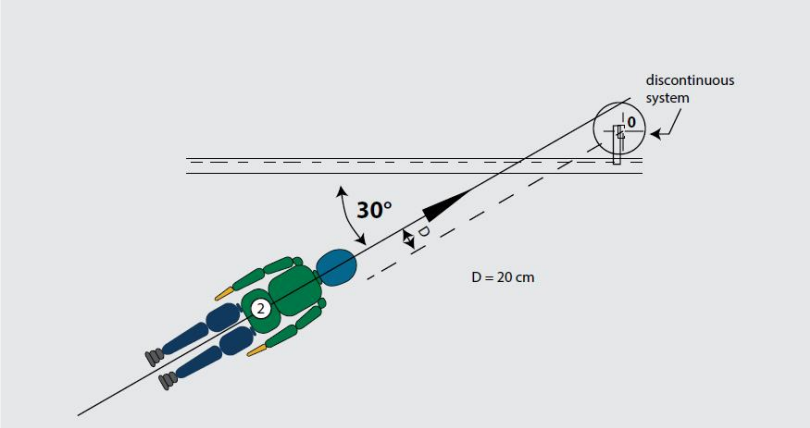

Figure 4.10 Second test (discontinuous barriers) [113]**.**

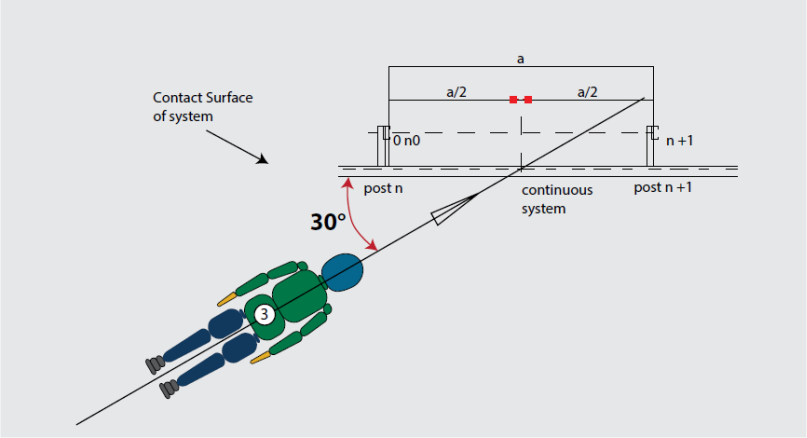

Figure 4.11 Third test (continuous barrier only) [113]**.**

The acceptance criteria for the UNE 135900 were already discussed in the Chapter: Injury criteria for the neck.

The German Federal Bureau for Road Safety (**BASt**) has devised a homologation process aimed at endorsing protective systems for motorcyclists. This procedure categorizes devices into two classes: Class 1, subjected to testing at 20 km/h, and Class 2, subjected to testing at 35 km/h. The prescribed acceptance criteria entail that the recorded peak deceleration must remain below 60 g, and the mean acceleration within a 3 ms timeframe should not surpass 40 g.

4.2 Numerical testing of safety measures

4.2.1 Helmet testing

4.2.1.1 Material and methods

The focus of this part of the study revolves around the creation of a simplified finite element model for helmets and its subsequent numerical testing to meet European regulations [108]. This model is intended to be integrated with the existing human body model for evaluating the safety of motorcycle riders. The AVG-T2 helmet [106, 107]served as the basis for geometry. To ensure compatibility with the human body model (Virthuman), the finite element mesh was developed in accordance. An additional advantage of this helmet is the simplicity of having the calculation time step comparable to Virthuman. The helmet comprises two distinct components: the outer shell, 4 mm thick, and the inner protective padding, measuring 40 mm in thickness, as depicted in Figure 4.12, and Figure 4.13. Material properties were adopted from C. Deck [114], as illustrated in Figure 4.14.

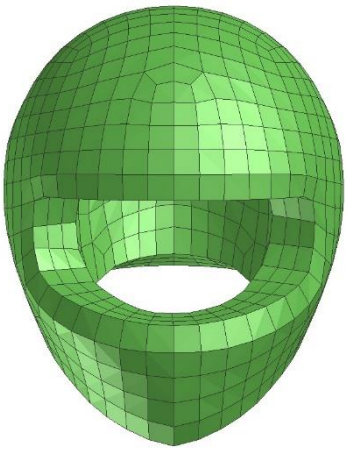

Figure 4.12 Frontal view of simplified helm FE model.

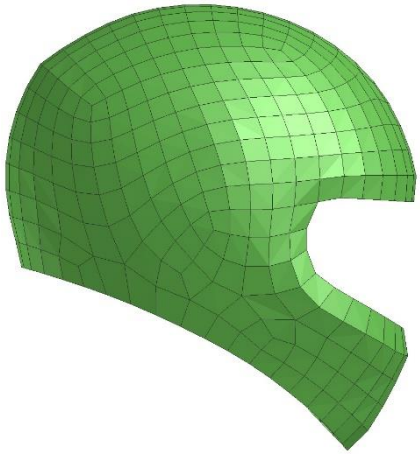

Figure 4.13 Side view of simplified helm FE model.

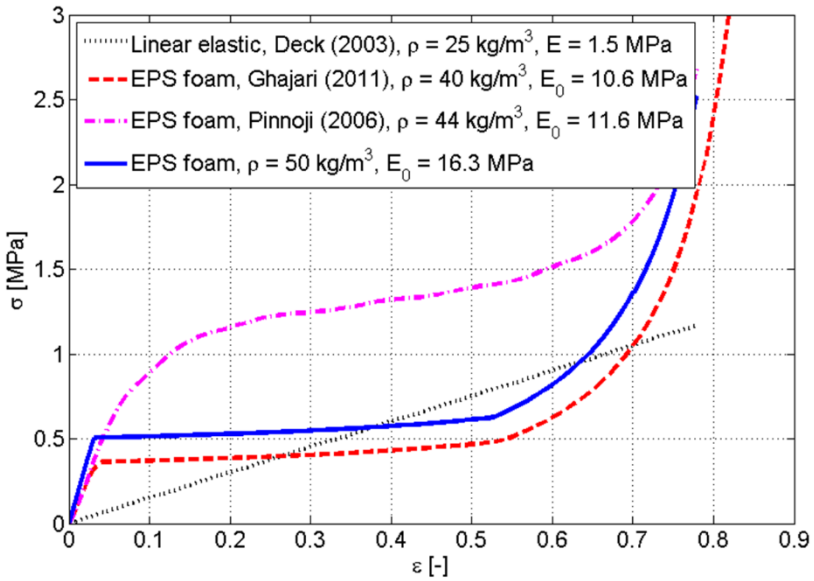

Figure 4.14 Material curve of the helmet liner

Following European regulations, every helmet introduced to the European market must comply with the ECE-R22.05 standard, which was outlined in the previous section (4.1.1). These standards encompass a dynamic retention system test, rigidity assessment, shock absorption evaluation, and a visor penetration resistance test. In terms of impact protection for the head, a drop test is conducted. As per the regulations, a helmet, complete with a headform, is dropped against an anvil at a velocity of 7.5 m/s. specifically, for the developed helmet size, the ECE R22.05 regulation employs the M-size headform (depicted in Figure 4.15), weighing 5.6 kg. Two distinct anvils, a flat one and a kerbstone (illustrated in Figure 4.16), are utilized, along with four designated impact points. These impact configurations (P, B, R, and X) for the flat anvil are displayed in Figure 4.17.

The developed helmet is subjected to testing across eight impact configurations, covering four impact directions for both anvils. According to the guidelines, the helmet must not exceed a maximum acceleration of 275 g, and the HIC should not surpass 2400 for each impact scenario to meet the regulation's requirements.

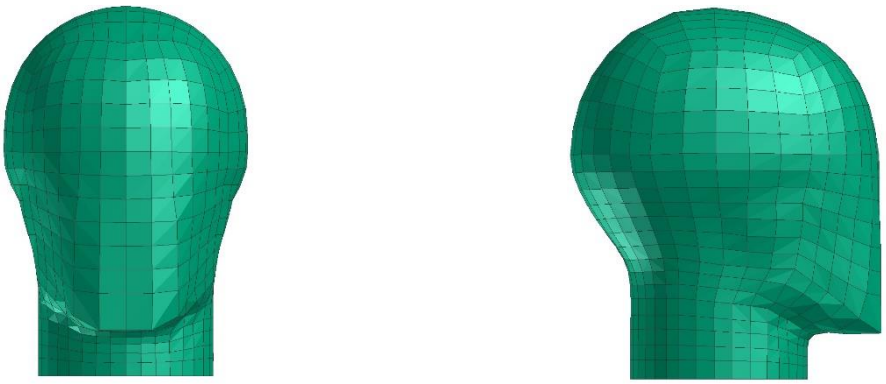

(a) Frontal view **(b) Side view**

Figure 4.15 A headform FE model.

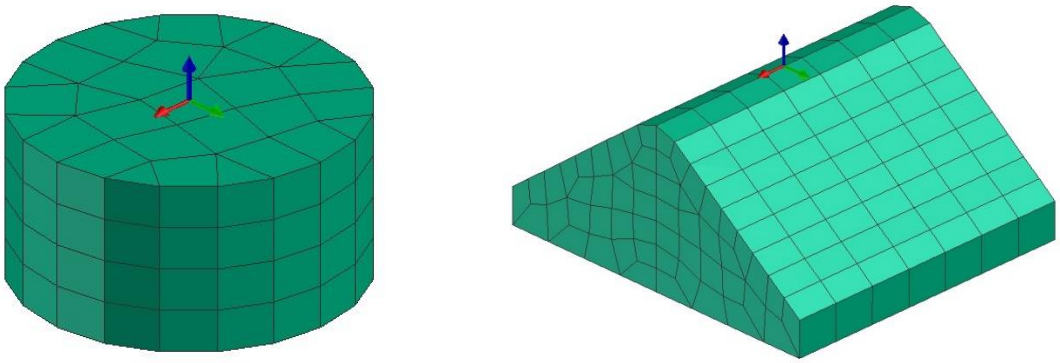

(a) Flat anvil **(b) Kerbstone**

Figure 4.16 Two FE models of the anvil from ECE R22.05.

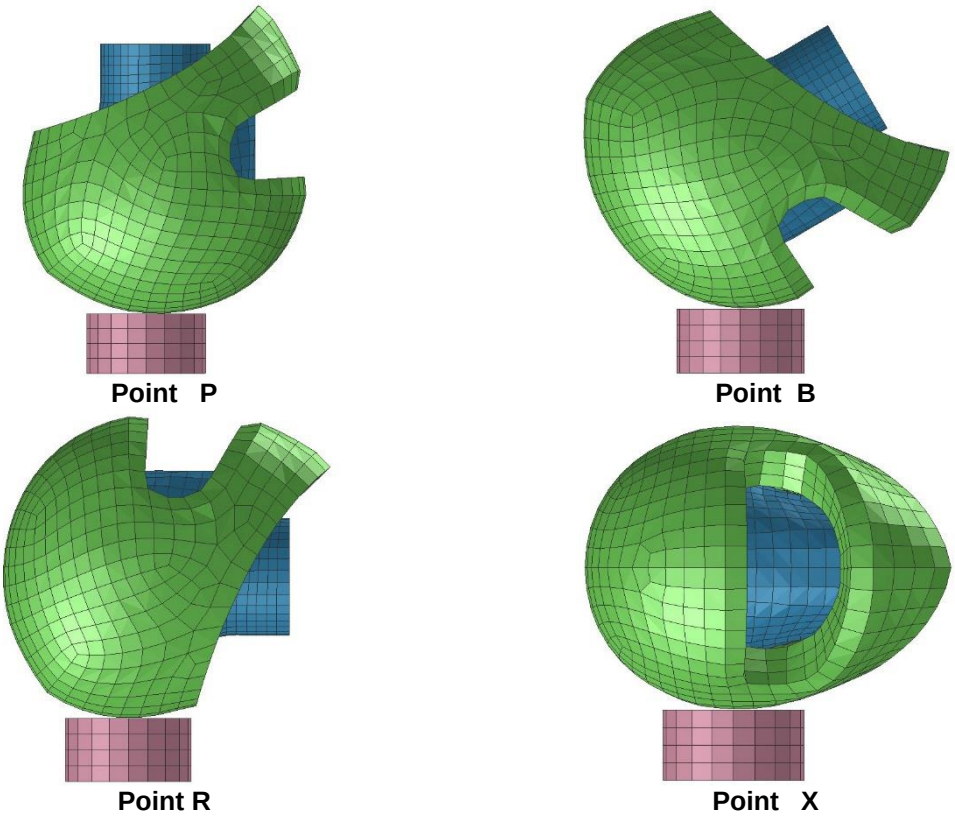

Point P **Point B**

Point R **Point X**

Figure 4.17 Four impact configurations of MC helmet.

4.2.1.2 Results

The impacts were evaluated according to the example presented in Figure 4.5. For each anvil (flat, circular) and impact point four types of liner's material model were assessed (LE, EPS 40, EPS 44, EPS 50). The example of HIC and PLA threshold evaluation for this study is depicted in Figure 4.18.

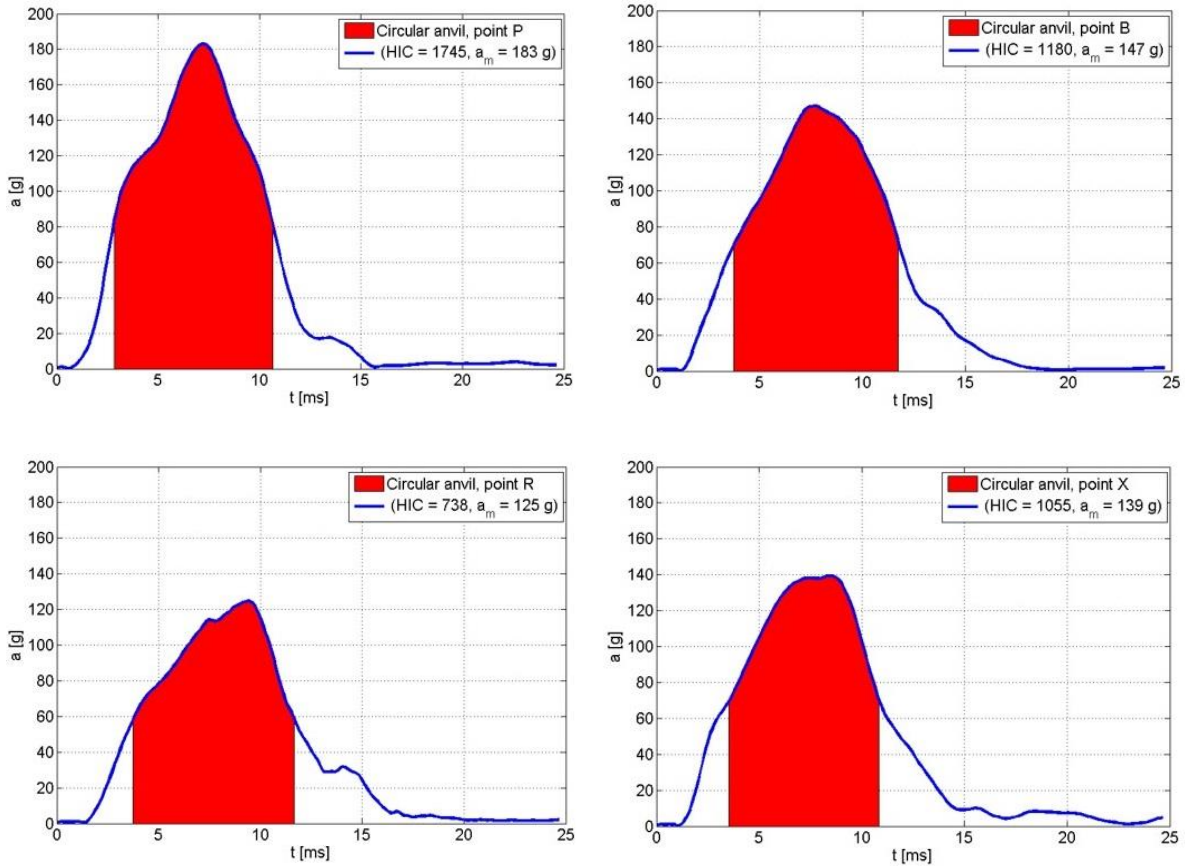

Figure 4.18 Acceleration curve and HIC of headform in flat anvil impact simulation (liner: linear elastic).

The simulated HICs and PLAs of the headform are presented in Table 4.2 and Table 4.3. Per the regulations, the maximum acceleration should not surpass 275 g, and the maximum HIC must remain below 2400 for each impact test to meet the stipulated criteria. Notably, the red values in both tables indicate instances where a specific material model (as well as the helmet model itself) failed to meet the requirements. Notably, the results in these tables highlight that the EPS with a density of 50 kg/m³ successfully fulfills the requirements across all impact simulations.

The helmet equipped with a linear elastic shell and linear foam liner meet the requirements of the ECE-R22.05 tests only when subjected to the flat anvil impact. On the other hand, the helmet featuring a linear elastic shell and an EPS foam liner with a density of 44 kg/m³ successfully meets the ECE-R22.05 tests except for the P impact on the flat anvil. Remarkably, the helmet fitted with a linear elastic shell and an EPS foam liner of 50 kg/m³ density meets all ECE-R22.05 test criteria. Particularly noteworthy is that the EPS foam with a density of 50 kg/m³ passed all tests, thus validating the model. This validated model is recommended for future utilization in motorcycle accident reconstructions and the assessment of injury risk.

Table 4.2 HIC assessment for particular liner material model.

HIC	ECE R22.05	Flat anvil				Kerbstone anvil			
		LE	EPS 40	EPS 44	EPS 50	LE	EPS 40	EPS 44	EPS 50
Point B	2 400	1 180	1 338	2 209	1 425	5 339	2 834	1 231	1 108
Point P		1 745	1 994	3 224	2 160	8 427	3 316	1 650	1 447
Point R		738	941	1 704	972	4 335	1 147	1 065	802
Point X		1 055	1 055	2 222	1 207	4 636	2 064	1 338	1 090

Table 4.3 PLA assessment for particular liner material model.

a_{max} [g]	ECE R22.05	Flat anvil				Kerbstone anvil			
		LE	EPS 40	EPS 44	EPS 50	LE	EPS 40	EPS 44	EPS 50
Point B	275	147	172	207	164	496	392	129	163
Point P		183	212	274	204	589	415	171	186
Point R		125	152	173	137	442	232	137	128
Point X		139	146	208	153	464	330	158	161

4.2.2 Population diversity helmet testing

4.2.2.1 Methods and simulation setup

This study aimed to investigate the influence of diversity factors such as age and sex on helmet testing using a hybrid scalable human body model. The Virthuman model was employed as the HBM, which was further scaled to cover six age categories (16, 17, 18, 22, 26, and 34 years) for both males and females. The selection of these age categories was guided by an analysis of the MAIDS database, as illustrated in Figure 2.2.

Each scaled Virthuman model was combined with the Finite Element (FE) representation of the T2 AGV helmet [106, 107]. To accommodate differences between material law implementations in LS-Dyna [102] and VPS, the T2 AGV helmet was reconfigured within the VPS environment. The coefficient of friction between the VH and the helmet was set at 0.5, following [115]. After being integrated with the helmet, the VH was oriented at a 15° angle between the model's coronal plane and the ground [105], as depicted in Figure 4.19. The initial velocity of 7.5 m/s adhered to the European Standard for helmet testing utilized in the previous chapter. Throughout the simulation, the acceleration of the head's COG was continuously tracked. The signal was filtered by the SAE J211-1 standard, employing the CFC 1000 filter.

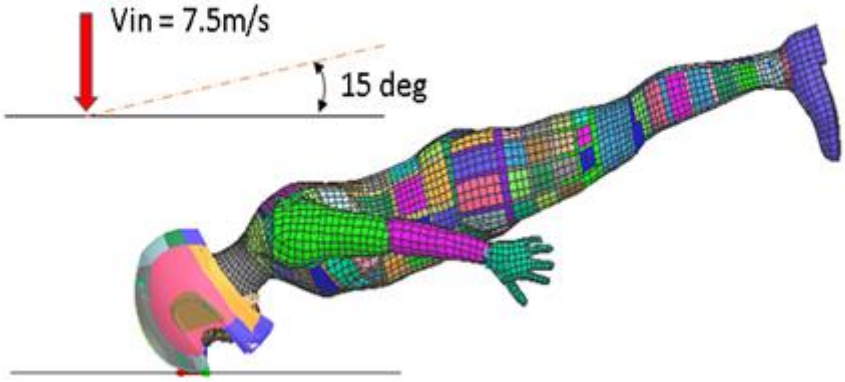

Figure 4.19 Simulation setup.

4.2.2.2 Results

Table 4.4 displays the variations in HIC at 15 ms time intervals for the scaled models. The outcomes indicate that in all instances, the T2 AGV helmet successfully met the certification criteria of ECE R22.05 (where the maximum HIC must not exceed 2400). However, it's noteworthy that only the scenarios involving male VH models approached the HIC threshold for significant head injuries (HIC = 1500). Conversely, the evaluation of HIC for female VH models exhibited an increase ranging from 13.8% to 20.4% compared to their male VH counterparts of the same age.

Table 4.4 HIC evaluation for particular sex, mass, and height.

	Age [years]	**16**	**17**	**18**	**22**	**26**	**34**
Female	*mass[kg]*	56	59	58	61	59	62
	height[m]	1.64	1.66	1.66	1.67	1.66	1.65
	HIC	1811	1849	1819	1817	1799	1837
Male	*mass[kg]*	66	70	72	77	76	78
	height[m]	1.76	1.77	1.78	1.79	1.78	1.76
	HIC	1502	1471	1565	1522	1551	1519

A comprehensive analysis, coupling finite element (helmet) and hybrid (VH) models, was conducted to investigate the variations in HIC assessment within a diverse population. The focal point was the acceleration of the head's COG resulting from helmet impact.

The outcomes demonstrate that the employed helmet successfully meets the requirements of ECE R22.05 certification for both genders. The evaluation of HIC revealed no noteworthy disparities within the same-gender groups. However, the simulations unveiled noticeable differences in HIC values between females and males. Specifically, the HIC value for females was 13.8% to 20.4% higher than that for males. This dissimilarity might be attributed to the smaller head diameter of the VH model, scaled to the dimensions of females.

4.2.3 Virthuman-based barrier assessment

In the present context, a range of national standards and test protocols is currently in place across Europe to evaluate the protective capacity of barriers for motorcyclists, these norms were described in section 4.1.2. Generally, the prescribed impact tests entail utilizing an ATD placed in a supine position and impacting the barrier at a 30-degree angle and a velocity of 60 km/h. The ATD in the protocol is outfitted with motorcyclist protective attire and a helmet, with particular attention to the performance of the head and neck. In the direction of harmonization, the CEN formulated the European Technical Specification (TS) CEN TS 1317-8, outlining a comprehensive impact test that involves launching a dummy at a predetermined speed towards a barrier, as depicted in Figure 4.20. The sole disparities between TS 1317-8 and UNE 135900 lie in the fact that the Technical Specification permits segments of the barrier to detach during testing and allows for the ATD's hand to penetrate and traverse the barrier, which in our case is irrelevant due to the utilization of simplified barrier model [113].

4.2.3.1 Method

Given that barrier impact testing involves intricate body motion at high velocities and encompasses personal protective equipment, virtual simulations have emerged as a suitable avenue for evaluating such impacts and designing secure barriers. To execute barrier impact simulations, the Virthuman model, which has previously undergone development and validation for intricate impact scenarios, is linked with the same helmet as above. Currently, there isn't specialized protective attire, and the interaction between the Virthuman model and protective clothing solely hinges on frictional contact. Although protective clothing can significantly influence the ROM in specific joints, its effect is minimal in the present context, as the extremities remain close to the body. The simulation setup looks as follows:

- VH lying on his back impacting the barrier by 60 km/h at 30^{o},
- Motorcyclist protective helmet coupled,
- Head and neck performance monitored,
- Critical values of HIC and neck moments (levels I and II) evaluated according to UNE 135900 / CEN TS 1317-8,
- Three types of virtual models of barrier evaluated (rigid, thin steel barrier, thick steel barrier),
- Barrier material parameters: E = 210 GPa, ν = 0.3, γ = 200 MPa

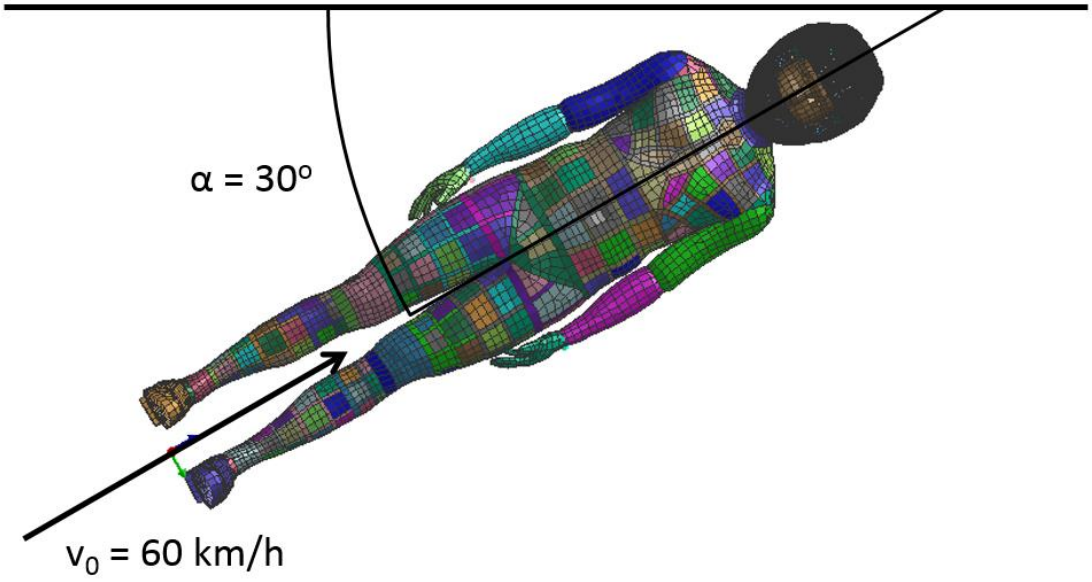

Figure 4.20 Barrier impact simulation setup.

4.2.3.2 Results

Upon evaluating the results, it becomes evident that these uncomplicated barrier models fail to meet the criteria outlined in the UNE 135900 / CEN TS 1317 – 8 regulations. The thin steel barrier comes closest to satisfying the criteria, with the shear force during impact slightly surpassing the safe envelope. For each of the barrier simulations, the neck initially experiences shear and compression forces beyond acceptable limits (around 7-10 ms into the simulation), followed by tension forces around 20 ms into the virtual experiment (depicted in Figure 4.22, Figure 4.23, Figure 4.24). These tension forces also exceed the II severity level. However, for the thick and rigid barrier, the maximum peak of this tension force is approximately 30% lower than that of the thin barrier. Table 4.5 shows that all the barriers were close to meeting the max. flexion momentum criterion.

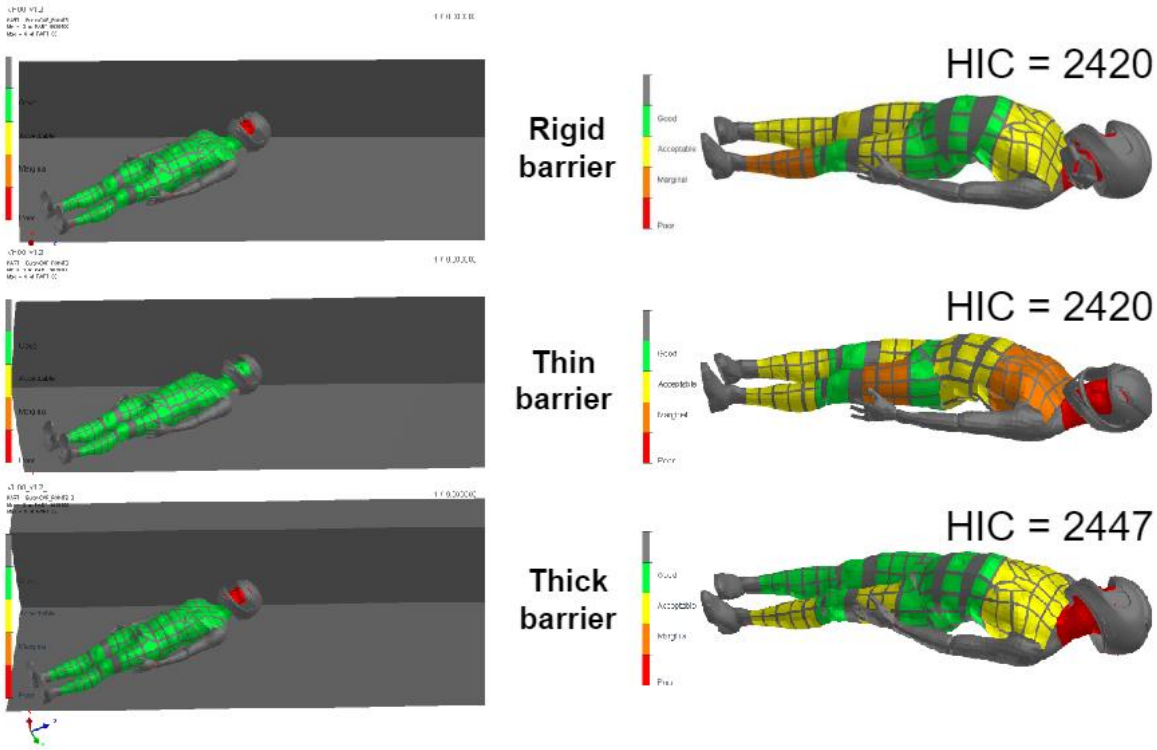

Figure 4.21. First and last time-frame of simulation, with IC color coding according to Table 3.8.

This study demonstrates the utilization of the Virthuman human body model in the evaluation of safety barriers. Simulations were conducted using hypothetical barriers, positioning the human body model as specified in UNE 135900 / CEN TS 1317–8. By subjecting the model to impacts at a velocity of 60 km/h, specific outputs were compared against the criteria defined in UNE 135900 / CEN TS 1317–8. The research underscores the capability of virtual human body models in the advancement and design of secure PTW infrastructure.

Table 4.5 UNE 135900 / CEN TS 1317 - 8 head and neck severity evaluation.

Segment	Criterion	Severity level	Limit	Rigid	Thin	Thick
Head	HIC	I	650	2418	2420	2447
		II	1000			
Neck	Shear	I	Next Figures			
		II				
	Tension	I				
		II				
	Compression	I				
		II				
	Lateral flexion	I	134 Nm	260	254	257
		II	134 Nm			
	Extension	I	42 Nm	109	180	111
		II	57 Nm			
	Flexion	I	190 Nm	197	191	196
		II	190 Nm			

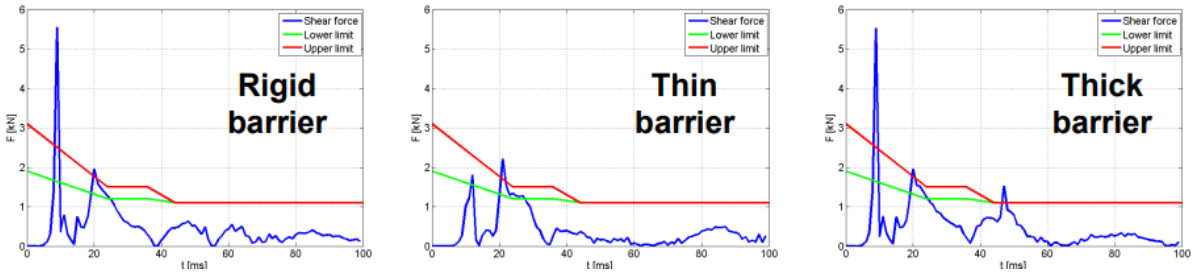

Figure 4.22 Evaluation of neck shear force limits.

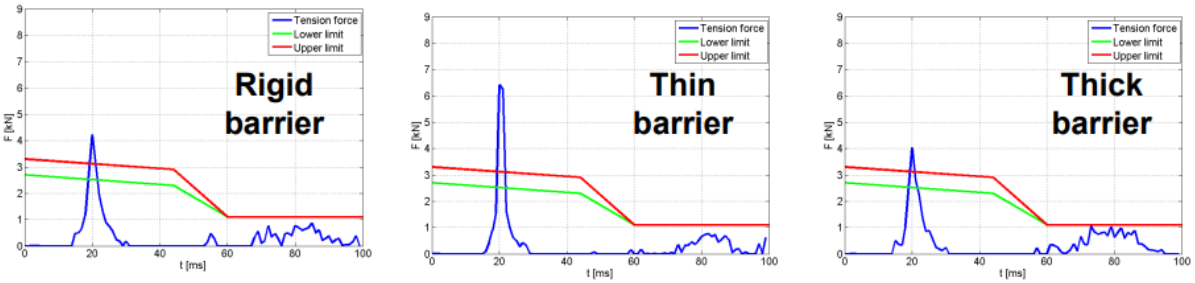

Figure 4.23 Evaluation of neck tension force limits.

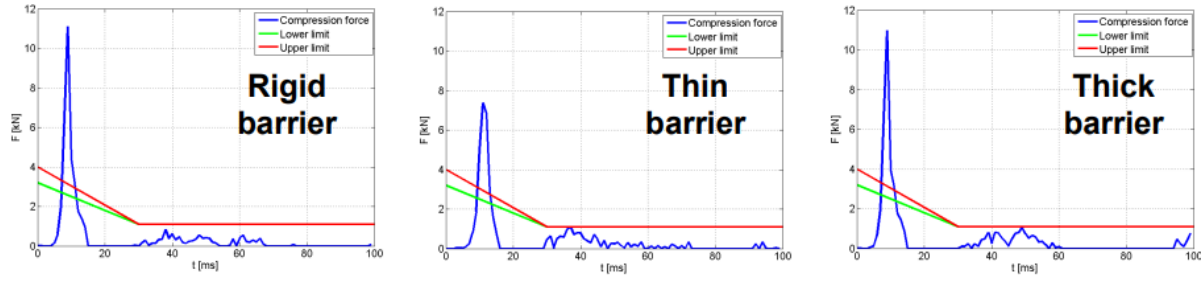

Figure 4.24 Evaluation of neck compression force limits.

4.3 Summary

The primary focus of this part of the dissertation was the numerical development of helmets and virtual testing of safety barriers following established standards. The discussion encompassed various aspects, including helmet finite element modeling, impact testing methodologies, and injury assessment criteria. The examination of helmet standards such as ECE-R22.05, DOT FMVSS 218, and Snell M2015, as well as the testing procedures for head protection against impact, was a central theme.

Additionally, attention was given to the evaluation of safety barriers for motorcyclists, involving multiple national standards such as UNE 135900, CEN TS 1317–8, and others. The process included the use of human body models like Virthuman, coupled with helmet models, to assess barrier impact performance. Virthuman's successful utilization as an alternative to ATD in numerical barrier development further underscored its significance.

Moreover, the development of a numerical model for a simple helmet, which is set to be employed in subsequent chapters, was another crucial aspect discussed in this conversation. This model holds the potential to enhance the understanding of helmet performance and contribute to the broader context of safety for motorcyclists.

In summary, this chapter delved into the intricacies of injury countermeasures testing, ranging from helmet development and impact assessment to safety barrier evaluation. It underscored the significance of virtual testing methodologies for enhancing safety measures and designing protective equipment and infrastructure for motorcyclists. The promising use of Virthuman as an ATD substitute and the introduction of the developed helmet model lay the groundwork for future chapters' exploration and analysis.

5 Accident Reconstruction

5.1 State of the Art

An accident is an incidental (unplanned) event that causes unintentional injury and/or damage to property. Using accident reconstruction, we can describe the process of recreating the causal link between accident outcomes and the circumstances leading to it. This process can be based on the remaining traces and testimony of eyewitnesses. In this chapter, the term "accident reconstruction" will be used to describe the reconstruction of traffic accidents. Particular emphasis is placed on traffic accidents that involve PTW with the presence of the rider in de form of a numerical surrogate. Accident reconstruction is one of the components of forensic sciences. Usually, this term describes the application of scientific principles to determine accident mechanics.

The development of this forensic area was accelerated by the Industrial Revolution. The first recorded automobile accident happened in 1891 in Ohio City, Ohio. This accident involved a gasoline-powered buggy driven by engineer James Lambert. After hitting a tree root, Lambert lost control of his buggy and crashed into a hitching post. Because of this accident, the driver and his passenger suffered minor injuries [116]. Later on, in the times when the Ford-T became the common household good, the number of traffic accidents rose. To improve the work of the police departments photography became one of the most important tools for reconstruction teams as can be seen in Figure 5.1.

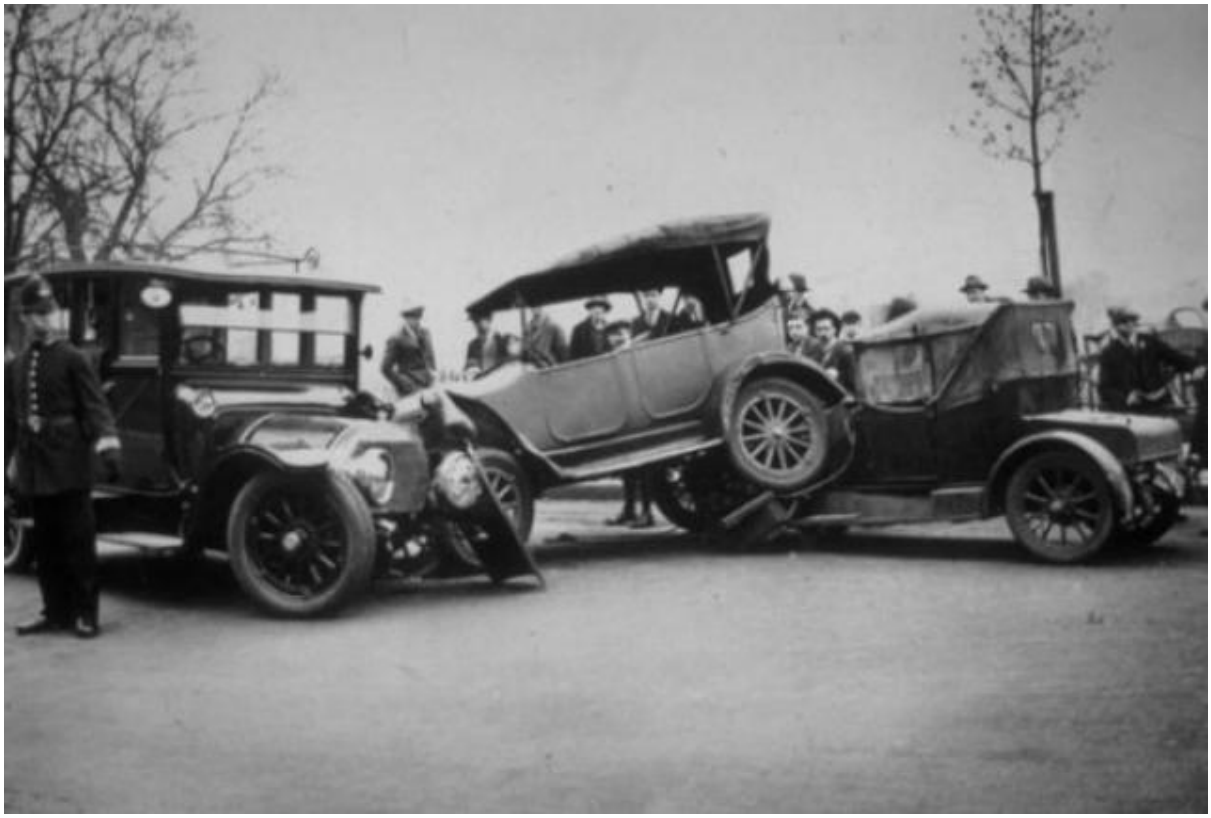

Figure 5.1. One of the first photographs shows a car accident with the Ford Model T [116]**.**

The first basic concept that should be applied during accident reconstruction is a coordinate system. Without using a coordinate system, any mechanical analysis cannot go too far. A reference frame concept allows the creation of a description of the position of bodies and/or parts of vehicles involved in an accident. Often the Earth is taken as a reference. For events that are discussed during traffic accident reconstruction, the Earth could be assumed as an inertial reference frame. Coordinates attached to the Earth are usually called “global coordinates”. There is a second type of coordinates, which are not fixed to the Earth. For them, the term “local coordinates” is usually used. For the reconstructionist, they are affixed to the various aspects of the accident parts. It should be recalled that “local coordinates” are often described as the non-inertial reference frame (they are exposed to non-zero acceleration).

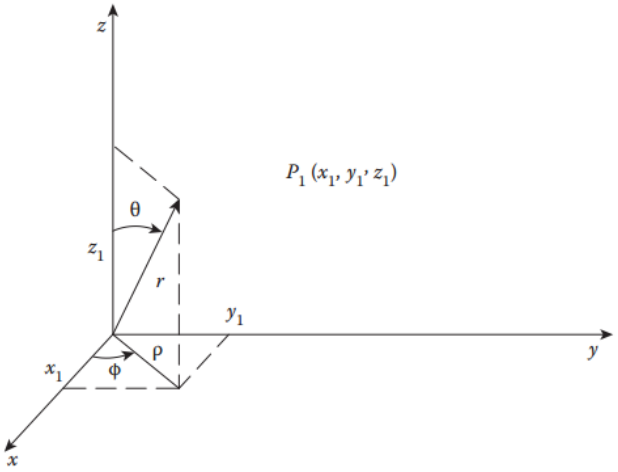

Figure 5.2. Cartesian coordinate system. [117]

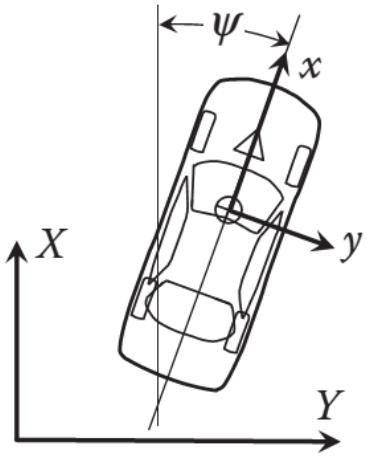

Figure 5.3. SAE coordinate system. [118]

Cartesian coordinates (depicted in Figure 5.2) are the most used system for accident reconstruction. The coordinates are described in three dimensions by mutually perpendicular coordinate axes. The convention of coordinate names goes in line with the right-hand rule. In this rule, the direction of the Z-axis is shown by the thumb during the rotation of the X-axis to the Y-axis position. The Society of Automotive Engineers (SAE International) has its own way of describing the “local coordinates” of a vehicle. This system is presented in Figure 5.3 It is also assumed to be right-handed; therefore, the Z-axis should point downwards. This system is widely known as SAE J670e-Vehicle Dynamics Terminology (1976).

One of the pivotal factors in determining the severity of a crash is the Energy Equivalent Speed (EES). In essence, EES signifies "The velocity of a vehicle impacting a fixed, rigid barrier that would yield a comparable level of damage to the observed damage on the analyzed vehicle"[119]. It's important to note that EES isn't synonymous with delta-V. Achieving a realistic simulation of an accident necessitates an accurate and realistic estimation of EES. Comparing the damage incurred by the vehicle with that of a vehicle possessing a known EES (sourced from various references) is integral. These references can encompass:

- Expert insights from accident reconstructionists,
- Databases of crash test results,
- Catalogs of EES values,

- Crash tests conducted by organizations like NCAP,
- Execution of dedicated crash tests (Figure 5.4).

Figure 5.4 Vehicle after an accident vs.
Vehicle after dedicated experimental reconstruction [119]**.**

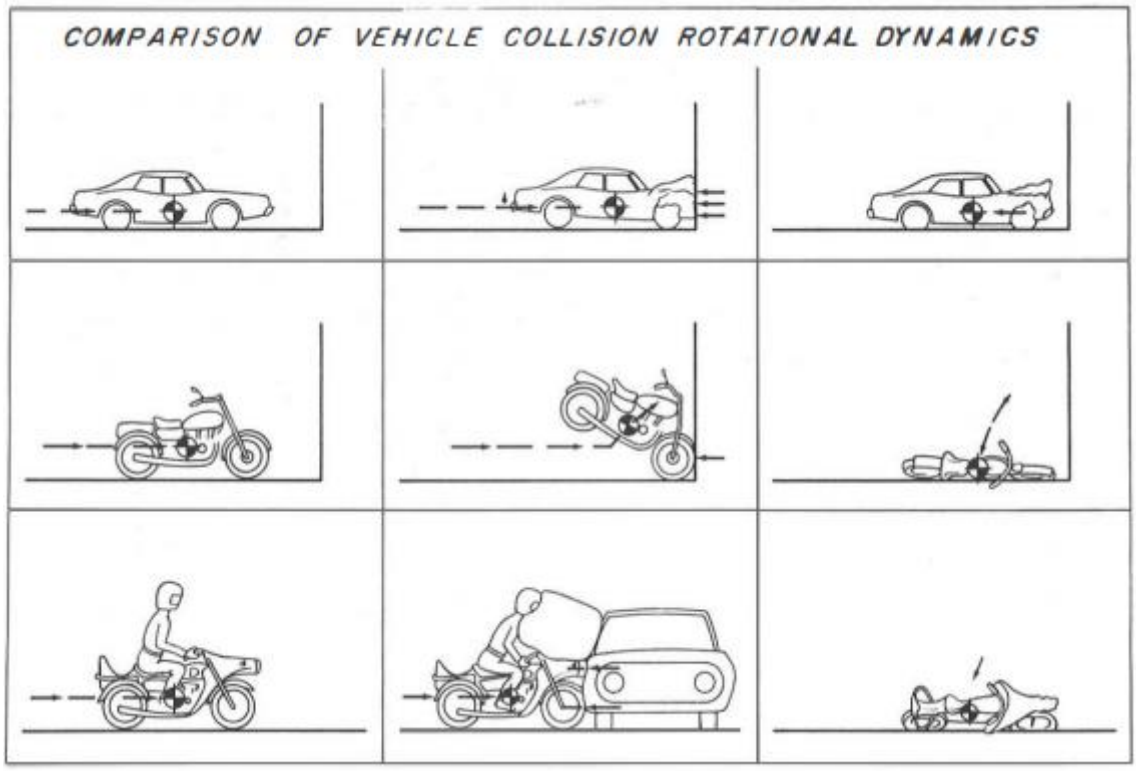

Figure 5.5 Rotational dynamics, car vs. powered-two-wheeler during a frontal crash [120]**.**

The comparison of the deformation observed on the vehicle that was crashed to the deformation on the reference crash-test vehicle allows us to estimate the absorbed energy. The EES is a quantity that is a more convenient derivative of the deformation energy and can be defined as:

$$EES = \sqrt{\frac{2 * E_{Def}}{m}}\ , \tag{5.1}$$

where: E_{Def} is the deformation energy of the vehicle [J], and the m is vehicle mass [kg]. The conservation of the energy after the accompanying deformation energy could be described by the following equation:

$$E'_{kin1} + E'_{kin2} = E_{kin1} + E_{kin2} - E_{Def1} - E_{Def2}\ , \tag{5.2}$$

where: E'_{kin1} and E'_{kin2} represents the kinetic energy of vehicles after impact, and E_{kin1} and E_{kin2} before the impact [121].

In 2012 O. Masory, in a series of papers [122, 123] presented a deep overview of current methods for motorcycle accident reconstruction. The first research paper analyzed the five most common methods for estimating the impact speed of the motorcycle to the side of the opposite vehicle (wheelbase reduction, two "total" crush models – with soft and stiff structure, conservation of linear momentum, and conservation of angular momentum). It was found that in the real accident scene the "total" crush models estimates the impact speed with highest confidence. The second paper [123] presented a preliminary study on applying adductive networks (AIM) for the estimation of the impact speed, the AIM studied in this paper was supervised trained with the experimental data. In his own words, the AIM method presents significant advantages: "It was obtained automatically using the AIM system and it is reasonably accurate. The model is explicit in contrast to non-explicit model that can be obtained by other learning procedures such an Artificial Neural Networks"[123]. A similar comparison of analytical and empirical methods in motorcycle accident reconstruction was presented by McNally [124], with case-by-case application of each method to the particular accident. This methodological effort allows the author to draw the conclusions about the limitations and applicability of the "momentum techniques ". Especially the differences in the motorcycle and opposite vehicle mass often seen in PTW collisions guided McNally to conclusion: "that momentum techniques are probably not appropriate, since even small changes in the input variables will produce large changes in the calculated speed of the motorcycle"[124]. However the author did not dismiss the methods which employ the conservation of angular momentum rule: "By properly evaluating the results of the momentum analysis with a sensitivity analysis, the reconstructionist can evaluate the applicability of these techniques to each individual collision."[124]

The Shanghai Jiao Tong University team led by Qian Wang conducted in 2020 advanced reconstruction of motorcycle accidents [125] by employing the MADYMO human body model, facet model of the opposite vehicle, and rigid model of PTW. The advantage of this research was to provide the kinematical validation of the simulation by utilizing the video recording from the real accident. Additionally, the MADYMO HBM has been modified to account for the realistic deformation of the lower and upper limb by changing the modeling approach for the lower limb and crating a hybrid human body model. The advantage of the Qian Wang research was the detailed modeling of the handlebar gripping by the PTW driver. The disadvantages of this approach was not to account for the deformation of the PTW structure which could led to the overestimation of the driver injury and also cause unrealistic kinematics from the time point of crash between the PTW and the OV.

Research expanding the reconstruction procedures to cases where the PTW has more than one occupant was published in 2019 by the team of Donghua Zou [126]. In his research, the MADYMO environment with the MBS modelling approach was employed for all accident participants (opposite

vehicle, PTW – scooter, and three scooter occupants). Besides reconstructing the real case, a parametric study on possible impact angle and crash speed was conducted. As with all reconstruction procedures that employ simulation also here the reconstruction approach could be described as forward-type, where by analyzing a large number of simulations the most fitted set of input parameters was chosen to find the best kinematical fit of the participants to the final position. The authors stated: "The most closely matched results were acquired when the speed of the microvan was set at 18 km/h and that of the scooter was set as 28.8 km/h."[126].

Besides the general purpose multi-body solvers (MADYMO, Adams) and general purpose explicit FEM environments (Ls-dyna, Pam-crash, Radioss) there are also special accident reconstruction software (PC-Crash [127], Virtual-Crash[128]) which can be used by forensic specialists without (or with reduced) labor intensive identification of material parameters. These softwares often utilized the same numerical methods as general-purpose environments. The main difference is the ease of use, already validated workflows for specific accidents, and build-in database of vehicles with their physical parameters (mass, inertia, coefficient of friction, etc.). They are especially useful for experts who needs working tool for accident reconstruction [129–131], without the time to deliberate the methods which stand behind the software.

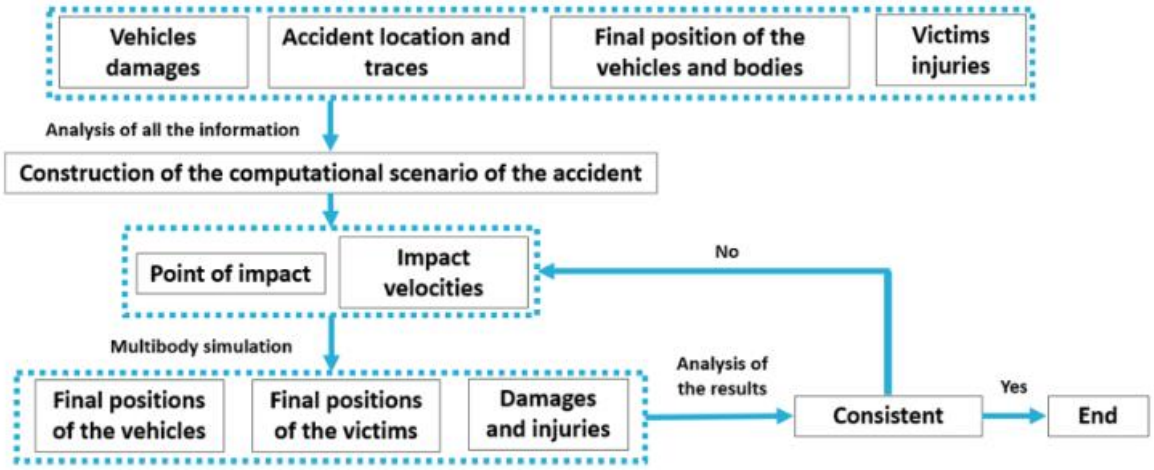

Figure 5.6. The forward(simulation-based) reconstruction methodology [130]**.**

The entire MBS-based reconstruction of 240 motorcycle accidents was conducted in the framework of "SECU2RM" project [132]. The reconstruction was made by the forward-looking approach by utilizing the MADYMO v7.5 software. The MBS 50th percentile human body model was weighted to body mass index (BMI) which represents the 5th, 50th, and 95th percentile of the population, BMI: 19 (1.76m, 59 kg), 24 (1.76m, 74 kg) and 32 (1,76, 99 kg) accordingly. To evaluate impact region to division for 15 impact zones was performed as depicted in Figure 5.7.

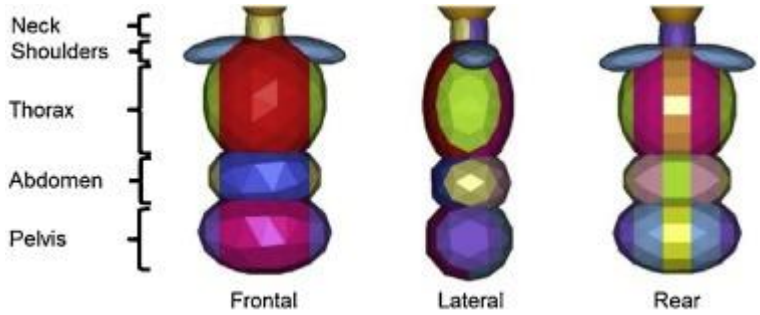

Figure 5.7. Division of body impact zones [132]**.**

5.2 Methodology

The inception of applying numerical methodologies to motorcycle passive safety can be traced back to as early as 1970 when LM models were employed to depict motorcycle crash scenarios [133]. The evolution of numerical simulations for PTW crash analysis has progressed from initial LM [134] to advanced MBS models and culminated in sophisticated FEM models, as succinctly summarized by Barbani [135]. Barbani also chronicled the historical trajectory of advancements in PTW crash simulations, which encompassed diverse studies [136–144] aiming to establish comprehensive numerical frameworks. These frameworks often incorporated models of the motorcycle itself, an opposing vehicle (OV), a surrogate for the motorcycle rider known as MATD, and, in select instances, even the helmet model (the most widely mandated protective gear by legal jurisdictions).

5.2.1 PTW Modelling

Noteworthy efforts were invested by researchers such as Chawla [145], Namiki [142], and Barbani [135] in the meticulous validation of their numerical representations of these accidents. However, as highlighted by Barbani [135], a universally accepted industry standard for motorcycle accident simulation remains elusive. This absence, coupled with the limitations in applying concepts like restraint or crashworthiness to PTW safety system development, perpetuates an unequal footing for PTW riders within the broader road transportation ecosystem, thereby underscoring the criticality of continued research in this domain.

In alignment with the findings from the MAIDS, the motorcycle was replicated as a PTW adopting a scooter-style configuration and mass characteristics that align with the L3 vehicle category (gross mass of 180 kg). This particular PTW archetype, commonly known as a Maxi Scooter, corresponds to models such as Suzuki Burgman or Piaggio Beverly. The depiction of this vehicle utilized a multi-body system framework, supplemented by an additional plastic joint hinge [146]. The multi-body system representation of the motorcycle encompassed 7 distinct bodies and 8 interconnecting joints (as depicted in Figure 5.8). The torque-rotation behavior of the plastic hinge joint was derived through the FEM simulation of a fork-bending test, adding an additional layer of detail to the model's realism.

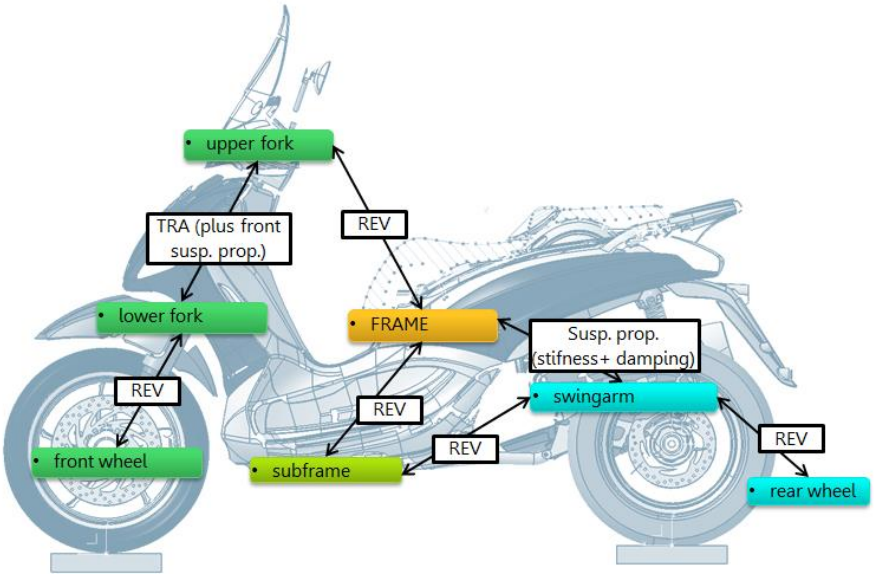

Figure 5.8 Conceptual MBS model of L3 scooter style PTW.

The numerical FEM experiment involved securing the fork's column in a stationary position, followed by the application of a bending force to the wheel mounting holes. Throughout the bending process, both the force exerted and the deflection angle were closely monitored. To determine the torque, the measurement of the distance from the region of peak stress to the mounting holes was utilized. Once a deflection angle of 0.25 radians was attained, the characteristics of the test were adjusted to replicate the interaction between the wheel and the chassis (depicted in Figure 5.9, Figure 5.10).

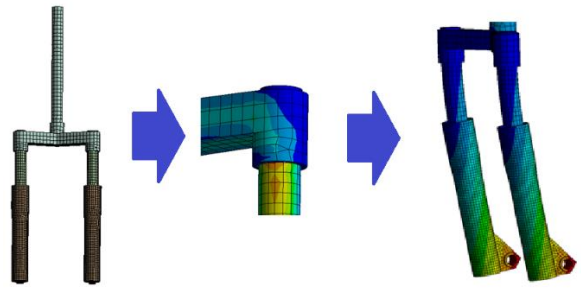

Figure 5.9 FEM procedure for obtaining bending characteristics for plastic hinges.

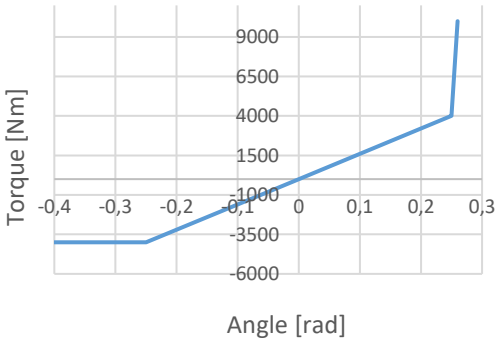

Figure 5.10 Fork plastic hinge characteristics.

The inertia properties of the PTW body parts have been obtained from the project partner in the MOTORIST project (Table 5.1). The inertia data were described in relation to the principal axis of particular motorcycle body part and can be found in the following table. The suspension properties were adopted from the Piaggio Beverly 350 PTW (depicted in Figure 5.12).

Table 5.1 PTW MBS model body part inertia and mass.

	Mass [kg]	I_{xx} [kg*m^2]	I_{yy} [kg*m^2]	I_{zz} [kg*m^2]
Frame	106.6	7.1	16.6	15.3
Fork upper	4.13	0.207	0.013	0.212
Fork lower	9.39	0.351	0.305	0.052
Front wheel	7.5	0.25	0.25	0.5
Rear wheel	7.5	0.25	0.25	0.5
Swing arm	50	1.26	3.6	1.26
Sub-frame	0.01	--	--	--

The coupling interfaces for the modeled PTW are: wheels meshed geometry by automatic contact 33), chassis and seat (by automatic contact 33), and handlebar to VH hands (by breakable spring joining hands and handlebar). The geometry of these parts (chassis with seat, wheels, handlebar) was modeled by using the shell elements with the Young modulus in the range which allows obtain quasi-realistic contact forces (here it is worth noting that the contact force by the PAM-Crash algorithm 33 between two parts has a component of Young modulus, that why it was necessary to tune this parameter, otherwise for the MBS body part the inertia parameters are enough to describe the dynamics of the system). Parts of the PTW in the MBS representation which are not expected to be in contact with another object did not receive their own geometrical representation besides the simple bar which depicts the distance between the joints connected to the particular part of the MBS. This strategy can be seen by comparing the images in Figure 5.8 and Figure 5.11 (subframe, swing arm, and the lower fork).

Figure 5.11 Implemented MBS model of maxi-scooter.

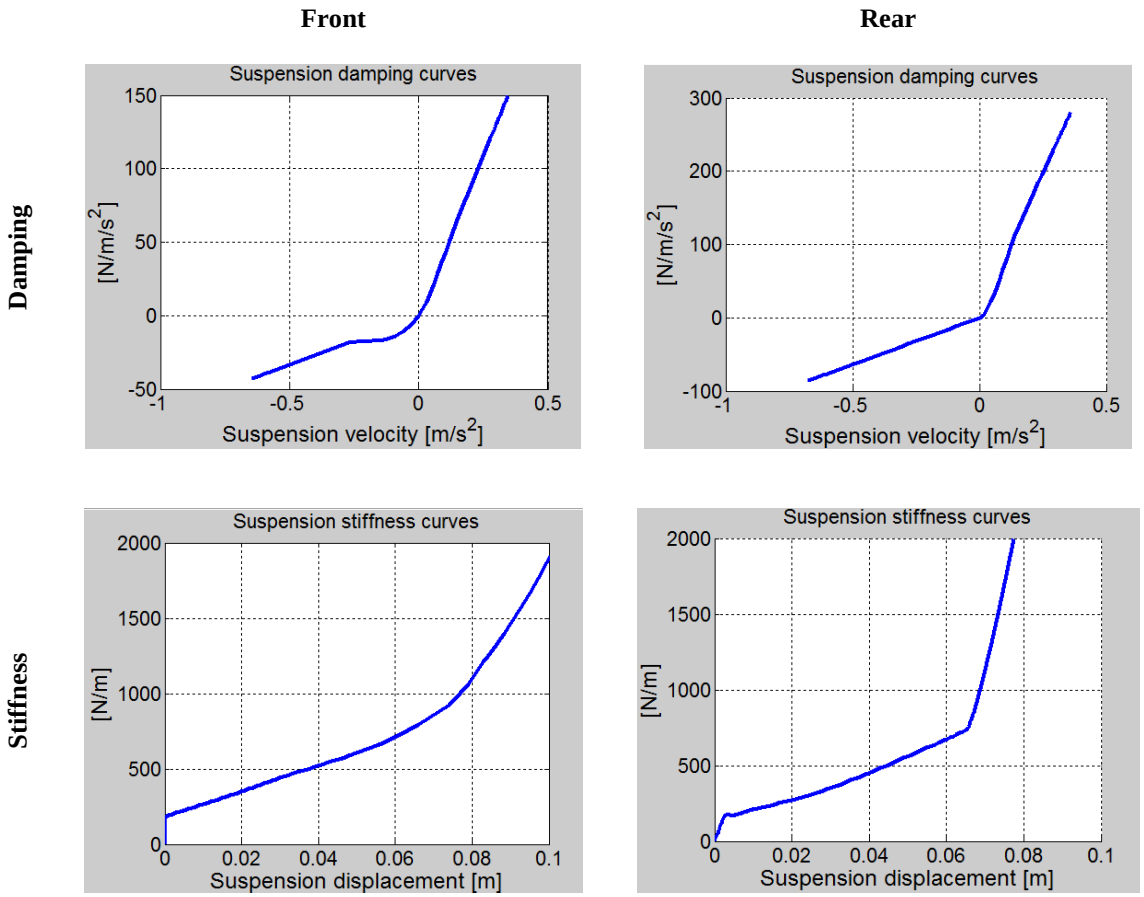

Figure 5.12 Implemented suspension characteristics.

5.2.2 OV Model and Simplification

5.2.2.1 Base model

The FEM approach was utilized by NCAC [147] to create the numerical model of the Chrysler vehicle. The initial iteration of this model was developed using the commercial FEM software, LS-Dyna 970-5434a. The components comprising the building blocks of the numerical Neon model are itemized in the subsequent table.

Table 5.2 Chrysler Neon FEM model parameters.

Parts	Nodes	Solids	Beams	Shells	Elements
336	283859	2852	122	267786	270768

The primary focus of the model's development was on frontal impact scenarios. Its validation was conducted through NCAP frontal crash procedures [147]. The NCAC validation process indicated the model's numerical stability up to speeds of approximately 40 miles per hour (~17.9 m/s). Additionally, the ESI Group recreated this specific car model in their software, as shown in Figure 5.14. In the cases discussed in this chapter, the differences in mass between the Chrysler and the opposing vehicles (OVs) were adjusted using the built-in "Mass Trimming" tool within VPS. This tool enables the

distribution of additional mass among all nodes of the model. It's worth noting that while a complete FEM model could prove valuable for real accident reconstructions, it might introduce high time step-related computational demands for parametric studies or optimization processes. To address this, model simplification could be considered, followed by an assessment of its behavior relative to the intended scenario configuration for which the model will be employed.

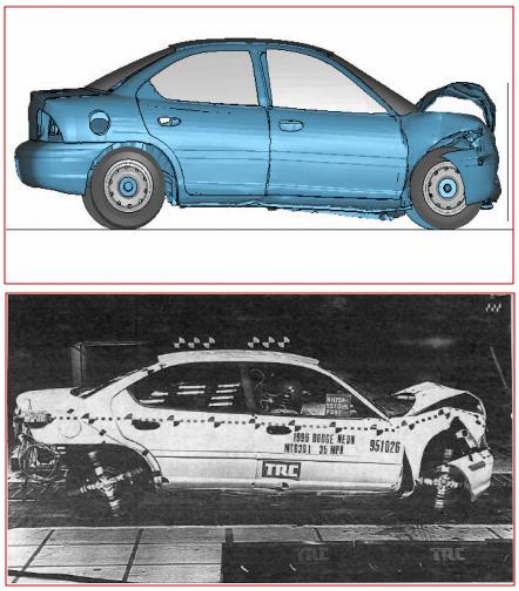

Figure 5.13 The NCAC validation of the Neon FE model [147]**.**

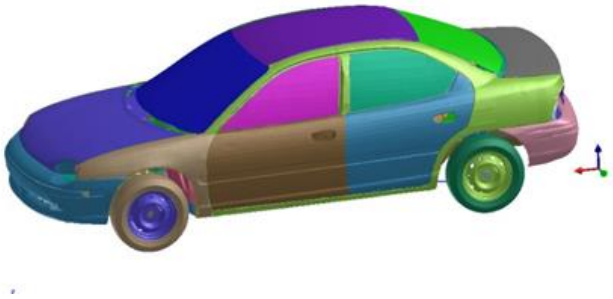

Figure 5.14 The VPS (PAM-Crash) version of the Chrysler Neon.

5.2.2.2 Simplified models and validation

Considering the substantial quantity of elements and components in the original vehicle base model (Table 5.2), a streamlined version of the vehicle model was devised, maintaining the same mass and inertia properties. Furthermore, to cater to prevalent real-world crash scenarios (frontal impact, side impact, rear impact), several simplified Neon models were formulated. During this simplification process, the primary structure responsible for energy absorption in impact simulations was preserved. Refer to Figure 5.15 for an illustration of the simplified Neon FE models designed for frontal, rear, and side impact simulations.

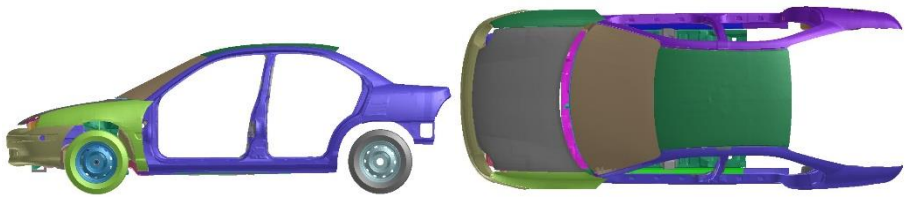

(a) Frontal impact

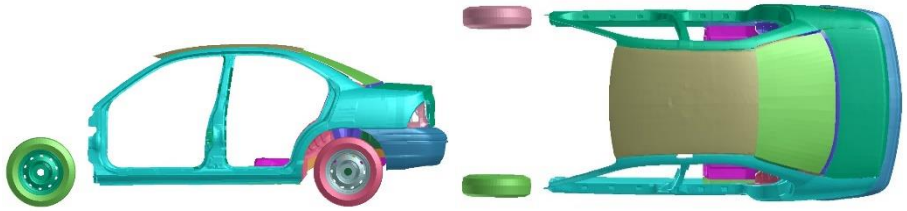

(b) Rear impact

(c) Side impact

Figure 5.15 Side view and top view of simplified Neon FE models.

To reconfirm the mechanical behavior of the simplified models, a procedure was employed that compares the deformation of these simplified models with their respective full models. The moving deformable barrier (MDB), possessing a gross mass of 950 kg, was utilized as the impactor in each revalidation scenario. Initial velocities of 30 km/h or 50 km/h were assigned for the MDB in each case.

The revalidation of the simplified frontal impact model encompassed four configurations: full frontal impact, 50% offset frontal impact, bumper end impact at 45 degrees, and side-impact onto the fender. Detailed setups for each scenario are outlined in the appendix. For the rear impact simplified Neon model, validation involved constructing simulations for 100% rear impact and 50% offset rear impact, with MDB speeds of 30 km/h and 50 km/h. The simplified side-impact model was validated in a single configuration with the MDB impacting the B pillar (see appendix). In each configuration, the maximum deformation of two horizontal and one vertical lines on the body part was assessed. The nodal line positions are illustrated in the appendix.

The outcomes of the revalidation efforts are summarized in Table 5.3. The results reveal that the frontal impact model conforms to the 5% error criterion for agreement with the full model in six out of eight cases. In the remaining two cases (side fender impact at 30 km/h and bumper end impact at 50 km/h), the deformation was within the threshold of 10% error. Evaluation of the simplified side model indicates that in every instance, the deformation satisfies the 10% error criterion.

Table 5.3 Simplified FE Neon model assessment.

	Frontal model				**Rear model**		**Side model**
	Full frontal	Frontal 50% offset	Bumper end (45 deg.)	Fender	100% rear impact	50% rear impact	B pillar impact
30 km/h							
50 km/h							

5.2.3 Models Coupling

Throughout the simulation, four key macroscopic entities were employed, including the PTW, the OV (opposite vehicle), the occupant, and the helmet. Prior to commencing the numerical calculations, it was imperative to meticulously position and integrate these entities. The coupling procedure encompassed the following steps:

1. Scaling the Virthuman in accordance with the PTW occupant's specifications.
2. Coupling the Virthuman with the PPE.
3. Placing the Virthuman in a seated posture.
4. Establishing coupling between the Virthuman and the PTW at their contact points.
5. Positioning the PTW alongside the occupant.
6. Defining the initial velocities of both the PTW and the OV.
7. These systematic steps ensured the coherent integration and alignment of the various entities involved in the simulation.

A symmetrical contact interaction between the rider and the motorcycle is established in the simulation. The connection between the hands and handlebars is represented through breakable springs with a stiffness of 9.36 kN/m [148] and a maximum force limit of 350 N [149] for each hand. The simulation is conducted until the point of reaching the most critical injury criterion.

The ground is modeled as a rigid plane with a consistent friction coefficient of 0.7 [150, 151, 152]. To ensure accuracy and compliance, the outputs of specific joints (forces and moments) and nodes (head center of gravity acceleration) are filtered according to the guidelines of the SAE J211 standard prior to result evaluation. For clarification, it should be noted that the entire model preparation – simulation – evaluation pipeline is performed under the ESI Virtual Performance Solution software package.

5.3 Results

The subsequent chapter of this work will delve into the practical application of the discussed concepts and methodologies. Specifically, it will focus on the numerical reconstruction of three different Powered Two-Wheeler (PTW) accidents. These reconstructions will utilize the forward reconstruction method outlined in the state of the art review, combined with the simulation pipeline detailed in the current chapter.

By implementing this approach, the chapter will aim to provide comprehensive insights into the dynamics of the selected PTW accidents. The simulation pipeline, incorporating the virtual human body model, motorcycle dynamics, and helmet interactions, will be employed to recreate and analyze the sequence of events leading to each accident scenario.

Through this numerical reconstruction, the chapter intends to demonstrate the applicability and effectiveness of the developed methodologies in shedding light on the critical factors and mechanisms involved in real-world PTW accidents. This approach offers a valuable opportunity to gain a deeper understanding of accident scenarios, contributing to the improvement of motorcycle safety measures and accident prevention strategies.

5.3.1 In-SAFE cases

The In-depth Study of Road Accidents in Florence (In-SAFE) initiative was established by creating the methodology involved forging a collaboration between the Department of Mechanics and Industrial Technologies at the University of Florence and the Intensive Care Unit of the Emergency Department at Careggi Teaching Hospital, Florence. The primary objective was to gather comprehensive information related to road accidents. The compiled dataset encompasses a range of details, including on-scene observations, vehicle examination findings, crash dynamics and kinematics data, injury documentation, treatment procedures, and injury mechanisms. Each injury is systematically coded using the AIS score, accurately localized using a three-dimensional human body model derived from computed tomography slices, and relevant key scores are computed. This data is subsequently linked to the specific causes of injuries and the technical parameters of the crashes. The entirety of this data is systematically stored and organized within the In-SAFE database [153]. The author of this dissertation obtains the records from the database by collaboration under the MOTORIST project.

5.3.1.1 Case 1

5.3.1.1.1 Accident description

The initial case under examination occurred in October 2012 and is centered on an incident that transpired on Dante Alighieri Street in the city of Calenzano during the evening hours. The collision entailed a Piaggio Beverly 400 and a 2004 Ford Fiesta. The nature of the accident can be categorized as a "Head-on-side collision." The event unfolded on a dry asphalt surface, and the street was illuminated by public street lights.

According to the site summary, the accident unfolded on a dark autumn afternoon, with the road visibility enhanced by public illumination. The driver of the car was proceeding in the direction of the oncoming PTW. The car driver had come to a halt in the middle of the road, with the intention of making a left turn into the vicinity of a petrol station. Unfortunately, the PTW rider became aware of

the driver's maneuver when it was too late to react effectively. Although the rider attempted to brake, the collision could not be averted [154].

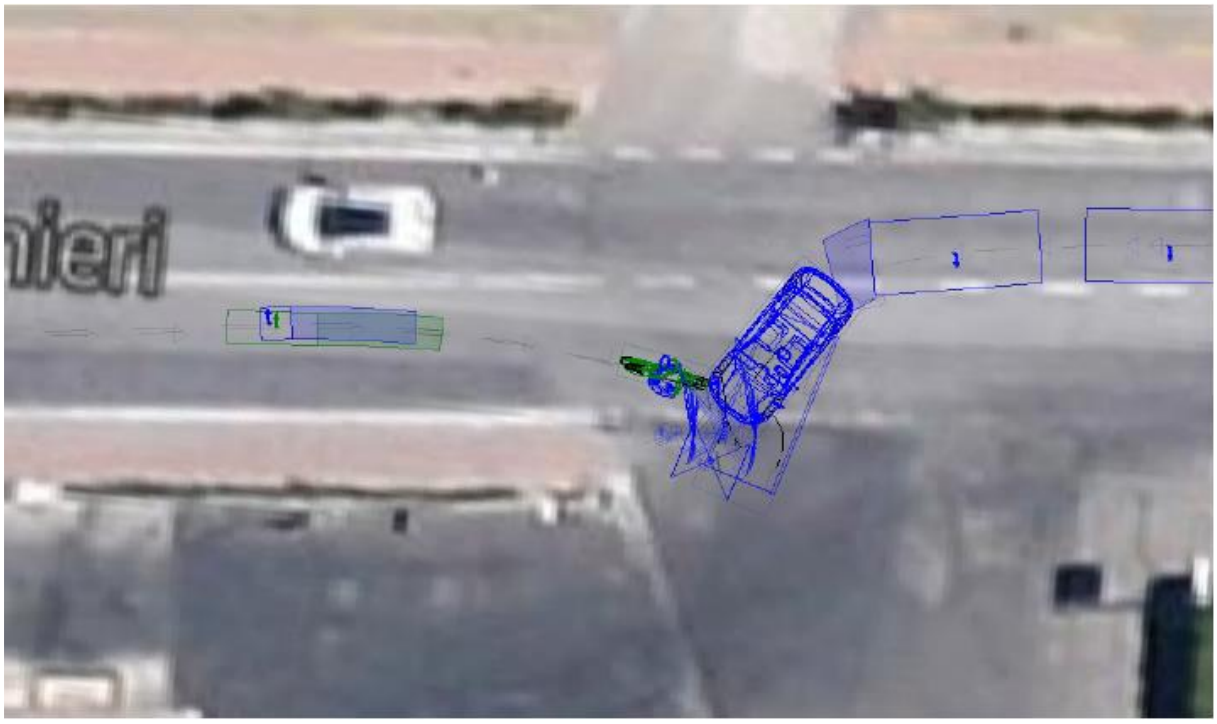

Figure 5.16 The Case 1 accident site [154]**.**

Employing cutting-edge technology, an investigative team conducted an examination of the site. A sketch of the scene was created, which was subsequently integrated into Google Maps for enhanced visualization (Figure 5.16). Furthermore, photographs capturing the damage sustained by the involved vehicles were taken and meticulously cataloged for reference (Figure 5.17 - Figure 5.23).

Figure 5.17 Case 1: Vehicle A front [154]**.**

Figure 5.18 Case 1: Vehicle A front glass [154]**.**

Figure 5.19 Case 1: Vehicle A crumple zone [154]**.**

Figure 5.20 Case 1: Vehicle A zoomed crumple zone [154]**.**

Figure 5.21 Case 1: Vehicle B [154]**.**

Figure 5.22 Case 1: Damages on vehicle B zoomed [154]**.**

Figure 5.23 Case 1: Vehicle B bended front fork [154]**.**

Subsequently, the configuration of the accident was determined by considering factors such as the final positions of the vehicles, the presence of skid marks, and the accounts provided by the drivers. The PTW collided with the car from its right side, specifically, it can be seen around the front lamp area (Figure 5.19). The angle formed between the Vertical longitudinal planes of the vehicles was approximately 114 ± 5 degrees (Figure 5.24), conforming to the guidelines set forth by the ISO 13232-2005 standard [155]. Vehicle A, a car with three occupants, had a mass of roughly 1300 kg, while the PTW weighed around 260 kg with the driver on board. Importantly, the PTW rider was wearing a helmet at the time of the accident, and he was identified as a male approximately 52 years of age.

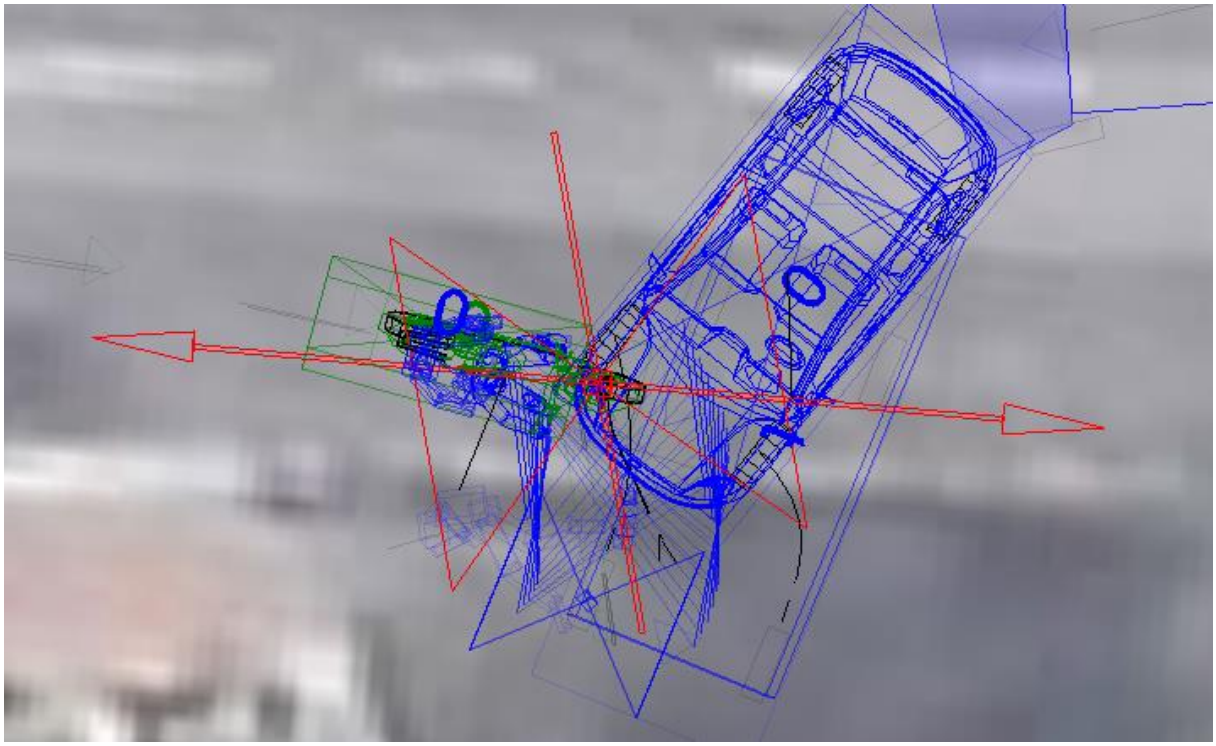

Figure 5.24 Case 1 accident configuration [154]**.**

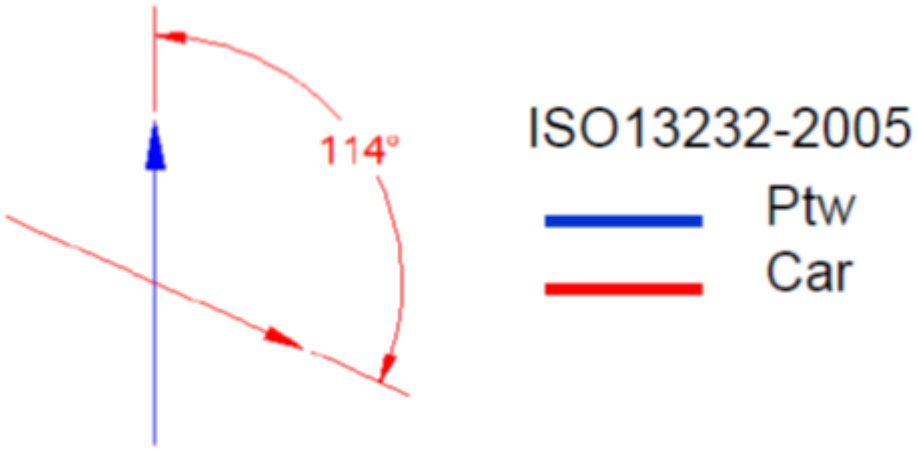

Figure 5.25 Case 1: ISO description [154]**.**

Utilizing the Virtual-Crash software (depicted in Figure 22), the IN-SAFE team undertook the reconstruction of the Case 1 accident. The analysis yielded the following findings:

Vehicle A, which corresponds to the car:

- Was in the process of executing a U-turn.
- Initiated braking approximately 2.5 seconds prior to the collision.
- Was traveling at an approximate speed of 15 ± 5 km/h.
- Collided with a speed of around 10 ± 3 km/h.
- Experienced the EES of about 12 ± 3 km/h.

Vehicle B, representing the PTW:

- Engaged in braking maneuvers around 0.5 seconds before the accident.
- Was traveling at a velocity of approximately 74 ± 5 km/h.
- Experienced a crash impact speed of about 55 ± 3 km/h.
- Had a roll angle of -90 degrees at the time of collision.
- Demonstrated the EES of approximately 12 ± 3 km/h.

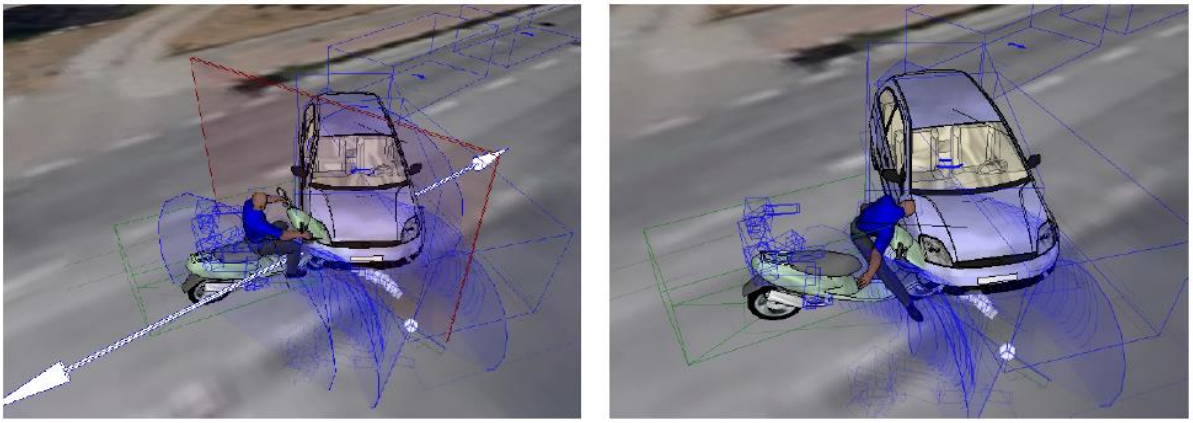

Figure 5.26 The reconstruction made by the IN-SAFE team [154]**.**

From a medical examination, the PTW driver´s injuries were found. The driver suffered four types of injuries:

- Serious injury of the left femur,
- Moderate injury of the left tibia,
- Moderate injury of the left fibula,
- Serious injury of the thorax.

5.3.1.1.2 Accident numerical setup

The first step for an accident simulation is the positioning of the vehicles and the occupant. In Case 1, the OV and the PTW were positioned according to the figures from the case description (Figure 5.24 - Figure 5.25). The angle between the vehicles was equal to 114 deg.

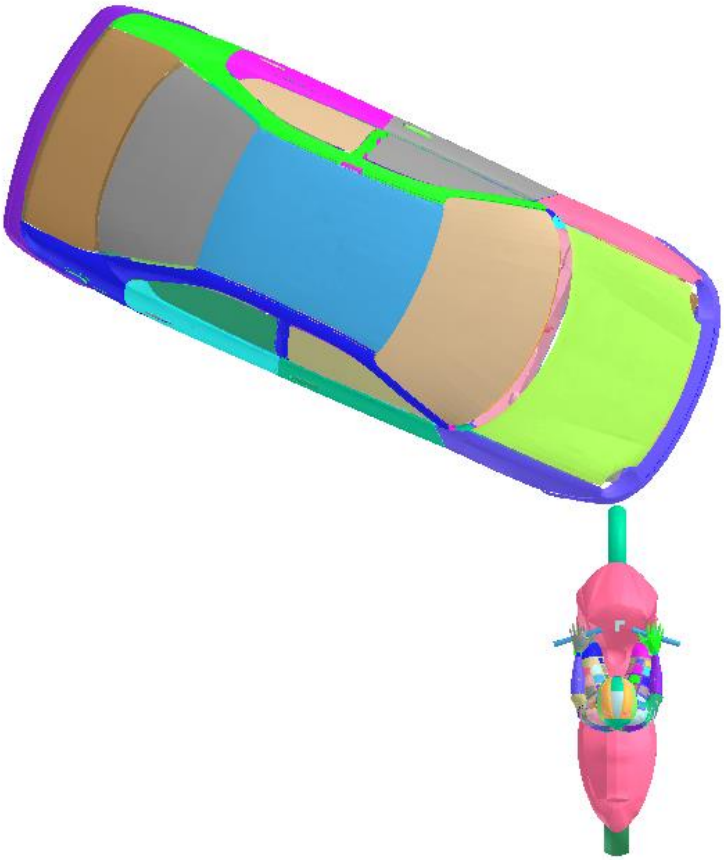

Figure 5.27 Case 1 simulation setup.

The initial velocities were as follows:

- The PTW: 55 km/h,
- The OV: 10 km/h.

5.3.1.1.3 Results and discussion

The accident's kinematics are illustrated in the preceding figures (Figure 5.28, Figure 5.29), showcasing distinct sub-phases of the PTW crash. These sub-phases reveal the progressive sequence of events. Initially, the PTW's front fork experiences compression (0 – 30 ms). Subsequently, deformation of the fork becomes evident (30 – 60 ms). The third phase of kinematics involves the PTW's rotation around the contact point. Simultaneously, the occupant's movement can be characterized as follows: Initially, the rider's body begins to slide forward from the seat due to the PTW's deceleration. As the PTW slows down, the rider's hands experience compression against the handlebar. Upon reaching the coupling spring force of 350 N between the hands and handlebar, the spring fractures. Subsequently, the upper part of the rider's body overtakes the PTW, while the lower part remains compressed by inertia forces acting on the PTW's front frame. Consequently, the lower extremities become immobilized by the PTW frame, leading to the generation of a torque affecting the rider's body. This torque induces rotation of the rider around the point of contact between the abdomen and the motorcycle (90 - 120 ms). As a result of this rotational motion, the rider's head ultimately makes contact with the hood of the OV.

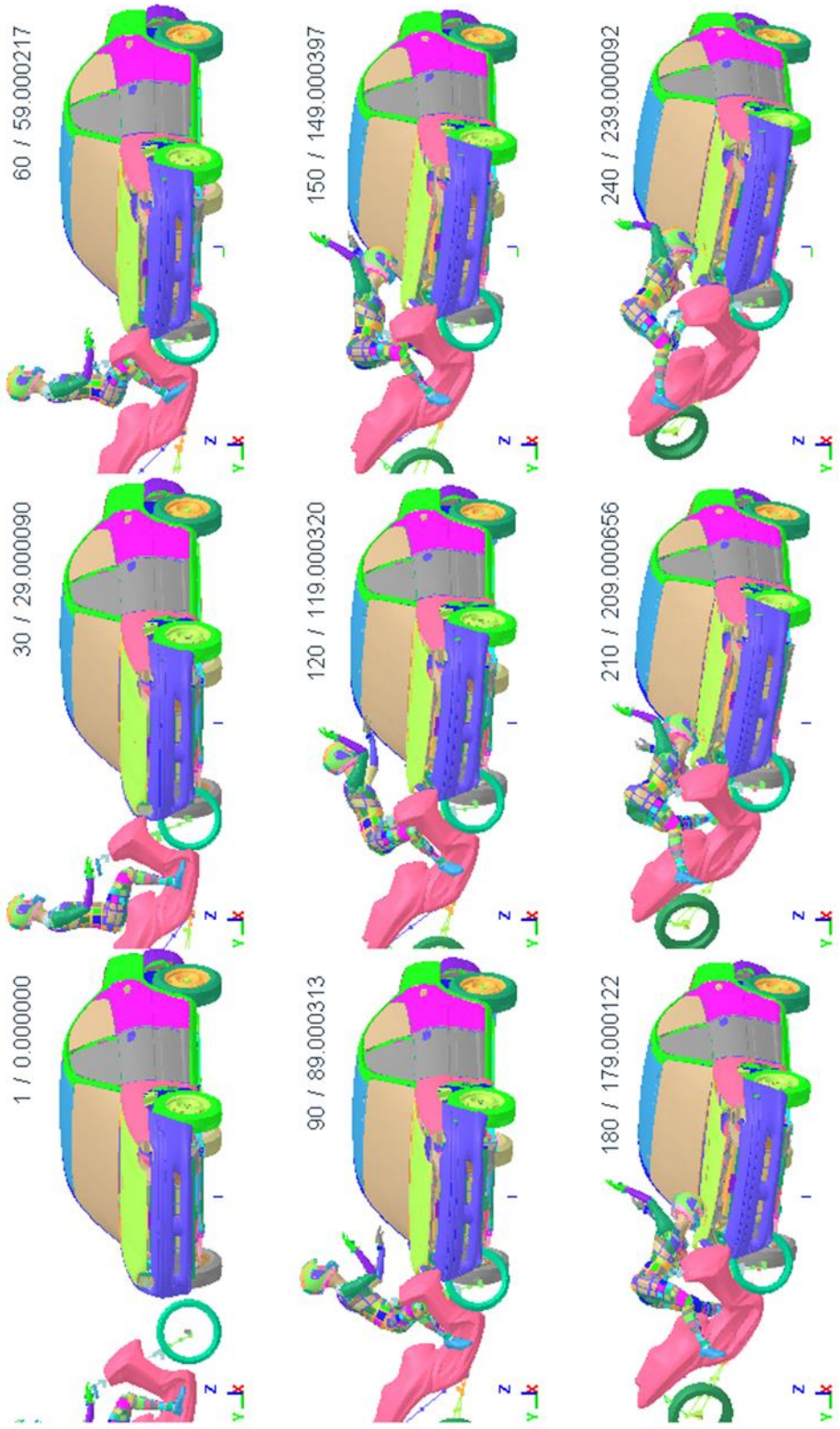

Figure 5.28 Side view on the Case 1 simulation time-frames.

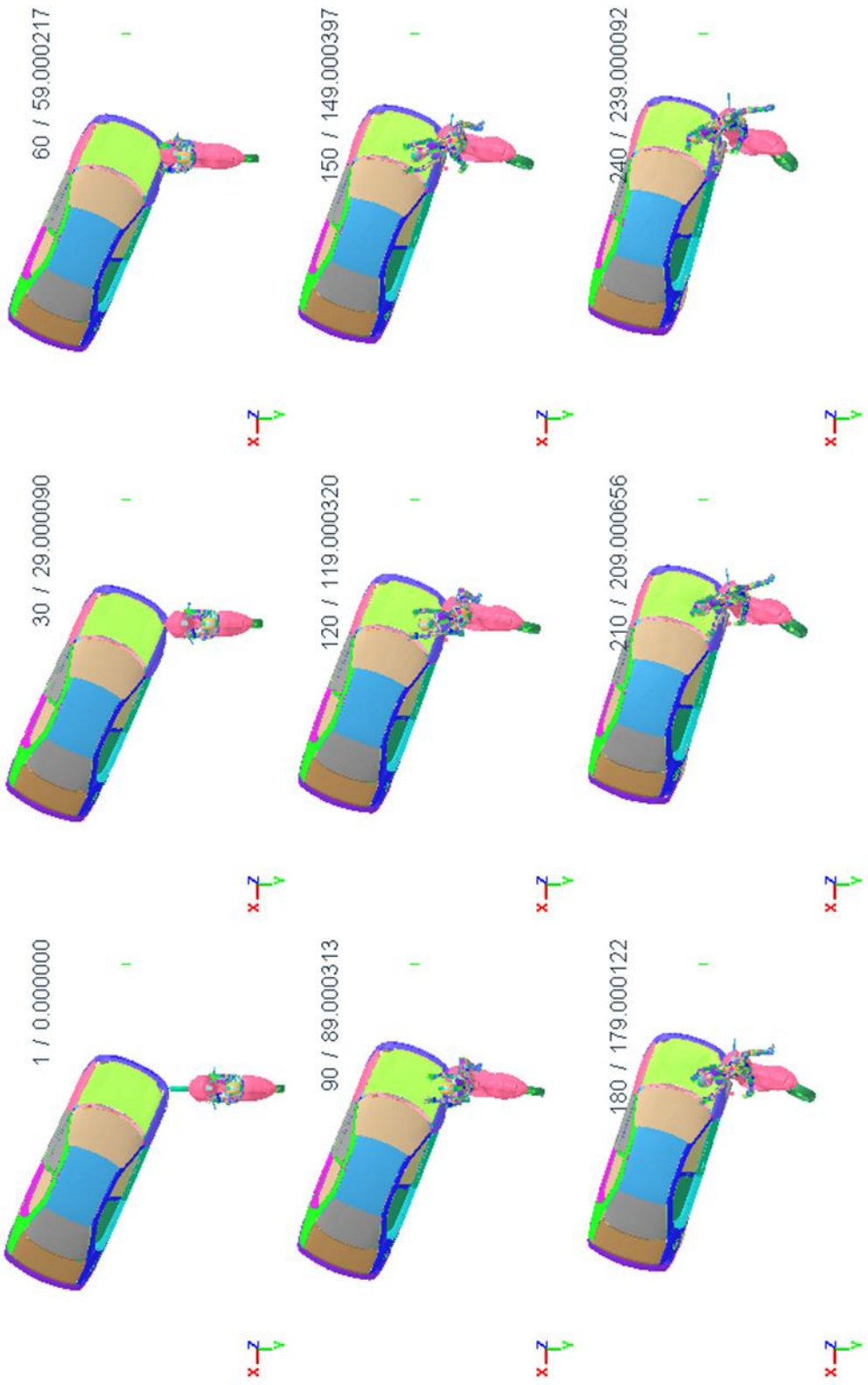

Figure 5.29 Top view on the Case 1 simulation time-frames.

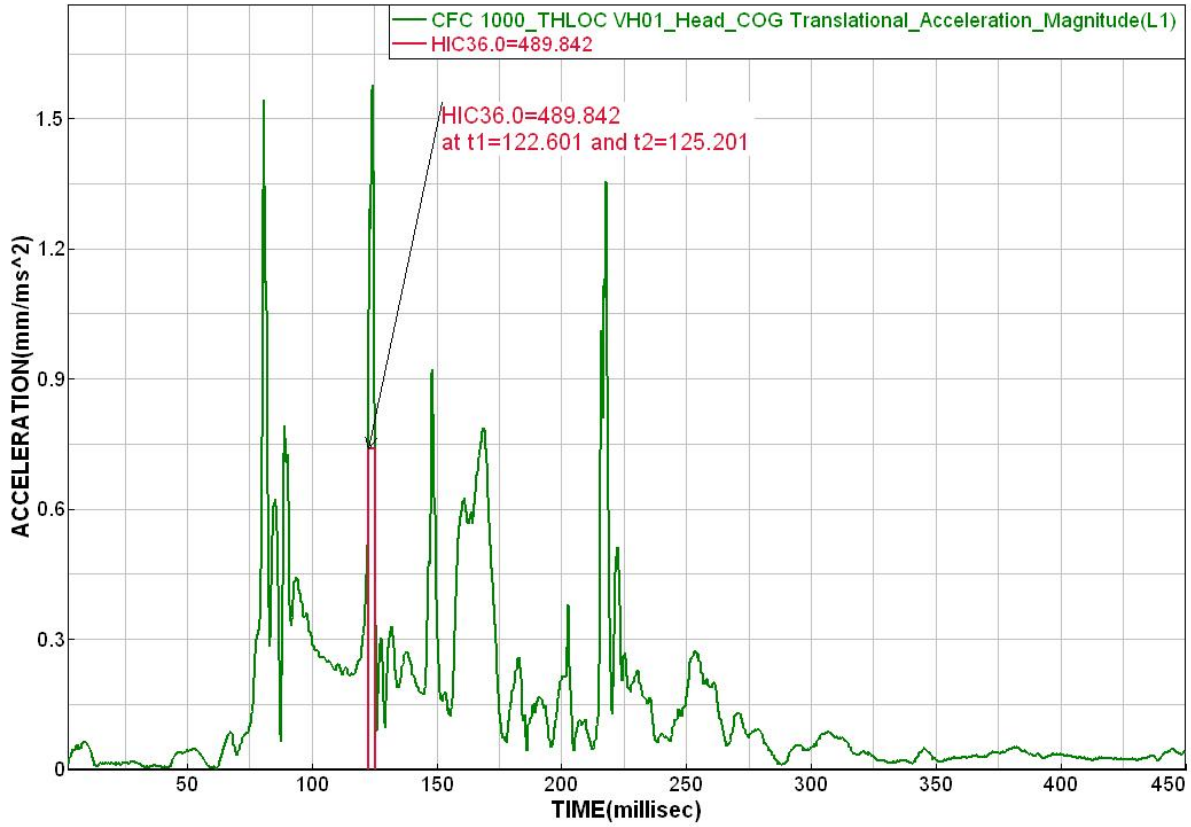

Figure 5.30 Head COG acceleration in Case 1.

The initial momentum and angle of the oncoming vehicle lead to a modification in the trajectory of the motorcycle (causing it to rotate clockwise). This adjustment results in contact between the left side of the motorcycle and the left leg of the rider (between 150 - 240 ms). The force of this contact between the leg and the motorcycle's side has the potential to induce significant leg injuries. By analyzing the acceleration experienced by the head's CO), it's possible to calculate the HIC. For this reconstructed case, the HIC is measured at 489 (as shown in Figure 5.30). This value aligns with the medical examination of the motorcycle rider, which reported injuries no higher than AIS1.

Assessment of the accelerations of the T1, T8, and T12 vertebrae (as seen in Figure 5.31-5.33) reveals that between 175 and 225 ms, the thoracic portion of the vertebral column encountered exceedingly high acceleration peaks (ranging from 6 to 24 mm/ms^2). Prior to analysis, the acceleration data was filtered according to the SAE standard [156], utilizing the CFC 1000 filter. Virtual accelerometers positioned at the 4th and 8th rib areas manifest similar acceleration peaks (as indicated in Figure 5.34, 5.37). This peak acceleration could be attributed to the extensive rib fractures documented by the hospital. Examination of the rider's kinematics unveils that these acceleration peaks coincide with the rotational movement of the rider's body. Throughout this rotational motion, the rider's ribcage came into contact with the front section of the motorcycle frame.

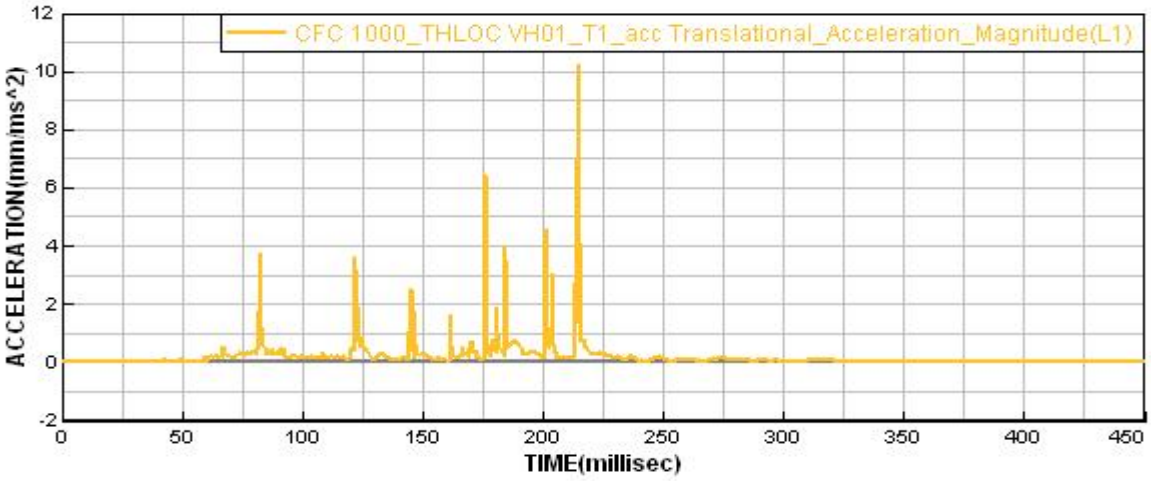

Figure 5.31 T1 vertebra acceleration.

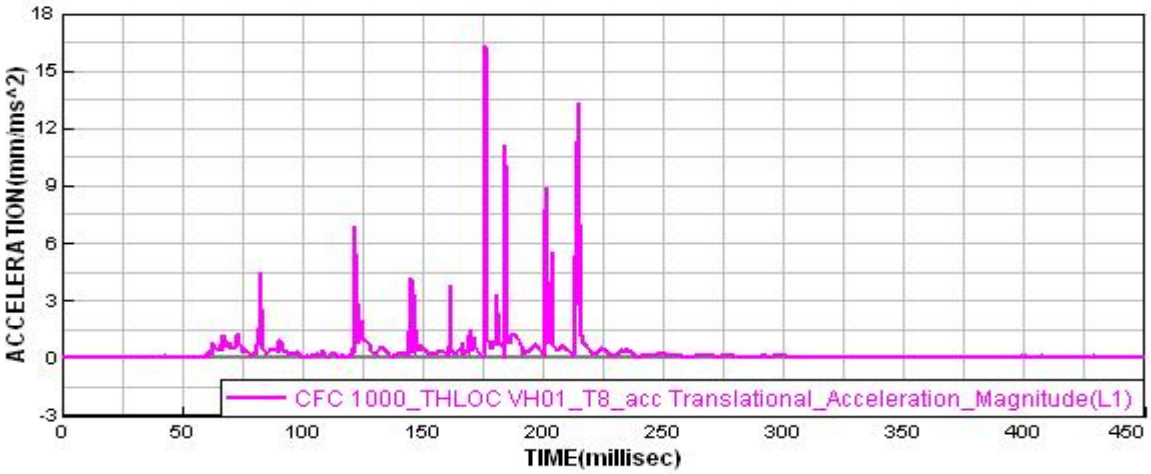

Figure 5.32 T8 vertebra acceleration.

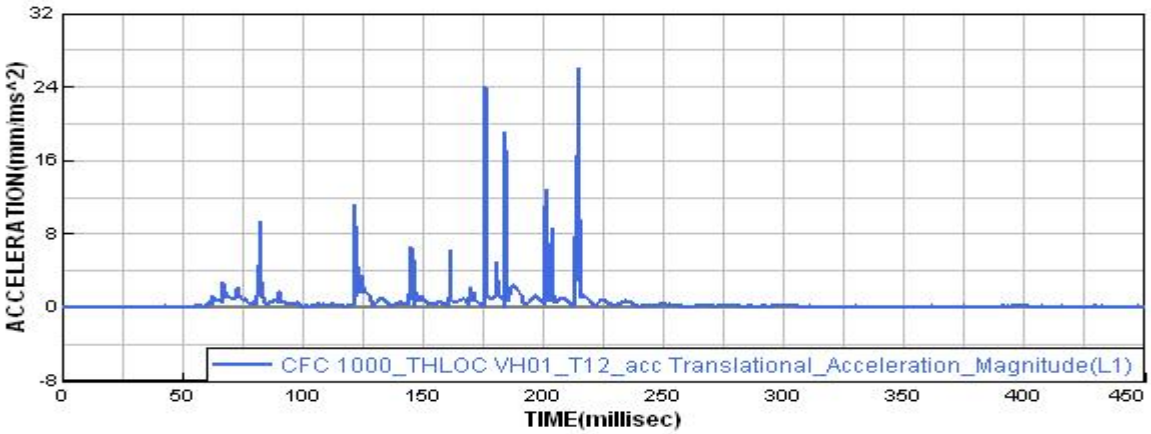

Figure 5.33 T12 vertebra acceleration.

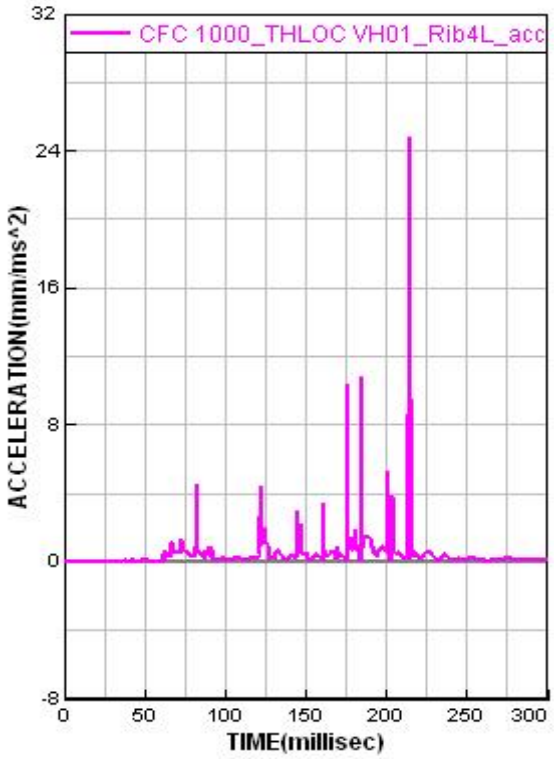

Figure 5.34 4th left rib acceleration.

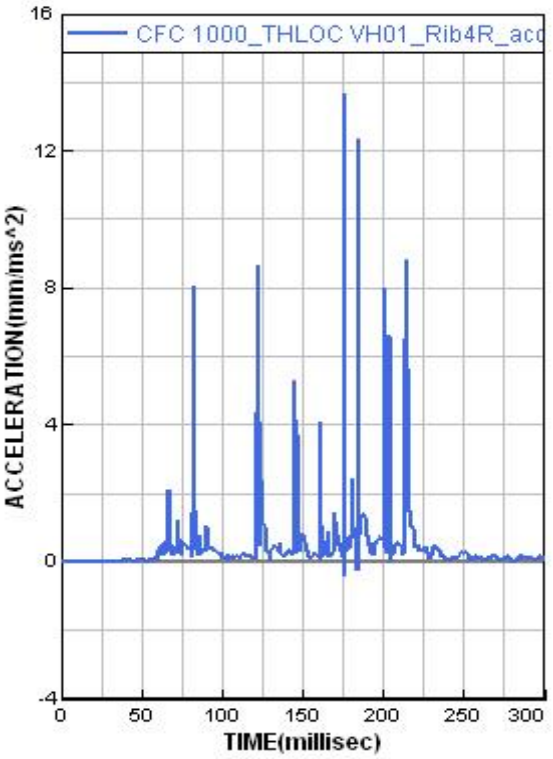

Figure 5.35 4th right rib acceleration.

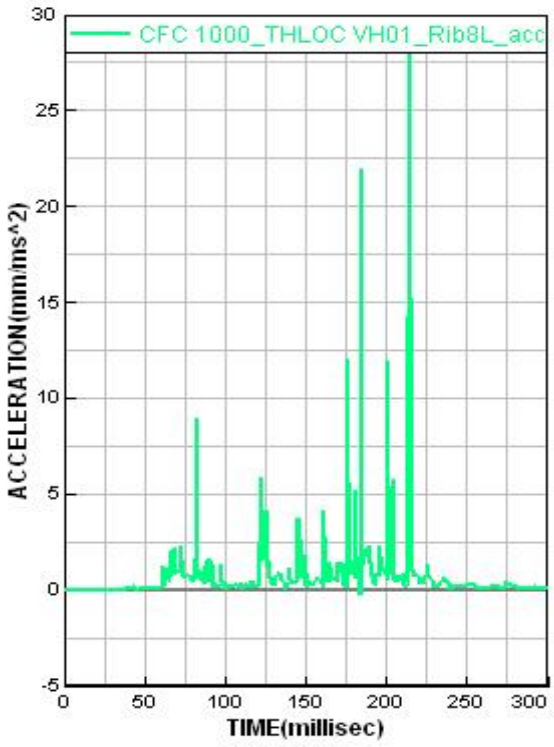

Figure 5.36 8th left rib acceleration.

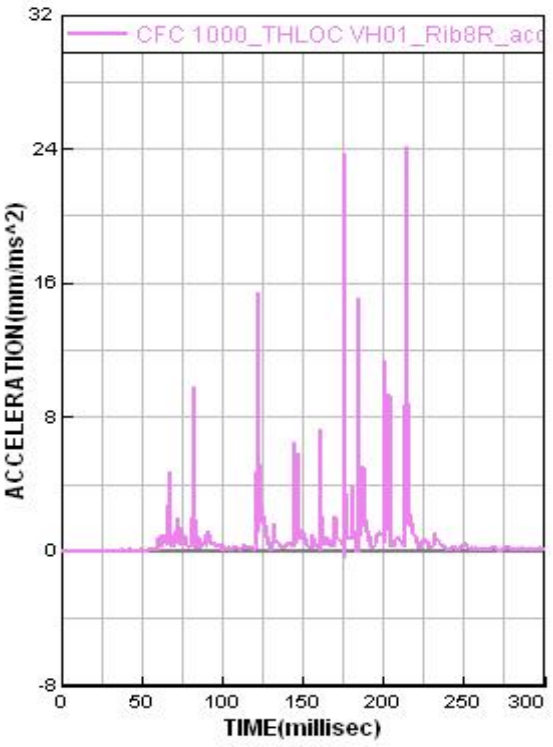

Figure 5.37 8th right rib acceleration.

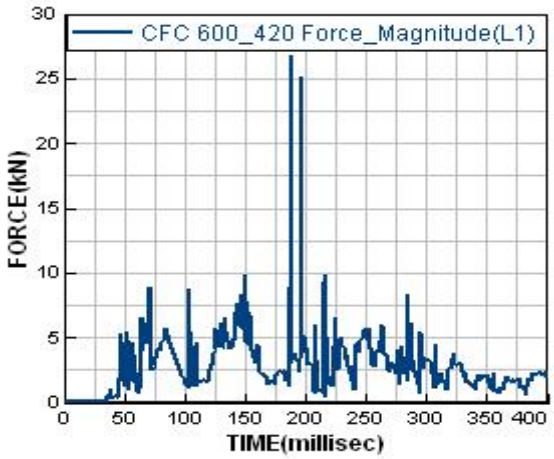

Figure 5.38 Force magnitude in joint 420.

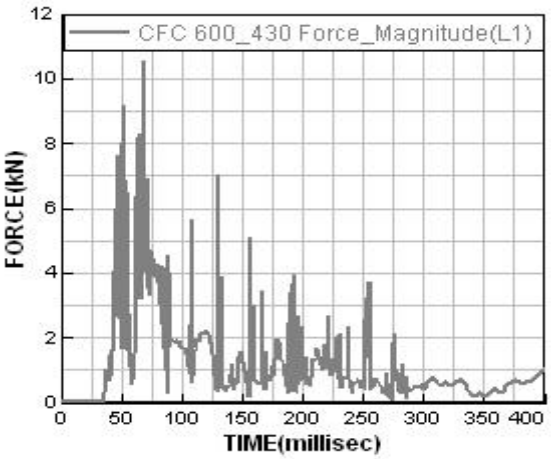

Figure 5.39 Force magnitude in joint 430.

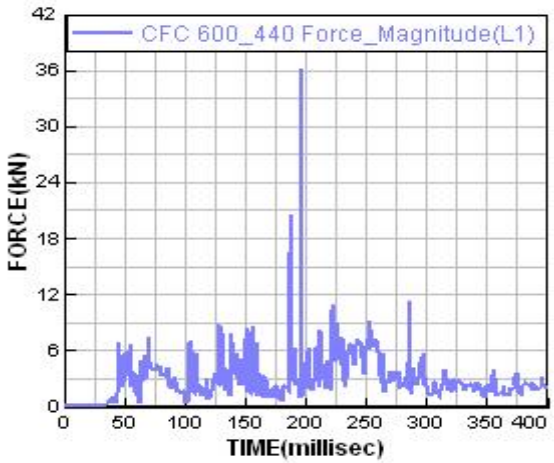

Figure 5.40 Force magnitude in joint 440.

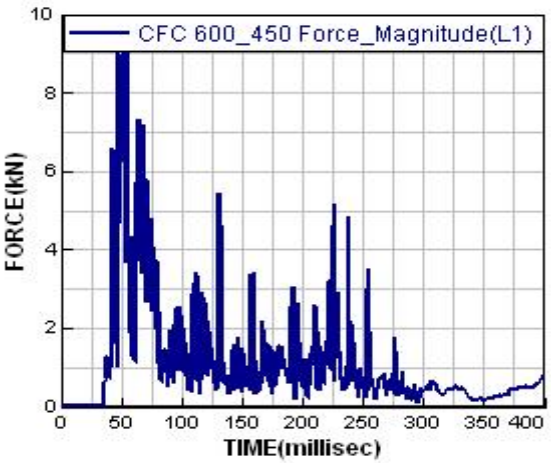

Figure 5.41 Force magnitude in joint 450.

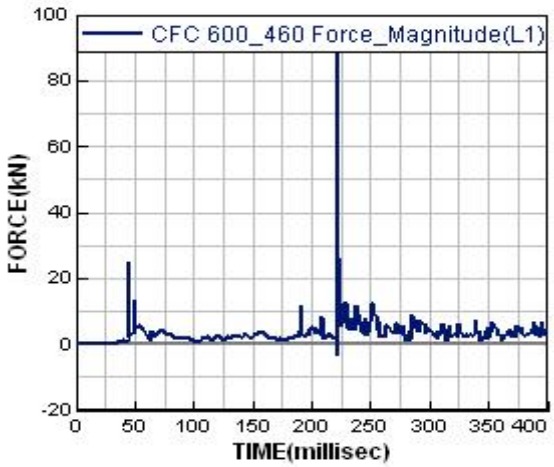

Figure 5.42 Force magnitude in joint 460.

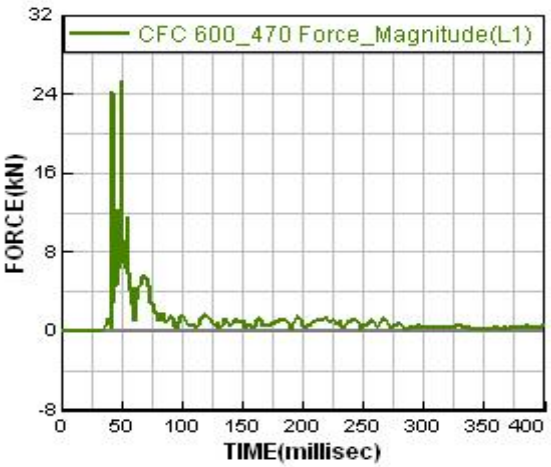

Figure 5.43 Force magnitude in joint 470.

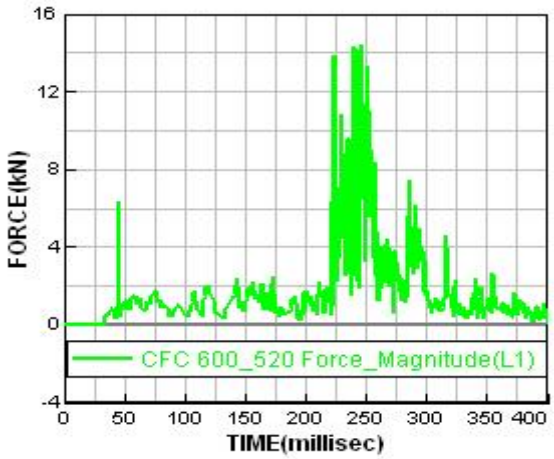

Figure 5.44 Force magnitude in joint 520.

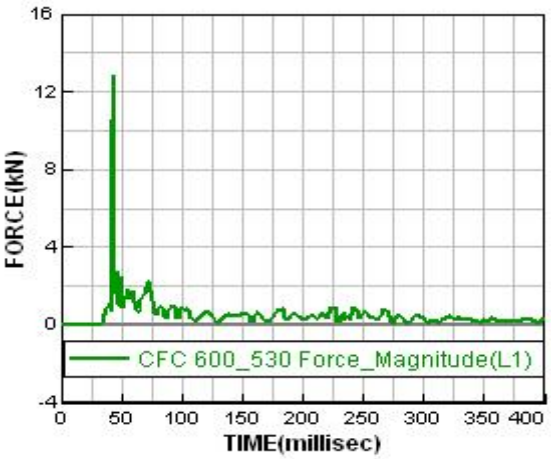

Figure 5.45 Force magnitude in joint 530.

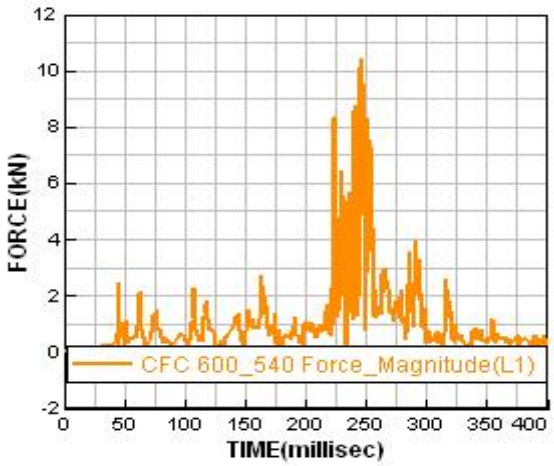

Figure 5.46 Force magnitude in joint 540.

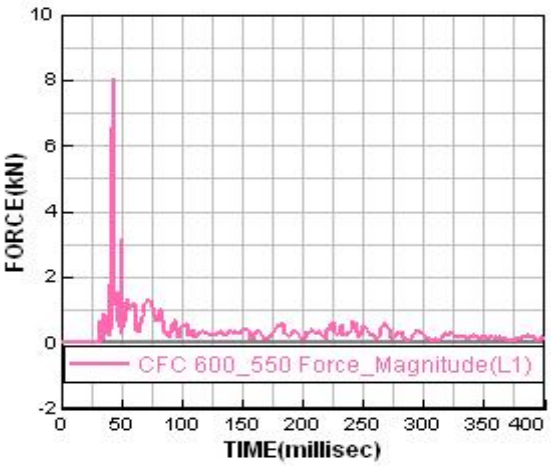

Figure 5.47 Force magnitude in joint 550.

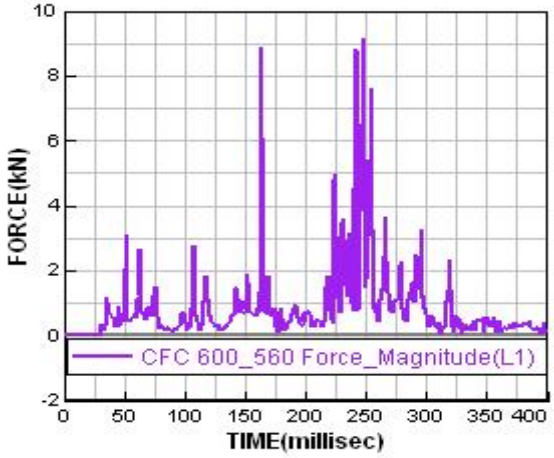

Figure 5.48 Force magnitude in joint 560.

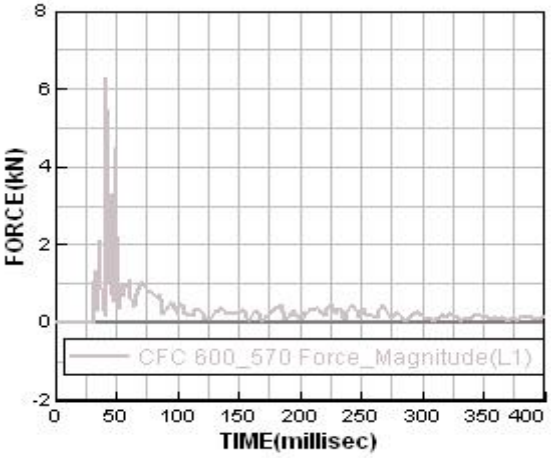

Figure 5.49 Force magnitude in joint 570.

The medical examination of the motorcycle rider revealed a fracture in the shaft of the left femur, classified with an AIS code of 3. In the region of the left femur, the Virthuman model incorporates three breakable joints:

- Joint 420 - upper femur,
- Joint 440 - middle femur,
- Joint 460 - lower femur.

The force magnitudes in these joints are depicted in Figure 5.38, Figure 5.40, Figure 5.42. These virtual force readings exhibit significant peaks between 175 and 250 ms. The peak forces in the respective joints were as follows:

- Joint 420: 27 kN,
- Joint 440: 36 kN,
- Joint 460: 90 kN.

Conversely, the right femur (joints 430, 450, and 470) did not experience such pronounced peaks. Similar, albeit lower magnitude, peaks were also observed in joints located within the area of the left fibula and the left tibia:

- Joint 520 - Figure 5.44,
- Joint 540 - Figure 5.46,
- Joint 560 - Figure 5.48.

Within this region, the peak forces range from 9 to 14 kN. The medical records also indicated injuries to the left tibia and left fibula (shaft fracture and fracture above the joint - AIS2). These injuries correspond with the aforementioned force peaks.

Neck forces and moments (as seen in Figure 5.50) were measured in the joint between the C0 and C1 vertebrae, following SAE regulations J1727 and J1733. The SAE standards define the measurement procedure for Nij calculation, involving the filtration of signals as follows:

- Moment: CFC600 filter,
- Forces: CFC180 filter.

The force signal filtration aligns with the SAE J211-1 standard [152]. While SAE recommends using a CFC600 filter for force signal filtration, it was observed that the CFC180 filter yields a higher signal-to-noise ratio (SNR).

Upon calculating Nij after filtration, the results were placed within the 50th percentile male corridor (as shown in Figure 5.51). The figure illustrates that the corridor was exceeded due to elevated neck extension force peaks at 75 ms and 120 ms. However, despite this, the medical examination did not report any neck injuries in the region.

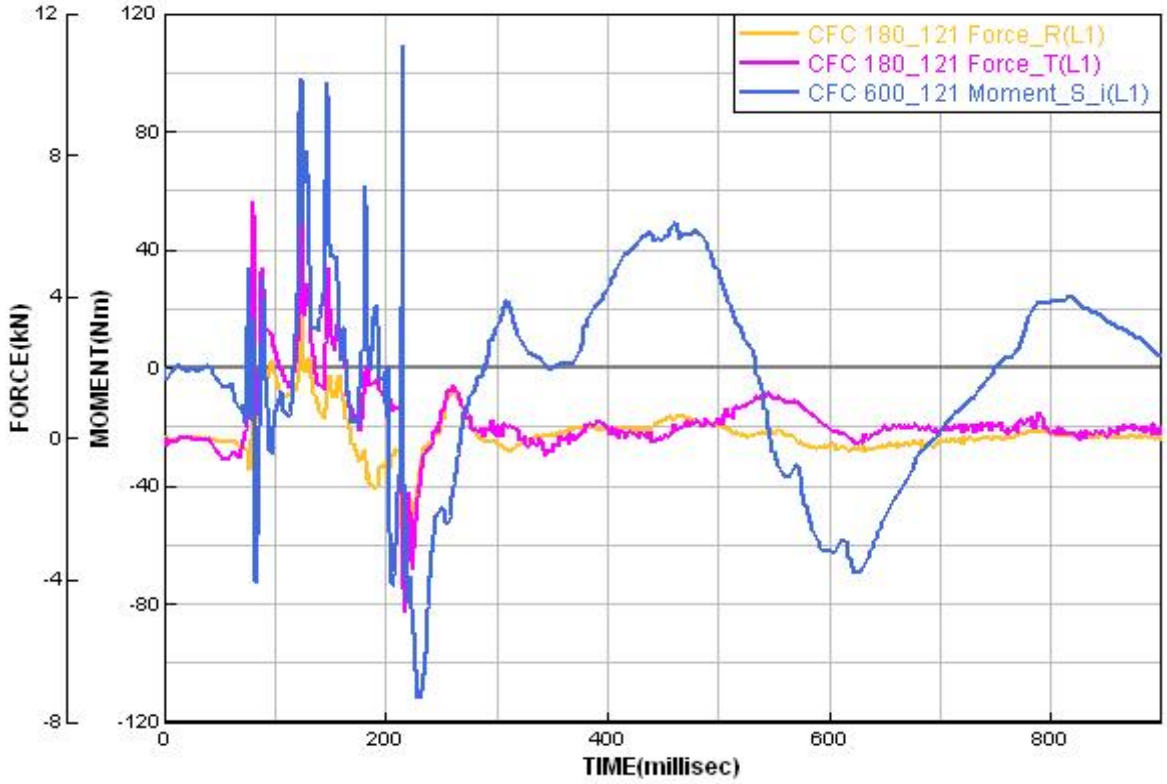

Figure 5.50 Moment and forces in the PTW occupant´s neck.

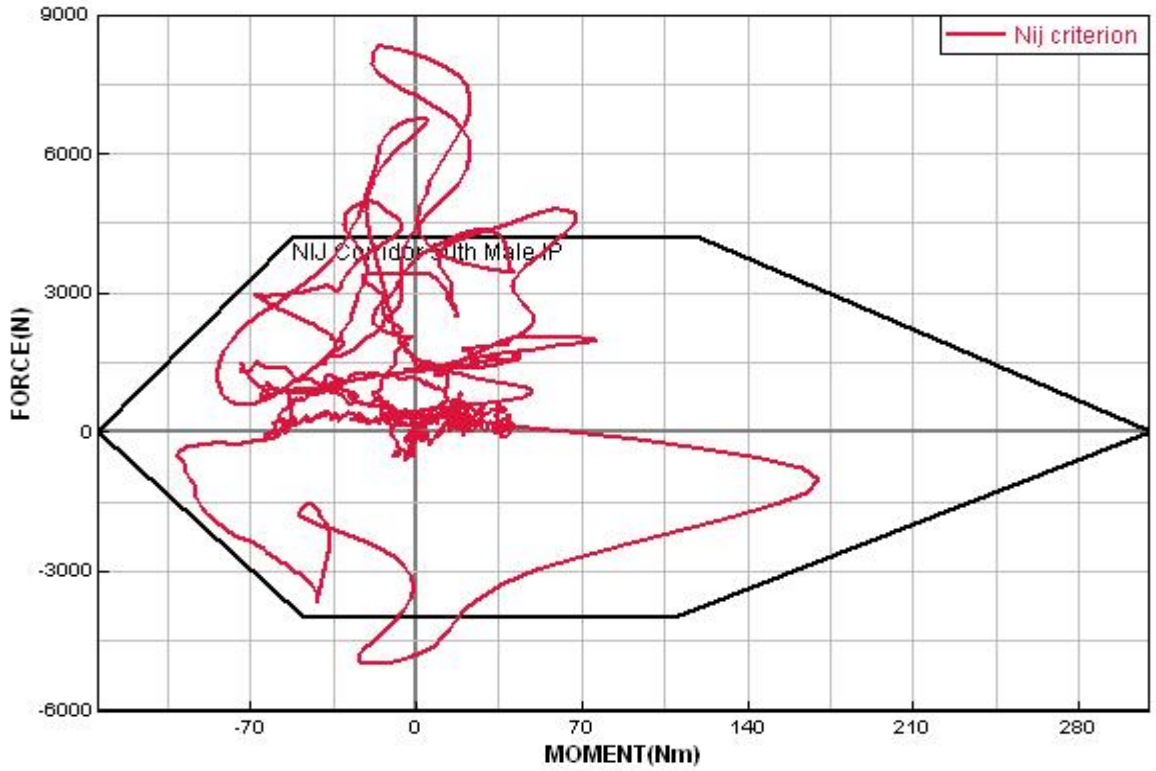

Figure 5.51 Case 1 Nij evaluation corridor.

5.3.1.2 Case 2

5.3.1.2.1 Accident description

The second scenario involves a collision on Forlivese Street in Dicomano, occurring around 2:30 p.m. The accident took place during daylight hours on a dry asphalt road. According to the site summary, "It was a summer afternoon with sunny and clear visibility conditions. The driver came to a halt at a Stop sign. Upon proceeding and accelerating, the driver executed a left turn, colliding with the PTW. The motorcycle rider was approaching rapidly from the left side of the driver. The rider only noticed the impending danger 0.5 seconds before the collision" [157].

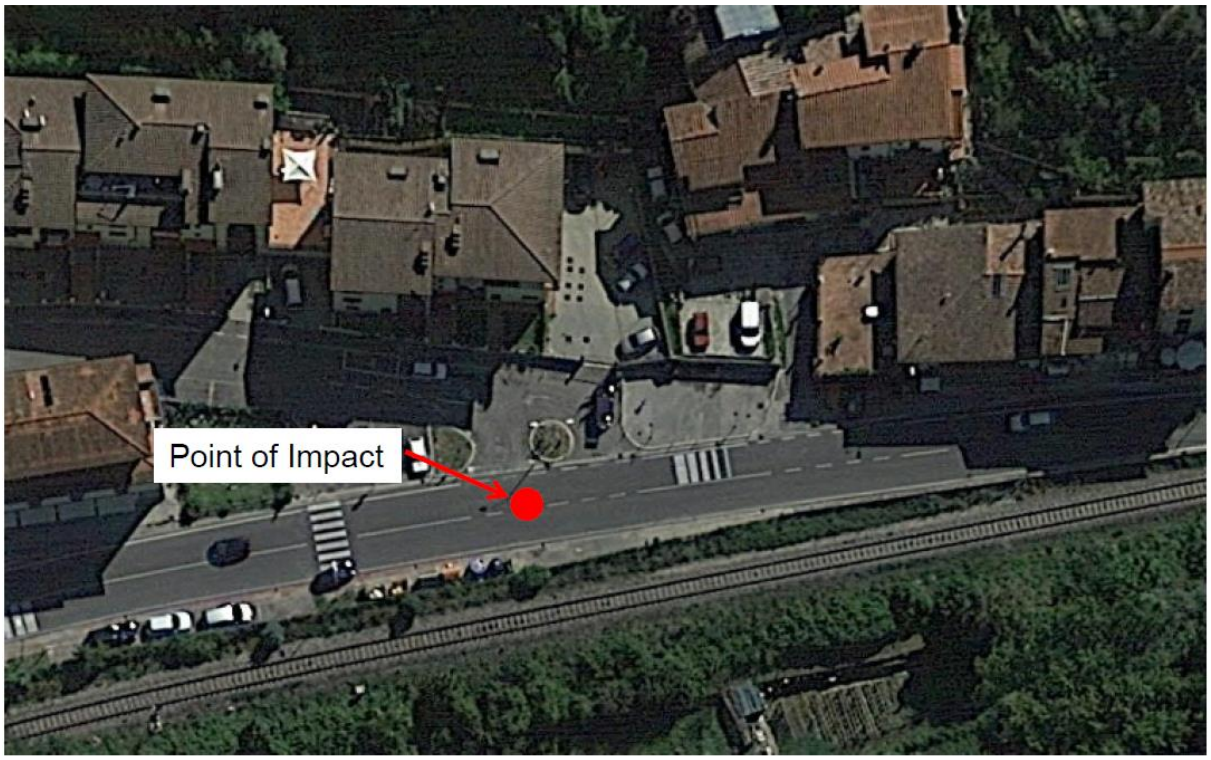

Fig. 1 Case 2 accident site on Google Maps [157]**.**

The accident location was documented through both a sketch and a series of photographs (Figure 5.52 - Figure 5.57). The incident involved two vehicles: a Piaggio Beverly 300 cc PTW (with a total mass of 180 kg, including an 80 kg rider) and an Opposite Vehicle (OV) - a Fiat Grande Punto with a single occupant (the combined mass of the vehicle and driver was approximately 1130 kg).

Figure 5.52 Case 2 accident site - the front of the car [157]**.**

Figure 5.53 Case 2 accident site - the PTW and left side of the car [157]**.**

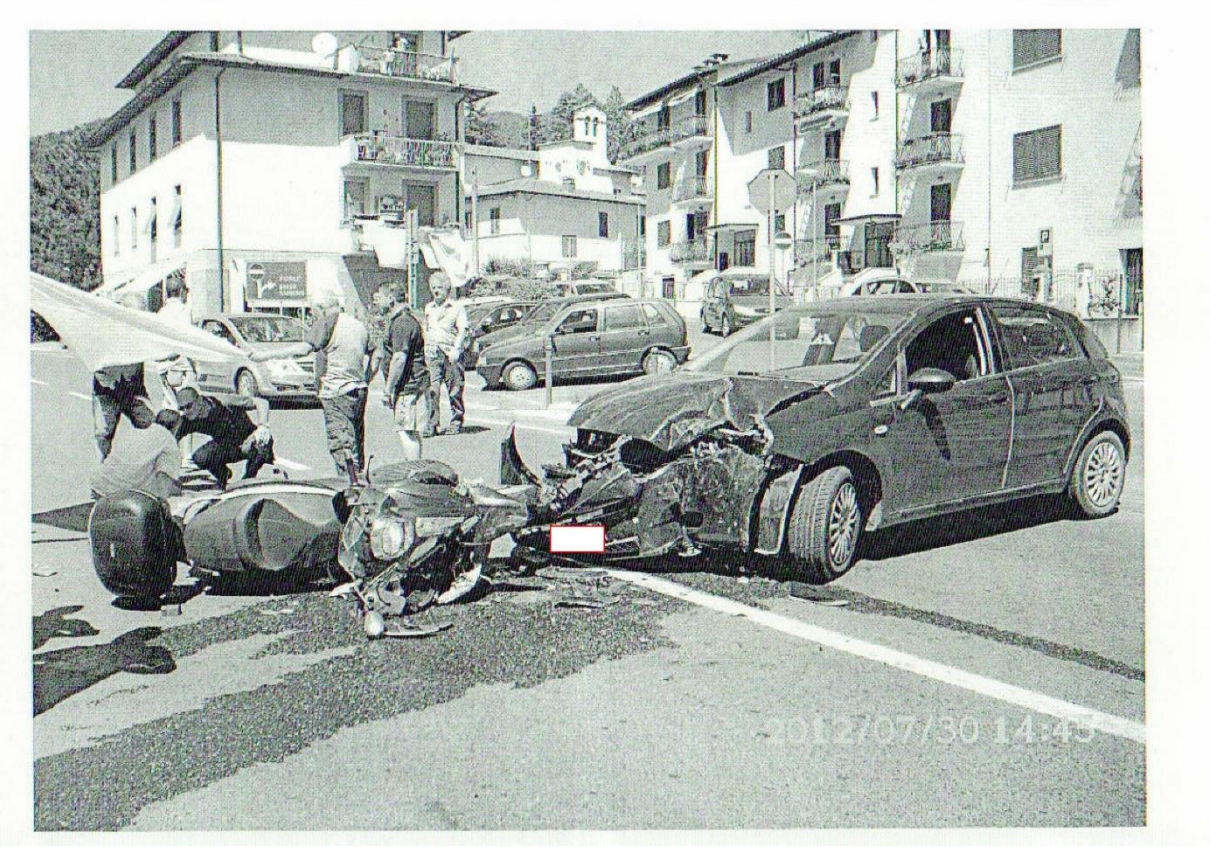

Figure 5.54 Case 2 accident site - the post-crash configuration [157]**.**

Figure 5.55 Case 2 accident site - rear view of the car [157]**.**

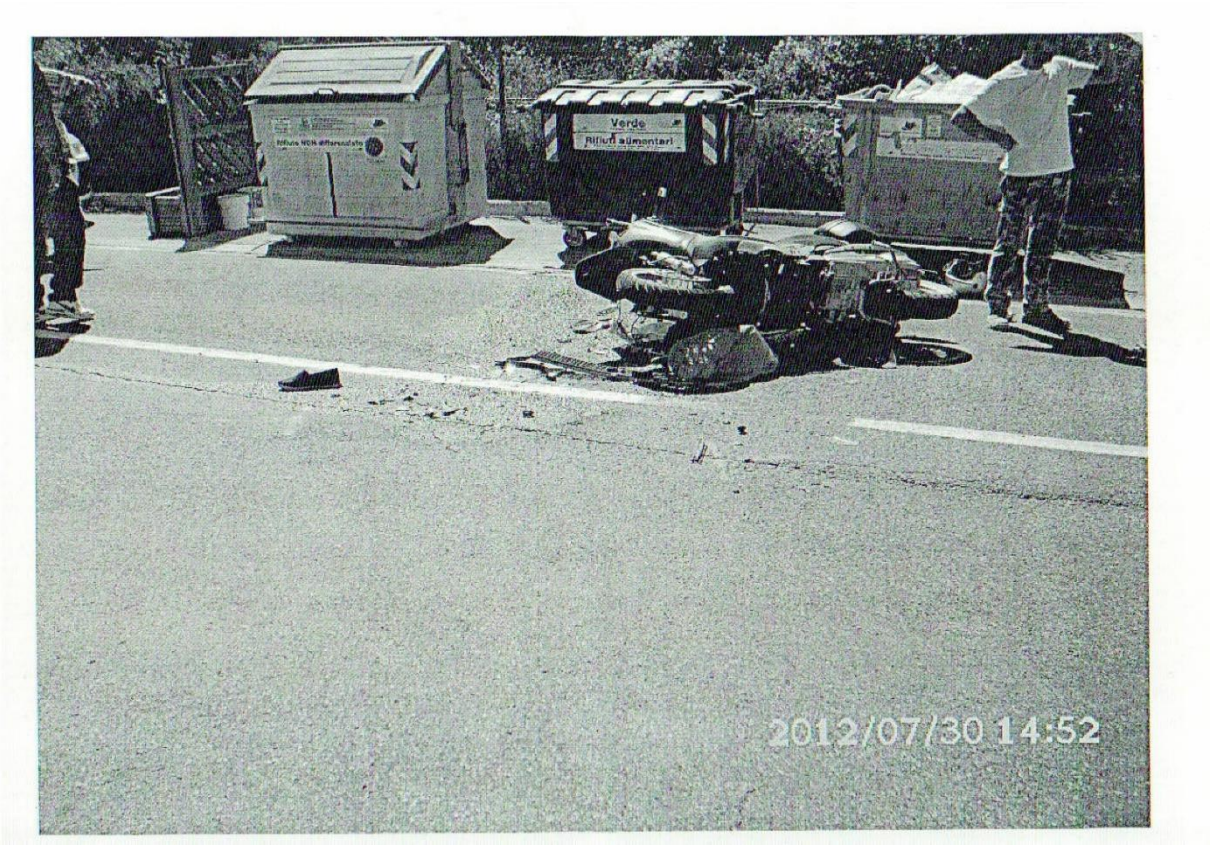

Figure 5.56 Case 2 accident site - the PTW position after the crash [157]**.**

Figure 5.57 Case 2 accident site - the view of the accident surroundings [157]**.**

The Reconstructionist from the IN-SAFE team analyzed the available evidence. The investigation revealed that the PTW collided with the OV from its left side (depicted in Figure 5.58). The angle between the two vehicles was measured to be 111 degrees (Figure 5.59).

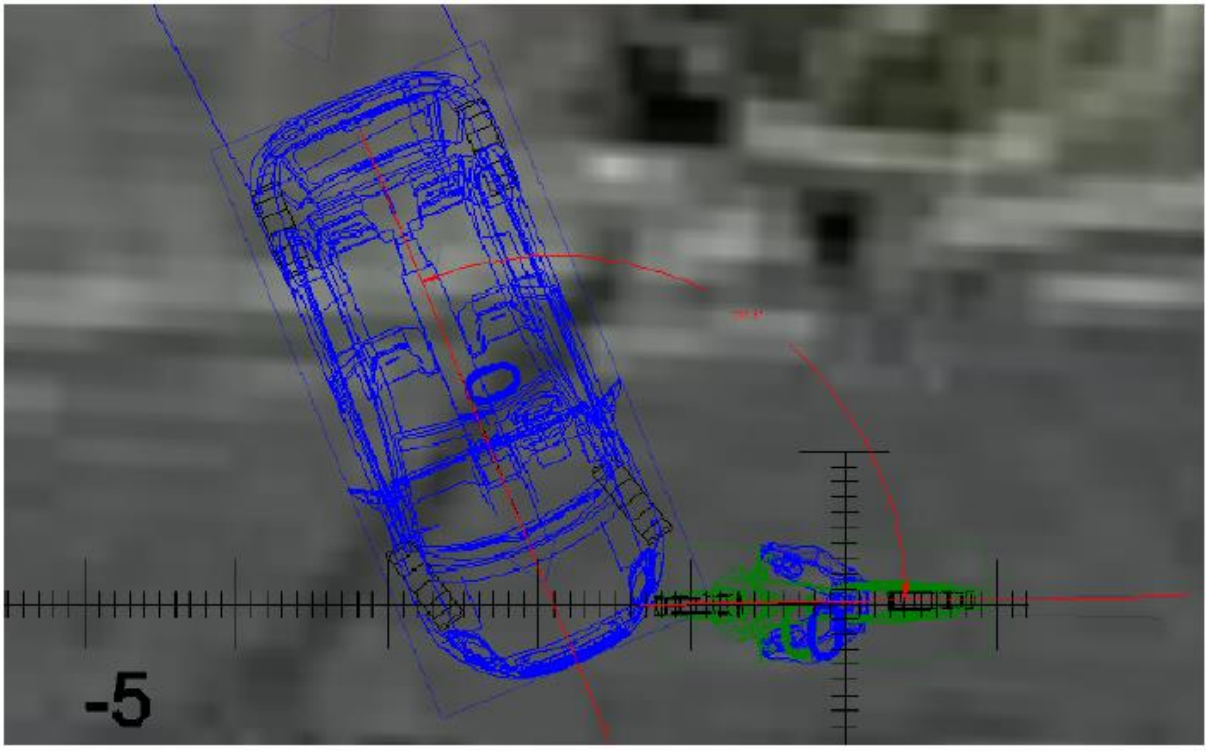

Figure 5.58 Case 2 configuration [157]**.**

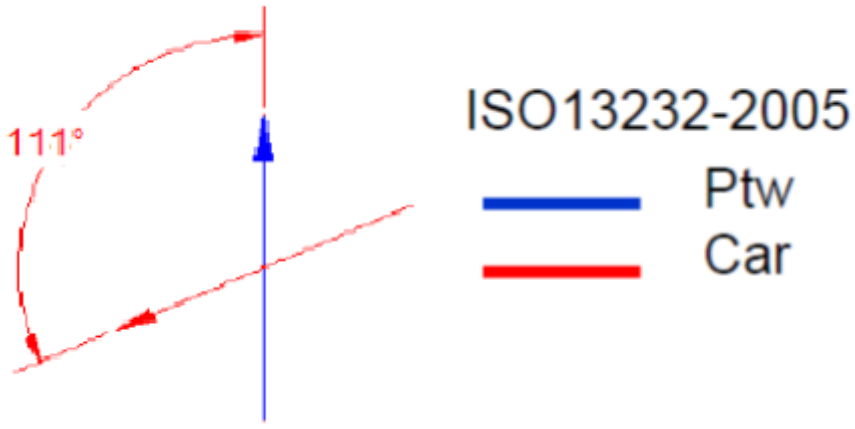

Figure 5.59 The ISO description of Case 2 configuration [157]**.**

It was found that:

Vehicle A – the Car

- Executed a left turn maneuver,
- Accelerated 1.8 seconds before the collision,
- Moved at a speed of 0 ± 5 km/h,
- Had a collision speed of 9.5 ± 3 km/h,
- EES was 13.8 ± 3 km/h.

Vehicle B - the PTW

- Applied brakes 0.5 seconds before the accident,
- Traveled at a speed of 67 ± 5 km/h,
- Had a collision speed of 56 ± 3 km/h,
- EES was 38.5 ± 3 km/h.

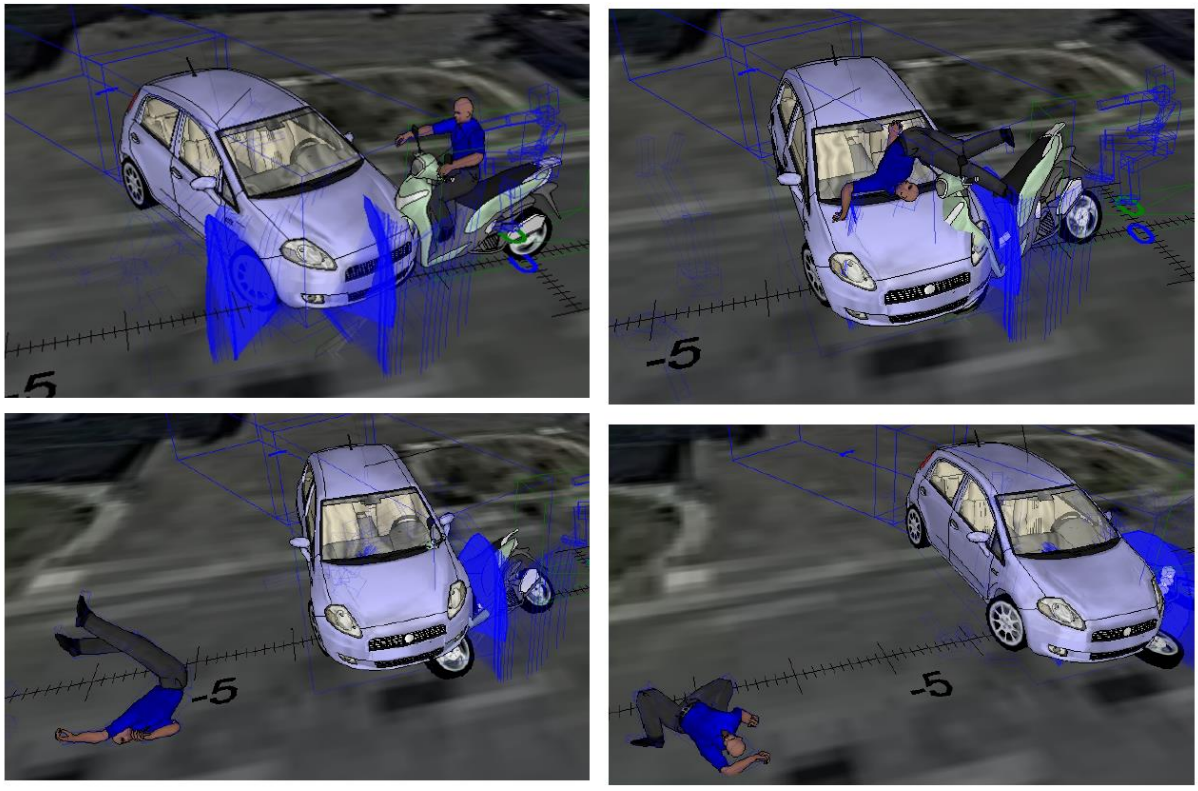

Figure 5.60 The IN-SAFE team Case 2 reconstruction [157]**.**

Based on a medical examination, the PTW driver sustained injuries of various types, including:

- Serious and moderate injuries to the rib cage,
- Moderate injury to the spine in the T8 region,
- Moderate injury to the right fibula,
- Severe injury to the internal organs of the thorax.

5.3.1.2.2 Accident numerical setup

Following the established procedure, the initial phase involved scaling the Virthuman model to match the anthropometric characteristics of the actual PTW occupant. Subsequently, the scaled model was positioned, integrated with the helmet, and linked with the PB350. The OV model was then adjusted to align with the reported mass from the police documentation (1130 kg). Upon completing these adjustments, the PTW model was placed adjacent to the OV model (as shown in Figure 5.61), with an approximate angle of 111 degrees between the vehicles.

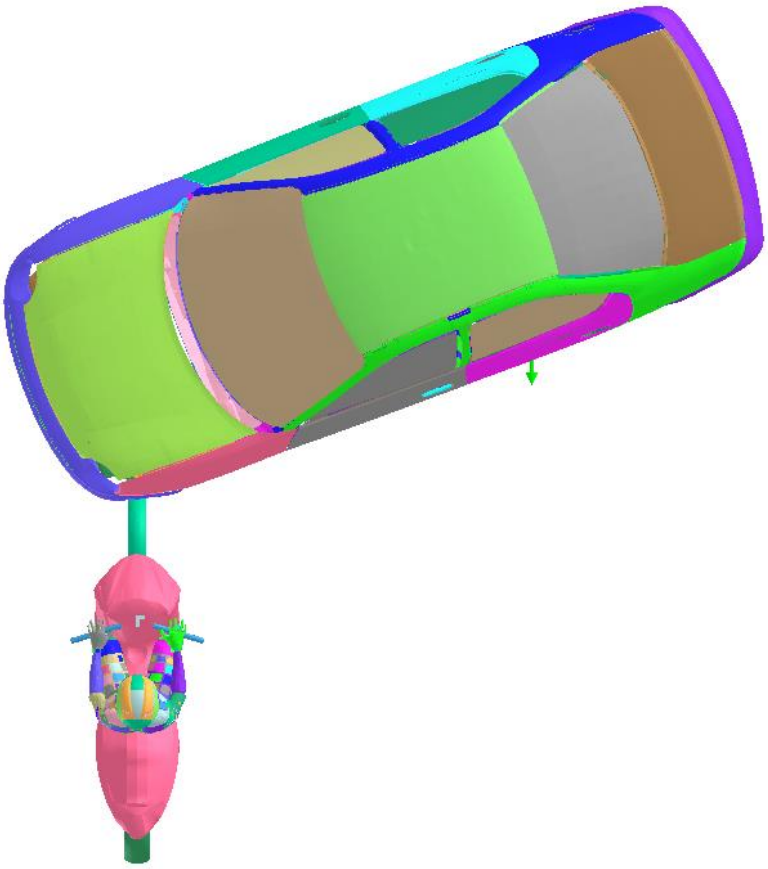

Figure 5.61 Case 2 numerical setup.

The initial velocities were as follows:

- The PTW: 56 km/h,
- The OV: 9.5 km/h.

5.3.1.2.3 Results and discussion

The sequence of events during the crash is visualized in the preceding figures (Figure 5.62- 5.63). The collision initiates with the PTW's front wheel contacting the left fender of the OV. Within the initial 20 ms, the PTW's fork undergoes compression. Subsequently, from 20 to 45 ms, the fork begins to bend until contact occurs between the PTW's front wheel and its frame. At the 45 ms mark, the PTW starts rotating around the point of contact with the OV (Y-axis of the PTW). This rotation causes the rear part of the PTW to lift.

Throughout the crash, the movement of the PTW driver unfolds through the following stages:

- 0 – 30 ms: Sliding on the seat
- 30 ms: Reaching the maximum handlebar grip force (350 N) and releasing the hands
- 30 – 60 ms: Continuous sliding from the seat
- 60 ms: First contact between the occupant's abdomen and the PTW frame
- 60 - 180 ms: Rotation of the body leading to the head-to-hood impact (175 - 185 ms)

Analyzing the signal from the virtual accelerometer at the head's center of gravity (Figure 5.64) reveals the largest acceleration peak occurring around 180 ms, which corresponds with the simulation's contour plot at 180 ms (Figure 5.62). The calculated HIC value (399) aligns with the medical records that indicate no head injuries were sustained.

The acceleration time series recorded from the T1, T8, and T12 vertebrae (Figure 5.65-5.67) exhibits pronounced peaks:

- T1: 68 ms – 4 mm/ms2; 90 ms – 4.8 mm/ms2
- T8: 68 ms – 7.1 mm/ms2; 90 ms – 6.9 mm/ms2
- T12: 68 ms – 12.1 mm/ms2; 90 ms – 10.5 mm/ms2

Within the same time frame (68, 90 ms of simulation), substantial acceleration peaks (ranging from 4 to 14 mm/ms2) are recorded in the regions of the 4th and 8th ribs (Figure 5.68- 5.71). Medical assessments of the PTW driver report rib cage fractures categorized as AIS2 and 3. These fractures potentially stem from the impact of the driver's body with the PTW's upper front frame. The hospital's records also note injuries to the spinal cord around the T8 and T9 vertebrae. The acceleration peaks at 68 and 90 ms could be implicated in causing these injuries.

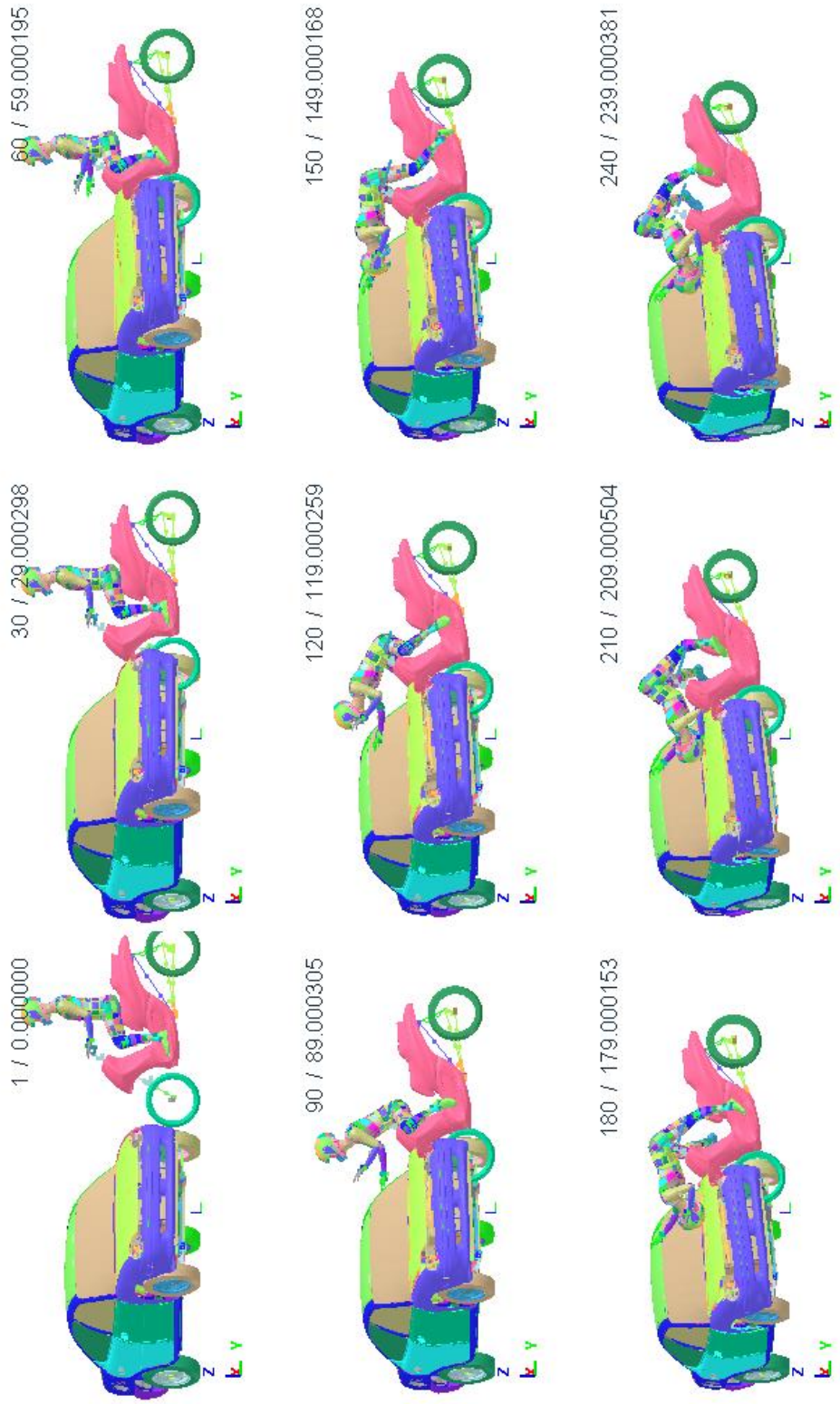

Figure 5.62 Case 2 reconstruction - side view.

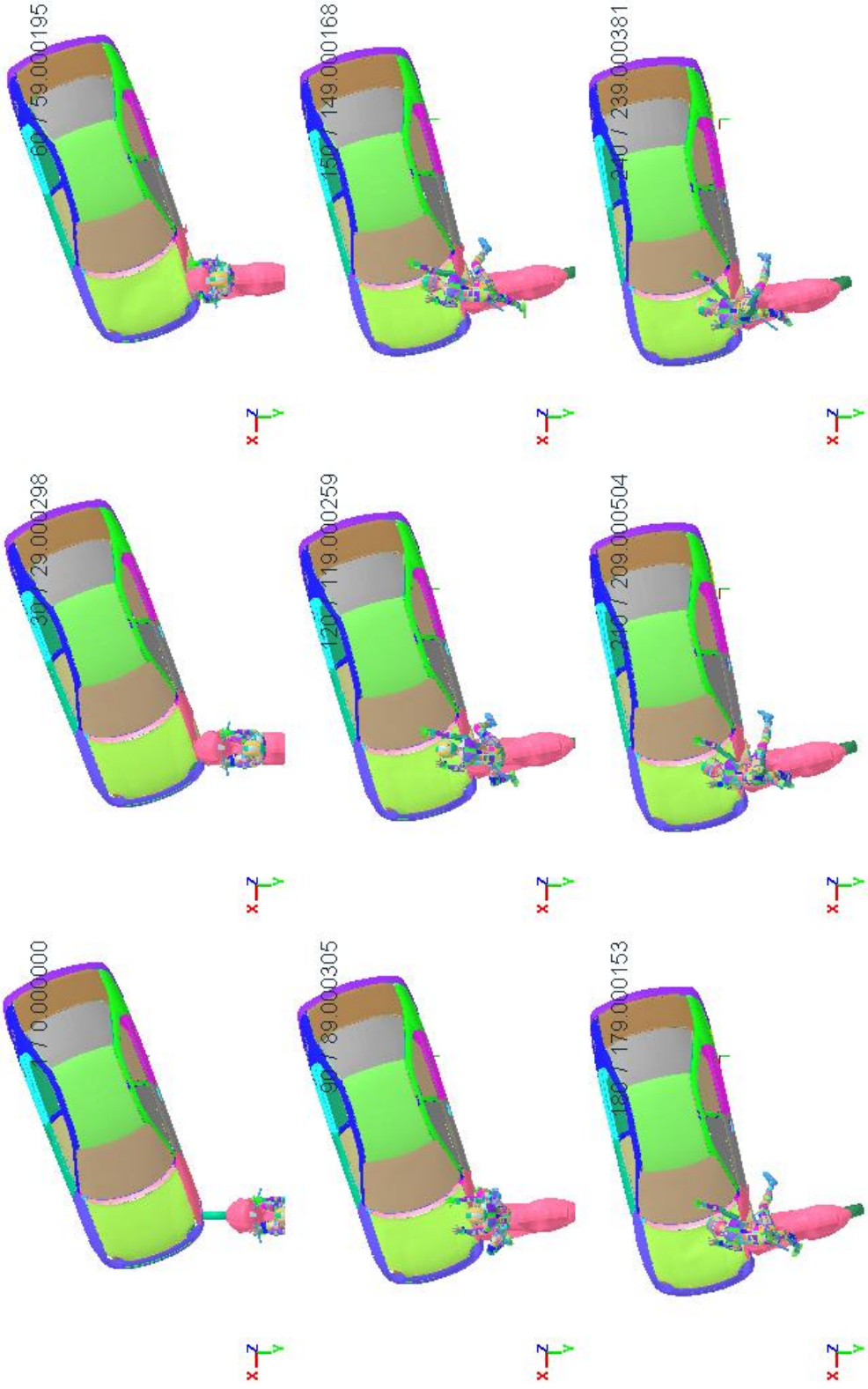

Figure 5.63 Case 2 reconstruction - top view.

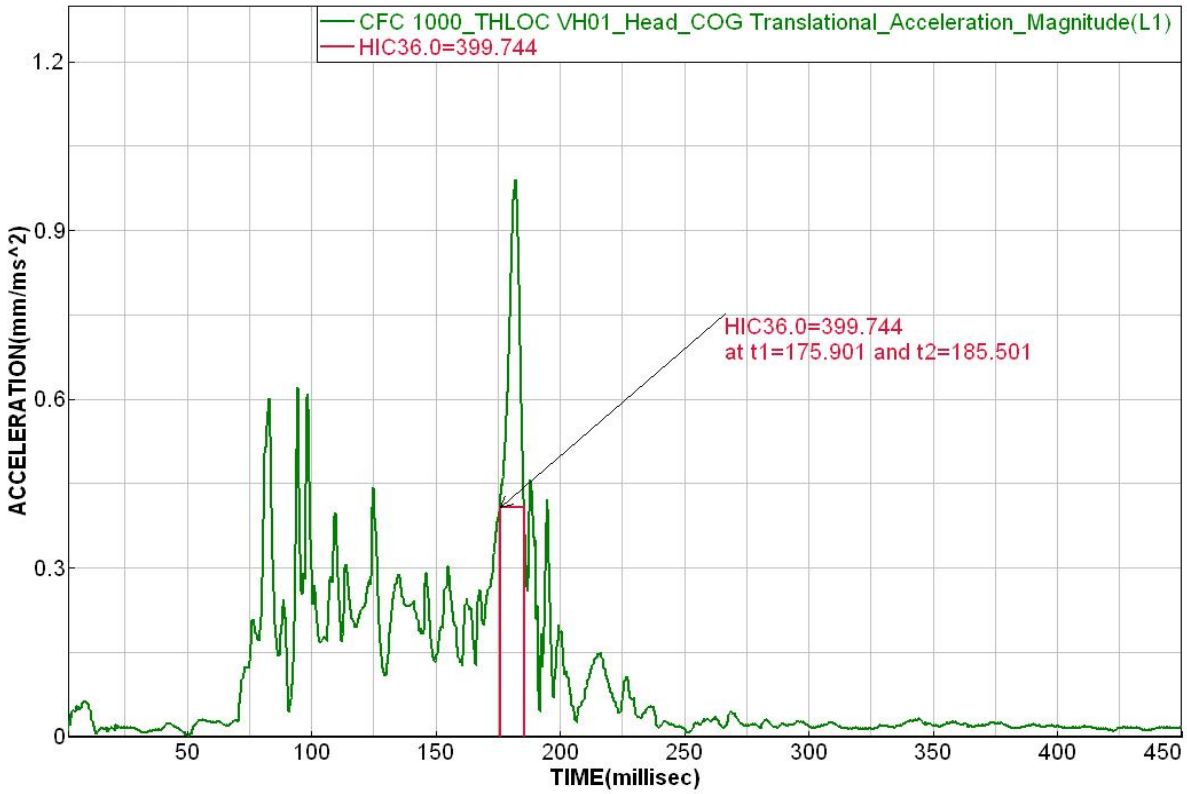

Figure 5.64 Head COG acceleration in Case 2.

The PTW driver also sustained an injury to the lower extremity, specifically a fracture above the joint in the right fibula, categorized as AIS2. Regrettably, the assessment of the force in the region of the right fibula and tibia (joints: 530, 550, 570 - Figure 5.79, Figure 5.81, Figure 5.83) indicates no evident correlation.

An examination of the Nij criterion (Figure 5.84-5.85) reveals that throughout the accident, the PTW occupant consistently remained within the safe corridor for neck injuries. This outcome corresponds with the medical examination, as no neck injuries were documented.

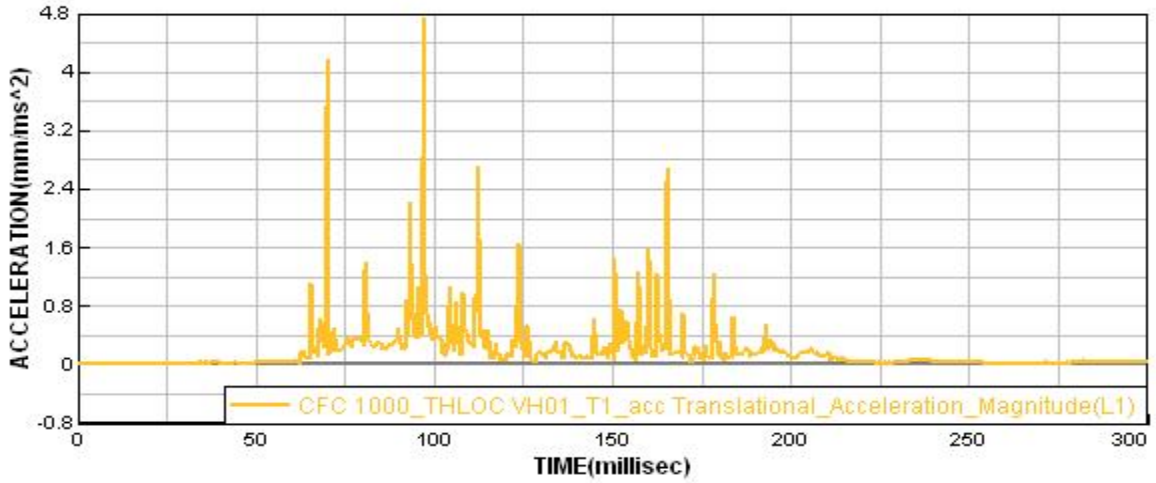

Figure 5.65 T1 vertebra acceleration.

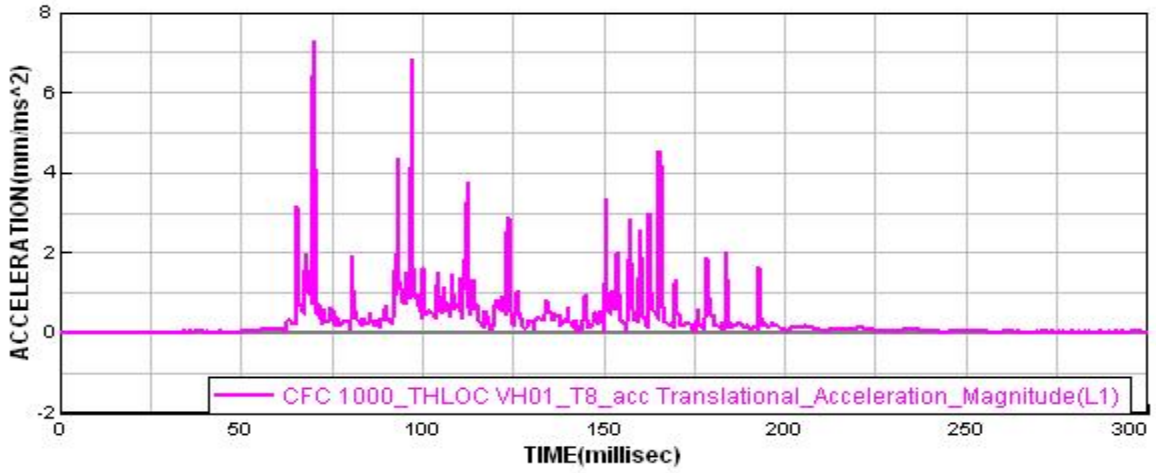

Figure 5.66 T8 vertebra acceleration.

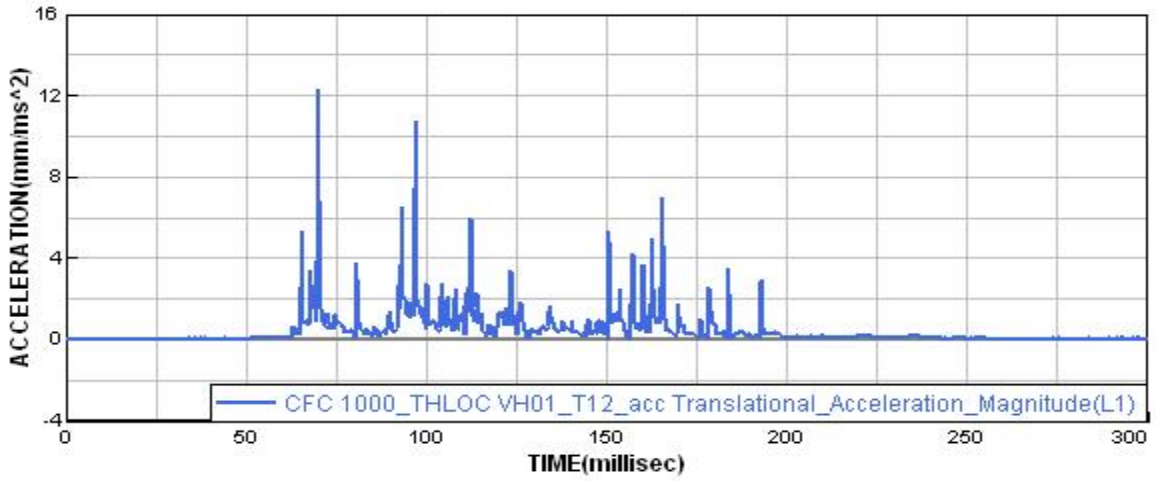

Figure 5.67 T12 vertebra acceleration.

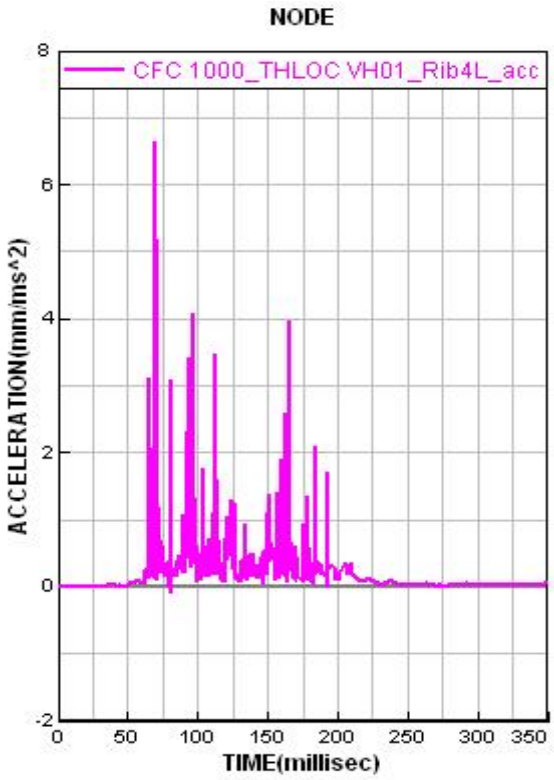

Figure 5.68 4th left rib acceleration.

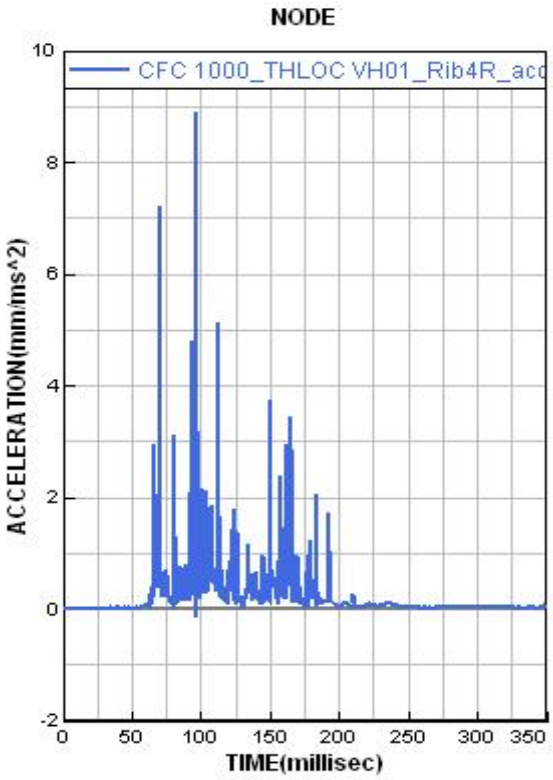

Figure 5.69 4th right rib acceleration.

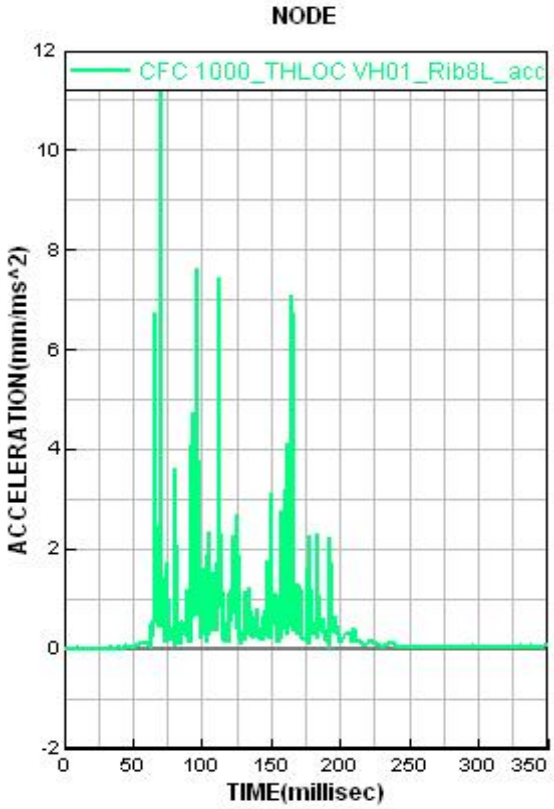

Figure 5.70 8th left rib acceleration.

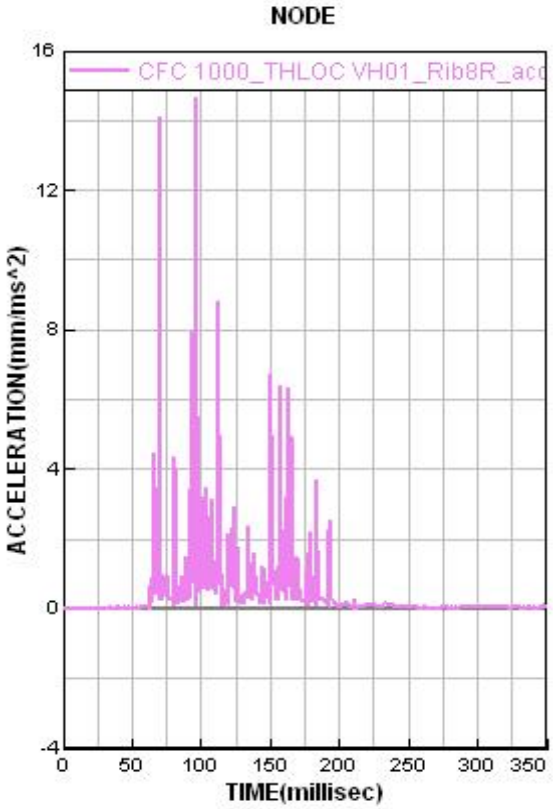

Figure 5.71 8th right rib acceleration.

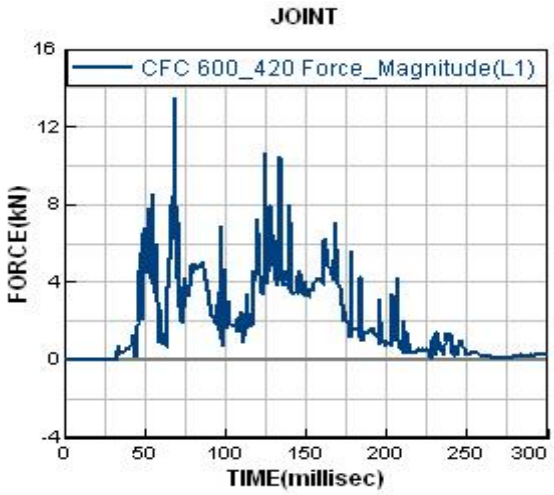

Figure 5.72 Force magnitude in joint 420.

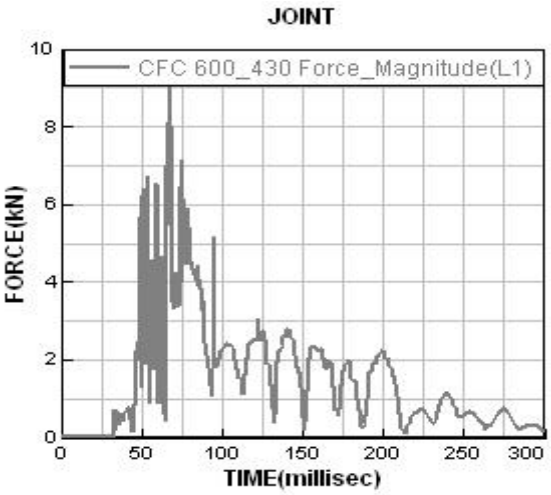

Figure 5.73 Force magnitude in joint 430.

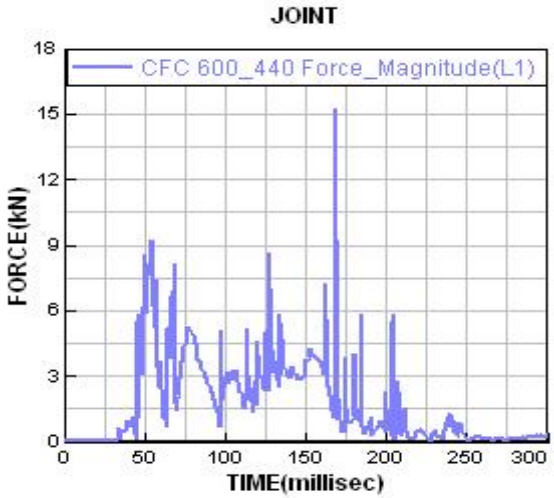

Figure 5.74 Force magnitude in joint 440.

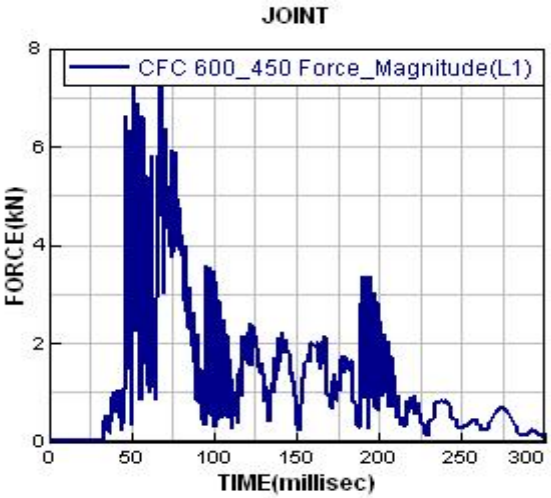

Figure 5.75 Force magnitude in joint 450.

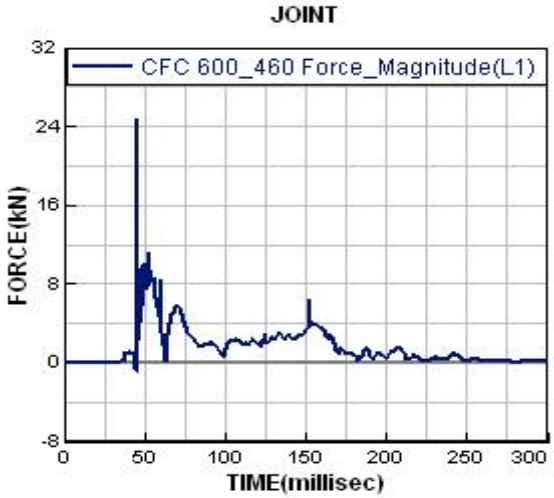

Figure 5.76 Force magnitude in joint 460.

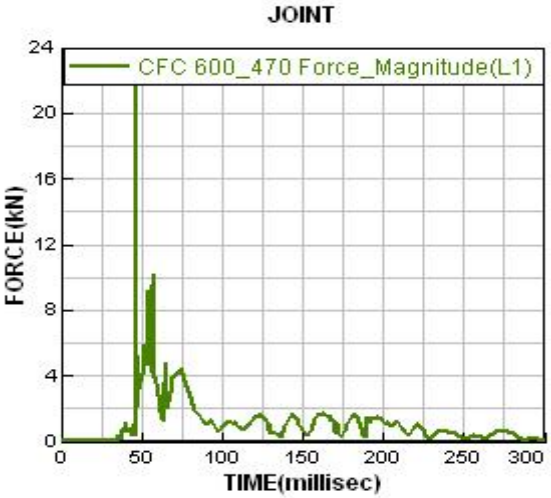

Figure 5.77 Force magnitude in joint 470.

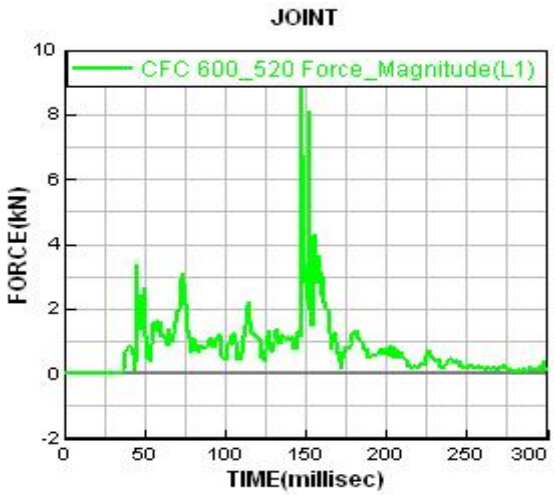

Figure 5.78 Force magnitude in joint 520.

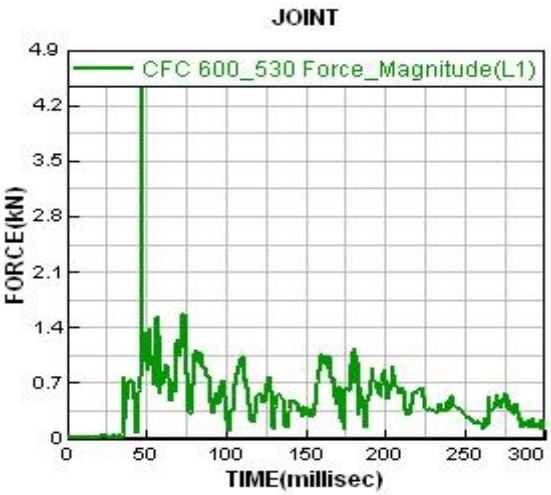

Figure 5.79 Force magnitude in joint 530.

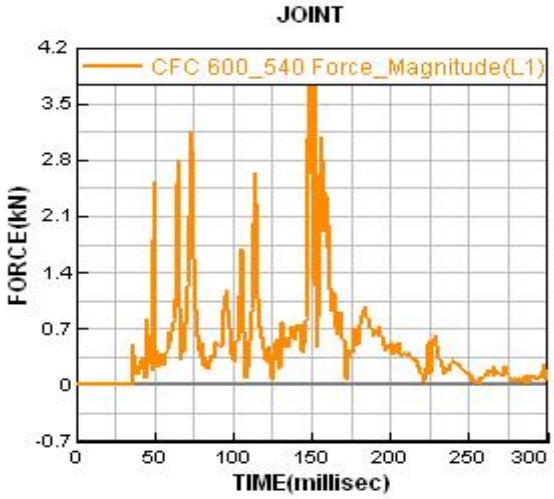

Figure 5.80 Force magnitude in joint 540.

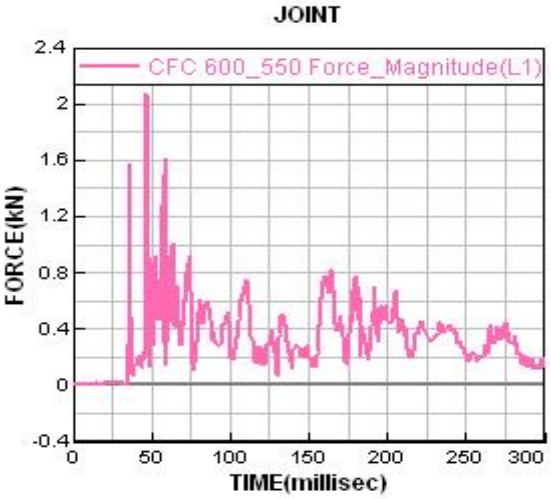

Figure 5.81 Force magnitude in joint 550.

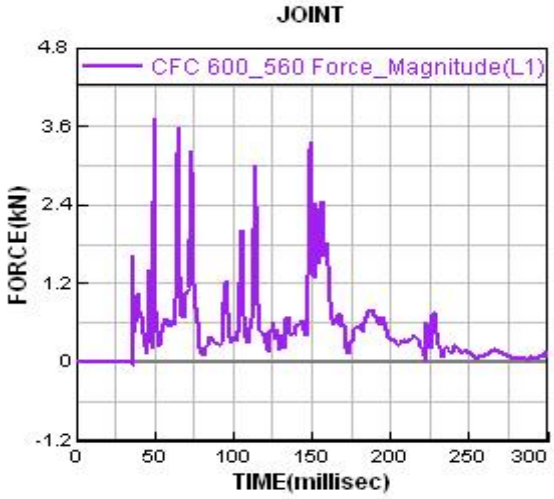

Figure 5.82 Force magnitude in joint 560.

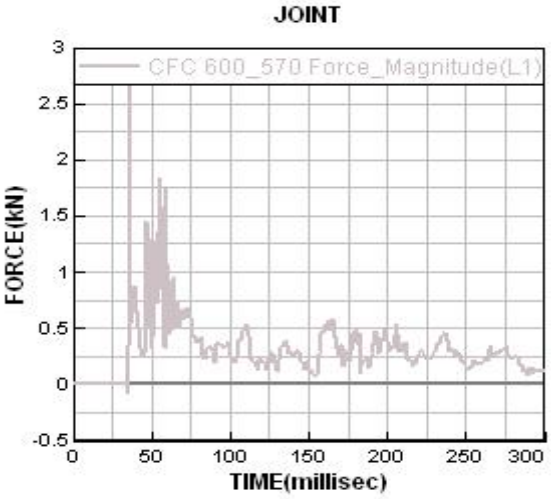

Figure 5.83 Force magnitude in joint 570.

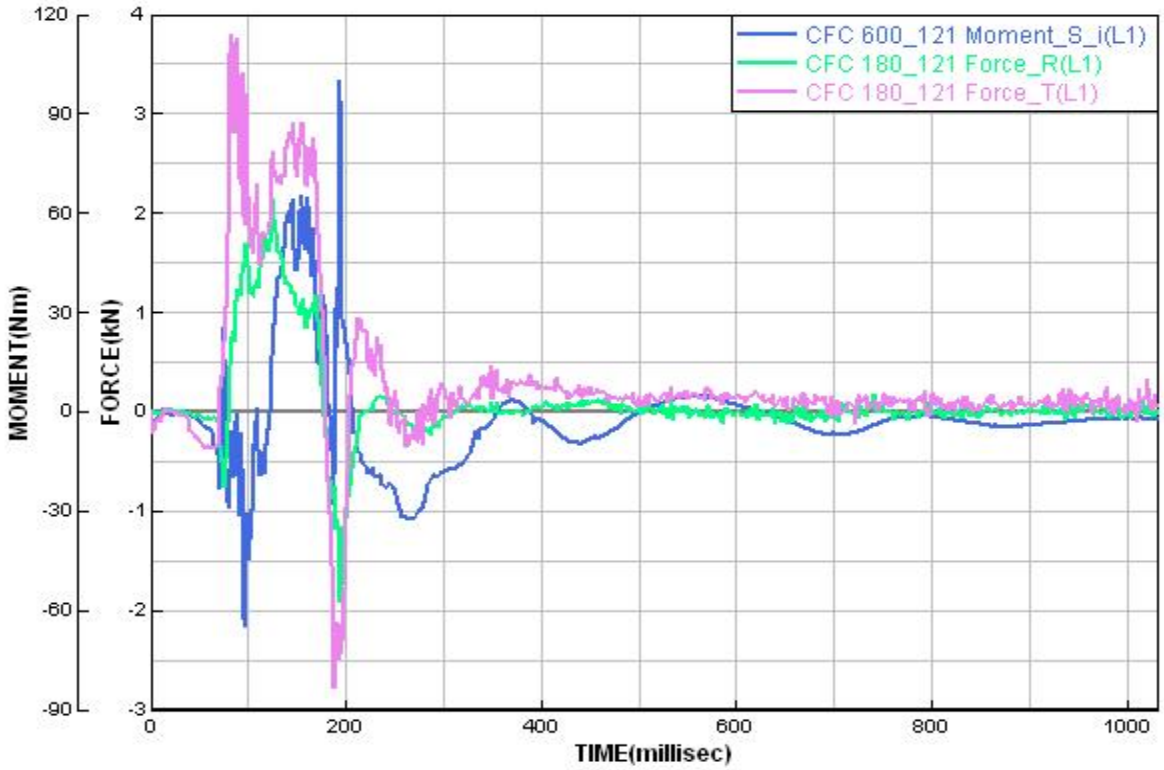

Figure 5.84 Moment and forces in the PTW occupant´s neck.

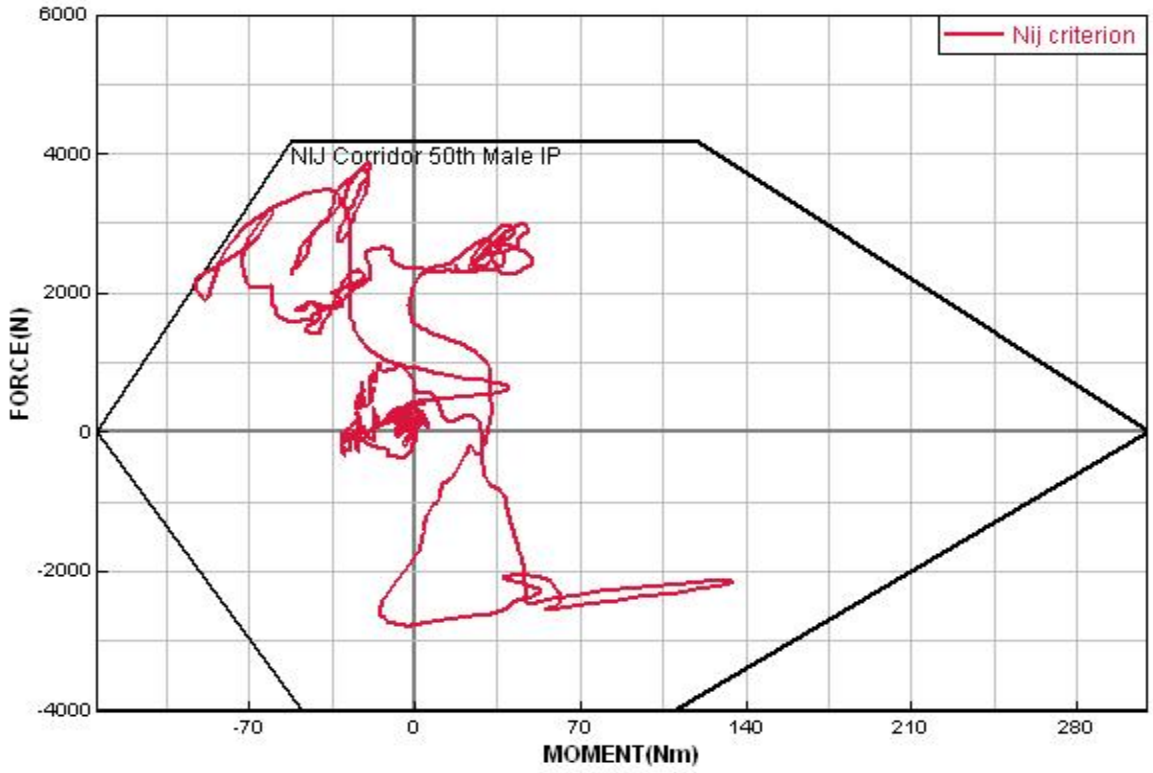

Figure 5.85 Case 2 Nij evaluation corridor.

5.3.2 LMU Institute for Legal Medicine case

Established in 1472 as Bavaria's inaugural university under papal concession, Ludwig Maximilian University of Munich (LMU) has evolved into a prominent institution renowned for its academic excellence and pioneering research endeavors. Positioned as a major beneficiary of Germany's excellence program, LMU stands as one of Europe's foremost research universities today.

Within LMU, the Institute for Legal Medicine holds a significant role as part of one of Germany's premier faculties of medicine. Since its inception in 1909, the institute has consistently contributed groundbreaking research in its field. With a dedicated team of 11 permanent researchers, the Institute for Legal Medicine possesses a diverse range of interdisciplinary expertise encompassing Engineering, Computational Mechanics, Medicine, Anthropometry, Biology, Physics, and Epidemiology.

The institute boasts extensive proficiency in areas such as anthropometry and image-based modeling, Impact-Biomechanics, Crash Simulation, and comprehensive accident analysis. With a specific emphasis on road traffic incidents, the institute has garnered significant experience in data acquisition, accident reconstruction, and the nuanced analysis of accidents.

One of the central objectives of the institute is the advancement of accident analysis and prevention. Leveraging its multi-disciplinary knowledge base and state-of-the-art methodologies, the Institute for Legal Medicine at LMU seeks to enhance the understanding of accidents and their underlying mechanisms. By focusing on road traffic accidents, their research aims to contribute to the overall improvement of road safety and accident prevention strategies [158].

5.3.2.1 Case 3

5.3.2.1.1 Accident description

Accident reconstruction serves as a crucial means of acquiring comprehensive insights into accidents, encompassing their dynamics and outcomes. It plays a pivotal role in building extensive accident databases, essential for enhancing safety systems through optimization across various impact scenarios.

The motorcycle accident under analysis occurred at an intersection. The opposing vehicle came to a halt at a red traffic signal, and the motorcycle collided with the rear of the car. The accident configuration is visually depicted in Figure 5.86.

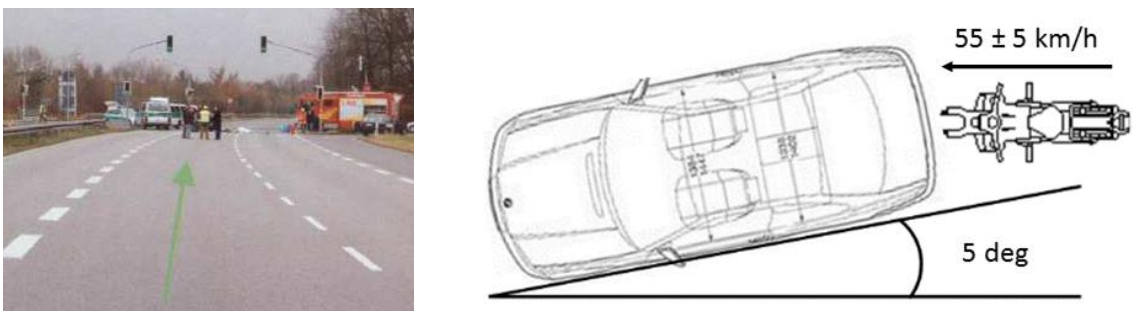

Figure 5.86 LMU Case accident scenario depicted on the left, sourced from accident case documentation, alongside the simulation setup sketch on the right [159]**.**

The accident involved two vehicles, one being a BMW 318i Cabrio (depicted on the left in Figure 5.87) with a dry mass of 1370 kg. The car was operated by a single occupant, the driver, whose mass amounted to 70 kg. Consequently, the overall mass of the car, including the driver, was 1440 kg.

The other vehicle in question was a Suzuki Burgman 200 maxi scooter (illustrated on the right in Figure 5.87) with an empty mass of 161 kg. The rider, a 66-year-old individual with a height of 171 cm, weighed 70 kg. Hence, the total mass of the motorcycle, encompassing the rider, tallied at 241 kg. The recorded impact speed, as determined by the accident analysis team, was within the range of 55±5 km/h.

Figure 5.87 Depiction of OV [160] **and PTW** [161]**.**

The motorcycle rider sustained severe injuries, including extensive head and brain trauma, displacement of the skull base from the spine, multiple rib fractures, a torn aorta, and substantial collarbone and sternum fractures. The severity of these injuries, assessed using the maximum abbreviated injury scale (MAIS [6]), were categorized as follows: a MAIS of 6 for the head, 6 for the neck, 5 for the thorax, 5 for the abdomen, and 1 for the extremities. The most critical injuries sustained by the scooter rider included significant head and brain trauma, skull base dislocation from the spine, a series of rib fractures, an aortic tear, and substantial collarbone and sternum fractures.

5.3.2.1.2 Accident numerical setup

The reconstructed accident scenario by LMU was subjected to thorough analysis. Numerical models were created for both vehicles involved in the accident. The PTW model was developed following the aforementioned method, incorporating an elastic joint on the front fork. The mass and inertia properties were adjusted to match those of the Suzuki Burgman. As a specific model for the BMW 318i Cabrio was unavailable, the existing finite element model of the Neon was adapted and customized to align with the vehicle's dimensions and mass. Given that extensive parametric study wasn't needed to apply the framework to the accident reconstruction, the non-simplified OV model was employed.

While the mass of the opposite vehicle driver is encompassed in the total mass of the opposing vehicle, the motorcycle rider's representation was created by scaling the Virthuman model to specific dimensions (66 years, 70 kg, 171 cm). This rider model was then linked to the personal protective equipment, including the detailed numerical helmet model (AGV–T2). The helmet was attached symmetrically to the head, making contact with the helmet foam and head as well as being secured by the chinstrap (refer to Figure 5.88).

The human body model was positioned in a sitting posture on the motorcycle and connected to the motorcycle structure that holds the handlebars. This connection featured a sliding contact with a stiffness of 9.36 kN/m and a maximum force limit of 350 N for each hand, following the prescribed approach. Subsequently, the numerical models representing the involved parties (motorcycle, motorcycle rider, and opposite vehicle) were positioned based on the accident's configuration (see Figure 5.88). The passenger car was positioned at a 5-degree angle with zero speed. The motorcycle's initial velocity was set at 55 km/h, aligned with its vector in the vertical longitudinal plane. The simulation was executed within the VPS numerical environment.

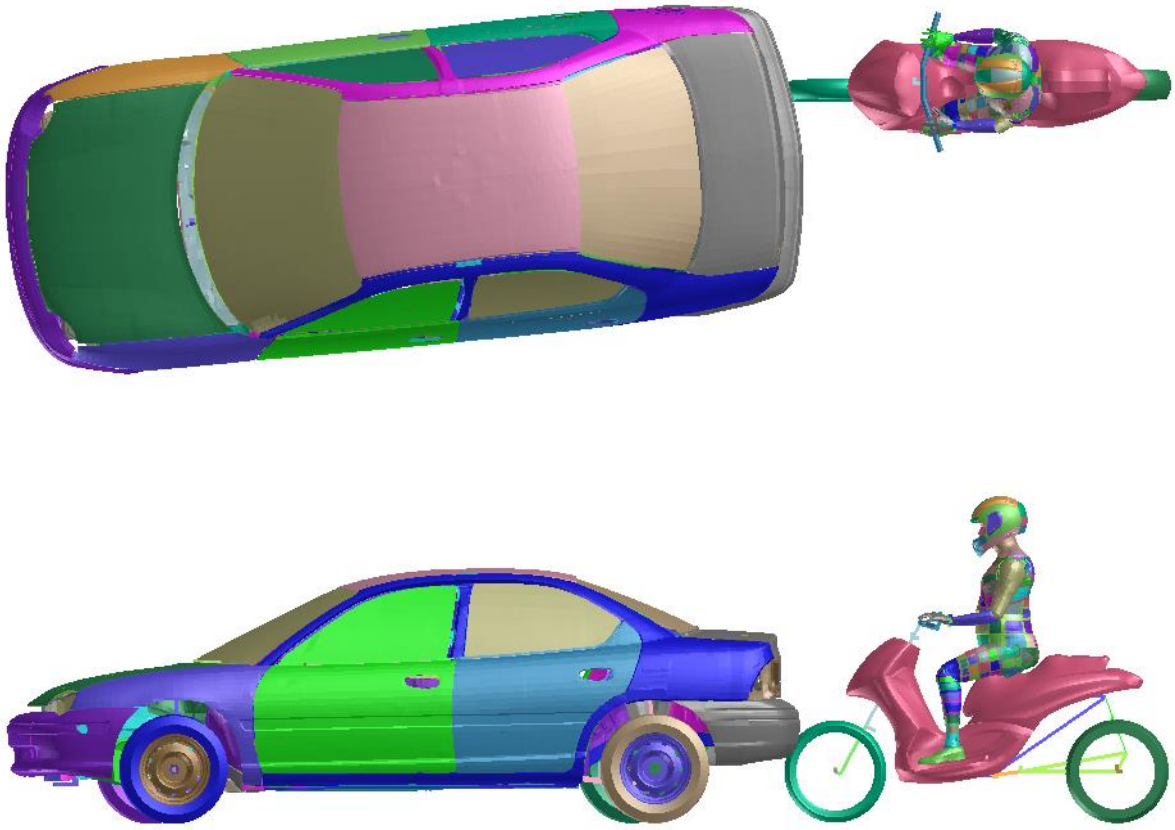

Figure 5.88 Numerical setup of LMU case.

5.3.2.1.3 Results and discussion

The initial 300 ms of the accident scenario were meticulously simulated, and the outcomes were juxtaposed with the actual accident occurrences (see Figure 5.89-5.90). Notably, there are observable resemblances in the deformation patterns between the real accident and the simulation results. A notable divergence in the numerical outcomes is identified in the modest deformation of the car's upper rear, resulting in a less direct head impact and consequently lower head acceleration. This discrepancy highlights the need to integrate a genuine car model tailored to the specific accident scenario for improved simulation accuracy.

Figure 5.89 Deformations of the vehicles involved in the accident.

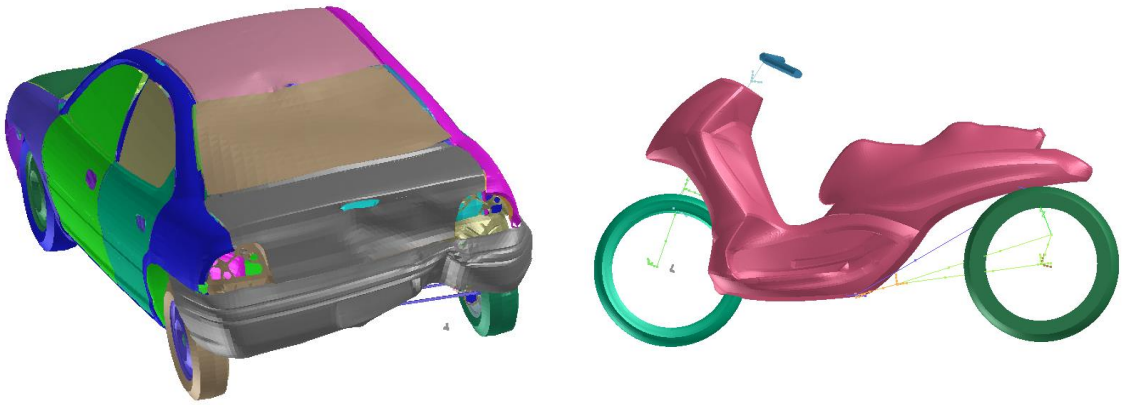

Figure 5.90 Deformations of the simulated vehicles.

The sequence of events involving the accident participants' kinematics is vividly depicted in Figure 5.91. In the initial phase of the collision, the motorcycle's wheel came into contact with the rear bumper of the car. This contact triggered the bending of the elastic joint positioned on the fork, leading to wheelbase shortening. The above figures effectively demonstrate a commendable congruence between actual and virtual deformation trends. As the scenario progresses, at 35 ms, the motorcycle rider begins to slide off the seat, losing contact between the hands and the handlebars. By 55 ms, full-scale deformation of the vehicles became apparent, halting the rider's linear motion and initiating body rotation around the handlebars.

A whiplash effect manifested prior to the head's impact with the rear window at 105 ms, resulting in a severe neck injury. Ultimately, the rotational motion culminated in the head striking the rear window at 150 ms.

Table 5.4 Comparison between the numerical results and the real injuries from the LMU case.

Body part	**Degree of injury by numerical simulation**	**MAIS from accident report** [159]
Head	Green (Good)[5]	6 (Fatal)
Neck	Red (Poor)	6 (Fatal)
Thorax	Orange (Marginal)	5 (Critical)
Abdomen	Yellow (Marginal)	5 (Critical)
Extremities	Yellow / Red (Marginal / Poor)	1 (Minor)

Figure 5.91 LMU case numerical reconstruction accident kinematics with the ongoing fast IC evaluation.

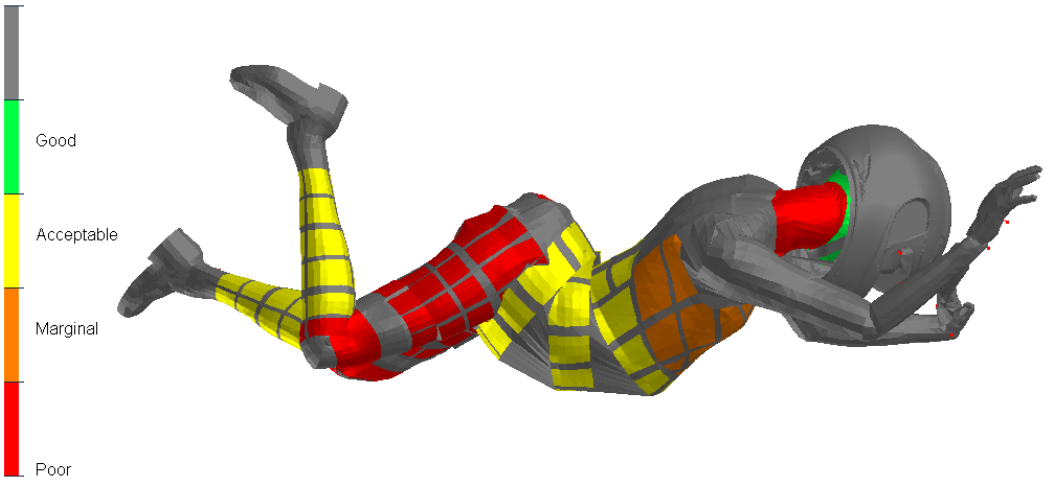

Figure 5.92 Final injury risk prediction.

[5] *The head was seriously injured in the real case. The numerical simulation results might be influenced by the used model of the helmet, where in real case the particular type of helmet is unknown.*

The evaluation of driver injuries in this case was undertaken using a tool designed for swift accident outcome assessment (refer to Figure 3.49 and Figure 3.50). In brief, injury criteria across major body regions (head, neck, thorax, abdomen, pelvis, legs) were gauged in line with EuroNCAP standards. The color code scheme employed signifies risk levels—red implies high injury risk, orange indicates marginal injury risk, yellow represents acceptable injury risk, and green signifies low or negligible injury risk.

The most substantial injury risks during the significant vehicle contact were observed in the neck (highlighted by red hues in Figure 5.91-5.92) and the abdominal region (indicated by orange tones in Figure 5.91-5.92). These findings align with the actual injury report. Table 5.4 offers a comparative analysis of the numerical and actual injury outcomes. Moreover, the simulation identified elevated injury risks in the lower extremities. On the contrary, the head did not exhibit a heightened injury risk, potentially attributed to the utilization of a highly protective helmet model (AGV T2) for the simulation in this case.

The selected crash scenario extracted from the LMU accident dataset is emulated through the harmonious coupling of multiple components: a FEM passenger car model, a Multibody System MBS motorcycle, and an anthropometry-scaled model. This anthropometry-scaled model embodies the physical attributes of the motorcycle driver. The model is enhanced with a helmet, a standard protective gear for motorcycle riders. Employing virtual simulation techniques, the reconstruction process effectively replicates the intricate kinematics and dynamics of the motorcycle driver's actions during the accident event.

The evaluation of injury criteria exhibits a notable correspondence between the simulated outcomes and actual observed results. This alignment showcases the potential value of the virtual human body model, particularly in scenarios characterized by intricate kinematic and loading patterns. It points towards promising applications in scenarios where both complexity and accuracy are essential. Nonetheless, it is essential to underscore that while the virtual human body model proves valuable, the incorporation of a realistic vehicle model remains crucial to ensure the heightened predictability and reliability of the numerical simulations.

5.4 Summary

This chapter comprehensively delves into the intricate field of reconstructing accidents, encompassing both backward and forward reconstruction methodologies. By critically assessing the current state of the art in this domain, the chapter establishes a solid foundation for the subsequent analyses. Moreover, the chapter presents a detailed exploration of three distinct accident cases, with two cases originating from Florence and one from Munich, which were meticulously reconstructed using the proposed framework.

The first critical building block pertains to the PTW model, a fundamental representation of the motorcycle involved in the accidents. This model employs advanced techniques to adapt the motorcycle's mass and inertia properties, allowing it to mimic the behavior of the specific PTW in question. The PTW model's coupling with other elements is meticulously facilitated through various contact points, facilitating accurate replication of interaction scenarios.

In conjunction with the PTW, HBM adds another layer of complexity to the reconstruction process. Scaled and tailored to match the real-life rider's anthropometric attributes, the HBM brings the human element into the simulation. This model is meticulously coupled to the PTW and the PPE represented by a detailed helmet FE model, which is integrated through symmetrical contact and breakable spring mechanisms, simulating realistic interactions.

The chapter highlights the utilization of the proposed framework to successfully reconstruct the accident scenarios. It underscores the integration of both backward and forward reconstruction methods to yield accurate insights into the accident dynamics, sequences, and outcomes. Additionally, the efficacy of the framework in analyzing real-world accidents underscores its relevance in improving accident analysis and prevention strategies.

A noteworthy aspect of the framework is the introduction of simplified OV models, which are effectively employed in subsequent chapters. These models streamline the simulation process while retaining essential energy absorption structures for relevant impact scenarios.

In essence, the chapter serves as a pivotal juncture in the research journey, effectively applying advanced methodologies to replicate and understand intricate real-world accident scenarios. The comprehensive analyses of three distinct cases underscore the applicability and effectiveness of the proposed framework, positioning it as a promising avenue for enhancing accident reconstruction techniques and contributing to the broader field of PTW passive safety.

6 Full-scale crash tests

Full-scale crash tests are pivotal components of modern vehicle safety research and development. These tests involve subjecting entire vehicles to controlled, real-world collision scenarios to assess their crashworthiness, occupant protection, and overall structural integrity. Unlike computer simulations or small-scale experiments, full-scale crash tests provide comprehensive and accurate insights into how vehicles and their occupants respond to impact forces in actual crash situations. However numerical approach slowly started to become a standard not only in initial development but also in consumer testing [162].

These tests play a critical role in ensuring that vehicles meet stringent safety standards and regulations, ultimately aiming to reduce the severity of injuries sustained in accidents. They offer a means to evaluate the effectiveness of various safety systems, such as airbags, seat belts, crumple zones, and structural reinforcements. Moreover, full-scale crash tests help researchers and engineers refine vehicle designs, optimize safety features, and develop new technologies to enhance passenger and pedestrian safety.

The information gathered from these tests contributes to a deeper understanding of how different types of collisions impact vehicle occupants and the structural components of the vehicle itself. By observing and measuring forces, accelerations, and deformations during controlled crash scenarios, researchers can fine-tune safety systems and assess the potential for injury reduction. This empirical data forms the foundation for improving vehicle safety across a wide range of crash scenarios, including frontal, side, rear, and rollover collisions.

Full-scale crash tests provide invaluable data that inform regulatory agencies, manufacturers, and consumers about a vehicle's safety performance. As technology continues to advance, these tests remain indispensable tools in the ongoing efforts to create vehicles that better protect passengers and mitigate the consequences of accidents on our roads.

6.1 State of the Art

Full-scale crash tests are common procedures for the assessment of the crashworthiness and passive safety of new cars introduced to the market. These experimental tests must be conducted to achieve the type approval and prove the fulfilling the certain safety criteria (described for example in ECE-R 94 [163], FMVSS 208 [164], and similar standards). Another type of crash test are the customer test, these sets of test are not mandatory for the car manufacturers and often have far higher requirements according to the vehicle safety. The most common and recognized customer test organization is the European New Car Assessment Programme (Euro NCAP).

One of the first applications of the ISO 13232 standard for the full-scale motorcycle crash tests was done by the Berg F. from the DEKRA [3]. As a second part of the research paper, the four full-scale crash tests made in the DEKRA laboratories were presented. The constellations ISO 413 and ISO 414 with stationary and moving opposite vehicle were investigated. Due to the cost of the MATD the Hybrid III ATD was used as the driver surrogate. One of the evaluations of the accident participant's kinematics with the assessment of injury criteria is shown in Figure 6.1. One of the direct findings from the crash tests was "The results of these tests indicate that crash tests featuring a frontal impact of the motorcycle with the side of the standing vehicle tend to lead to higher loadings on the dummy head than corresponding collisions with moving vehicles."[3]. The decelerations of the ATD chest and head were measured below the injurious limit of SI = 1000 and a_3ms = 60 g respectively.

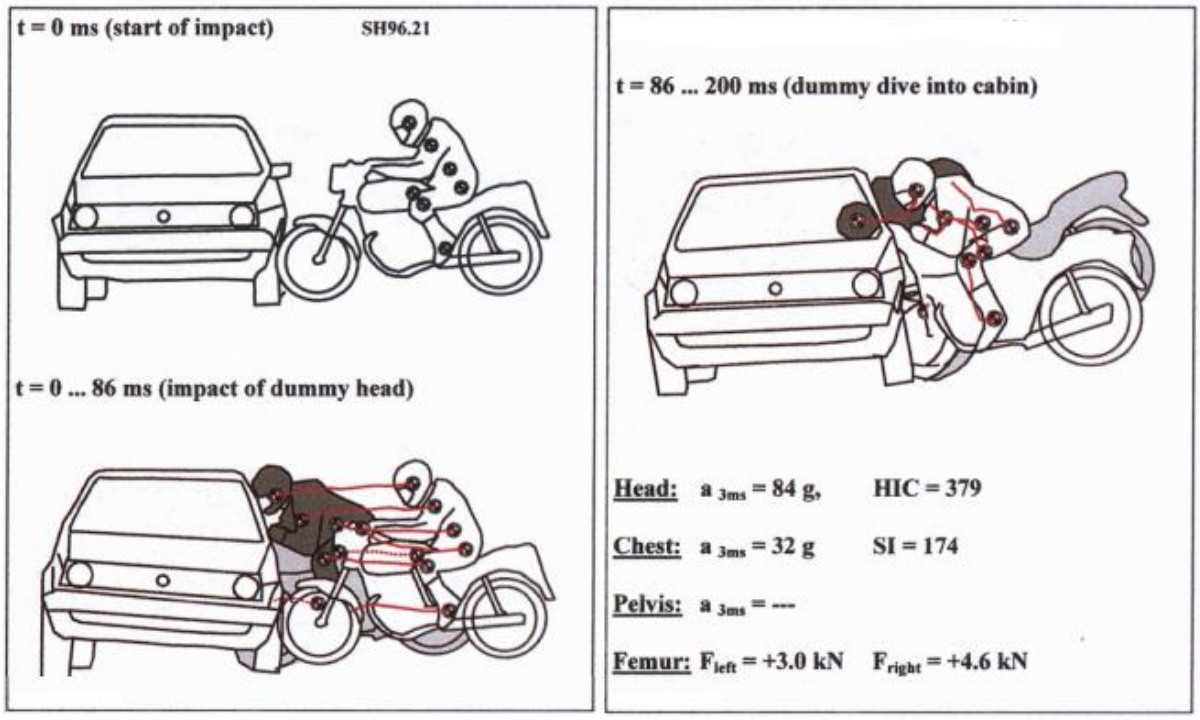

Figure 6.1. Evaluation of the ISO 413 constellation with stationary vehicle [3]**.**

To understand the retrospective analysis of the statistical data from the field accident research the team of researchers from Opel A.G and DEKRA [165] carried out the two most relevant (based on real accidents) types of full-scale crash tests. Namely frontal and side impacts of moving PTW into the opposite vehicle (car). The constellations of full-scale crash tests are depicted in Figure 6.2.

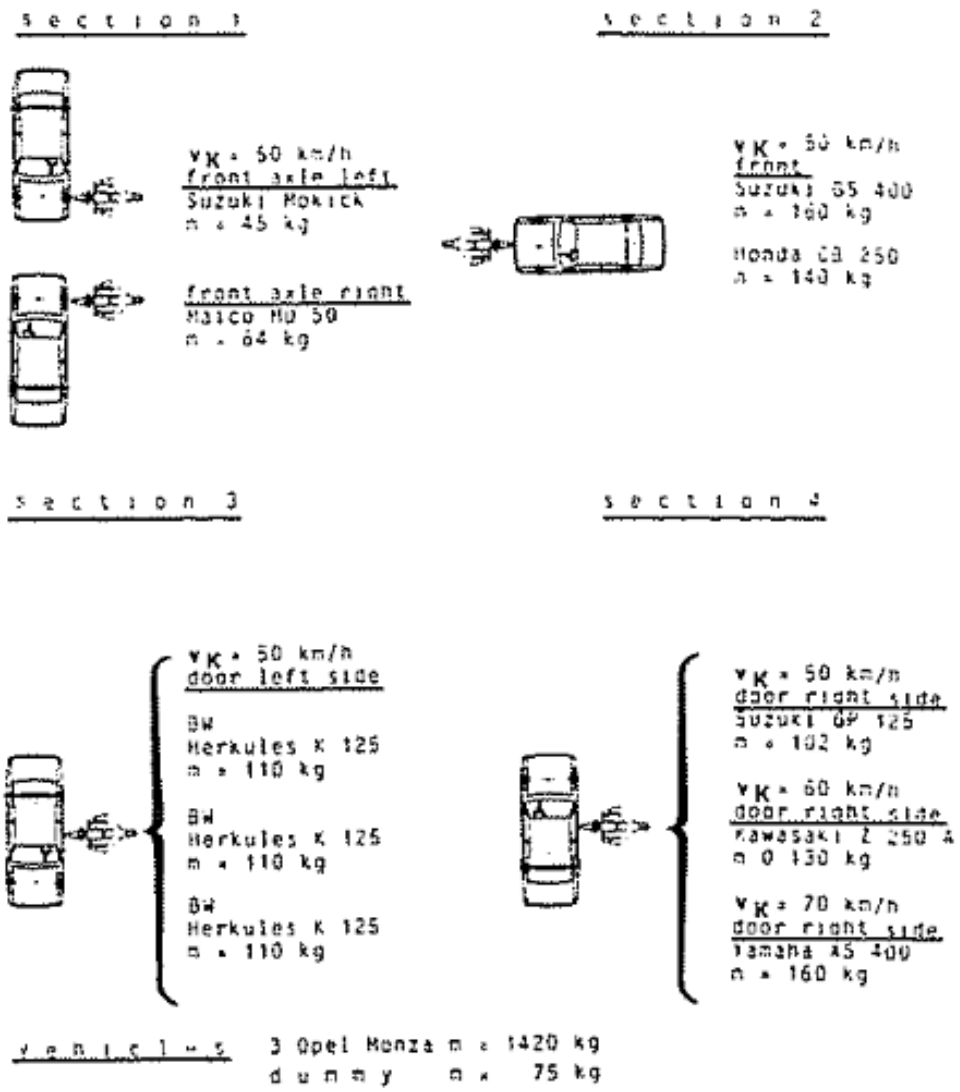

Figure 6.2. Motorcycle full-scale crash tests were performed in 1985 in Opel facility [165]**.**

This study allows to draw conclusions about the rider's kinematics and the deformation of the motorcycle during the accident. It was found that the fork usually deforms in the close time range of 10ms from the start of the crash. The analysis of the velocity correlated with the video analysis allows to draw the conclusion that most of the kinetic energy is dissipated/converted in the second crush phase (between 20 and 50 ms). The lifting of the rear wheel starts around 36 to 84 ms after contact. From all the constellations (with the dependence on initial velocity) the event stops at 54 to 120 ms, with the full conversion of the PTW kinetic energy to plastic or elastic deformation. The elastic deformation then causes the rebound phase which could be horizontal or upward around the front wheel.

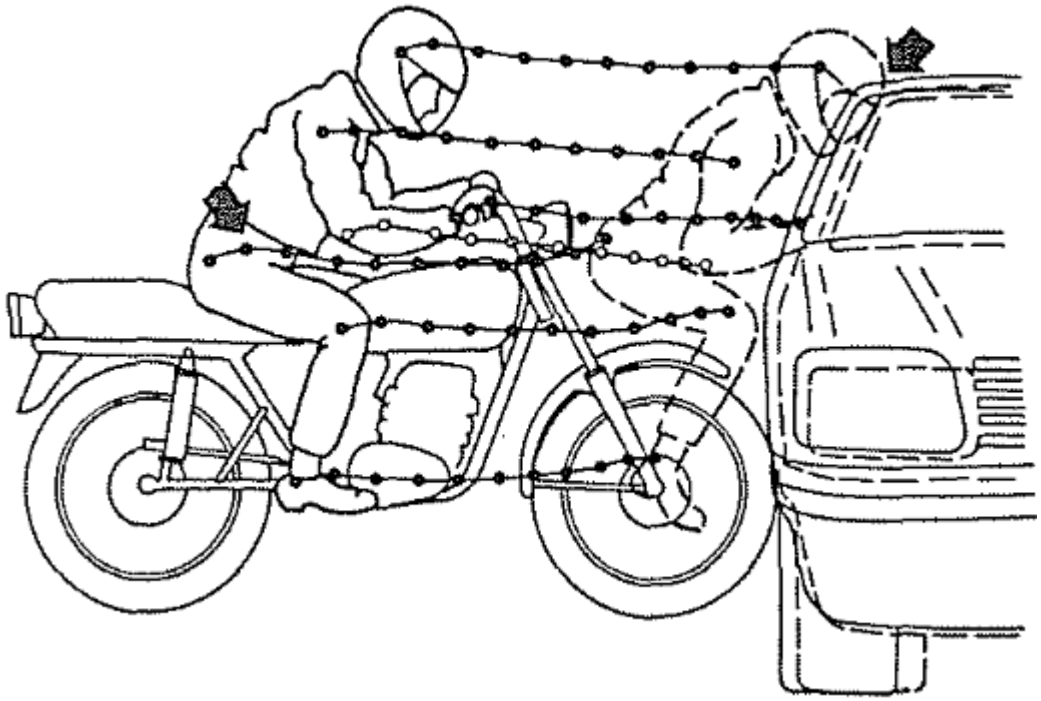

Figure 6.3. Kinematics of the rider's body parts during impact [165]**.**

The conclusions about the interaction of the motorcycle and dummy (ATD) kinematics were found as follows: “when finally rider's legs are trapped by the handle bars, while cycle is already rebounding, this input increases cycle's upward rotation considerably” [165]. That means in means that is reasonable to expect higher rear motorcycle wheel raising in case of the trapping of the surrogate between the handlebars. This conclusion could be also used for the design of crash energy management systems for particular PTWs’ design. The results depicted in Figure 6.3 show that during the accident ATD head continues the almost horizontal movement on the initial path (up to the roof contact).

Full-scale motorcycle crash tests could be also performed without the utilization of any driver surrogate, such a situation occurred during the 2016 World Reconstruction Exposition [166]. During the exposition, the researchers prepared and ran eleven instrumented crash tests with the Harley-Davidson motorcycles. The aim of this study was to update the empirical equations that are used for the estimation of the impact speed by measuring the wheelbase reduction or total crush. By applying the experimental data to the “Modified Eubanks” [167, 168] equations a new set of “Modified Bartlett Equations (MBEs)” has been derived:

$$Axle: \quad S = 2.16 * (L + C) + 17.33, \tag{2}$$

$$Bumper\ or\ pillar: \quad S = 1.36 * (L + C) + 19.50, \tag{3}$$

$$Door: \quad S = 1.50 * (L + C) + 9.27, \tag{4}$$

$$Fender: \quad S = 1.26 * (L + C) + 22.95, \tag{5}$$

where: S is impact speed in [mph], L is wheelbase reduction in [in], C is opposite vehicle crush in [in], and L+C is total crush in [in].

Since the PTW group of motorcycles is not only limited to the supersport, touring, or chopper style bikes, crash-tests of two-wheeler PTW with the scooter/ pedelec style are also in the interest of the safety research groups. This is especially true in countries like Malesia where the PTWs are often used as a main mode of transportation. This type of full-scale scooter crash test was presented by a research team from the Malaysian Institute of Road Safety Research (MIROS) [169]. The method section describes and preparation of three crash tests with the PTW in the scooter style with the average mass of 94 kg, and with the 29.3 km/h, 43.6 km/h, and 52.1 km/h impact speed respectively. As the driver surrogate the official MATD manikin was used. The total mass of the pre-crash accelerated system was in the range of 180 kg. Constellation was not described in the ISO 13232 terms, however from the pictures it can be assumed as the ISO 413 configuration with the small city car (perhaps Hyundai i10, model year 2008, which according to the datasheet has a 948kg dry mass) acting as a stationary opposite vehicle. The entire kinematics can be seen in Table 6.1, which in detail describes each phase of the post-impact movement. Regarding the injuries, the researchers summarized that the highest injury was recorded in the ATD chest (on the level of AIS 6, but the injury criteria were not indicated). The HIC criterion was evaluated to be in the range of 104, the team summarized it could indicate the good performance of the used helmet. However by re-analyzing the high-speed footing (100 – 130 ms of Table 6.1), it can be seen that most of kinetic energy from the MATD was dissipated during the contact of the chest to the dashboard and handlebar (AIS 6 injury confirms there was high transfer of the energy in this body region), and finally the head impacted and broke the side glass, where some of the remained head kinetic energy was also transformed into plastic, elastic deformation of the glass up to the ultimate strength of the side window. These experiments confirm the conclusions of the D. Schaper team [165], that the body/handlebar interaction can cause the uplifting of the rear wheel (depicted between 100 - 350 ms), and that in the interaction with the standing vehicle, the path of the head is uninterrupted up to the contact with the OV structure (-20 – 100 ms).

Table 6.1. Accident kinematics of crash test performed by the MIROS team at 43.6 km/h impact speed [169]**.**

Time	Description	High-Speed Image
-20 ms	Motorcycle position immediately before impact.	

0 ms	Beginning of the impact sequence, the wheel contacted the car side sill.	
20 ms	The front wheel started to deform and the front suspension began to deflect inward.	
50 ms	The front wheel and the suspension experienced maximum crush. At this moment, the rear suspension springs begin to expand and the rider slide forward.	
100 ms	The rear wheel began to lift. and the rider slide to the maximum distance with lower extremities hitting the plastic fairing and handle frame. Subsequently, the rider helmet started to hit the side glass.	
130 ms	The wheel rotation increased. The rider abdomen pivoted around the handle bar and the helmet penetrated through the car window while the chest hit the window frame.	

350 ms	The motorcycle rotated completely off the ground. Riders head + helmet stuck momentarily in the car compartment.	
640 ms	The motorcycle rotated to the maximum height as the front wheel subsequently hit the ground.	
700 ms	The motorcycle started to drop to the ground. The rider's head began to flex out of the car.	

Another conclusion drawn from these three crash tests was the graph which was correlating the impact speed with the wheelbase shortening. However, the equation in the form of Eubanks [167] of Bartlett was not derived. This deficiency could be easily fixed by applying the linear fit curve to the bare data provided by the MIROS paper:

$$V_{crash} = 0.1314 * delta_p + 25.026, \quad (5)$$

where: V_{crash} is crash speed in [km/h], and $delta_p$ is wheelbase shortening in [mm], it should be added that the symbols are not similar to Bartlett's equations due to the different unit systems (SI vs. Imperial).

The full-scale crash tests of the motorcycles are not limited to the constellations with the stationary opposite vehicle, which by common sense comes from the real-world PTW crash. However the preparation of a reliable and robust setup for conducting a crash test with two accelerated vehicles, in which one is single track is far more complicated than with a stationary target. These tests are especially important because due to the direct interaction of the front wheel (and its sidewise rotation) and front suspension of the PTW with the moving opposite vehicle, it's almost impossible to make an accurate approximation with just one moving vehicle test. The extensive methodology for conducting above-mentioned tests has been developed over the years by Exponent's Test and

Engineering Centre [170]. One of the Exponent team publications [171] describes a set of four crash tests as presented in Table 6.2.

Table 6.2. Parameters of Exponent Inc. moving to moving vehicle crash tests [171]**.**

Test Num.	Bullet Vehicle	Bullet Vehicle Speed [mph]	Target Vehicle	Target Vehicle Speed [mph]
1	1981 Kawasaki KZ750E	30.0	1986 Ford Mustang	14.0
2	1981 Kawasaki KZ750E	29.9	1986 Ford Mustang	30.1
3	2007 Kawasaki Ninja ZX-10R	63.2	1986 Jaguar XJ6	41.9
4	2006 Kawasaki Ninja ZX-10R	68.1	1985 Jaguar XJ6	46.6

The full-scale crash tests of the motorcycles in recent years were not only conducted in Germany and the USA but also in Poland. The detailed analysis of the post-crash movement of the motorcycle [172] and rider surrogate [173] was published by the team led by Prof. Prochowski. As input data for the detailed analysis, his team has used high-speed camera recordings from a crash-test case conducted by the Automotive Industry Institute (PIMOT) in Warsaw (Figure 6.4). The main outcome was that in the analyzed case a motorcycle rear wheel is reaching the 2.5m/s lifting speed and that around 15% of pre-crash kinetic energy is consumed by the rotation movement. From the point of the PTW driver injury the published analysis concluded that “the head hit the car with a velocity of 14.2 m/s and a force of 23 kN and the maximum acceleration value measured in the center of mass of the head reached a level of 110 g”.

Figure 6.4 Motorcycle crash test conducted in Polish Automotive Industry Institute (PIMOT) in Warsaw

In 2010 M. Toma, with the team from the MYMOSA project was conducting the research on finding the optimal foam liner for the motorcycle helmet. As an inter-step, the full-scale numerical crash test was employed in their research. The side impact of the motorcycle to the 50% length (the B pillar) was utilized to find the impact conditions for the optimization of the liner. The disadvantage of this study was the employment of the “semi-rigid” Hybrid III ATD model as a driver. This limitation could (and

probably has) influence the “realistic” behavior of the driver's neck, as the Hybrid III did not have a biofidelic neck for this type of configuration. [174]

The team of Zhi Xiao [175] by utilizing the numerical approach to the full-scale crash test, conducted a parametric study on the impact speed to find which speed level is critical for the occurrence of the driver injury described by the HIC and CSDM (Cumulative Strain Damage Measure). For HIC the threshold was found on 15m/s and for CSDM on 10m/s.

6.2 Numerical full-scale crash test

6.2.1 Standard Configurations – ISO 13232

The ISO 13232 standard [155], titled "Motorcycles - Test and analysis procedures for research evaluation of rider crash protective devices fitted to motorcycles," provides guidelines and procedures for assessing and testing rider crash protective devices on motorcycles. This standard is crucial in evaluating the safety and effectiveness of various protective measures designed to minimize injuries to motorcycle riders during crashes. One of the key components of the ISO 13232 standard is the definition of seven standardized motorcycle crash configurations. These configurations serve as specific testing scenarios that replicate common real-world crash situations. These standardized configurations help ensure consistent and reproducible testing procedures across different testing facilities and studies. Each configuration aims to assess the performance of protective devices under specific crash conditions.

The seven standard motorcycle crash configurations defined by the ISO 13232 standard are as follows and depicted in Figure 6.5.

Configuration 143 - Side Stationary Motorcycle Impact:

Impact Velocities: 9.8 m/s (OV), 0 m/s (PTW)

Description: In this scenario, the OV crashes into the side of the PTW. This evaluates the impact's effect of the moving OV into the PTW and its rider when impacted by the OV.

Configuration 114 - Frontal Skew Impact:

Impact Velocities: 6.7 m/s (OV), 13.4 m/s (PTW)

Description: A PTW collides obliquely into an opposite vehicle the OV that is moving at a lower speed. This configuration assesses the impact of a skewed frontal collision between two vehicles.

Configuration 413.1 - Side Opposite Vehicle Impact:

Impact Velocities: 6.7 m/s (OV), 13.4 m/s (PTW)

Description: A PTW crashes into the side of an OV that is in motion. This scenario evaluates the consequences of a side impact between a motorcycle and an opposite vehicle.

Configuration 412 - Side Rear Skew Vehicle Impact:

Impact Velocities: 6.7 m/s (OV), 13.4 m/s (PTW)

Description: The PTW collides obliquely into the side of the OV that is moving at a lower speed. The tangential component of the PTW velocity vector in this situation has the same direction as the OV

speed vector. This configuration assesses the outcome of a skewed side collision between a motorcycle and a vehicle.

Configuration 414 - Side Front Skew Vehicle Impact:

Impact Velocities: 6.7 m/s (OV), 13.4 m/s (PTW)

Description: The PTW collides obliquely into the side (B pillar) of the OV that is moving at a lower speed. The tangential component of the PTW velocity vector in this situation has different direction than the OV speed vector. This scenario examines the consequences of a skewed side collision between a motorcycle and a vehicle.

Configuration 225 - Near-Miss Frontal Impact:

Impact Velocities: 0 m/s (OV), 13.4 m/s (PTW)

Description: The PTW approaches an opposite vehicle OV head-on but avoids the direct collision, however slightly touches the side of the OV fender. This configuration evaluates the rider's responses and dynamics during a near-miss situation.

Configuration 413.2 - Side Stationary Opposite Vehicle Impact:

Impact Velocities: 0 m/s (OV), 13.4 m/s (PTW)

Description: The PTW crashes into the side of a stationary OV normally to the B pillar. This scenario assesses the impact of the moving motorcycle on a stationary object.

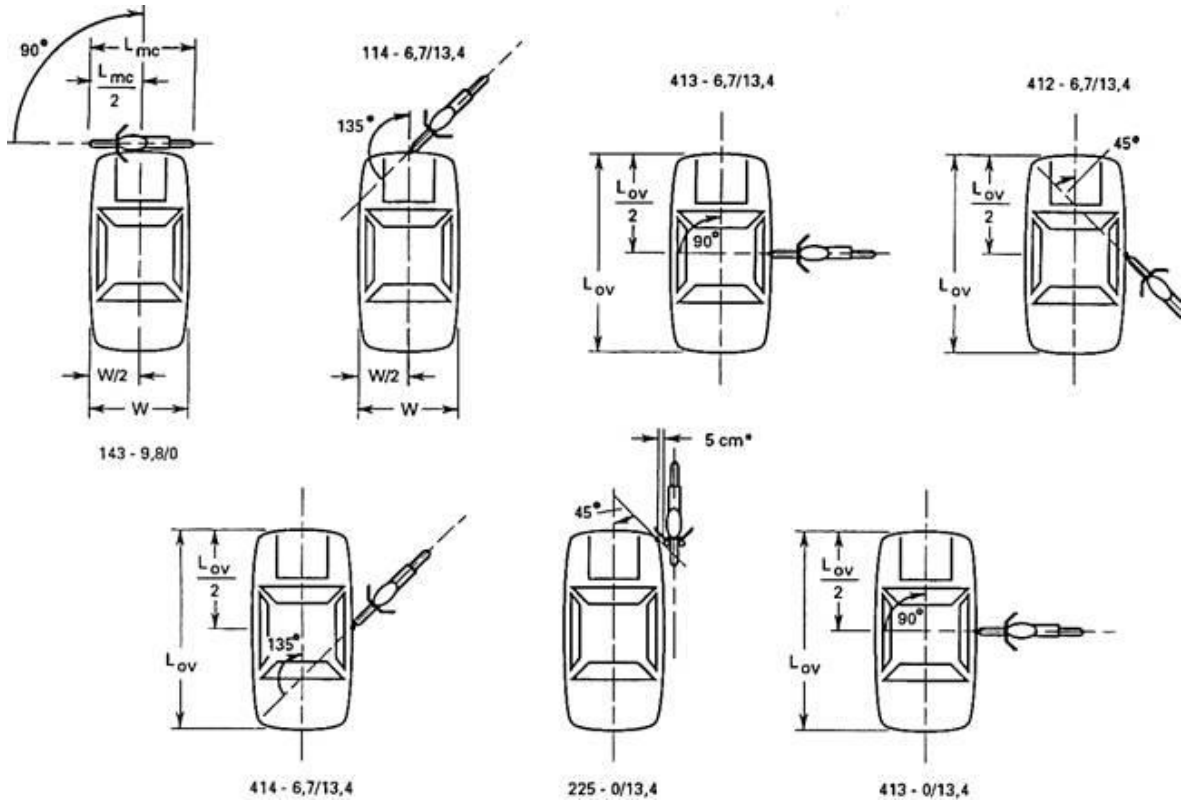

Figure 6.5 ISO 13232 seven standard configurations [155]**.**

These standardized crash scenarios provide valuable insights into the dynamics and potential injuries associated with different types of motorcycle crashes, aiding in the development of safety measures and protective equipment for motorcyclists. These configurations have become a standard practice in

the industry for conducting real-world crash tests on motorcycles, as well as for conducting numerical research studies on the PTWs [176–181]. The drawback of this standard is the utilization of mechanical ATD – MATD, in which biofidellity is far from being validated for the abovementioned vide range of different dynamical configurations, and due to the cost its implementation is rarely used [182].

6.2.1.1 Methods

The above-mentioned configurations were detail modeled using the proposed framework in the ESI VPS software package. For each ISO 13232 configuration, the motorcycle rider model represented by VH is integrated with a simplified FE helmet model and positioned on the motorcycle, maintaining an appropriate gap between the hip and the motorcycle seat. To recap the framework procedure: symmetrical contact between the rider and the motorcycle is established then the interaction between the hands and handlebars is simulated using breakable springs, characterized by a stiffness of 9.36 kN/m and a limiting force of 350 N for each hand. The simulation is executed until the highest possible injury criterion is reached. The ground is represented as a rigid plane with a consistent friction coefficient of 0.7. The OV in this part is represented by two simplified models of Neon (frontal and side), developed in the previous chapter.

Prior to result evaluation, specific joint forces, moments, and node accelerations, including the head center of gravity, are filtered following the SAE J211 standard. To enhance result clarity, each ISO configuration is assigned a descriptive name, as detailed in Table 6.3.

Table 6.3 ISO 13232 cases description [155]**.**

ISO 13132 Configuration	Impact velocity OV/PTW [m/s]	Descriptive name
143	9.8/0	side stationary motorcycle impact
114	6.7/13.4	frontal skew impact
413 (413.1)	6.7/13.4	side opposite vehicle impact
412	6.7/13.4	side rear skew vehicle impact
414	6.7/13.4	side front skew vehicle impact
225	0/13.4	near-miss frontal impact
413 (413.2)	0/13.4	side stationary opposite vehicle impact

Side Stationary Motorcycle Impact (ISO 143 9.8/0)

ISO 13232 outlines the side stationary motorcycle impact configuration as an occurrence where the OV undergoes a frontal impact onto the side of the PTW, which is positioned perpendicular to the OV (Figure 6.6). In this specific setup, the PTW remains stationary, while the OV's impact velocity is set at 9.8 m/s. For the numerical simulation of this arrangement, the simplified frontal OV model is utilized.

Notably, in this instance, the presence of the elastic joint within the front fork, which is usually instrumental in replicating fork bending dynamics, has a lesser significance.

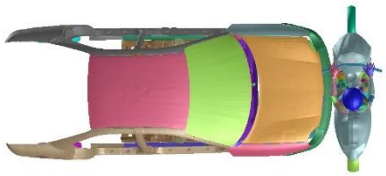

Figure 6.6 ISO 143 simulation setup configuration.

Frontal Skew Impact (ISO 114 6.7/13.4)

The frontal skew impact scenario (Figure 6.7) portrays a situation where the motorcycle impacts the front of a car at a 45-degree angle relative to the car's symmetry plane. Notably, this configuration holds the distinction of being the 3rd highest Configuration Risk Index (CRI) according to Grassi's assessment [183], and it's identified as the 1st highest CRI in the MAIDS and Hanover-Los Angeles databases. Both involved vehicles are in motion in this case, with the initial velocity of the PTW set at 13.4 m/s, while the OV's velocity is set at 6.7 m/s.

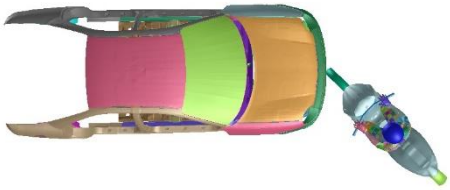

Figure 6.7 ISO 114 simulation setup configuration.

Side Opposite Vehicle Impact (ISO 413 6.7/13.4)

The side opposite vehicle impact configuration is a frequently encountered scenario at intersections, where the PTW collides with the centerline of the opposite vehicle (OV) at 90 deg. angle (Figure 6.8). The final rider's kinematics in this setup can be notably affected by the OV's design, particularly concerning the placement of the B pillar. In this particular study, the B pillar's position did not align with the 50% length of the OV. Consequently, the impact point of the PTW's front wheel falls on the front doors. In this configuration, the PTW collides with a moving OV at a speed of 13.4 m/s. The OV's velocity at the time of impact was set at 6.7 m/s in accordance with the established standard.

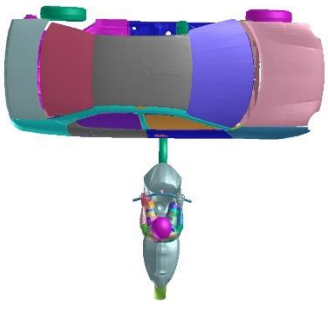

Figure 6.8 ISO 413.1 simulation setup configuration.

Side Rear Skew Vehicle Impact (ISO 412 6.7/13.4)

The side rear skew vehicle impact configuration diverges from the side opposite vehicle impact setup in terms of the relative heading angle of the PTW (Figure 6.9). In this particular case, the motorcycle collides with the side of the OV at a 45-degree angle to the OV's vertical longitudinal plane. By conducting a basic vector analysis of the velocities, it's reasonable to anticipate a lower impact speed of the rider's head. The initial velocity values remain identical to those in the side opposite vehicle impact case, with the OV traveling at 6.7 m/s and the PTW at 13.4 m/s.

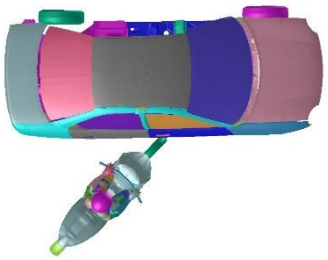

Figure 6.9 ISO 412 simulation setup configuration.

Side Front Skew Vehicle Impact (ISO 414 6.7/13.4)

In the scenario involving a side front skew vehicle impact (Figure 6.10), the position of the PTW is a mirror reflection across the vertical transverse plane of the PTW's position in the side rear skew vehicle impact configuration. The initial velocities of both vehicles remain unchanged.

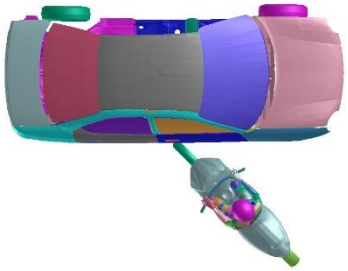

Figure 6.10 ISO 414 simulation setup configuration.

Near-Miss Frontal Impact (ISO 225 0/13.4)

The ISO 13232 configuration involving a near-miss frontal impact depicts a scenario where the motorcycle narrowly avoids a collision with the OV. In this setup, the OV is stationary, while the PTW starts with an initial velocity of 13.4 m/s. The configuration (Figure 6.11) is constructed through the following steps:

- Identifying the vertical longitudinal plane of the OV (Y),
- Creating a plane perpendicular to the horizontal plane of the OV (Z),
- Rotating the plane from the previous step until it achieves a 45-degree angle to the Y plane of the OV,
- Translating the plane to establish a single-point contact with the front fender,

- Constructing a plane parallel to the Y plane of the OV, which is shifted 5 cm outward from the car body at the contact point from the previous step,
- Positioning the PTW by aligning its vertical longitudinal plane with the plane from the preceding step, ensuring that the X-axes of both vehicles face opposite directions,
- Adjusting the position of the PTW to ensure clearance for the contact algorithm (preventing initial penetration).

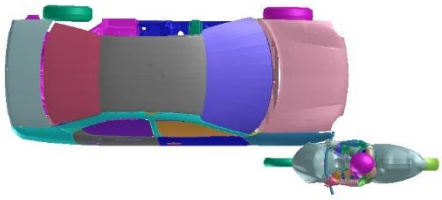

Figure 6.11 ISO 225 simulation setup configuration.

Side Stationary Opposite Vehicle Impact (ISO 413 0/13.4)

The scenario involving a side stationary opposite vehicle impact is a simplified version of the side opposite vehicle impact configuration. In this setup, the OV remains stationary, and the PTW collides with the centerline of the OV at a velocity of 13.4 m/s (Figure 6.12).

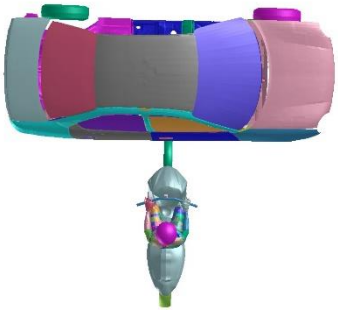

Figure 6.12 ISO 413.2 simulation setup configuration.

6.2.1.2 Results: kinematics

Side Stationary Motorcycle Impact (ISO 143 9.8/0)

The kinematics of the side stationary motorcycle impact simulation are depicted in Figure 6.13. The collision commences with the initial contact between the motorcycle frame and the rider's left shin against the front bumper of the Neon. Subsequently, the motorcycle topples over and skids along the ground. Throughout the crash, the movement of the rider follows these stages:

- From 0 to 150 ms, the motorcycle rider disengages from the motorcycle and undergoes clockwise rotation in tandem with the motion of the hood.
- Between 150 and 300 ms, the motorcycle rider maintains a clockwise rotation around the point of contact between the hip and the hood. The rider's back then makes contact with the front windshield.
- From 300 to 750 ms, the rider continues a clockwise rotation in conjunction with the front windshield. The rider's back remains in contact with the front windshield from a top-down perspective.

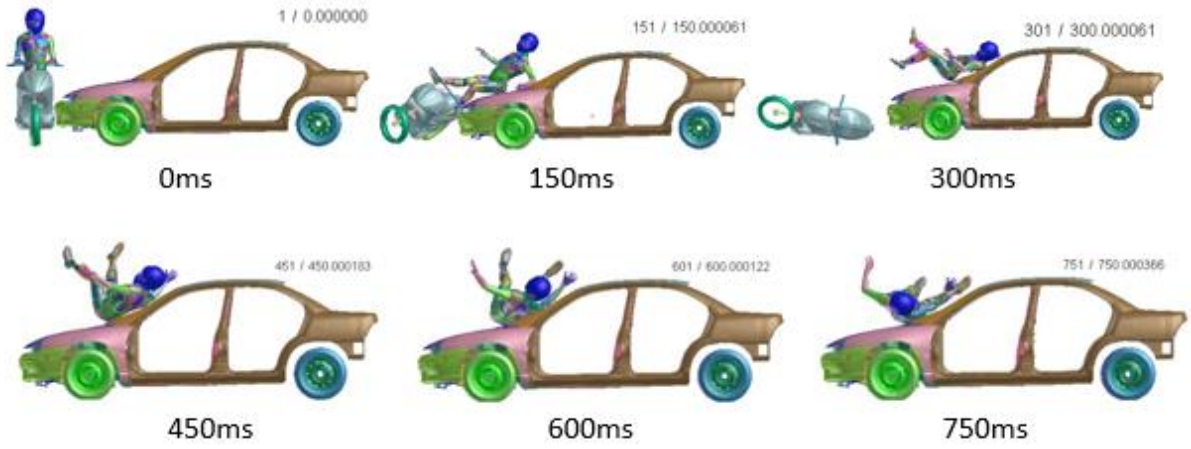

Figure 6.13 Kinematic responses of ISO 143-9.8/0 simulation

Frontal Skew Impact (ISO 114 6.7/13.4)

The kinematics of the frontal skew impact simulation are illustrated in Figure 6.14. The collision was initiated by the initial contact between the motorcycle's front wheel and the front bumper of the Neon. Following this, the motorcycle undergoes a clockwise rotation around the front wheel before ultimately falling to the ground and skidding. Throughout the crash, the movement of the motorcycle rider unfolds through the following phases:

- From 0 to 150 ms, the motorcycle rider glides along the motorcycle seat, disengaging from the motorcycle. The rider experiences clockwise rotation over the hood, leading to contact between the helmet and the front windshield.
- Between 150 and 300 ms, the motorcycle rider continues a clockwise rotation around the point of contact between the helmet and the front windshield. Concurrently, the contact point shifts to the lower right.
- From 300 to 1050 ms, the rider executes a rotation of approximately 270 degrees clockwise.
- Between 1050 and 1200 ms, the helmet gradually makes contact with the ground, and the rider maintains clockwise rotation. Subsequently, the back, hip, and lower limbs come into contact with the ground.

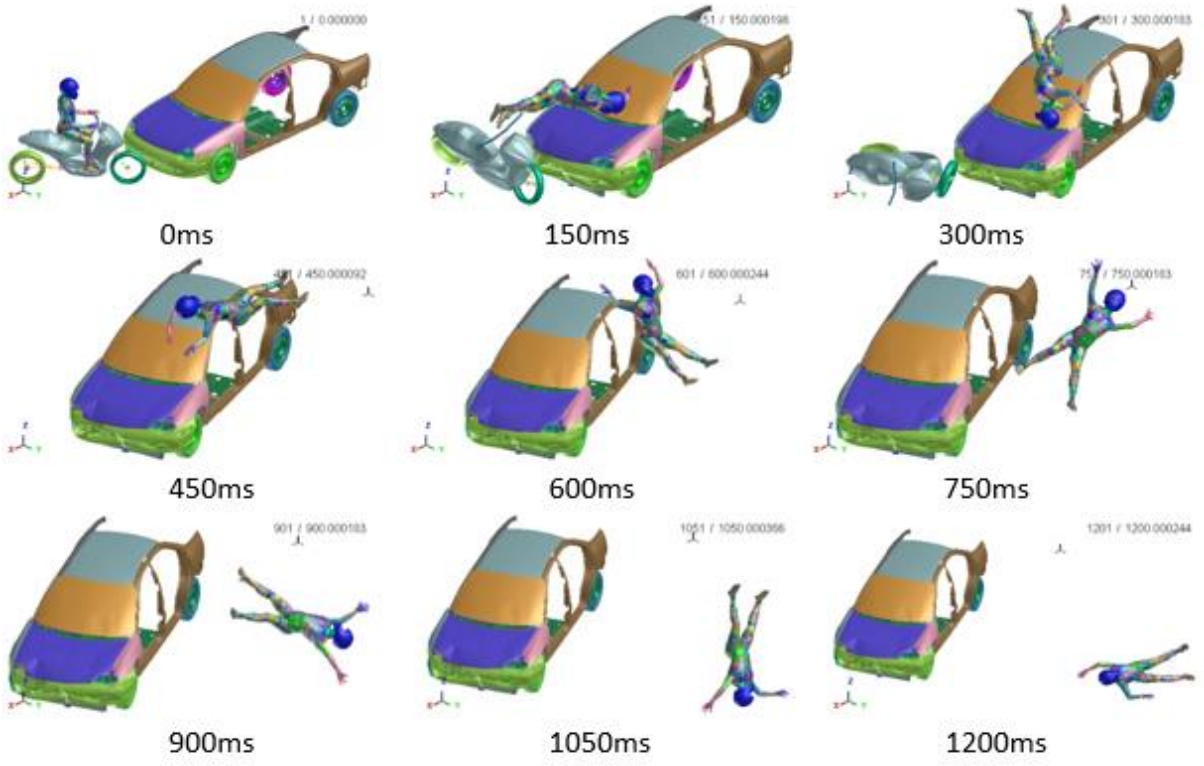

Figure 6.14 Kinematic responses of ISO 114-6.7/13.4 simulation.

Side Opposite Vehicle Impact (ISO 413 6.7/13.4)

Figure 6.15 presents the kinematics of the simulation for side opposite vehicle impact. The collision between the vehicle and motorcycle commences with the initial contact occurring between the motorcycle's front wheel and the left front door of the Neon. As a result, the motorcycle undergoes counterclockwise rotation around the front wheel. The front portion of the motorcycle frame comes into contact with the left rear door before the motorcycle eventually falls to the ground and skids. Throughout the crash, the motion of the motorcycle rider unfolds through the following phases:

- During the interval of 0 to 150 ms, the motorcycle rider glides along the motorcycle seat and disengages from the motorcycle. This is accompanied by counterclockwise rotation as observed from both the front view and the top view. Subsequently, the helmet makes contact with the roof.
- Between 150 and 900 ms, the motorcycle rider maintains a continuous counterclockwise rotation of about 180 degrees, as viewed from the top.
- From 900 to 1200 ms, the rider falls to the ground. The helmet, thorax, and lower limbs come into contact with the ground, and then subsequently slide along the ground.

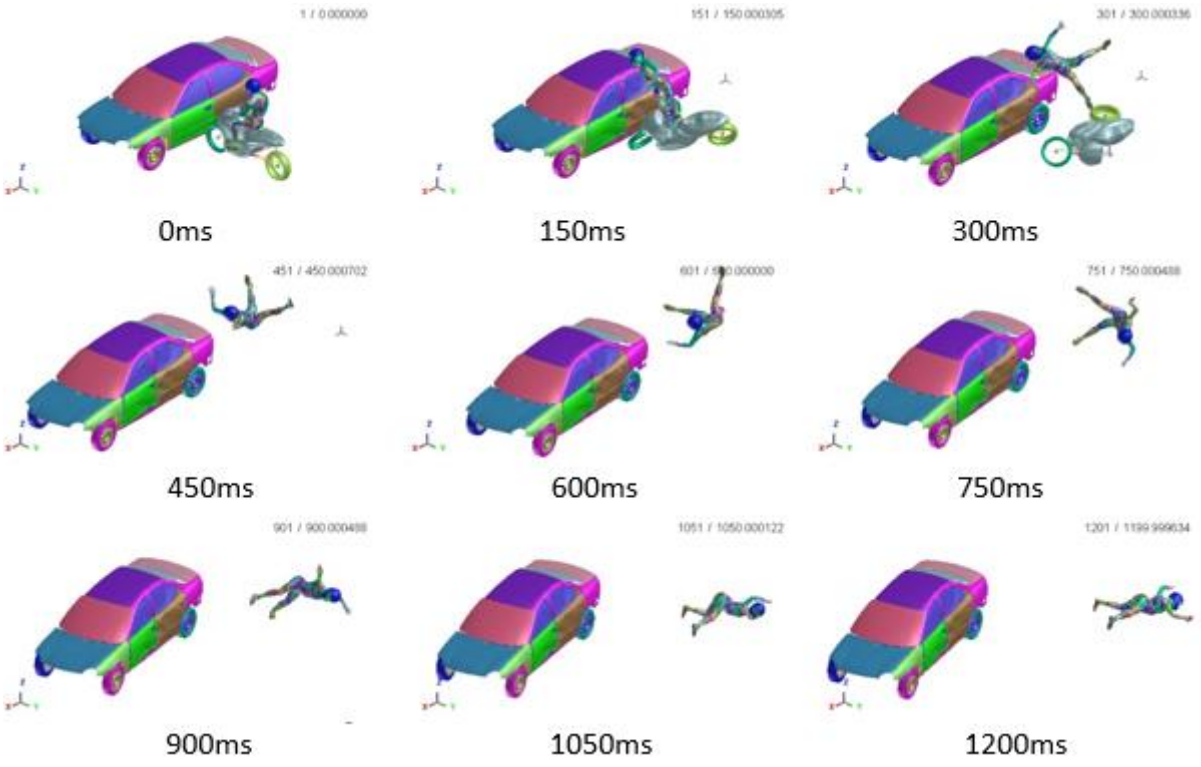

Figure 6.15 Kinematic responses of ISO 413-6.7/13.4 simulation.

Side Rear Skew Vehicle Impact (ISO 412 6.7/13.4)

Figure 6.16 illustrates the kinematics of the simulation for side rear skew vehicle impact. The interaction between the vehicle and motorcycle commences with the initial contact between the motorcycle's front wheel and the left front door of the Neon. Subsequently, the motorcycle undergoes counterclockwise rotation around the front wheel. The motorcycle frame then comes into contact with the left rear door, eventually leading to the motorcycle falling to the ground and sliding. Throughout the crash, the motion of the motorcycle rider unfolds through the following phases:

- In the time span of 0 to 150 ms, the motorcycle rider glides along the motorcycle seat and separates from the motorcycle. Concurrently, counterclockwise rotation is observed from the front view. At this point, the right upper limb and shoulder make contact with the left rear window.
- From 150 to 900 ms, the motorcycle rider continues to slide along the front windshield and hood.
- Between 900 and 1200 ms, the rider falls from the hood. The helmet and lower limbs come into contact with the ground, followed by the helmet bouncing off the ground.

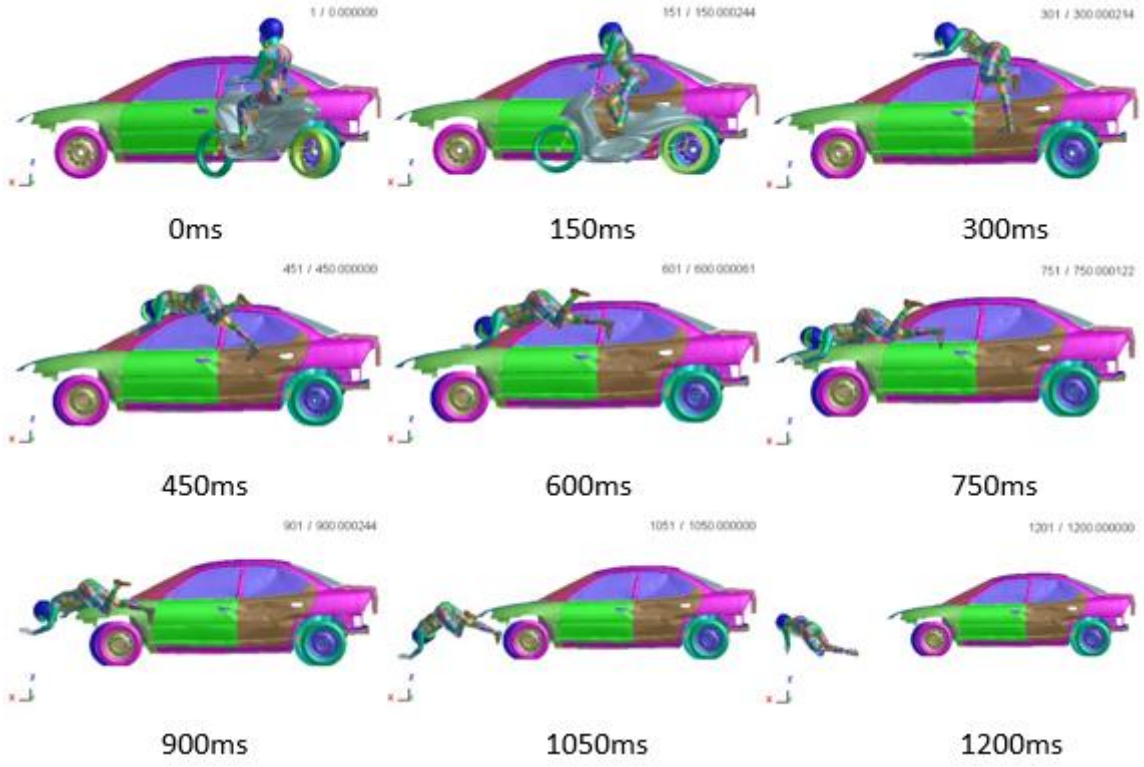

Figure 6.16 Kinematic responses of ISO 412-6.7/13.4 simulation.

Side Front Skew Vehicle Impact (ISO 414 6.7/13.4)

Figure 6.17 depicts the kinematics of the simulation for side front skew vehicle impact. The collision between the vehicle and motorcycle initiates with the initial contact between the motorcycle's front wheel and the left front door of the Neon. Consequently, the motorcycle undergoes clockwise rotation around the front wheel from the top view. The motorcycle frame makes contact with the left rear door, ultimately leading to the motorcycle toppling over and sliding on the ground. Throughout the crash, the progression of the motorcycle rider's motion unfolds through the following stages:

- In the time span of 0 to 100 ms, the motorcycle rider glides along the motorcycle seat and separates from the motorcycle. Concurrently, clockwise rotation is observed from the top view.
- From 100 to 200 ms, the motorcycle rider executes a clockwise rotation over the trunk as viewed from the side.
- From 200 to 900 ms, the rider completes a clockwise rotation of about 180 degrees when viewed from the side. Additionally, the helmet begins to make contact with the ground.

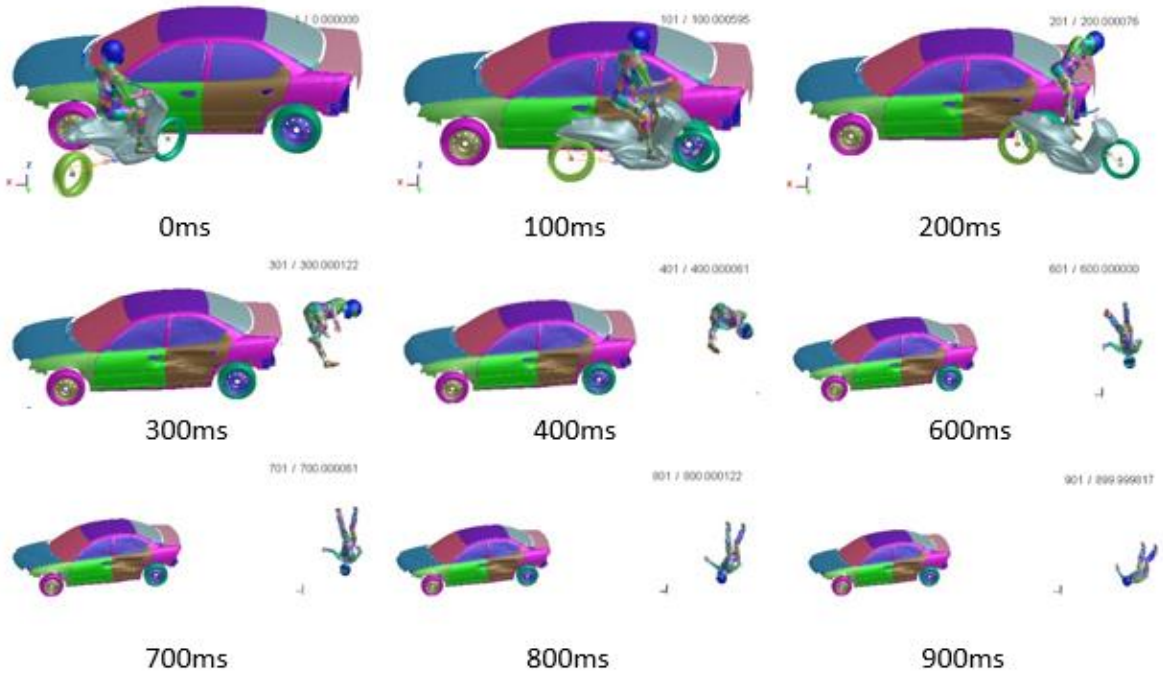

Figure 6.17 Kinematic responses of ISO 414-6.7/13.4 simulation.

Near Miss Frontal Impact (ISO 225 0/13.4)

Displayed in Figure 6.18 is the kinematics of the near-miss frontal impact simulation. The interaction between the vehicle and motorcycle is initiated by the initial contact between the motorcycle frame and the left front wheel of the Neon. Subsequently, the motorcycle experiences a fall and slides across the ground. Throughout the crash sequence, the motorcycle rider's movement unfolds in the subsequent stages:

- From 0 to 100 ms, the motorcycle rider glides along the motorcycle seat.
- From 100 to 200 ms, the rider disengages from the motorcycle.
- From 200 to 600 ms, the motorcycle rider undergoes clockwise rotation as observed from the side view. This motion ultimately leads to a fall, and the helmet begins to make contact with the ground.

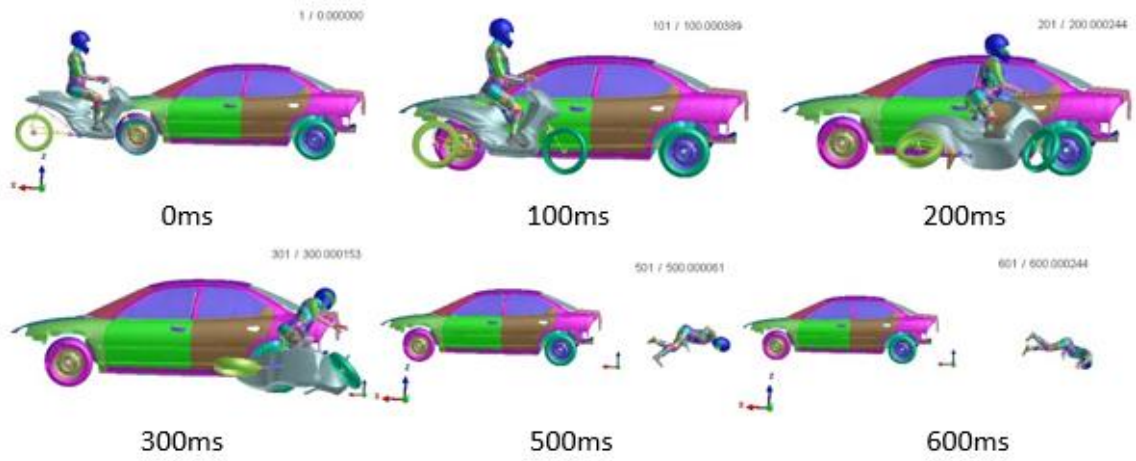

Figure 6.18 Kinematic responses of ISO 225-0/13.4 simulation.

Side Stationary Opposite Vehicle Impact (ISO 413 0/13.4)

Illustrated in Figure 6.19 is the kinematics of the side stationary opposite vehicle impact simulation. The collision sequence between the vehicle and the motorcycle is initiated by the initial contact between the motorcycle's front wheel and the left front wheel of the Neon. Subsequently, the PTW undergoes a counterclockwise rotation as observed from the front view, followed by a fall of the motorcycle. Throughout the crash scenario, the motorcycle rider's movement unfolds in the following steps:

- From 0 to 150 ms, the motorcycle rider glides along the motorcycle seat and separates from the motorcycle. Subsequently, the rider executes a counterclockwise rotation as viewed from the front, and the helmet establishes contact with the upper portion of the left front door.
- From 150 to 450 ms, the rider continues to execute a counterclockwise rotation of about 180 degrees from the front view.

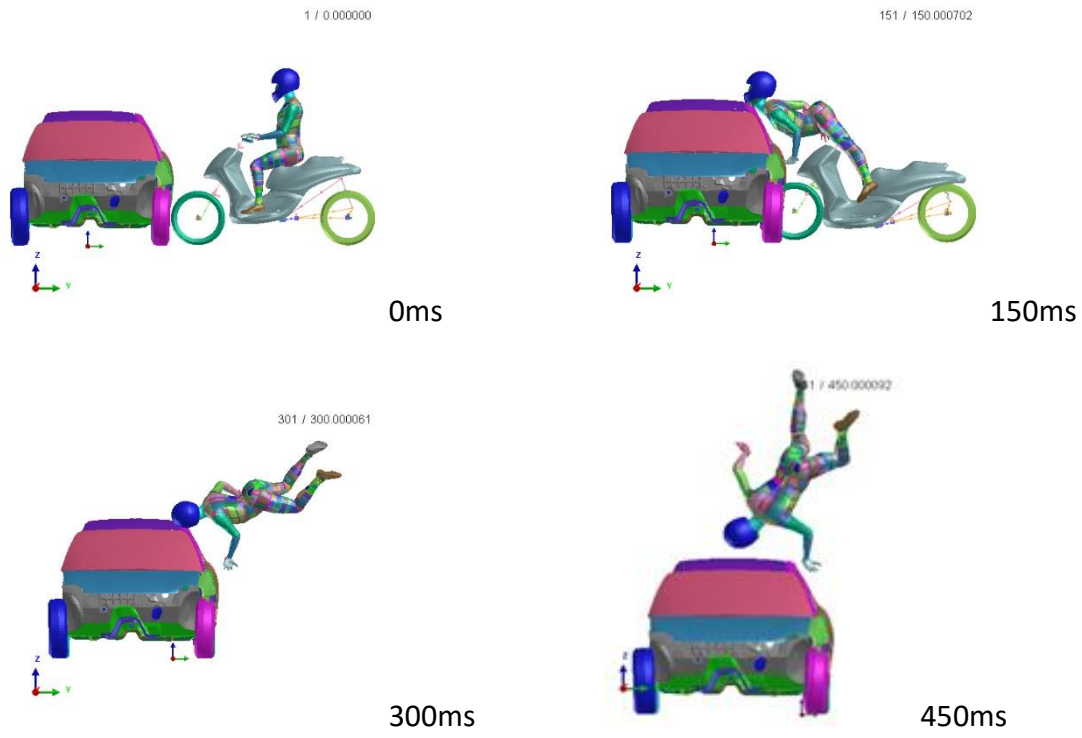

Figure 6.19 Kinematic responses of ISO 413-0/13.4 simulation.

6.2.1.3 Results: Injury assessment

Depicted in Figure 6.20 is the comparison of the head HIC 36ms criterion across the accidents outlined in ISO 13232. The evaluation of the HIC accounts for the secondary impact, a particularly important consideration in scenarios lacking direct contact between the car and the rider's head. In the figure, the impact type numbers 413.1 and 413.2 correspond respectively to side opposite vehicle impact and side stationary opposite vehicle impact. This simplified notation is employed to enhance the clarity of the visuals. The data presented in Figure 6.20 highlights several key observations. Specifically, the HIC for the side stationary opposite vehicle impact demonstrates notably higher values compared to other cases. Conversely, the HIC for the scenario involving side front skew vehicle impact registers lower values. These findings suggest that the simulation involving side stationary opposite vehicle impact presents a significantly elevated head injury risk compared to the simulation featuring side front skew vehicle impact. The HIC for the side stationary opposite vehicle impact is observed during the timeframe when the helmet makes contact with the upper portion of the left front door. On the other hand, the HIC associated with the side front skew vehicle impact occurs as the simulation progresses to around 900 ms, coinciding with the moment when the helmet interacts with the ground.

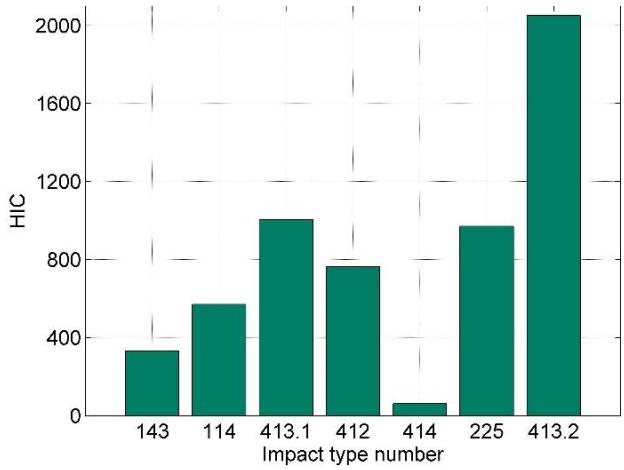

Figure 6.20 Configurations evaluation of HIC 36ms.

The highest peak moments in the rider model's neck are observed at the joint connecting the C0 and C1 vertebrae across all impact simulations, as depicted in Figure 6.22. These moments encompass both positive and negative C0-C1 values, representing flexion and extension bending moments, respectively. The figure indicates that the peak flexion bending moments at the C0-C1 joint during the side opposite vehicle impact, side rear skew vehicle impact, side front skew vehicle impact, and near-miss frontal impact are greater than the absolute values of the corresponding peak extension bending moments in the same scenarios. Notably, the side stationary opposite vehicle impact displays peak flexion bending moments at C0-C1, and the absolute value of peak extension bending moments during near-miss frontal impact exceeds that in other simulations.

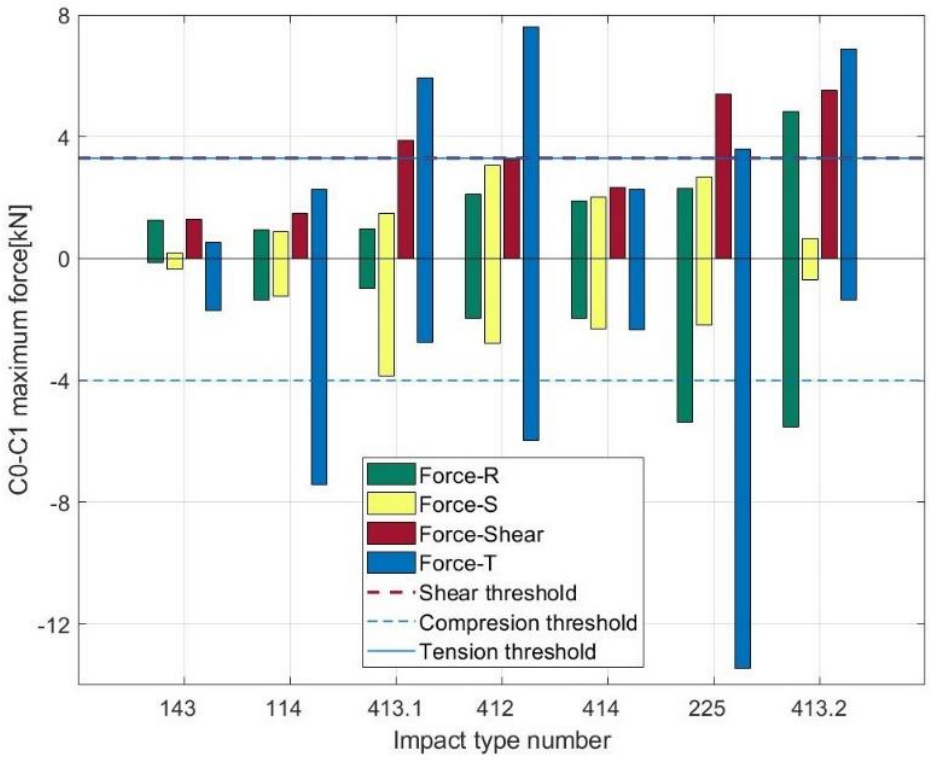

Figure 6.21 Comparison of C0-C1 forces in the motorcycle rider's neck with the UNE 135900 thresholds.

Figure 6.21 illustrates the peak shear neck forces (Force-R, Force-S) and the axial neck force (Force-T), all measured at the C0-C1 joint. Positive and negative axial forces signify tension and compression forces, respectively. The figure reveals that the peak tension force during side opposite vehicle impact, side stationary opposite vehicle impact, and side rear skew vehicle impact exceeds those in other scenarios. Furthermore, the peak compression force in the near-miss frontal impact simulation is the highest among all simulations. The figure also indicates that the positive peak shear force during the side stationary opposite vehicle impact surpasses that in other scenarios. Nevertheless, when evaluating the maximum magnitude of the vector sum of Force-R and Force-S (which together generate shearing force in the X-Y plane of the neck), it is found that only side stationary motorcycle impact, frontal skew impact, and side front skew vehicle impact remain below the UNE 135900 [184], [185] level II severity threshold of 3100N described in the chapter about neck injury criteria.

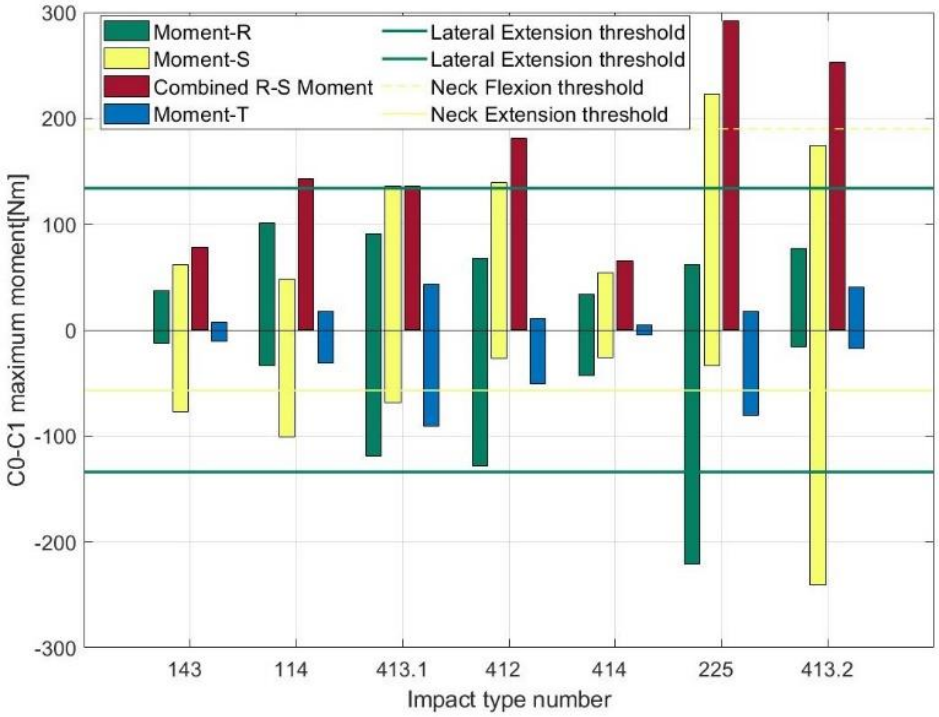

Figure 6.22 Comparison of C0-C1 moments in the motorcycle rider's neck with the UNE 135900 thresholds.

In evaluating neck injury potential, the initial consideration was the Nij criterion as a measure of neck protection or risk assessment (described deeply in the neck injury criteria chapter). However, this criterion only accounts for flexion/extension neck moments and tension/compression forces, addressing loads primarily in the coronal plane of the human body. Recognizing that the rider's neck loading, particularly during secondary impacts, extends beyond the coronal plane, it became evident that the Nij criterion wasn't comprehensive enough for assessing protection.

To address this limitation, criteria for upper neck injuries, encompassing loads in the sagittal, coronal, and transverse planes, are outlined in the UNE 135900 standard [184, 185]. Within this standard, threshold values for shearing force, compression/extension forces, and flexion/extension moments are derived from EuroNCAP, while the lateral bending limit [186] is adapted from FMVSS 208 [187].

Table 6.4 UNE 135900 criteria assessment (forces – level II severity thresholds).

Neck limit		143	114	413.1	412	414	225	413.2
3100 N	Neck Shear							
3300 N	Neck Tension							
4000 N	Neck Compression							
134 Nm	Neck Lateral Flexion							
57 Nm	Neck Extension							
190 Nm	Neck Flexion							

Table 6.4 presents the results of scenario assessments. Only the side front skew vehicle impact scenario adheres to the thresholds across all criteria. Conversely, the near-miss frontal impact scenario exceeds the limit in five of the six criteria. This assessment underscores that the thresholds for neck lateral flexion are surpassed in the near-miss frontal impact simulation.

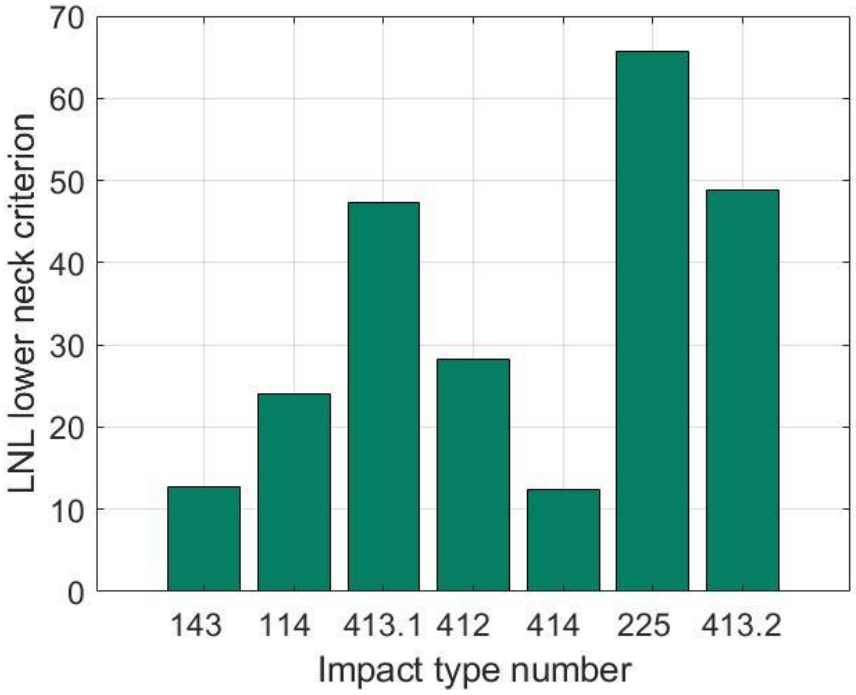

Figure 6.23 Lower neck criterion assessment.

The UNE 135900 criteria prove to be a suitable tool for assessing upper neck severity. However, they don't provide a single numerical value that can be universally evaluated across different scenarios or protective equipment within the same scenario. An exception to this lies in the Lower Neck Load Index

(LNL) criterion, the sole criterion considering loading in all five degrees of freedom (5 DOF) - encompassing three forces and two moments. Heitplatz [188] recommended the LNL criterion as a response to Prasad's [189] proposition, highlighting that existing criteria account for just one of several forces and moments potentially generated in the neck during impact. The LNL criterion is calculated based on lower neck loads, specifically employing C6-C7 joint forces and moments for its computation.

Scenario assessments concerning the LNL criterion are depicted in Figure 6.23. Nevertheless, Schmitt [76] summarized the LNL's limitations, including the absence of a firmly established biomechanical link to possible injury mechanisms and the lack of correlation with real-world injury outcomes. Additionally, the LNL is limited in its application due to the requirement of ATD instrumentation with a lower neck force/moment cell.

The thresholds used by the NCAP for injury criteria are respectively 1000 for the HIC. The HIC threshold was exceeded only in the side opposite vehicle impact and the side stationary opposite vehicle impact, but also for cases with the near-miss frontal impact, the value of the HIC was close to 1000, which means that for these cases probability of injury higher than AIS3+ was greater than 50 % [187]. The evaluation of the HIC shows that the cases with the side stationary motorcycle impact, the frontal skew impact, and the side front skew vehicle impact present the lowest risk of skull injury (HIC far below the 1000 threshold). For the case with the side stationary motorcycle impact, it means that the probability of injury higher than AIS3 is lower than 10 %, and the probability of injury higher than AIS2 is lower than 25 % [187]. Respectively for the case with the frontal skew impact, it means the probability of AIS3+ is around 19% and AIS2+ around 55 %. Where for the case with the side front skew vehicle impact there should not be any risk of skull injury [187].

The evaluation of the LNL criterion on the C6-C7 joint (Figure 6.23) shows that the configurations with the side opposite vehicle impact, the side stationary opposite vehicle impact, and the near-miss frontal impact could cause the highest load on the lower neck of the rider. On the other side, the configurations with the side stationary motorcycle impact and the side front skew vehicle impact have the lower LNL criterion (under 15). These results are in good correlation with the UNE 135900 criteria assessment. Due to the limited experience with the LNL criterion and lack of established biomechanical connection to the injury, the establishing of any hard threshold is not possible, but with the correlation to the UNE 135900 criteria, the LNL can be a simple and robust criterion for the neck load assessment.

6.2.1.4 Full-scale numerical testing summary

This sub-chapter outlines the framework applied for numerically simulating scenarios defined in the ISO 13232 standard within a virtual environment. This setup incorporates a multi-body system model of a PTW, a simplified FE model of the OV, a novel hybrid human body model (Virthuman), and a virtually "certified" model of a full motorcycle helmet. These models are interconnected using contact interfaces and breakable springs (representing handgrips). This approach introduces novelty compared to existing studies in the field, but it also presents challenges due to a lack of validation data. No studies were identified that utilized post-mortem human body surrogates as motorcycle riders in PTW crash tests, making validation challenging. Qualitative validation through accident reconstruction was considered, but finding real-life accident cases exactly matching ISO 13232 configurations is nearly impossible.

Detailed analysis of rider kinematics for each case was provided. Assessment of NCAP, UNE 135900, and LNL criteria was conducted, encompassing HIC, neck shear/tension/compression/lateral flexion/extension/flexion. Injury risk calculations [187] demonstrated that the likelihood of skull injury at the AIS3+ level was higher than 50% for side stationary opposite vehicle impact and near-miss frontal impact cases. Evaluating the LNL criterion with correlation to UNE 135900 criteria revealed that side opposite vehicle impact, side stationary opposite vehicle impact, and near-miss frontal impact could expose the neck to higher injury risks. Notably, the near-miss frontal impact configuration (Figure 6.21) exhibited the highest Neck Compression Criterion due to the compression force during ground contact, potentially leading to fatal injury [76]. Conversely, the scenario with side front skew vehicle impact posed the lowest risk of injury to both the neck and the skull.

6.2.2 Stature influence on accident outcome

The study of traffic accidents and their outcomes has been a critical focus of research aimed at enhancing road safety and reducing injury risks. One significant factor that plays a pivotal role in the dynamics of accidents and subsequent injuries is the stature of the individuals involved. Stature, a fundamental anthropometric measure representing a person's height, has been recognized as having a substantial influence on accident scenarios and outcomes. As vehicles, roads, and safety systems are designed to accommodate a wide range of individuals, understanding how stature impacts accident dynamics is crucial for developing effective safety strategies.

Anthropometry, which encompasses various measurements of the human body, provides insight into how different individuals interact with their surroundings, especially during accidents. Stature, being a major component of anthropometry, affects factors like seat positioning, visibility, restraint system effectiveness, and interaction with vehicle structures. These factors can significantly alter the biomechanics of injury during an accident and subsequently influence the severity and type of injuries sustained.

This research aims to delve into the intricate relationship between stature and accident outcomes. By employing advanced numerical simulations and computational models, we seek to unravel how varying statures can impact collision dynamics, occupant kinematics, and injury patterns. The insights gained from this investigation can aid in optimizing safety systems, such as airbags, seat belts, and restraints, to cater to a broader spectrum of individuals, ultimately contributing to more effective and inclusive road safety measures.

Throughout this study, we will explore various accident scenarios and outcomes, considering differing statures as a key variable. The simulations and analyses conducted will shed light on the role that stature plays in determining injury risks, highlighting areas where safety interventions can be refined to provide better protection for individuals of all sizes. As road safety standards continue to evolve, incorporating a nuanced understanding of stature's influence on accident outcomes is imperative for creating a safer environment for all road users.

6.2.2.1 Methods

A sequence of virtual human body models, employed as motorcycle riders, are produced through an automated scaling algorithm on the Virthuman model. This scaling approach builds upon a previously established algorithm [89], which factors in gender, geometry, mass distribution, and body stiffness. The models' particular age (Table 6.5) was chosen based on the analysis of the MAIDS database (depicted in Figure 2.2). Given the extensive components and elements in the numerical models, the representations of the car, motorcycle, and helmet are streamlined to maintain a coherent time step alongside the human body model. It was possible by employing the simplified FE models from the chapters 5.2.2.2, 5.2.1, 4.2.1 respectively.

Table 6.5 Mass, height, and corresponding helmet sizes of six age ranges of motorcycle riders.

	Age[years]	16	17	18	22	26	34
Female	mass[kg]	56	59	58	61	59	62
	height[m]	1.64	1.66	1.66	1.67	1.66	1.65
	helmet size	X	X	X	X	X	X
Male	mass[kg]	66	70	72	77	76	78
	height[m]	1.76	1.77	1.78	1.79	1.78	1.76
	helmet size	XL	XL	XL	XL	XL	XL

The impact simulation is rooted in an actual rear impact incident from the LMU dataset, in detail simulated in the previous chapter. The investigated motorcycle accident occurred at an intersection where a vehicle had come to a stop at a red traffic light, and the motorcycle collided with the car's rear end. This event is illustrated in Figure 5.86 By analyzing the accident reconstruction, it was determined that the angle between the vehicle's longitudinal symmetry plane and the motorcycle's velocity direction was approximately 5 degrees. The initial velocity of the motorcycle is established as 55 km/h based on the reported impact speed range of 55±5 km/h from the accident report [159], while the vehicle's velocity is set to zero. These simulations, which consider the rider's variable anthropometry, encompass 12 scenarios and are executed within the Virtual Performance Solutions platform. Following own framework every motorcycle rider model (VH) is linked to a simplified helmet model and accurately positioned on the motorcycle, maintaining an appropriate distance between the hip and the motorcycle seat. Symmetrical contact between the rider and the motorcycle is established, and the interaction between the hands and handlebars is represented using springs with a stiffness of 9.36 kN/m and a maximum force limit of 350 N for each hand.

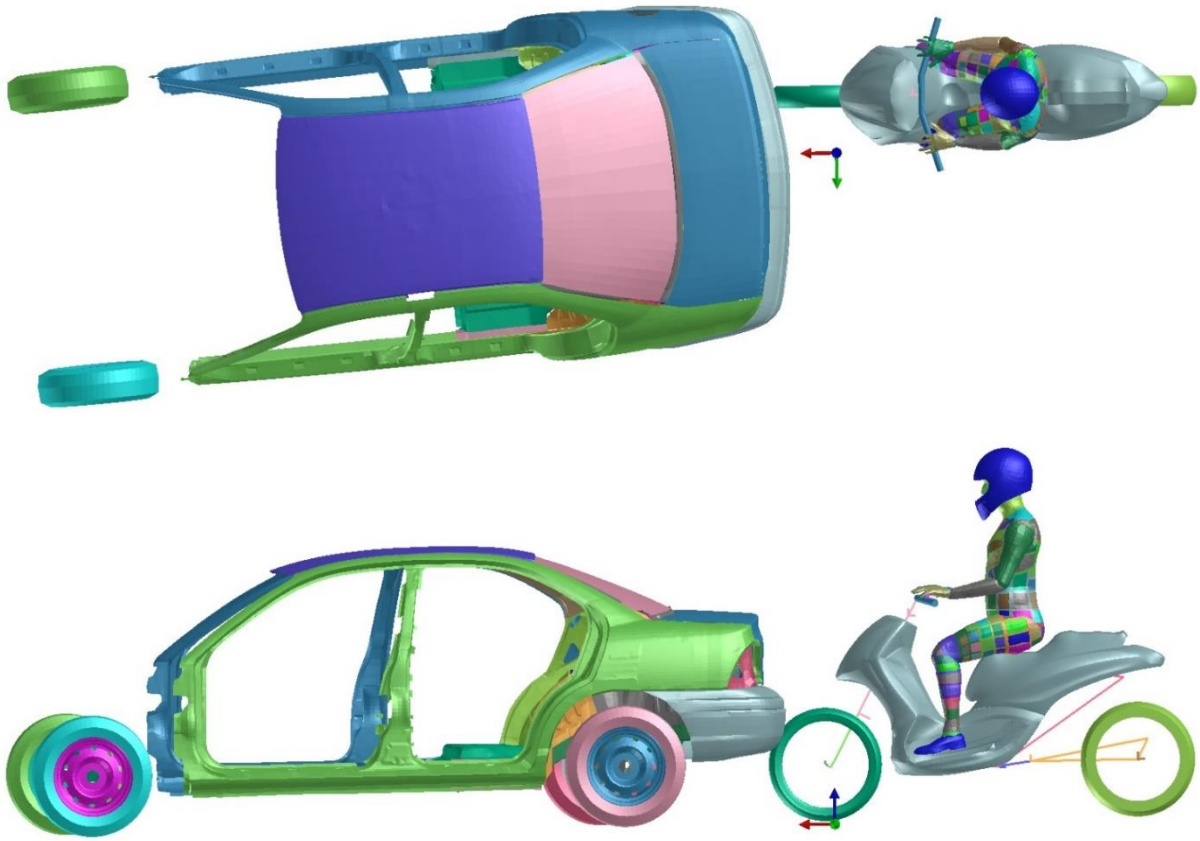

Figure 6.24 Numerical setup of the study based on the LMU case.

6.2.2.2 Results

Figure 6.25 displays the kinematic response of the simulation involving a 16-year-old female motorcycle rider, presented as an illustrative example. The entire impact simulation can be divided into three distinct phases. In the initial phase, characterized by the linear motion of both the rider and the motorcycle, the rider's body begins sliding away from the motorcycle seat due to the interplay of the rider's inertia and the decrease in motorcycle speed, concurrently with the compression of the motorcycle's front fork. The subsequent phase entails the rotation of both the rider and the motorcycle. Here, the rider's body undergoes a counterclockwise rotation around the point of impact between the knee and the motorcycle, while the motorcycle itself rotates counterclockwise around the point of contact between the front wheel and the rear bumper of the car. In this phase, the neck's movement encompasses a combination of extension and flexion, carrying a potential risk of neck injury. The concluding phase witnesses the movement of the head, coupled with the helmet, along the rear windscreen, simultaneous with the rotation of the rider's body around the contact point established between the helmet and the rear windscreen.

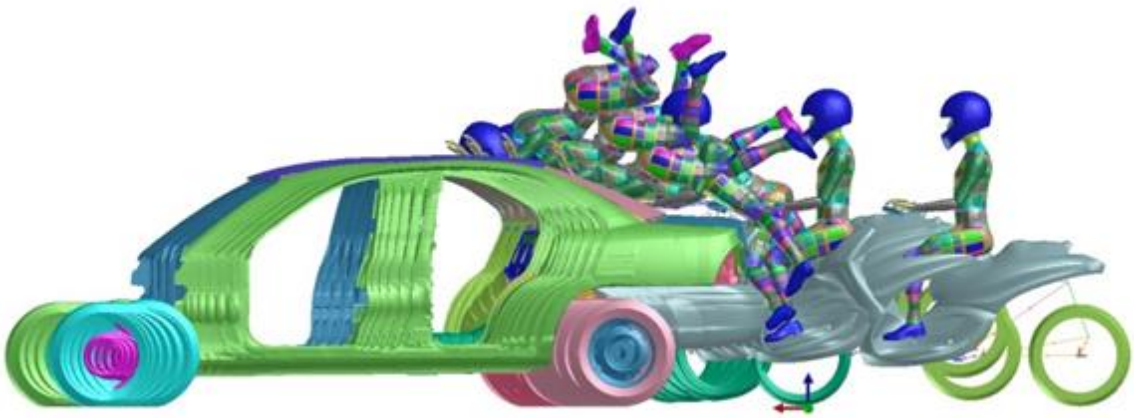

Figure 6.25 Kinematic response in the simulation with the 16-year-old female motorcycle rider.

Given the relatively subtle variations in height across the six age ranges within each gender group, this study predominantly focuses on investigating the connections between specific injury criteria and mass. Illustrated in Figure 6.26 is the HIC within the 36 ms time interval, encompassing all 12 motorcycle riders across the six age ranges. Notably, this figure reveals a marginally stronger correlation between the regression variable mass and the HIC for male riders compared to their female counterparts. For males, the HIC appears to be proportionate to mass, while for females, it displays an inverse relationship with mass. Furthermore, it becomes evident from Figure 6.26 that the mass's impact on the female HIC is more pronounced than its influence on the male HIC. All HIC values across these 12 cases remain below the ECE R22.05 certification threshold of 2,400.

In the context of peak moments, assessed at the joint between the C0 and C1 vertebrae as depicted in Figure 6.27, both positive and negative C0-C1 moments—indicative of flexion and extension bending moments—are considered. Notably, the regression variable mass showcases significantly stronger alignment with the bending moments of male riders as opposed to their female counterparts. The flexion bending moments for both genders, along with the extension bending moment for males, exhibit proportionality to mass. Conversely, the extension bending moment for females is inversely proportional to mass. A direct comparison between the absolute values of the regression lines' slopes in Figure 6.27 reveals that the flexion bending moments' absolute values surpass those of the extension bending moments. This highlights the stronger influence of mass on flexion bending moments in comparison to extension bending moments. The mass's effect on the extension bending moment for females is minimal.

Moving to peak shear force (Force-R) and axial force (Force-T) assessments at the C0-C1 joint—illustrated in Figure 6.28 and Figure 6.29—positive and negative axial forces represent tension and compression forces. Figure 6.28 demonstrates that the regression variable mass exhibits a much more pronounced correlation with male negative Force-R compared to female Force-R and male positive Force-R. For both genders, the negative Force-R and male positive Force-R display an inverse relationship with mass, while female Force-R is proportionate to mass. Furthermore, Figure 6.28 indicates that the mass's impact on negative peak shear forces exceeds its influence on positive peak shear forces.

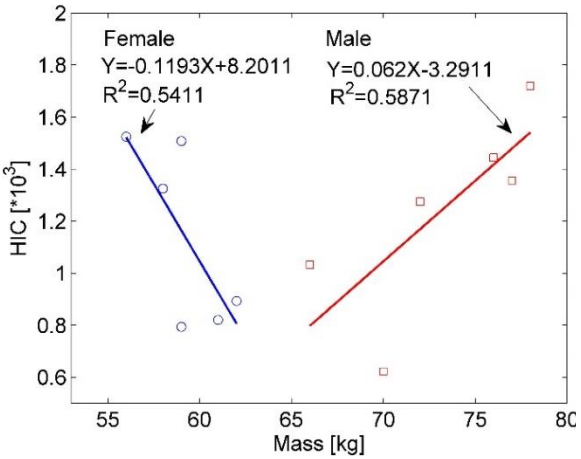

Figure 6.26 Linear regressions of HIC as a function of male/female mass.

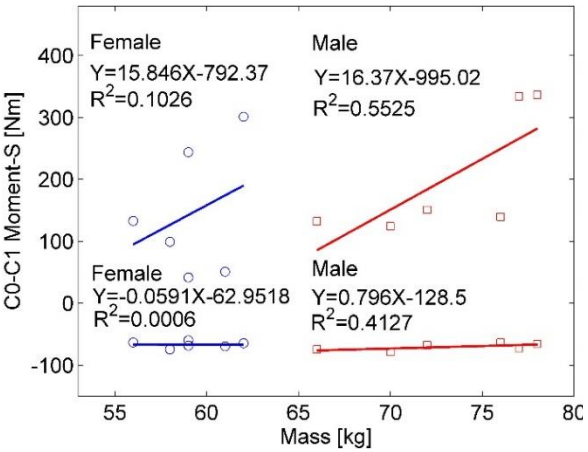

Figure 6.27 Linear regression of C0-C1 peak moment as a function of male/female mass.

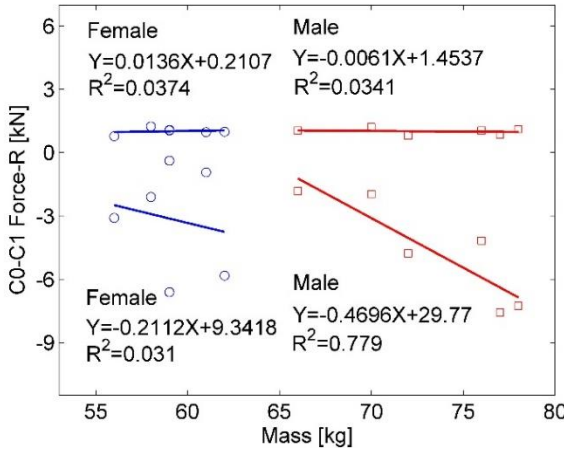

Figure 6.28 Linear regression of C0-C1 peak shear force as a function of male/female mass.

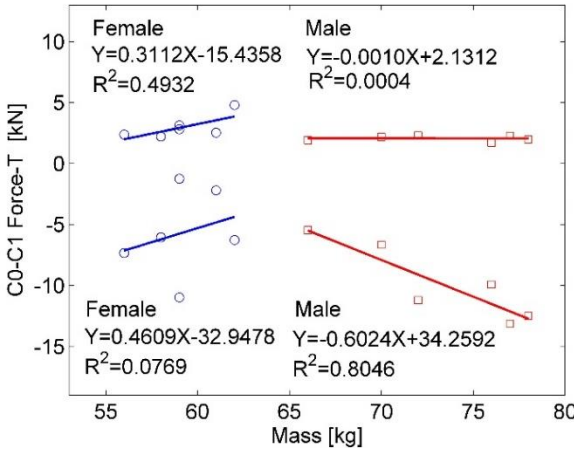

Figure 6.29 Linear regression of C0-C1 axial force as a function of male/female mass.

Considering Figure 6.29, the regression variable mass shows notably stronger alignment with female peak tension force and male peak compression force in comparison to male peak tension force and female peak compression force. Female peak tension and compression forces are proportionate to mass, whereas male peak tension and compression forces are inversely proportional to mass. Additionally, the impact of mass on male peak tension force is minor compared to its effect on other peak axial forces.

Figure 6.30 depict the Nij criteria for ages 16, 17, 18, 22, 26, and 34, encompassing both male and female riders. The Nij criteria are juxtaposed against the 50th percentile male corridor to gauge the potential neck injury risk. Examining the envelopes, it becomes evident that the Nij criteria for ages 17 and 22 among female riders closely align with the established corridor. However, for the other Nij criteria, they exceed the corridor due to the pronounced peak region in C0-C1 compression force during specific time intervals—164 to 173 ms for males and 158 to 166 ms for females. This discrepancy implies that neck injury risk might manifest earlier for female riders than their male counterparts in the course of impact simulations. The distribution and trend variations for male riders at ages 18, 26, and 34 mirror those for female riders.

Further observation from the figures unveils a conspicuous distinction in Nij criteria between male and female riders, underscoring the notable influence of rider stature on the Nij criterion at ages 16, 17, and 22. Specifically, male riders of 22 years of age exhibit considerably higher shear forces in the neck (as depicted in last graph Figure 6.30) in comparison to their female counterparts. This phenomenon can be attributed to the presence of stiffer joints within the male neck. However, as age increases and subsequently neck stiffness rises, this gender difference becomes less discernible.

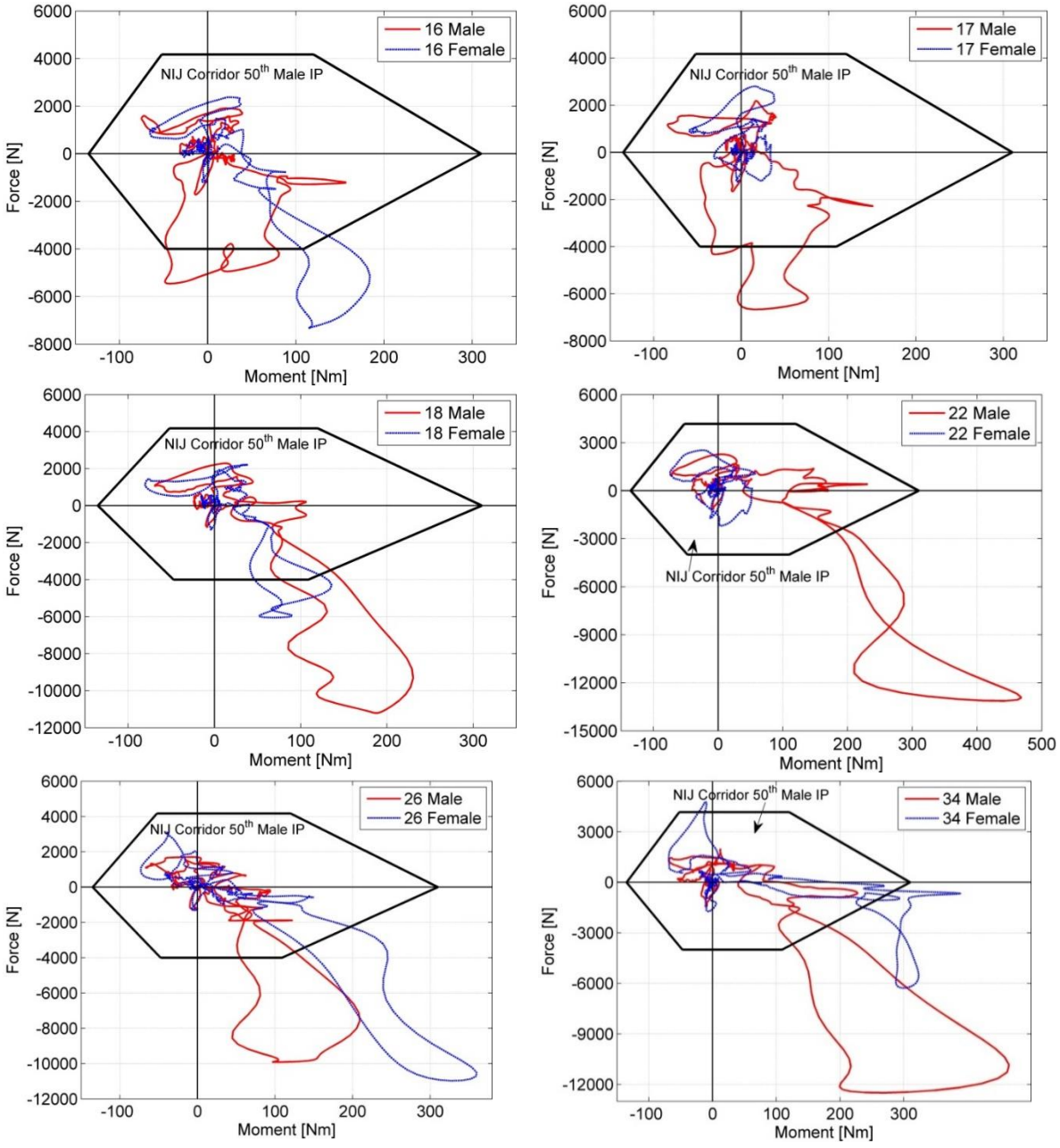

Figure 6.30 Nij criterion evaluation for all age groups

The findings of this study reveal distinct patterns regarding the influence of rider stature on various injury criteria. Specifically, the male HIC and C0-C1 flexion bending moments in both genders, the male C0-C1 extension bending moment, the female peak C0-C1 shear force, and the female peak C0-C1 axial forces exhibit a direct proportionality to mass. In contrast, the female HIC, the female C0-C1 extension bending moment, the male peak C0-C1 shear force, the female negative peak C0-C1 shear force, and the male peak C0-C1 axial force display an inverse proportionality to mass. Importantly, the impact of mass on the HIC, the C0-C1 flexion bending moments in both genders, the male peak C0-C1 shear force, the female peak C0-C1 axial force, and the male peak C0-C1 compression force is more pronounced than on other corresponding parameters investigated in this study. These trends are anticipated to be observed in motorcycle-to-car frontal and rear impacts with diverse impact angles. Moreover, the influence of rider stature on the HIC (for ages 16, 22, and 34) and on the Nij criterion (for ages 16, 17, and 22) is found to be significant.

This study underscores the advantages of employing virtual approaches in the realm of vehicle safety technology. Such methods prove invaluable for applications ranging from accident reconstruction and optimization of personal protective equipment to the mitigation of injury risks.

6.3 Summary

In this chapter, the focus was on conducting full-scale virtual crash tests following the guidelines of the ISO 13232 standard. These tests were aimed at comprehensively understanding the effects of rider stature on injury outcomes in motorcycle accidents. The proposed framework provided a structured approach to simulate and analyze various impact scenarios.

The first part of the chapter revolved around the execution of full-scale virtual crash tests. Following the ISO 13232 standard, a range of impact scenarios was simulated using a combination of motorcycle, vehicle, and human body models. These simulations captured different types of collisions, including frontal, rear, and lateral impacts, providing a holistic perspective on injury dynamics during motorcycle accidents. The virtual environment allowed for meticulous observation of rider kinematics and the correlation of these observations with injury criteria.

The second part of the chapter involved a parametric study specifically investigating the influence of rider stature on injury outcomes. The framework presented by the author facilitated the systematic variation of rider anthropometry across different age groups. By examining a comprehensive set of injury criteria, including HIC, neck bending moments, shear forces, axial forces, and Nij criterion, the study provided a nuanced understanding of how rider stature interacts with injury risk. Notably, the study highlighted the complex relationships between stature, gender, and injury criteria, revealing both proportional and inversely proportional trends.

Overall, this chapter showcases the versatility and power of full-scale virtual crash tests in evaluating injury outcomes in motorcycle accidents. By aligning with international standards like ISO 13232 and employing a systematic approach to studying rider stature effects, the research advances our understanding of how different factors influence injury patterns

The introduced virtual framework has the potential for simulating and optimizing personal protective equipment, complementing ECE 22.05 [108], EN 13634 [190], and EN 1621 [191–194] standards. However, further efforts are necessary to gather more real-life motorcycle accident cases for enhanced validation of the established setup.

7 Conclusions

In summation, this dissertation presents a comprehensive exploration into the intricate realm of impact biomechanics, human body modeling, and the imperative considerations surrounding the passive safety of powered two-wheeler (PTW) drivers. The diverse objectives laid out in the research outline have not only effectively met but have culminated in the establishment of an extensive and robust framework that stands poised to significantly impact the realm of motorcyclists' safety.

The overarching goal that has guided this study is the establishment of a solid and scientifically grounded foundation in the domain of injury biomechanics. This foundation aims to pave the way for a rigorous and comprehensive evaluation of passive safety measures for PTW drivers, bridging the gap between theoretical models and practical real-world applications. The meticulously planned sequence of steps, stemming from the initial problem statement, has been the backbone of achieving this overarching objective, each contributing its unique facet to the tapestry of knowledge and advancement.

The journey began with a meticulous and detailed statistical analysis of accident databases, a critical exercise that yielded invaluable insights into the macroscopic impact conditions and the prevalence of certain accident configurations. This analytical phase helped anchor the study in real-world scenarios, grounding it in the complexities and dynamics of actual accidents.

The research encompasses a range of compelling HBM applications. It commences with the study of real MotoGP accident, utilizing the sliding simulations of the VH model to gain a profound understanding of accident dynamics. Further exploration involves ground surrogate impacts involving helmets, with a meticulous comparison of injury criteria against the well-established THUMS model. This comparative analysis elucidates helmet performance across different scenarios.

Following this, the research dived into the intricate task of modeling helmets, the paramount protective gear for motorcyclists. These simplified helmet models were seamlessly integrated into HBM, effectively merging the tangible physicality of helmets with the anatomical intricacies of the human body. Validation against established standards ensured the accuracy and reliability of these helmet models, a pivotal aspect in building the foundation for comprehensive virtual testing.

The evaluation of ECE 22.05 certified helmet performance within diverse population segments is another pivotal facet of the research. This examination underscores the practical efficacy of HBM in assessing and enhancing helmet safety standards, catering to a wide array of potential users.

The versatility of HBM extends to motorcycle barrier testing, where they serve as effective surrogates for evaluating safety measures with a view to current safety standards. This application could facilitate a comprehensive experimental assessment of the barrier impact by providing a cost-effective tool in the initial state of barrier design.

Additionally, the research significantly contributes to accident reconstruction by employing HBM as a driver in the meticulous reconstruction of two real accidents from the In-Safe project database and a single LMU case. This real-world application underscores the practical utility of HBM in translating theoretical insights into tangible solutions for accident reconstruction, and proves that the results from the backward reconstruction technique could be comparable to the real injuries from the accident scene.

The subsequent stride saw the creation of a full-scale PTW numerical accident model, a substantial step that harmonized various accident scenarios into a singular framework. This inclusive model, representing diverse accident situations, served as the backbone for the subsequent research endeavors. Building upon this foundation, the creation and meticulous validation of the numerical PTW model fortified the research with a realistic and versatile tool, expanding its application across various scenarios.

Moreover, HBM's role as an ATD substitute is evident in its utilization for evaluating seven standard configurations defined by ISO 13232. This application could act as a culmination of the VH application for the PTW passive safety, and be used as a virtual range to test the motorcycle safety measures in their early stage of design/ development. The ISO 13232 is already a solid and established standard but with one drawback which lies in the application only the MATD as HS. This limitation has been overtaken by the application of VH which contains a scaling algorithm The focus here was on representing diverse populations to assess the influence of stature on accident injury outcomes. This application provides valuable insights into injury patterns based on different driver stature and builds a scaffolding for personalized protective equipment development.

Further enhancements ensued with the streamlining of the occupant vehicle model and the careful reconstruction of actual PTW-OV-driver collision cases. These refinements added layers of realism to the research, simulating real-world accidents and refining the scope of the research.

7.1 Thesis objectives evaluation

The particular thesis objectives were fulfilled in the following chapters of the work.

- Statistical analysis of the accident database to obtain macroscopic realistic impact conditions and most common accident configurations; - **Chapter 2.2** MAIDS analysis
- Modeling of simplified helmet and coupling with HBM;
  - Standard-based helmet validation; - **Chapter 4.2.1** Helmet testing
- Creation of full-scale multi-scenario PTW numerical accident model; -
  - Creation and validation of the numerical PTW model; - **Chapter 5.2.1** PTW Modelling
  - Coupling of HBM, MC, and method on HBM – PPE coupling; - **Chapter 5.2.3** Models Coupling
  - Simplification of the OV model; - **Chapter 5.2.2.2** Simplified models and validation
- Reconstruction of real cases involving PTW, OV, and driver; - **Chapter 5.3** Results
- Simulation of most common PTW - OV accidents with injury criteria assessment - **Chapter 6.2.1** Standard Configurations – ISO 13232

Table 7.1 Explanation of framework models application for particular tasks.

Model / Application	Virthuman		PTW		Helmet		Chrysler Neon	
	Base	Scaled	Base	Mass -trimmed	Detailed	Simplified	Detailed	Simplified
Basic simulations								
Sliding simulation								
Ground impact								
Population diversity								
Barrier assessment								
Accident reconstruction								
IN-SAFE case 1								
IN-SAFE case 2								
LMU case								
Full-scale tests								
ISO 13232								
LMU case stature influence								

Legend:

Performed	Non-essential	Non-recommended

8 Future Research

In the near future author is planning to continue his interest in the Passive Safety of motorcycle drivers by conducting the following research (but not limited to):

- Research on the development of helmets with the shear layer which will help to prevent oblique impact-induced injuries;
- Research on improving Virthuman by altering the joint properties to express the ROM of PTW driver in motorcycle garments;
- Development of virtual sled test methodology for the PTW's;
- Work on extending the developed framework to a wider range of vehicles (PTW with different geometry, OV different type).

9 References

[1] K. Santos, J. P. Dias, C. Amado, J. Sousa, and P. Francisco, “Risk factors associated with the increase of injury severity of powered two wheelers road accidents victims in Portugal,” *Traffic Inj. Prev.*, vol. 22, no. 8, pp. 646–650, Nov. 2021, doi: 10.1080/15389588.2021.1987421.

[2] A. Delhaye and L. Marot, “Traffic Management and ITS, Deliverable 6 of the EC/MOVE/C4 project RIDERSCAN.,” 2015.

[3] F. A. Berg, H. Bürkle, F. Schmidts, and J. Epple, “Analysis of the Passive Safety of Motorcycles Using Accident Investigations and Crash Tests,” in *16th International Technical Conference on the Enhanced Safety of Vehicles, Paper 98-S 1 O-O- 11*, 1998, pp. 2221–2236.

[4] M. Ptak, “Method to Assess and Enhance Vulnerable Road User Safety during Impact Loading,” *Applied Sciences* , vol. 9, no. 5. 2019. doi: 10.3390/app9051000.

[5] H. J. Hurt, J. Ouellet, and D. Thom, “Motorcycle Accident Cause Factors and Identification of Countermeasures: Volume 1 Technical Report,” vol. January, no. Contract No. DOT HS-5-01160, p. 425 pgs, 1981.

[6] “CARE - Community database on Accidents on the Roads in Europe.” https://ec.europa.eu/transport/road_safety/specialist/observatory/methodology_tools/about_care_en

[7] M. Wisch, “20 Jahre GIDAS,” Germany, 2019. [Online]. Available: https://www.gidas.org/pdf/190711_GIDAS_20_JAhre_Vortrag_Wisch_BASt.pdf

[8] ACEM, “MAIDS: In-depth investigations of accidents involving powered two wheelers.”

[9] J. Compagne, “Motorcycle Accidents In-Depth Study. Presentation of the study MAIDS.,” p. 54, 2008.

[10] J. R. Crandall *et al.*, “Human surrogates for injury biomechanics research,” *Clin. Anat.*, vol. 24, no. 3, pp. 362–371, 2011, doi: 10.1002/ca.21152.

[11] P. S. Nolet, L. Nordhoff, V. L. Kristman, A. C. Croft, M. P. Zeegers, and M. D. Freeman, “Is acceleration a valid proxy for injury risk in minimal damage traffic crashes? A comparative review of volunteer, adl and real-world studies,” *Int. J. Environ. Res. Public Health*, vol. 18, no. 6, pp. 1–18, 2021, doi: 10.3390/ijerph18062901.

[12] S. Parija and J. Mandal, “Ethics of involving animals in research,” *Trop. Parasitol.*, vol. 3, no. 1, p. 4, 2013, doi: 10.4103/2229-5070.113884.

[13] Dwindrim, “Sierra Sam,” vol. 2018, no. May 21. 2004. [Online]. Available: https://commons.wikimedia.org/wiki/File:Sam4.jpg

[14] “‘Sierra Sam’ Photo Op.” [Online]. Available: https://www.secretsdeclassified.af.mil/News/Photos/igphoto/2000345084/

[15] “The Humble History of the Crash Test Dummy.” 2017. [Online]. Available: https://www.motorbiscuit.com/the-humble-history-of-the-crash-test-dummy/

[16] “More on Sierra Susie - Science Museum Blog.” 2009.

[17] D. C. Herbert and D. Cutting, “Crash protection for children after their third birthday,” New South Wales, 1978.

[18] B. Naylor, “How Crash Tests Help Bring Traffic Deaths Down.” 2009. [Online]. Available: https://www.npr.org/2009/11/23/120628434/how-crash-tests-help-bring-traffic-deaths-down

[19] National Institute of Standards and Technology, “Crash test dummies.jpg - Wikimedia Commons.” [Online]. Available: https://commons.wikimedia.org/wiki/File:Crash_test_dummies.jpg

[20] Humanetics, “Humanetics History.” [Online]. Available: https://www.humaneticsgroup.com/about-us/history

[21] JASTI, “JASTI PRODUCT CATALOG 2020,” 2020. [Online]. Available:

https://www.highvisionsys.com.br/catalogos/catalogue2020_Jasti_en.pdf
[22] "Dummy-mounted sensors for hybrid Ⅲ dummy in frontal impact | KYOWA." [Online]. Available: https://www.kyowa-ei.com/eng/product/sector/automobile/application_111.html
[23] J. A. Newman, J. W. Zellner, and K. D. Wiley, "A Motorcyclist Anthropometrie Test Device MATD," in *Proceedings of the 1991 International IRCOBI Conference on the Biomechanics of Impacts*, 1991, pp. 285–193.
[24] C. Withndll and E. Fourier, "A New Neck for Motorcycle Crash Testing," in *16th International Technical Conference on the Enhanced Safety of Vehicles*, 1998, pp. 2375–2383.
[25] P. V Bhosale, "Exploratory study on the suitability of an airbag for an Indian motorcycle using finite element computer simulations of rigid wall barrier tests," *23rd Interna- tional Tech. Conf. Enhanc. Saf. Veh.*, no. 13, pp. 1–16, 2013.
[26] W. Christopher and F. Edmund, "A new Neck for Motorcycle Crash Testing," *Proc. 16th Enhanc. Saf. Veh. Conf.*, 1998, [Online]. Available: https://www-nrd.nhtsa.dot.gov/pdf/Esv/esv16/98S10W27.PDF
[27] F. A. Berg, P. Rücker, and J. König, "Motorcycle crash tests - An overview," *Int. J. Crashworthiness*, vol. 10, no. 4, pp. 327–339, 2005, doi: 10.1533/ijcr.2005.0349.
[28] J. Carroll, B. Been, M. Burleigh, and B. Li, "A Powered Two-Wheeler Crash Test Dummy," in *IRCOBI conference 2022*, 2022, pp. 114–115.
[29] WORKING GROUP 12 ADULT CRASH, "DEVELOPMENT AND EVALUATION OF THE ES-2 DUMMY," 2001. [Online]. Available: https://unece.org/DAM/trans/main/wp29/wp29wgs/wp29grsp/grspinf/30/30infp6.pdf
[30] B. Friedel, H. Henssler, I. D. Neilson, G. Silvestri, and J. Wismans, "The European side-impact dummy 'Eurosid.'"
[31] TASS_International, "Madymo Dummy Models," *Time*. https://tass.plm.automation.siemens.com/madymo-dummy-models
[32] A. E. Louden, *WorldSID 50th Percentile Male Dummy Seating Procedure Evaluation and Revision*, no. DOT HS 812 694. 2019. [Online]. Available: https://rosap.ntl.bts.gov/view/dot/41900
[33] M. JW, "Advanced Anthropomorphic Test Device (AATD) Development Program. Phase 1 Reports: Concept definition," in *ESV*, 1985, vol. DTNH22-83-, p.
[34] D. Parent, M. Craig, and K. Moorhouse, "Biofidelity Evaluation of the THOR and Hybrid III 50th Percentile Male Frontal Impact Anthropomorphic Test Devices," *SAE Tech. Pap.*, no. November, 2017, doi: 10.4271/2017-22-0009.
[35] Humanetics, "THOR-50M." https://www.humaneticsgroup.com/products/anthropomorphic-test-devices/frontal-impact/thor-50m/thor-50m
[36] Humanetics, "BioRID-II." https://www.humaneticsgroup.com/products/anthropomorphic-test-devices/rear-impact/biorid-ii
[37] J. Davidsson, "BioRID II Final Report," *J. Penelit. Pendidik. Guru Sekol. Dasar*, vol. 6, no. August, p. 128, 1999, [Online]. Available: http://webfiles.ita.chalmers.se/~mys/BioRID/BioRIDIIFinal.pdf
[38] J. H. Ash, D. J. Lessley, J. L. Forman, Q. Zhang, C. G. Shaw, and J. R. Crandall, "Whole-Body Kinematics: Response Corridors for Restrained PMHS in Frontal Impacts," in *Proceedings of IRCOBI Conference*, 2012, vol. IRC-12-21, pp. 142–154.
[39] C. R. Bass, R. S. Salzar, S. R. Lucas, K. A. Rafaels, A. M. Damon, and J. R. Crandall, "Re-evaluating the neck injury index (NII) using experimental PMHS tests," *Traffic Inj. Prev.*, vol. 11, no. 2, pp. 194–201, 2010, doi: 10.1080/15389580903501864.
[40] C. L. Ewing and D. J. Thomas, *Human Head and Neck Response To Impact Acceleriation*. Naval Aerospace Medical Research Laboratory, Naval Aerospace Medical Institute, Naval Aerospace and Regional Medical Center, Pensacola, Fla., 1972.
[41] J. A. C. Ambrosio, *Crashworthiness. Energy management and occupant protection*. 2001.
[42] "Stapp, John Paul: National Aviation Hall of Fame." https://www.nationalaviation.org/our-

enshrinees/stapp-john-paul/
[43] "National Air and Space Museum - Smithsonian Institution: The Man Behind High-Speed Safety Standards," *22 August*, 2018. https://airandspace.si.edu/stories/editorial/man-behind-high-speed-safety-standards
[44] R. Willinger and D. Cesari, "Determination of Cerebral Motion at Impact through Mechanical Impedance Measurement," in *IRCOBI Conference Proceedings*, 1990, pp. 203–213. [Online]. Available: https://doi.org/10.1080/13588265.2019.1593290
[45] R. Willinger, T. Guimberteau, A. Mclean, R. Anderson, and M. Farmer, "Experimental and theoretical modelling of head impact: influence of head modelling.," in *IRCOBI Conference Proceedings*, 1996, pp. 21–34.
[46] R. R. McHenry, "Analysis of the dynamics of automobile passenger restraint systems," in *Proc. 7th Stapp Car Crash Conference*, 1963, pp. 207–249.
[47] P. Du Bois *et al.*, *Vehicle crashworthiness and occupant protection*. Michigan: American Iron and Steel Institute, 2004. [Online]. Available: https://doi.org/10.1080/13588265.2019.1593290
[48] J. Wismans, R. Happee, and J. A. W. van Dommelen, "Impact Biomechanics: From Fundamental Insights to Applications," in *IUTAM Symposium on Impact Biomechanics*, M. D. Gilchrist, Ed. 2005, pp. 417–429. [Online]. Available: http://www.springerlink.com/content/q642098115531q14/
[49] "HUMOS: Human Model for Safety," 2000. https://cordis.europa.eu/project/id/BRPR970475
[50] S. Robin, "HUMOS : Human Model for Safety – A Joint Effort Towards the Development of Refined Human-Like Car Occupant Model," in *SAE Technical Paper*, 2001, vol. 06, pp. 1–9.
[51] P. Vezin and J. P. Verriest, "Development of a set of numerical human models for safety," 2005. [Online]. Available: http://wbldb.lievers.net/10060576.html
[52] S. . Peldschus, E. . Schuller, J. . Koenig, M. . Gaertner, D. G. . Ruiz, and A. Mansilla, "Technical Bases for the development of a test standard for impacts of powered two-wheelers on roadside barriers," in *Proceedings of the 20th Enhanced Safety of Vehicles Conference*, 2007, no. June.
[53] S. Kuppa, R. H. Eppinger, F. McKoy, T. Nguyen, F. A. Pintar, and N. Yoganandan, "Development of Side Impact Thoracic Injury Criteria and Their Application to the Modified ES-2 Dummy with Rib Extensions (ES-2re)," *SAE Tech. Pap.*, vol. 2003-October, no. October, 2003, doi: 10.4271/2003-22-0010.
[54] L. Thollon, Y. Godio, S. Bidal, and C. Brunet, "Evaluation of a new security system to reduce thoracic injuries in case of motorcycle accidents," *Int. J. Crashworthiness*, vol. 15, no. 2, pp. 191–199, Jun. 2010, doi: 10.1080/13588260903102062.
[55] M. Iwamoto, Y. Nakahira, and H. Kimpara, "Development and Validation of the Total HUman Model for Safety (THUMS) Toward Further Understanding of Occupant Injury Mechanisms in Precrash and During Crash," *Traffic Inj. Prev.*, vol. 16, pp. S36–S48, 2015, doi: 10.1080/15389588.2015.1015000.
[56] Toyota Motor Corporation and Toyota Central R&D Labs, "Total Human Model for Safety ("THUMS ")," 1997. https://www.jsol-cae.com/en/product/structure/thums/
[57] W. Wang, J. Ji, Z. Yue, D. Zhang, H. Tian, and H. Zhao, "Research on secondary impact safety of train driver based on THUMS Dummy," *MATEC Web Conf.*, vol. 81, pp. 2–6, 2016, doi: 10.1051/matecconf/20168102016.
[58] F. S. Gayzik *et al.*, "A Multi-Modality Image Data Collection Protocol for Full Body Finite Element Model Development," *SAE Tech. Pap. 2009-01-2261*, Jun. 2009, doi: 10.4271/2009-01-2261.
[59] T. A. Gennarelli and E. Wodzin, *Abbreviated injury scale 2005 : update 2008*. Association for the Advancement of Automative Medicine, 2008.
[60] J. D. States, "The abbreviated and the comprehensive research injury scales," *SAE Tech. Pap. 690810*, pp. 2625–2634, 1969, doi: 10.4271/690810.

[61] “Agency for Clinical Innovation (ACI): Injury Severity Score.” https://aci.health.nsw.gov.au/networks/institute-of-trauma-and-injury-management/data/injury-scoring/injury_severity_score

[62] S. P. BAKER, B. O’NEILL, W. J. R. HADDON, and W. B. LONG, “THE INJURY SEVERITY SCORE: A METHOD FOR DESCRIBING PATIENTS WITH MULTIPLE INJURIES AND EVALUATING EMERGENCY CARE,” *J. Trauma Acute Care Surg.*, vol. 14, no. 3, 1974, [Online]. Available: https://journals.lww.com/jtrauma/Fulltext/1974/03000/THE_INJURY_SEVERITY_SCORE__A_METHOD_FOR_DESCRIBING.1.aspx

[63] E. R. Welbourne, “Use of the Head Injury Criterion as a Measure of Vehicle Occupant Protection Performance,” in *Proceedings of IRCOBI Conference*, 1994, pp. 151–162.

[64] C. Gadd, “Criteria for Injury Potential,” in *Impact acceleration stress symposium, National Academy of Sciences, Washington, National Research Council Publication No. 977*, 1961, vol. 991, pp. 141–144.

[65] M. Kleinberger, E. Sun, R. Eppinger, S. Kuppa, and R. Saul, “Development of Improved Injury Criteria for the Assessment,” no. September, pp. 1–120, 1998, [Online]. Available: http://citeseerx.ist.psu.edu/viewdoc/summary?doi=10.1.1.180.2

[66] W. R. Bourdet N, Deck C, Mojumder S, “Comparative Evaluation of DOT vs. ECE,” in *IRCOBI Conference Proceedings*, 2018, pp. 470–479.

[67] J. A. Newman, “a Generalized Acceleration Model for Brain Injury Threshold (Gambit),” in *International Conference on the Biomechanics of Impact IRCOBI*, 1986, pp. 121–131.

[68] J. Newman *et al.*, “A new biomechanical assessment of mild traumatic brain injury, part 2: results and conclusions,” in *In Proceedings of the 2000 International Conference on the Biomechanics of Impact (IRCOBI)*, 2000, pp. 223–233.

[69] R. M. Greenwald, J. T. Gwin, J. J. Chu, and J. J. Crisco, “Head impact severity measures for evaluating mild traumatic brain injury risk exposure,” *Neurosurgery*, vol. 62, no. 4, pp. 789–798, 2008, doi: 10.1227/01.neu.0000318162.67472.ad.

[70] H. Kimpara and M. Iwamoto, “Mild traumatic brain injury predictors based on angular accelerations during impacts,” *Ann. Biomed. Eng.*, vol. 40, no. 1, pp. 114–126, 2012, doi: 10.1007/s10439-011-0414-2.

[71] E. G. Takhounts, S. a Ridella, S. Rowson, and S. M. Duma, “Kinematic Rotational Brain Injury Criterion (BRIC),” in *22nd Enhanced Safety of Vehicles Conference Proceedings*, 2011, p. Paper No. 11-0263.

[72] E. G. Takhounts, M. J. Craig, K. Moorhouse, J. McFadden, and V. Hasija, “Development of brain injury criteria (BrIC).,” in *Stapp car crash journal*, 2013, vol. 57, pp. 243–266.

[73] J. Antona-Makoshi, J. Davidsson, S. Ejima, and K. Ono, “Development of a comprehensive injury criterion for moderate and mild traumatic brain injuries,” *Int. J. Automot. Eng.*, vol. 7, no. 2, pp. 69–75, 2016, doi: 10.20485/jsaeijae.7.2_69.

[74] T. Yanaoka, Y. Dokko, and Y. Takahashi, “Investigation on an Injury Criterion Related to Traumatic Brain Injury Primarily Induced by Head Rotation,” *SAE Tech. Pap.*, vol. 2015-April, no. April, 2015, doi: 10.4271/2015-01-1439.

[75] D. R. Namjoshi *et al.*, “Towards clinical management of traumatic brain injury: A review of models and mechanisms from a biomechanical perspective,” *DMM Dis. Model. Mech.*, vol. 6, no. 6, pp. 1325–1338, 2013, doi: 10.1242/dmm.011320.

[76] K. U. Schmitt, P. F. Niederer, D. S. Cronin, M. H. Muser, and F. Walz, *Trauma biomechanics an introduction to injury biomechanics*, vol. 9783642539. 2014. doi: 10.1007/978-3-642-53920-6.

[77] SAE, “Sign Convention for Vehicle Crash Testing,” 1994. doi: https://doi.org/10.4271/J1733_201811.

[78] O. Bostrom and et al., “A New Neck Injury Criterion Candidate Based on Injury Findings in the Cervical Spine Ganglia after Experimental Sagittal Whiplash,” in *Ircobi*, 1996, pp. 123(119)-136(133).

[79] N. Yoganandan, F. A. Pintar, and J. F. Cusick, “Biomechanical analyses of whiplash injuries

using an experimental model," *Accid. Anal. Prev.*, vol. 34, no. 5, pp. 663–671, 2002, doi: 10.1016/S0001-4575(01)00066-5.

[80] K.-U. Schmitt, M. H. Muser, F. H. Walz, and P. F. Niederer, "N km --A Proposal for a Neck Protection Criterion for Low-Speed Rear-End Impacts," *Traffic Inj. Prev.*, vol. 3, no. 2, pp. 117–126, Jun. 2002, doi: 10.1080/15389580212002.

[81] AENOR (Asociación Española de Normalización y Certificación), "UNE 135900-1: Standard on the evaluation of performance of the protection systems for motorcyclists on safety barriers and parapets. Part 1: Terminology and test procedures," 2008.

[82] AENOR (Asociación Española de Normalización y Certificación), "UNE 135900-2: Standard on the evaluation of performance of the protection systems for motorcyclists on safety barriers and parapets. Part 2: Performance classes and acceptance criteria," 2008.

[83] "Regulation No 94 of the Economic Commission for Europe of the United Nations (UN/ECE) — Uniform provisions concerning the approval of vehicles with regard to the protection of the occupants in the event of a frontal collision," 2012.

[84] H. Yamada and F. G. Evans, *Strength of Biological Materials*. Robert E. Krieger Publishing Company, 1973. [Online]. Available: https://books.google.cz/books?id=w1LVAAAACAAJ

[85] L. Kovář and J. Hluchá, "ESI VIRTHUMAN models for impact," in *DHM and Posturography*, Elsevier, 2019, pp. 169–185. doi: 10.1016/B978-0-12-816713-7.00015-5.

[86] L. Hyncik, V. Novacek, P. Blaha, O. Chvojka, and P. Krejci, "On scaling of human body models," *Appl. Comput. Mech.*, vol. 1, pp. 63–76, 2007.

[87] J. Maňas, L. Kovář, J. Petřík, H. Čechová, and Stanislav Špirk, "Validation of Human Body Model VIRTHUMAN and its Implementation in Crash Scenarios," in *Mechanisms and Machine Science*, vol. 8, J. Beran, M. Bílek, M. Hejnova, and P. Zabka, Eds. Dordrecht: Springer Netherlands, 2012, pp. 351–356. doi: 10.1007/978-94-007-5125-5_46.

[88] J. Vychytil, J. Manas, H. Cechova, S. Spirk, L. Hyncik, and L. Kovar, "Scalable multi-purpose virtual human model for future safety assessment," *SAE Tech. Pap.*, vol. 1, 2014, doi: 10.4271/2014-01-0534.

[89] L. Hyncik, H. Cechova, L. Kovar, and P. Blaha, "On scaling virtual human models," *SAE Tech. Pap.*, vol. 1, 2013, doi: 10.4271/2013-01-0074.

[90] J. Vychytil *et al.*, "Prediction of Injury Risk in Pedestrian Accidents Using Virtual Human Model VIRTHUMAN: Real Case and Parametric Study," *SAE Tech. Pap.*, 2016, doi: 10.4271/2016-01-1511.

[91] J. Vychytil *et al.*, "Novel Approach in Vehicle Front-End Modeling for Numerical Analyses of Pedestrian Impact Scenarios," Mar. 2017. doi: 10.4271/2017-01-1451.

[92] S. Špirk, J. Špička, J. Vychytil, M. Křížek, and A. Stehlík, "Utilization of the Validated Windshield Material Model in Simulation of Tram to Pedestrian Collision," *Materials (Basel).*, vol. 14, no. 2, p. 265, Jan. 2021, doi: 10.3390/ma14020265.

[93] A. Talimian and J. Vychytil, "Numerical study of frontal collision effects on an occupant's safety, in autonomous vehicles, with non-standard seating configurations," *Acta Polytech. Hungarica*, vol. 18, no. 6, pp. 127–140, 2021, doi: 10.12700/APH.18.6.2021.6.7.

[94] L. Hynčík, T. Bónkowski, and J. Vychytil, "Virtual hybrid human body model for PTW safety assessment," *Appl. Comput. Mech.*, vol. 11, no. 2, pp. 137–144, 2017, doi: 10.24132/acm.2017.389.

[95] J. Špička and M. Čermák, "Forensic Analysis and a New Investigation into the Death of the Czechoslovak Minister of Foreign Affairs in 1948," *J. Forensic Identif.*, vol. 72, no. 3, pp. 245–286, 2022.

[96] SAE, "CAESAR® Executive Summary." https://www.sae.org/standardsdev/tsb/cooperative/caesumm.htm

[97] P. E. Nikravesh, *Computer-Aided Analysis of Mechanical Systems*. 1988.

[98] P. E. Nikravesh, *Planar multibody dynamics: Formulation, programming and applications*. 2007.

[99] P. Flores, *Kinematics and Dynamics of Multibody Systems with Imperfect Joints*, vol. 34. Berlin, Heidelberg: Springer Berlin Heidelberg, 2008. doi: 10.1007/978-3-540-74361-3.
[100] P. Bláha, "Anthropometry of Czech and Slovak Population from 6 till 55 years," 1985.
[101] Mecas ESI, "Mecas ESI Virthuman User Manual V1.5," 2020.
[102] Mecas ESI, "Virthuman Postprocessing Manual V1.5," 2020.
[103] T. Bońkowski *et al.*, "Contact forces on motorcycle rider overall during high speed low side sliding accident," in *31st Computational Mechanics 2015*, 2015, no. November, p. 2.
[104] T. Bońkowski, "MOTORIST project overview, presentation for the Mons University." Pilsen, p. 74, 2016.
[105] B. Chinn *et al.*, "COST 327 Motorcycle Safety Helmets," *COST 327 Mot. Saf. Helmets*, p. 327, 2001, [Online]. Available: http://scholar.google.com/scholar?hl=en&btnG=Search&q=intitle:COST+327+Motorcycle+Safety+Helmets#0
[106] M. Ghajari, S. Peldschus, U. Galvanetto, and L. Iannucci, "Effects of the presence of the body in helmet oblique impacts," *Accid. Anal. Prev.*, vol. 50, pp. 263–271, 2013, doi: 10.1016/j.aap.2012.04.016.
[107] M. Ghajari, U. Galvanetto, L. Iannucci, and R. Willinger, "Influence of the body on the response of the helmeted head during impact," *Int. J. Crashworthiness*, vol. 16, no. 3, pp. 285–295, 2011, doi: 10.1080/13588265.2011.559798.
[108] UNECE, "Uniform Provision Concerning the Approval of Protective Helmets and Their Visor for Drivers and Passengers of Motor Cycles and Mopeds, Report ECE R22, Revision 5," 2002. [Online]. Available: www.unece.org/%0Afileadmin/DAM/trans/main/wp29/wp29regs/r022r4e.pdf
[109] NHTSA, "Traffic Safety Facts. DOT HS 808953," 1998.
[110] Snell Memorial Foundation, "SA2015 STANDARD FOR PROTECTIVE HEADGEAR," 2014. [Online]. Available: https://smf.org/standards/sa/2015/SA2015Final3252014.pdf
[111] N. Bourdet, S. Mojumder, S. Piantini, C. Deck, M. Pierini, and R. Willinger, "Proposal of a new motorcycle helmet test method for tangential impact," in *2016 IRCOBI Conference Proceedings - International Research Council on the Biomechanics of Injury*, 2016, pp. 479–489.
[112] F. A. O. Fernandes and R. J. Alves De Sousa, "Motorcycle helmets - A state of the art review," *Accid. Anal. Prev.*, vol. 56, pp. 1–21, 2013, doi: 10.1016/j.aap.2013.03.011.
[113] FEMA, "Designing Sefer Roadsides for Motorcyclists - New Standards for Road Restraint Systems for Motorcyclists," Belgium, 2012.
[114] C. Deck, R. Willinger, and D. Baumgartner, "Helmet optimisation based on head-helmet modelling," *WIT Trans. Built Environ.*, vol. 67, pp. 319–328, 2003.
[115] G. Milne *et al.*, "Assessment of bicyclist head injury risk under tangential impact conditions," in *2013 IRCOBI Conference Proceedings - International Research Council on the Biomechanics of Injury*, 2013, pp. 736–746.
[116] L. S. Bailey, "Historic Discovery: 1891 Lambert, New Claim for America's First Car," *Antiq. Automob.*, vol. 24, no. 5, pp. 342–400, 1960.
[117] H. Franck and D. Franck, *Mathematical methods for accident reconstruction: A forensic engineering perspective*. Boca Raton: CRC Press, 2009. doi: 10.1201/9781420089011.
[118] D. E. Struble, *Automotive accident reconstruction: Practices and principles*. Boca Raton: CRC Press, 2013.
[119] D. Otte, "Limitation and Possibilities of Cat to Car Accident Reconstruction. How to handle in Prexis?," 2016.
[120] P. V. Hight, A. . Siegel, and A. N. Nahum, "Injury Mechanisms and Motorcycle Design," in *Proceedings of the 1976 International IRCOBI Conference on the Biomechanics of Impact*, 1976, pp. 65–74.
[121] H. Steffan, "ACCIDENT INVESTIGATION | Determination of Cause: Reconstruction," no. 1986,

J. A. B. T.-E. of F. S. Siegel, Ed. Oxford: Elsevier, 2000, pp. 16–24. doi: https://doi.org/10.1006/rwfs.2000.0395.

[122] O. Masory *et al.*, "Motorcycle Accident Reconstruction Part I - Physical Models," 2012.

[123] O. Masory *et al.*, "Motorcycle Accident Reconstruction Part II - Self Learning Models," in *Florida Conference on Recent Advances in Robotics*, 2012, pp. 1–4.

[124] B. F. McNally and W. Bartlett, "Motorcycle Speed Estimates Using Conservation of Linear and Rotational Momentum (imp)," *20th Annu. Spec. Probl. Traffic Crash Reconstr. Inst. Police Technol. Manag. Univ. North Florida, Jacksonville, Florida*, pp. 1–33, 2002.

[125] Q. Wang, Y. Lou, X. Jin, L. Kong, C. Qin, and X. Hou, "Reverse reconstruction of two-wheeled vehicle accident based on Facet vehicle model and hybrid human model," *Int. J. Crashworthiness*, vol. 0, no. 0, pp. 1–16, Oct. 2020, doi: 10.1080/13588265.2020.1836840.

[126] D. Zou *et al.*, "Prediction of injury risks and features among scooter riders through MADYMO reconstruction of a scooter-microvan accident: Identifying the driver and passengers.," *J. Forensic Leg. Med.*, vol. 65, pp. 15–21, Jul. 2019, doi: 10.1016/j.jflm.2019.04.006.

[127] S. Datentechnik, "PC-Crash A simulation program for Vehicle-Accidents - Operating and Technical Manual 11.0," Linz, Austria, 2016.

[128] "Virtual CRASH Accident Reconstruction Software User's Guide," 2020. [Online]. Available: https://www.vcrashusa.com/guide

[129] D. Farooq and J. Juhasz, "In-Depth Investigation of Contributing Factors to Car-Motorcycle Accidents in Budapest City," *Rom. J. Transp. Infrastruct.*, vol. 8, no. 2, pp. 30–43, 2019, doi: doi:10.2478/rjti-2019-0009.

[130] K. Santos and J. P. Dias, "Motorcycle accident reconstruction: Influence of structural deformation or failure," *Eng. Fail. Anal.*, vol. 115, p. 104597, 2020, doi: https://doi.org/10.1016/j.engfailanal.2020.104597.

[131] F. Y. Zhang, "Vehicle Accident Reconstruction Based on Pc-crash," *Int. J. Res. Eng. Sci.*, vol. 5, no. 5, pp. 16–20, 2017.

[132] O. Cherta Ballester *et al.*, "Analysis of trunk impact conditions in motorcycle road accidents based on epidemiological, accidentological data and multibody simulations," *Accid. Anal. Prev.*, vol. 127, pp. 223–230, 2019, doi: https://doi.org/10.1016/j.aap.2019.03.006.

[133] P. Bothwell, R. E. Knight, and H. C. Petersen, "Dynamics of Motorcycle Impact, Vol. I, Tech. Rep. DOT HS 800 906," Washington, DC, 1971.

[134] J. Happian-Smith, M. A. Macaulay, and B. P. Chinn, "Motorcycle Impact Simulation and Practical Verification," 1987.

[135] D. Barbani, N. Baldanzini, and M. Pierini, "Development and validation of an FE model for motorcycle-car crash test simulations," *Int. J. Crashworthiness*, vol. 19, no. 3, pp. 244–263, 2014, doi: 10.1080/13588265.2013.874672.

[136] A. Chawla, S. Mukherjee, D. Mohan, M. Singh, M. Sakurai, and T. Nakatani, "A methodology for car-motorcycle crash simulation," *JARI Res. J.*, vol. 23, no. 2, pp. 98–101, 2003.

[137] M. Deguchi, "Modeling of a motorcycle for collision simulation," in *18th International Technical Conference on the Enhanced Safety of Vehicles*, 2003, no. 157, pp. 1–7. [Online]. Available: http://scholar.google.com/scholar?hl=en&btnG=Search&q=intitle:Modeling+of+a+Motorcycle+for+Collision+Simulation#0

[138] M. Deguchi, "Simulation of motorcycle-car collision," in *19th international Technical Conference on Experimental Safety of Vehicles*, 2005, no. 05, pp. 1–7. [Online]. Available: http://www-nrd.nhtsa.dot.gov/pdf/nrd-01/ESV/esv19/05-0041-O.pdf

[139] S. Kanbe, M. Deguchi, and Y. Hannya, "Basic Research for a new airbag system for motorcycles," *20th Int. Tech. Conf. Enhanc. Saf. Veh.*, vol. 20076606, no. 1, pp. 1–9, 2007, [Online]. Available: http://www-nrd.nhtsa.dot.gov/pdf/nrd-01/ESV/esv20/07-0095-O.pdf

[140] T. Kuroe, H. Namiki, and S. Iijima, "Exploratory Study of an Airbag Concept for a Large Touring Motorcycle : Further Research Second Report," in *Honda R&D Co., Ltd. Asaka R&D Center*

Japan , 2005, no. Paper Number 05-0316.
[141] S. Mukherjee, A. Chawla, D. Mohan, M. Singh, M. SAKURAI, and Y. Tamura, “Motorcycle-car side impact simulation,” 2001.
[142] H. Namiki, T. Nakamura, and S. Iijima, “A computer simulation for motorcycle rider-motion in collision,” *SAE Tech. Pap.*, 2003, doi: 10.4271/2003-32-0044.
[143] H. Namiki, T. Nakamura, and S. Iijima, “A Computer Simulation for Motorcycle Rider Injury Evaluation in Collision,” *Honda R&D Tech. Rev.*, vol. 17.2, p. 153, 2005.
[144] J. J. Nieboer, J. Wismans, A. C. M. Versmissen, M. T. P. Van Slagmaat, I. Kurawaki, and N. Ohara, “Motorcycle crash test modelling,” *SAE Tech. Pap.*, 1993, doi: 10.4271/933133.
[145] A. Chawla *et al.*, “FE simulations of motorcycle-car frontal crashes, validations and observations,” *Int. J. Crashworthiness*, vol. 10, no. 4, pp. 319–326, 2005, doi: 10.1533/ijcr.2005.0344.
[146] J. Ambrósio and J. Dias, “A road vehicle multibody model for crash simulation based on the plastic hinges approach to structural deformations,” *Int. J. Crashworthiness*, vol. 12, no. 1, pp. 77–92, 2007, doi: 10.1533/ijcr.2006.0171.
[147] National Crash Analysis Center, “Finite Element Model of Dodge Neon FE Model of Dodge Neon,” 1996. [Online]. Available: http://www.ncac.gwu.edu/vml/archive/ncac/vehicle/neon-0.7.pdf
[148] R. Happee, E. De Vlugt, and A. C. Schouten, “Posture Maintenance of the Human Upper Extremity, Identification of Intrinsic and Reflex Based Contributions,” *SAE Int. J. Passeng. Cars - Mech. Syst.*, vol. 1, no. 1, pp. 2008-01–1888, Jun. 2008, doi: 10.4271/2008-01-1888.
[149] V. Mathiowetz, N. Kashman, G. Volland, K. Weber, M. Dowe, and S. Rogers, “Grip and pinch strength: normative data for adults,” *Arch. Phys. Med. Rehabil.*, vol. 66, no. 2, pp. 69–74, 1985, [Online]. Available: https://pubmed.ncbi.nlm.nih.gov/3970660/
[150] C. Y. Warner, G. C. Smith, M. B. James, and G. J. Germane, “Friction Applications in Accident Reconstruction,” *SAE Tech. Pap. 830612*, 1983, doi: https://doi.org/10.4271/830612.
[151] T. D. Day and J. R. Smith, “Friction Factors for Motorcycles Sliding on Various Surfaces,” *SAE Tech. Pap. 840250*, 1984.
[152] C. J. Medwell, J. R. McCarthy, and M. T. Shanahan, “Motorcycle slide to stop tests,” *SAE Tech. Pap. 970963*, Feb. 1997, doi: 10.4271/970963.
[153] S. Piantini *et al.*, “Advanced accident research system based on a medical and engineering data in the metropolitan area of Florence,” *BMC Emerg. Med.*, vol. 13, no. 1, 2013, doi: 10.1186/1471-227X-13-3.
[154] S. Piantini, “IN-SAFE ID – 85 (ICU - 285),” Florence, 2016.
[155] International Organization for Standardization (ISO), “Motorcycles—Test and Analysis Procedures for Research Evaluation of Rider Crash Protective Devices Fitted to Motorcycles, Parts 1 to 8. 2nd.” 2005. [Online]. Available: https://www.iso.org/home.html.
[156] SAE, “SAE J211-1 (1995): Instrumentation for Impact Test, Part 1, Electronic Instrumentation,” 1995.
[157] S. Piantini, “IN-SAFE ID – 135 (ICU – 266),” Florence, 2016.
[158] K. Bauer, “MOTORIST Mid-Term Meeting: Ludwig-Maximilians-University,” Pilsen, 2015.
[159] Ludwig-Maxmilians-Universität München., “Biomechanics and Accident Analysis Group.”
[160] “Accident by car (2011) Review BMW E36 323i Sporty.” https://accidentbycar.blogspot.cz/2011/01/review-bmw-e36-323i-sporty.html
[161] “Trade motorcycles (2015) Suzuki Burgman 200 Review.” http://www.trademotorcycles.com.au/2015-suzuki-burgman-200-review
[162] C. Klug and J. Ellway, “Pedestrian Human Model Certification v3.0.1,” 2021, [Online]. Available: blob:https://web.telegram.org/df1a9333-4ea4-4540-b499-9e6bf8cc083f
[163] *Regulation No 94 of the Economic Commission for Europe of the United Nations (UN/ECE) — Uniform provisions concerning the approval of vehicles with regard to the protection of the occupants in the event of a frontal collision*. 2010.

[164] NHTSA, *49 CFR § 571.208 - Standard No. 208; Occupant crash protection.*
[165] D. Schaper and J. Grandel, “Motorcycle collisions with passenger cars-analysis of impact mechanism, kinematics, and effectiveness of full face safety helmets,” *SAE Technical Papers 850094*. 1985. doi: 10.4271/850094.
[166] L. Peck, J. Manning, W. Bartlett, C. Dickerson, and E. S. Deyerl, “Eleven Instrumented Motorcycle Crash Tests and Development of Updated Motorcycle Impact-Speed Equations,” *SAE Int. J. Transp. Saf.*, vol. 7, no. 1, pp. 41–68, 2019, doi: 10.4271/09-07-01-0004.
[167] J. Eubanks, “Motorcycle Speed-from-Damage Estimates Update,” *Soc. Accid. Reconstr.*, vol. 22, 1991.
[168] W. Bartlett, “Motorcycle crush analysis,” *Accid. Reconstr. J.*, vol. 19, no. 2, pp. 25–28, 2009.
[169] A. Hamzah, M. K. Rahman, A. H. Ariffin, and M. S. Solah, “Motorcycle Structural Response in Simulated Vehicular Collision,” in *Proceeding of International Crashworthiness Conference*, 2014, no. August.
[170] J. Smith, T. Frank, G. Fowler, and S. M. Werner, “Motorcycle Crash Testing and Reconstruction: Selected Exponent Publications”.
[171] J. W. Smith, T. A. Frank, K. E. Bosch, G. F. Fowler, and J. W. Carter, “Full-scale moving motorcycle into moving car crash testing for use in safety design and accident reconstruction,” *SAE Tech. Pap.*, 2012, doi: 10.4271/2012-01-0103.
[172] L. Prochowski and T. Pusty, “Analysis of the rotation and lifting of a motorcycle following an impact against a motor car side,” *Arch. Motoryz.*, vol. Nr 4, pp. 13–29, 2012.
[173] L. Prochowski and T. Pusty, “Analysis of Motorcyclist’S Body Movement During a Motorcycle Impact Against a Motor Car Side,” *J. KONES. Powertrain Transp.*, vol. 20, no. 4, pp. 371–379, 2015, doi: 10.5604/12314005.1137849.
[174] M. Toma, F. E. A. Njilie, M. Ghajari, and U. Galvanetto, “Assessing motorcycle crash-related head injuries using finite element simulations,” *Int J Simul Model*, vol. 9, pp. 143–151, 2010, doi: 10.2507/IJSIMM09(3)3.164.
[175] Z. Xiao, L. Wang, F. Mo, X. Lv, and C. Yang, “Influences of impact scenarios and vehicle front-end design on head injury risk of motorcyclist,” *Accid. Anal. Prev.*, vol. 145, no. August, p. 105697, 2020, doi: 10.1016/j.aap.2020.105697.
[176] N. M. Rogers, “Further crash tests of motorcycle leg protectors as proposed in the UK draft specification,” in *Proceedings of the ESV*, 1991, p. 1.
[177] N. M. Rogers and J. W. Zellner, “Application of ISO13232 to motorcyclist productive device research,” in *International Technical Conference on the Enhanced Safety of Vehicles (ESV)*, 1996, p. 1.
[178] N. M. Rogers and J. W. Zellner, “An overall evaluation of UKDS motorcyclist leg protectors based on ISO13232,” in *International Technical Conference on the Enhanced Safety of Vehicles (ESV)*, 1998, p. 1.
[179] J. W. Zellner, J. A. Newman, and M. Nicholas, “Preliminary research into the feasibility of motorcycle airbag systems,” in *International Technical Conference on the Enhanced Safety of Vehicles (ESV)*, 1994, p. 1.
[180] J. W. Zellner, K. D. Wiley, N. L. Broen, and J. A. Newman, “A standardized Motorcyclist Impact Dummy for Protective Device Research,” in *International Technical Conference on the Enhanced Safety of Vehicles (ESV)*, 1996, p. 1.
[181] S. K. Kebschull, J. W. Zellner, R. Van Auken, and N. Rogers, “Injury risk/benefit analysis of motorcyclist protective devices using computer simulation and ISO 13232,” in *International Technical Conference on the Enhanced Safety of Vehicles (ESV)*, 1998, pp. 2357–2374. [Online]. Available: http://www-nrd.nhtsa.dot.gov/pdf/Esv/esv16/98S10W26.PDF
[182] S. Maier, F. Kempter, S. Kronwitter, and J. Fehr, “Positioning and Simulation of Human Body Models on a Motorcycle with a Novel Restraint System,” in *Conference proceedings International Research Council on the Biomechanics of Injury, IRCOBI*, 2022, vol. 2022-Septe, pp. 82–96.

[183] A. Grassi, N. Baldanzini, D. Barbani, and M. Pierini, “A comparative analysis of MAIDS and ISO13232 databases for the identification of the most representative impact scenarios for powered 2-wheelers in Europe,” *Traffic Inj. Prev.*, vol. 19, no. 7, pp. 766–772, 2018, doi: 10.1080/15389588.2018.1497791.
[184] AENOR (Asociación Española de Normalización y Certificación):, “UNE 135900-1: Standard on the evaluation of performance of the protection systems for motorcyclists on safety barriers and parapets. Part 1: Terminology and test procedures,” Spain, 2008.
[185] AENOR (Asociación Española de Normalización y Certificación):, “UNE 135900-2: Standard on the evaluation of performance of the protection systems for motorcyclists on safety barriers and parapets. Part 2: Performance classes and acceptance criteria,” Spain, 2008.
[186] F. J. Lopez-Valdes, D. , García, D. Pedrero, and J. L. Moreno, “Accidents of Motorcyclists Against Roadside Infrastructure.,” in *In IUTAM Symposium on Impact Biomechanics*, 2005.
[187] R. Eppinger, E. Sun, S. Kuppa, and R. Saul, “Supplement: Development of improved injury criteria for the assessment of advanced automotive restraint systems - II,” *Natl. Highw. Traffic Saf. Adminstration (NHTSA); Natl. Transp. Biomech. Res. Cent.*, no. March, p. SES-1--SR-2, 2000.
[188] F. Heitplatz, R. Sferco, and P. Fay, “An evaluation of existing and proposed injury criteria with various dummies to determine their ability to predict the levels of soft tissue neck injury seen in real world accidents.,” in *In: Proceedings of the 18th Technical Conference on the Enhanced Safety of Vehicles,Nagoya, Japan,* 2003, vol. pp, pp. 1-7.
[189] P. Prasad and A. Kim, “Critical evaluation of low speed rear impacts,” in *IRCOBI Conf. Symposium*, 2001, pp. 1–2.
[190] CEN, “Protective footwear for motorcycle riders - Requirements and test methods, EN 13634:2010.”
[191] CEN, “Motorcyclists’ protective clothing against mechanical impact - Part 1: Motorcyclists’ limb joint impact protectors - Requirements and test methods, EN 1621-1:2012.”
[192] CEN, “Motorcyclists’ protective clothing against mechanical impact - Part 2: Motorcyclists’ back protectors - Requirements and test methods, EN 1621-2:2013.”
[193] CEN, “Motorcyclists’ protective clothing against mechanical impact - Part 3: Motorcyclists’ chest protectors - Requirements and test methods, EN 1621- 3:2010.”.
[194] CEN, “Motorcyclists’ protective clothing against mechanical impact - Part 4: Motorcyclists’ inflatable protectors - Requirements and test methods, EN 1621-4:2012.”.

10 List of outputs during Ph.D. Study

[v1] **T. Bońkowski**, L. Hynčík "Helmet with a multi-directional suspension system and a procedure for assembling the helmet", PCT patent application PCT/CZ2022/050066

[v2] J. Špička, L. Hynčík, **T. Bońkowski**, P. Kochová, R. Cimrman, S. Kaňáková, M. Pašek. Testing and identification of the LLDPE material for impact applications. In Virtual Development In Passive Safety And Human Models For Future Mobility. Pilsen, 21.09.2021

[v3] J. Špička, M. Čermák, **T. Bońkowski**, R. Kroft,J. Vychytil, Support of the numerical mechanics in the clarification of the mysterious death of Jan Masaryk. Proceedings of the Computational Mechanics conference, 2021

[v4] J. Špička, A. Talimian, L. Hynčík**, T. Bońkowski**, P. Kochová, A. Hanuliak, L. Kovář, On the development of a new vehicle safety system for a standard and non-standard seating configurations. In proceedings of the ICCB 2022 conference 11 - 13 April 2022, Lisbon, Portugal. ISBN 979-989-99424-9-3.

[v5] L. Hynčík, H. Čechová, **T. Bońkowski**, On developing subject-specific human body models for clinical and industrial applications. In The Ninth International Conference on Computational Bioengineering (ICCB2022), 11 - 13 April 2022, Lisbon, Portugal. ISBN 979-989-99424-9-3.

[v6] **T. Bońkowski**, V. Beránek, V. Nováček, P. Šťastný. Forces in upper limb strikes in mix martial art athletes during ground and pound tactics. In 9th World Congress of Biomechanics, Tapei, Taiwan, 10-14 July 2022.

[v7] L. Hynčík, H. Čechová, **T. Bońkowski**, G. Kavalířová, P. Špottová, V. Hampejsová, H. Meng, Personalization of a Human Body Model Using Subject-Specific Dimensions for Designing Clothing Patterns. Appl. Sci. 2021, 11, 10138. https://doi.org/10.3390/app112110138.

[v8] J. Špička, **T. Bońkowski**, L. Hynčík, A. Hanuliak, Assessment of Nanobag as a New Safety System in the Frontal Sled Test. Appl. Sci. 2022, 12, 989. https://doi.org/10.3390/app12030989

[v9] P. Kochova, A. Malečková, R. Pálek, V. Liška, **T. Bońkowski**, M. Horák, M. Grajciarová, Z. Tonar, Porcine spleen as a model organ for blunt injury impact tests: An experimental and histological study, Anatomia, Histologia, Embryologia, 10.1111/ahe.12831

[v10] A. Malečková, P. Kochová, R. Pálek, V. Liška, P. Mik, **T. Bońkowski**, M. Horák, Z. Tonar, (2021) Blunt injury of liver – mechanical response of porcine liver in experimental impact test, Physiological Measurement, Q2, OBD ID: 43932013

[v11] L. Hynčík, P. Kochová, J. Špička, **T. Bońkowski**, R. Cimrman, S. Kaňáková, R. Kottner, M. Pašek, Identification of the LLDPE Constitutive Material Model for Energy Absorption in Impact Applications. Polymers 2021, 13, 1537. https://doi.org/ 10.3390/polym13101537, Q1

[v12] **T. Bońkowski**, L. Hynčík, L. Šoltés, R. Kottner, Range of motion in motorcycle garment: experimental study, Joint International Conference Clothing-Body Interaction 2021, 2-3.06.2021 https://mt.webspace.tu-dresden.de/cbi/doku.php?id=program

[v13] **T. Bońkowski**, L. Hynčík, Preliminary evaluation of motorcycle suit impact on rider range of motion, Studentská vědecká konference Fakulty aplikovaných věd 2021, 10.6.2021 , http://svk.fav.zcu.cz/download/sbornik_svk_2021.pdf

[v14] **T. Bońkowski**, J. Vychytil, Může antroppometrie řidiče ovlivnit výpočet rizika poranění? - Case study, Human Biomechanics 2021, Prague, 18.6.2021, https://sites.google.com/view/humanbiomechanics2021/schedule?authuser=0

[v15] **T. Bońkowski**, J. Špička, Virthuman in Vulnerable Road Users Passive Safety, In proceedings of VPS User Conference 2019, 1-2. 10. 2019 Nesuchyně, Czech Republic

[v16] **T. Bońkowski**, L. Hynčík, W. Lyu, Anthropometry Influence On The Real Ptw Accident Outcomes- A Numerical Study. In The 2nd International Symposium on Automobile Traffic Safety Problems in New Mobility Arena., 2019. OBD ID: 43928277 (příspěvek) ID 43929305 (konference)

[v17] L. Hynčík, **T. Bońkowski**, W. Lyu, Numerical Assessment of Motorcyclist Accident, Journal of the Society of Automotive Engineers Malaysia, Volume 3, Issue 2, pp 210-217, 2019, OBD ID: 43927714

[v18] R. Kottner, **T. Bońkowski**, S. Kaňáková , Experimental Investigation of Foams Suitable for Motorcycle Protectors, Journal Of Mechanics Of Continua And Mathematical Sciences ,4, NOV 2019,58-69, OBD ID: 43927732

[v19] **T. Bońkowski**, L. Hynčík, W. Lyu. (2020) PTW Passive Safety: Numerical Study of Standard Impact Scenarios with Rider Injury Risk Assessment, SAE Technical Paper 2020-01-0930, 2020, ISSN 0148-7191 (Q2 Journal)

[v20] R. Kottner, S. Kaňáková, **T. Bońkowski**, R. Yeung, A. Pukaro (2020) Improvement of impact protection by KORDCARBON-CPREG-200-T-3K-EP1-4-A composite, Materials Today: Proceedings ,https://doi.org/10.1016/j.matpr.2020.02.084, OBD ID: 43928819

[v21] L. Hynčík, **T. Bońkowski**, Helmet to head coupling by multi-body system,. Applied and Computational Mechanics, 2019, vol. 13, no. 1, s. 21-28. ISSN: 1802-680X, DOI: 10.24132/acm.2019.432

[v22] W. Lyu, L. Hynčík, **T. Bońkowski**, "Rider Stature Influence to Injury Risk in Motorcycle Rear Impact to Car," SAE Technical Paper 2019-01-1436, 2019, https://doi.org/10.4271/2019-01-1436

[v23] R. Kottner, **T. Bońkowski**, S. Kaňáková, Experimental Investigation of Foams Suitable for Motorcycle Protectors. Journal of mechanics of continua and mathematical sciences, 2019, vol. 4, no. NOV 2019, s. 58-69. ISSN 2454-7190.

[v24] R. Kottner, S. Kaňáková, L. Šoltés, T. **Bońkowski,** J. Krystek , Mechanical Behaviour of Foam Used in Joint Protectors In EAN 2018 – Conference on Experimental Stress Analysis, 2018,

[v25] J. Vychytil, J. Špička, L. Hynčík, T. **Bońkowski, L.** Kovář, P. Pavlata.; Application of Virthuman Model for Safety Assessment in Various Crash Configurations. In HMS, Berlin, 2018

[v26] S. Kaňáková, R. Kottner, **T. Bońkowski**, Influence of temperature on foam used in motorcycle protective equipment, Protectors In EAN 2019 – Conference on Experimental Stress Analysis, 2019

[v27] **T. Bońkowski**, J. Špička, L. Hynčík, Virthuman In PTW Passive Safety. In International Symposium on Automobile Traffic Safety Problems in New Mobility Arena. Tianjin: Tianjin University of Science and Technology, 2018. s. 11-12

[v28] **T. Bońkowski**, L. Hynčík, Combined forward-backward approach for reconstruction of powered two wheeler accidents with injury criteria assessment. In FISITA World Automotive Congress 2018. Chennai: SAEINDIA, 2018. ISBN: 978-0-9572076-5-3.

[v29] L. Hynčík, **T. Bońkowski**, R. Kottner, Virtual assessment of motorcycle helmet contribution to decreasing injury risk in impact. In FISITA World Automotive Congress 2018. Chennai: SAEINDIA, 2018. s. 1-6. ISBN: 978-0-9572076-5-3.

[v30] L. Hynčík, **T. Bońkowski** „Virtual approach for assessing safety“ European Conference on Injury Prevention and Safety Promotion 2017 (presentation) OBD ID: 43919194

[v31] L. Hynčík, **T. Bońkowski**, J. Vychytil, J. Špička, Motorcyclist barrier impact: a comparative study. In Computational mechanics - EXTENDED ABSTRACTS. Plzeň: University of West Bohemia, 2017. s. 41-42. ISBN: 978-80-261-0748-4, OBD ID 43919345

[v32] **T. Bońkowski**, Motorcycle helmet performance assessment for diverse population, 20th International Conference, AM2018

[v33] S. Kaňáková, R. Kottner**, T. Bońkowski**, V. Hrdlicka, Validace materialoveho modelu chranice pro motocyklisty, SVK 2018.

[v34] W. Lyu, **T. Bońkowski**, L. Hynčík, Development of a simple helmet finite element model. In Computational mechanics - BOOK OF EXTENDED ABSTRACTS. Plzeň: University of West Bohemia, 2018. s. 57-58. ISBN: 978-80-261-0819-1.

[v35] L. Šoltés, **T. Bońkowski**, R. Kottner, L. Hynčík, Drop Test of Foams used in Motorbike Protectors. In EAN 2017 - 55th Conference on Experimental Stress Analysis 2017. Košice: Technical University of Košice, 2017. p. 27-30. ISBN: 978-80-553-3167-6.

[v36] **T. Bońkowski**, L. Šoltés, L. Hynčík, R. Kottner, P. Kochová, Leather for motorcyclist garments: Multi-test based material model fitting in terms of Ogden parameters. Applied and Computational Mechanics, 2017, vol. 11(2), p. 129-136. ISSN: 1802-680X.

[v37] **T. Bońkowski**, L. Hynčík, L. Šoltés, Motorcycle Helmets: The Population Diversity Influence on Head Injury Criterion Assessment. In International Research Council on Biomechanics of Injury (IRCOBI) 2017. Zurich, Switzerland:(IRCOBI), 2017. p. 218-219, ISSN: 2235-3151.

[v38] **T. Bońkowski**, L. Šoltés, P. Kochová, R. Kottner, L. Hynčík, Motorcycle Suits: Uniaxial and Biaxial Tensile Tests of Leather. In EAN 2017 - 55th Conference on Experimental Stress Analysis 2017. Košice: Technical University of Košice, 2017. p. 435-440. ISBN: 978-80-553-3167-6.

[v39] L. Hynčík, **T. Bońkowski**, J. Vychytil, J. Špička, Motorcyclist barrier impact: a comparative study. In Computational mechanics - EXTENDED ABSTRACTS. Plzeň: University of West Bohemia, 2017. p. 41-42. ISBN: 978-80-261-0748-4.

[v40] **T. Bońkowski**, L. Šoltés, L. Hynčík, The coupling of the scaled Virthuman and the motorcycle helmet. In Studentská vědecká conference 2017 - magisterské a doktorské studijní programy, book of abstracts. Plzeň: ZČU v Plzni, 2017. s. 9-10. ISBN: 978-80-261-0706-4.

[v41] L. Hynčík, **T. Bońkowski, J**. Vychytil, Virtual hybrid human body model for PTW safety assessment. Applied and Computational Mechanics, 2017, vol 11 (2), p. 137-144. ISSN: 1802-680X.

[v42] J. Špička, M. Hajžman, **T. Bońkowski**, In-house multibody human model based on Euler parameters for the fast impact scenario calculation. In ECCOMAS Congress 2016. Kréta: National Technical University of Athens, 2016. p. 6556-6566. ISBN: 978-618-82844-0-1.

[v42] **T. Bońkowski**, R. Kottner, J. Krystek, L. Hubik, T. Görner, L. Hynčík, Tensile test of motorcycle garment leather. In 54th International Conference on Experimental Stress Analysis (EAN 2016). Plzeň, Czech Republic: Department of Mechanics, Faculty of Applied Sciences, University of West Bohemia, 2016. p. 23-29. ISBN: 978-80-261-0624-1.

[v43] **T. Bońkowski**, M. Hajžman, R. Kottner, T. Görner, L. Hubik, J. Vychytil, L. Hynčík, Contact forces on motorcycle rider overall during high speed low side sliding accident. In Computational mechanics 2015 - EXTENDED ABSTRACTS. Plzeň: Západočeská univerzita v Plzni, Univerzitní 8, 306 14 Plzeň, 2015. p. 13-14. ISBN: 978-80-261-0568-8.

[v44] **T. Bońkowski**, R. Kottner, L. Hynčík, Motorcycle crash parameters and its influence on driver injuries. In Studentská vědecká konference 2015 : magisterské a doktorské studijní programy. Plzeň: Západočeská univerzita v Plzni, 2015. p. 11-12. ISBN: 978-80-261-0505-3

11 Appendix 1 – Simplified Neon Validation

11.1 Frontal impact model – bumper impact

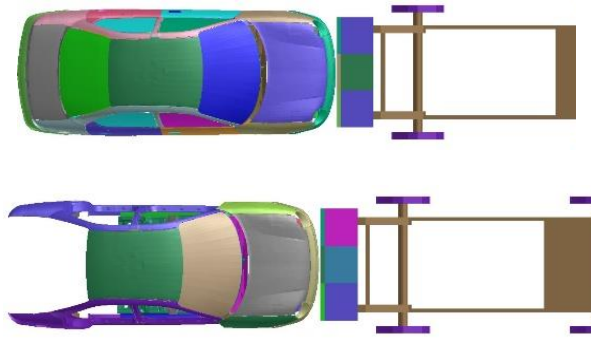

Figure 11.1. Validation setup for the full-frontal crash.

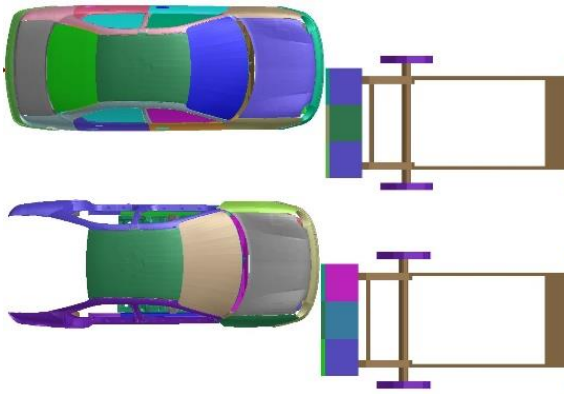

Figure 11.2. Validation setup for 50% offset frontal crash.

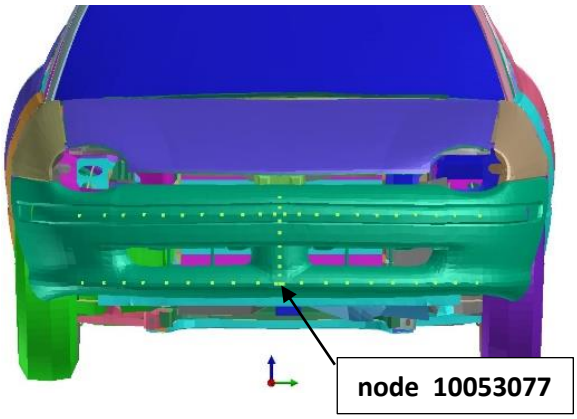

Figure 11.3. Nodes evaluated in validation for front bumper impact.

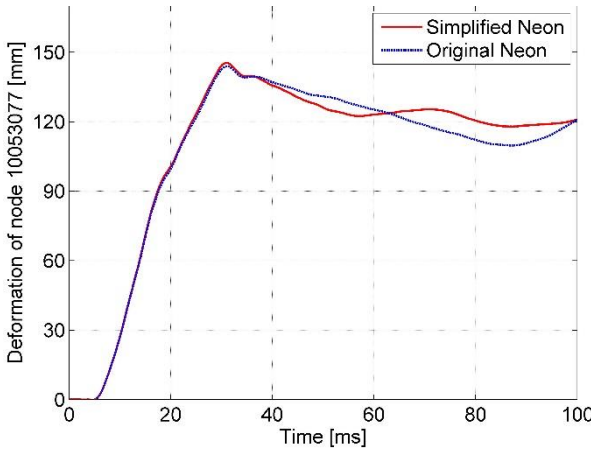

Figure 11.4. Deformation in time of node 10053077 of the front bumper (full frontal, 30 km/h).

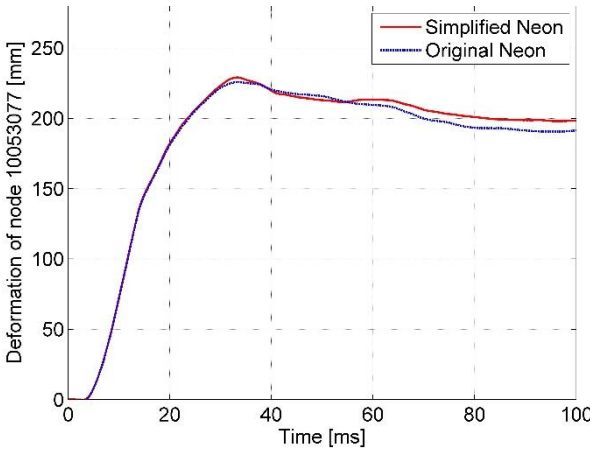

Figure 11.5. Deformation in time of node 10053077 of the front bumper (full frontal, 50 km/h).

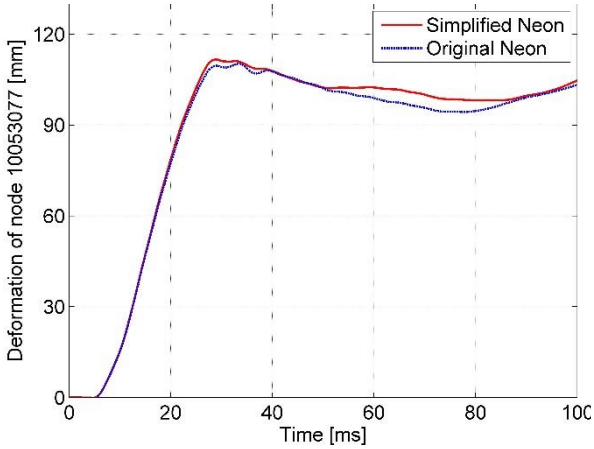

Figure 11.6. Deformation in time of node 10053077 of the front bumper (50% offset, 30 km/h).

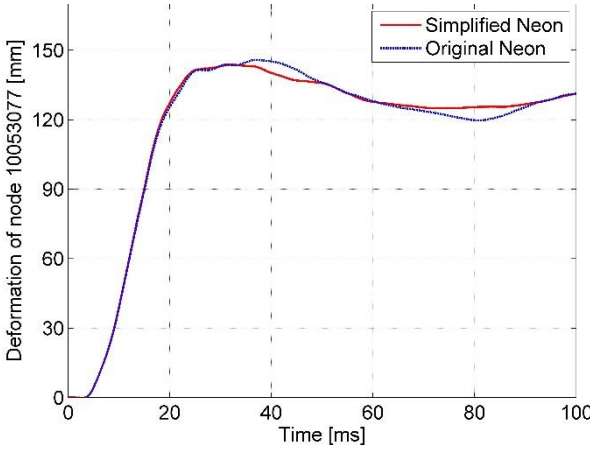

Figure 11.7. Deformation in time of node 10053077 of the front bumper (50% offset, 50 km/h).

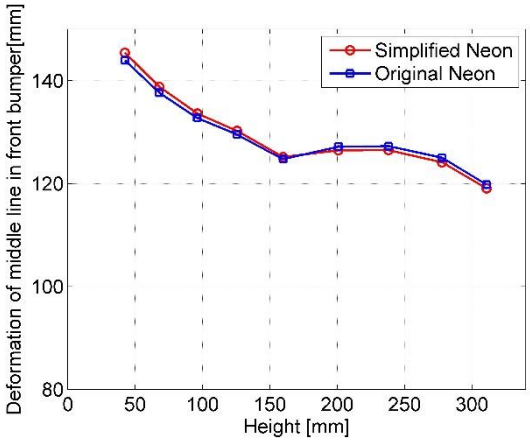

Figure 11.8. Maximum deformation of the central line of the bumper (full frontal, 30 km/h).

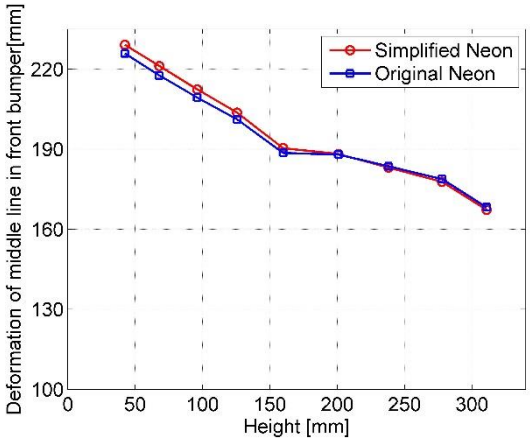

Figure 11.9. Maximum deformation of the central line of the bumper (full frontal, 50 km/h).

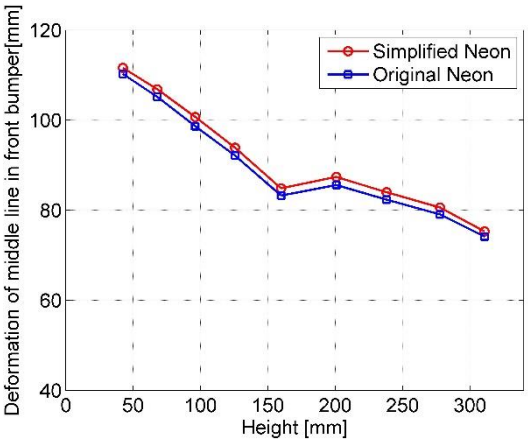

Figure 11.10. Maximum deformation of the central line of the bumper (50% offset, 30 km/h).

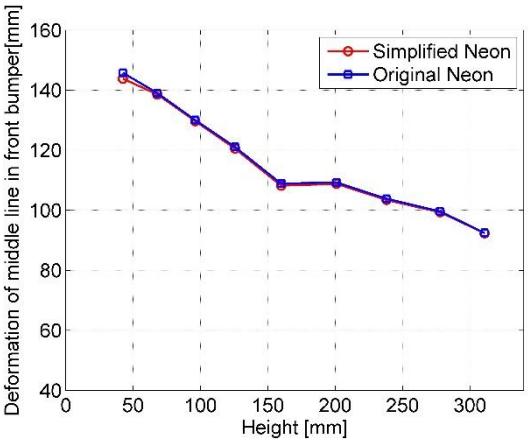

Figure 11.11. Maximum deformation of the central line of the bumper (50% offset, 50 km/h).

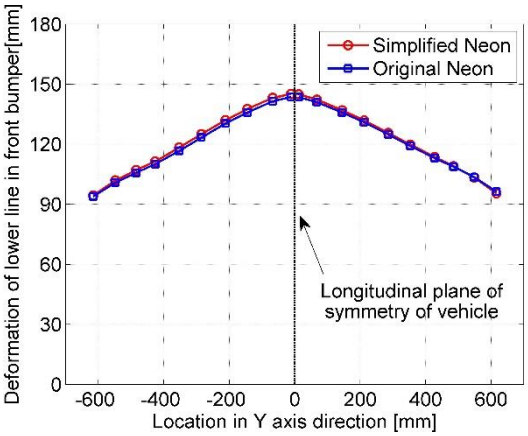

Figure 11.12. Maximum deformation of the lower line of the front bumper (full frontal, 30 km/h).

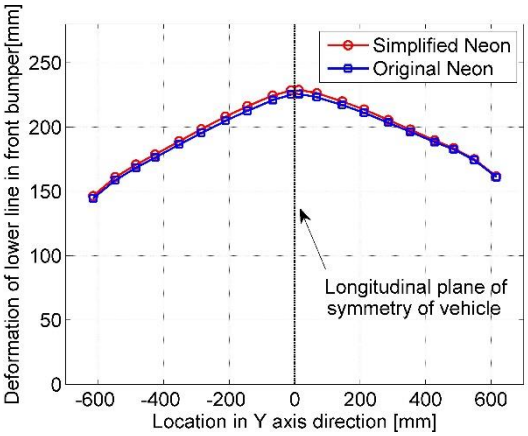

Figure 11.13. Maximum deformation of the lower line of the front bumper (full frontal, 50 km/h).

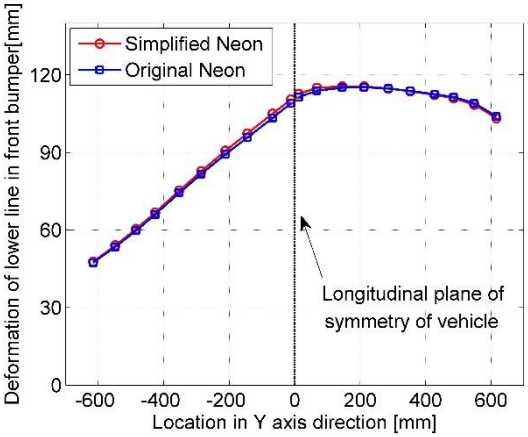

Figure 11.14. Maximum deformation of the lower line of the front bumper (50% offset, 30 km/h).

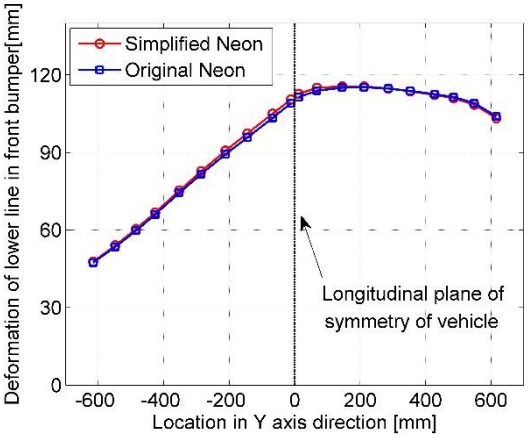

Figure 11.15. Maximum deformation of the lower line of the front bumper (50% offset, 50 km/h).

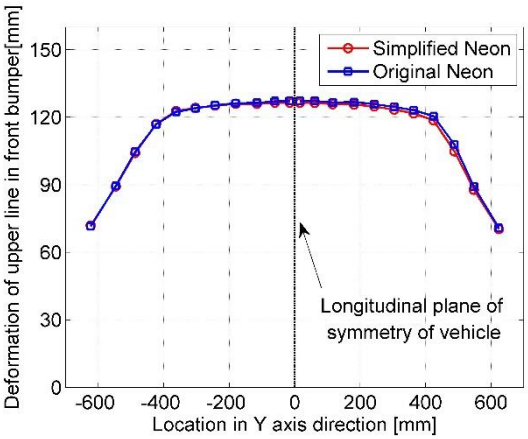

Figure 11.16. Maximum deformation of the upper line of the front bumper (full frontal, 30 km/h).

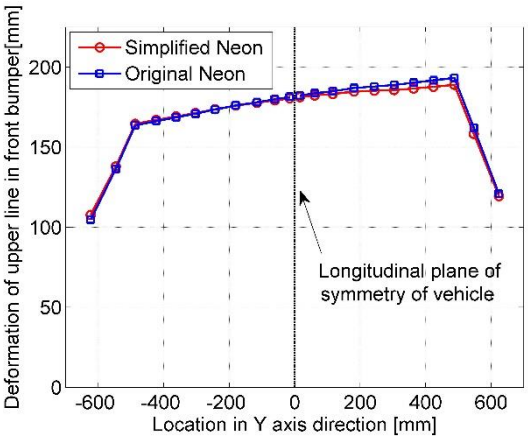

Figure 11.17. Maximum deformation of the upper line of the front bumper (full frontal, 50 km/h).

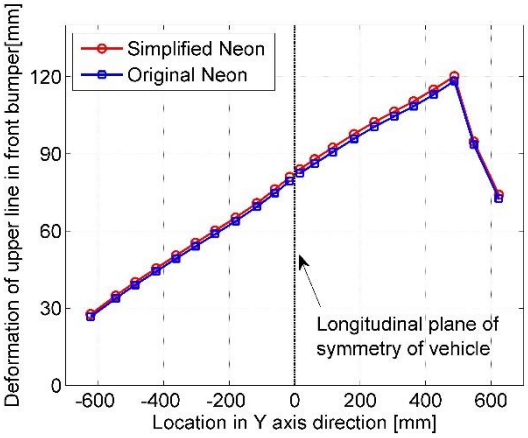

Figure 11.18. Maximum deformation of the upper line of the front bumper (50% offset, 30 km/h).

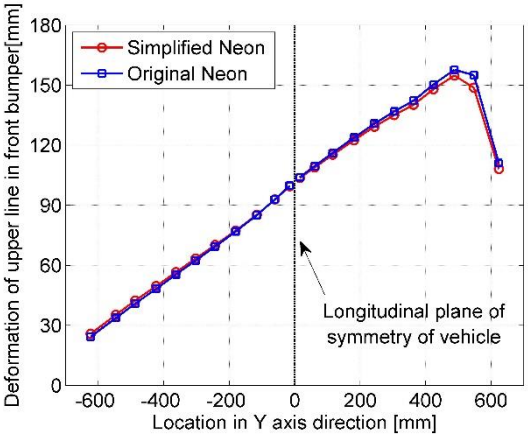

Figure 11.19. Maximum deformation of the upper line of the front bumper (50% offset, 50 km/h).

11.2 Frontal impact model – bumper end impact

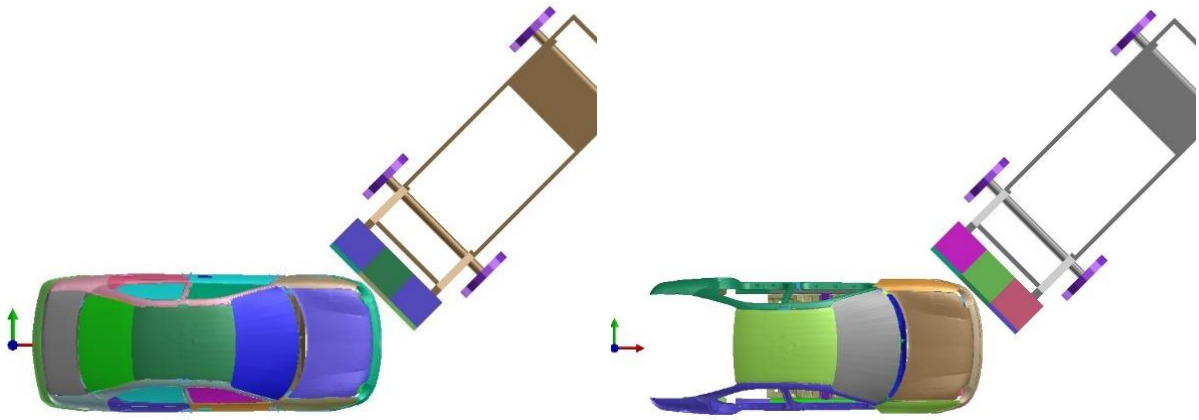

Figure 11.20. Setup for validation of bumper end impact (45 deg).

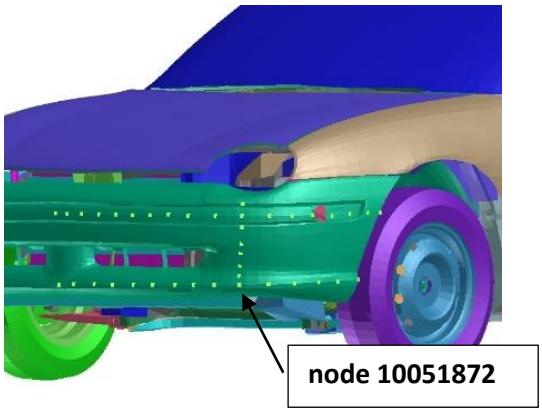

Figure 11.21. Nodes evaluated in 45 deg bumper end crash.

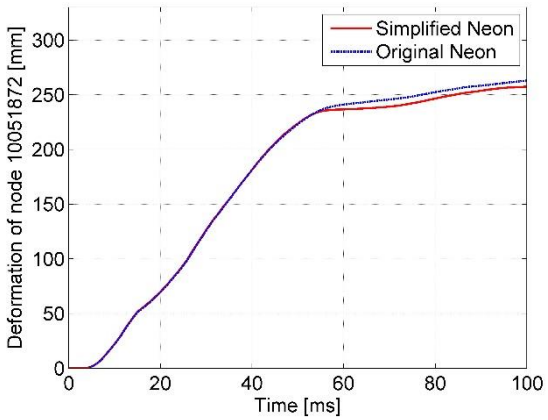

Figure 11.22. Deformation in time of node 10051872 of the front bumper end (45 deg impact, 30 km/h).

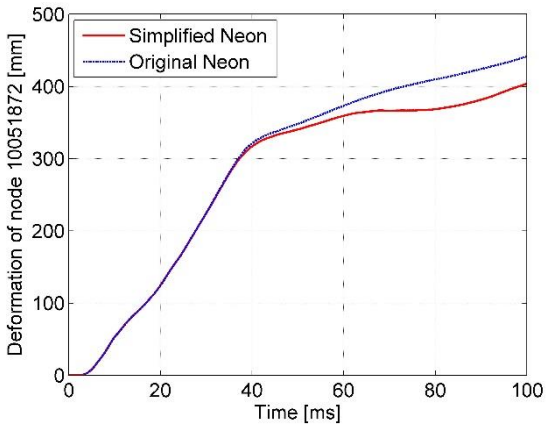

Figure 11.23. Deformation in time of node 10051872 of the front bumper end (45 deg impact, 50 km/h).

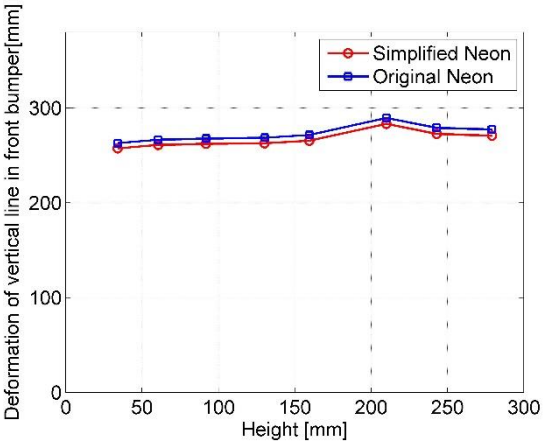

Figure 11.24. Maximum deformation of the vertical line of the front bumper end (45 deg impact, 30km/h).

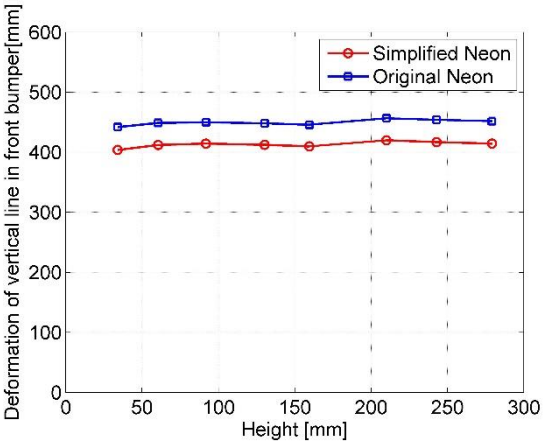

Figure 11.25. Maximum deformation of the vertical line of the front bumper end (45 deg impact, 50km/h).

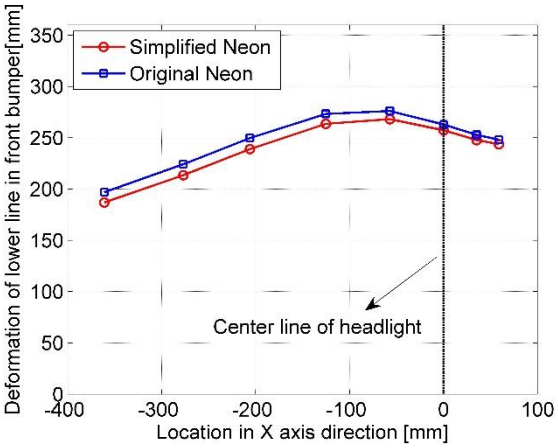

Figure 11.26. Maximum deformation of the lower line of the front bumper end (45 deg impact, 30km/h).

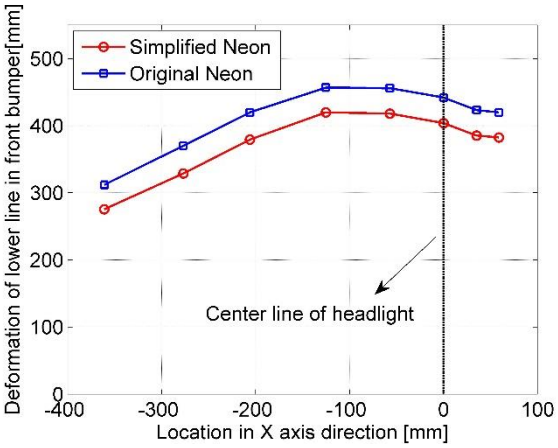

Figure 11.27. Maximum deformation of the lower line of the front bumper end (45 deg impact, 50km/h).

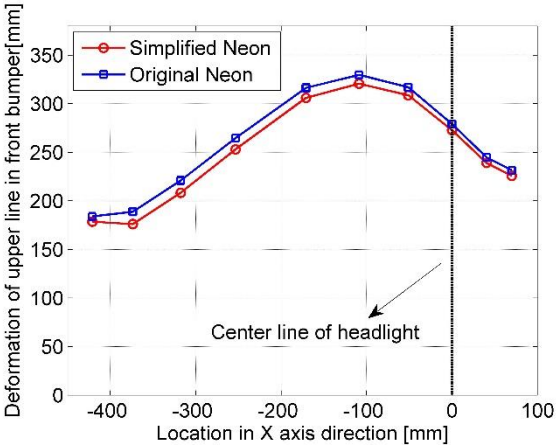

Figure 11.28. Maximum deformation of the upper line of the front bumper end (45 deg impact, 30km/h).

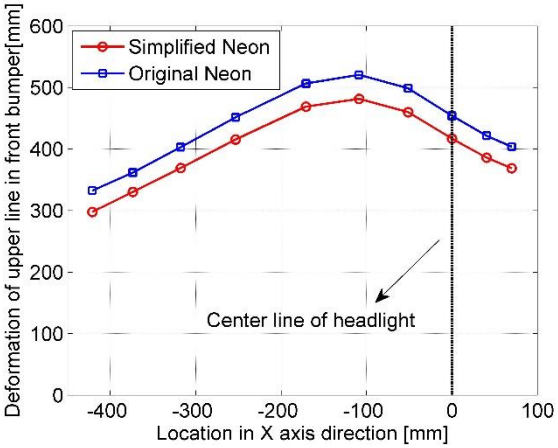

Figure 11.29. Maximum deformation of the upper line of the front bumper end (45 deg impact, 50km/h).

11.3 Frontal impact model – fender impact

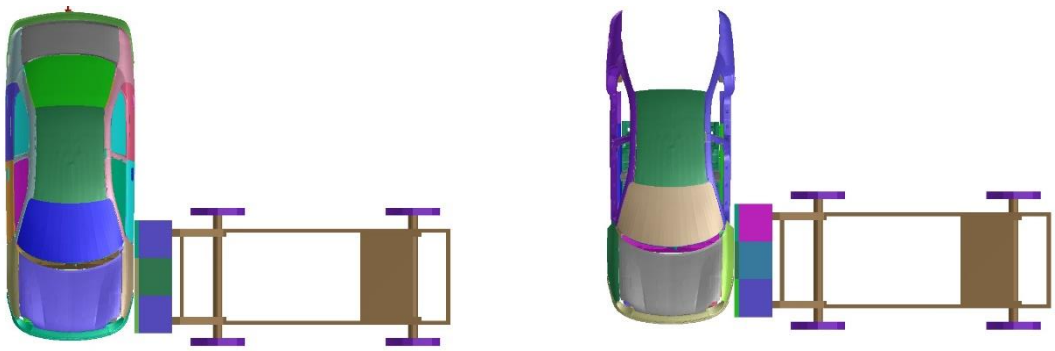

Figure 11.30. Setup for validation of side fender impact.

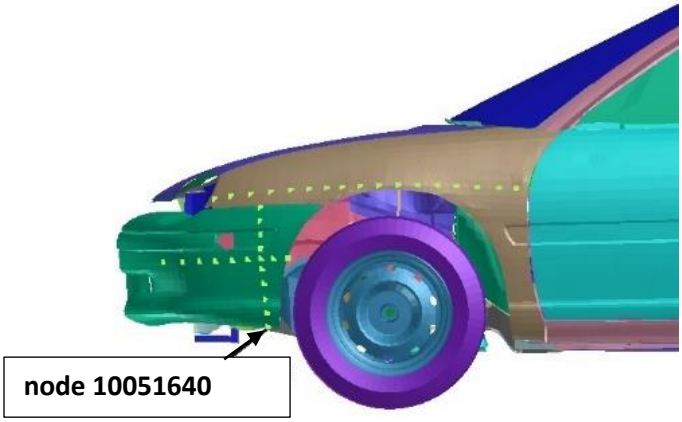

Figure 11.31. Nodes evaluated in side fender impact.

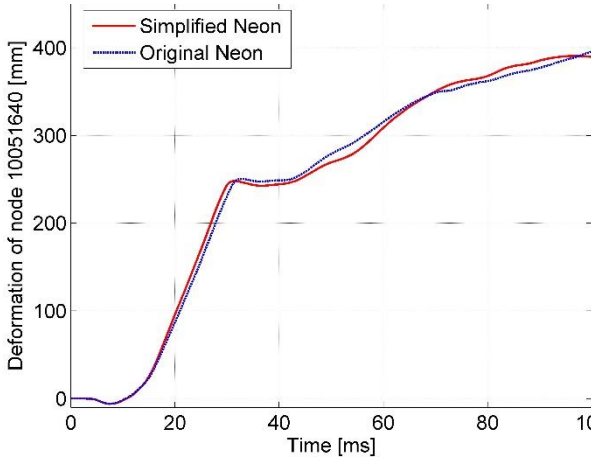

Figure 11.32. Deformation in time of node 10051640 of the fender (side-impact, 30km/h).

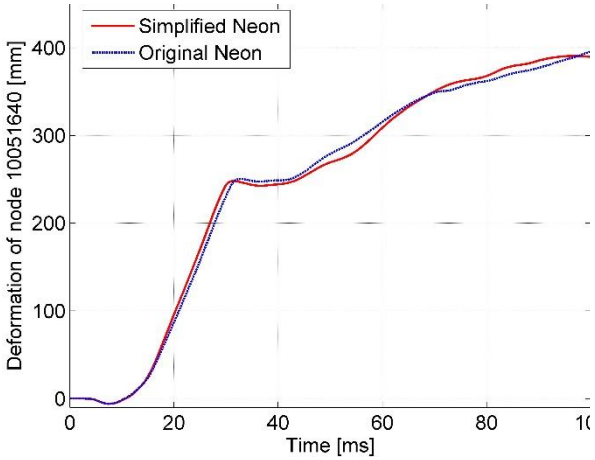

Figure 11.33. Deformation in time of node 10051640 of the fender (side-impact, 50km/h).

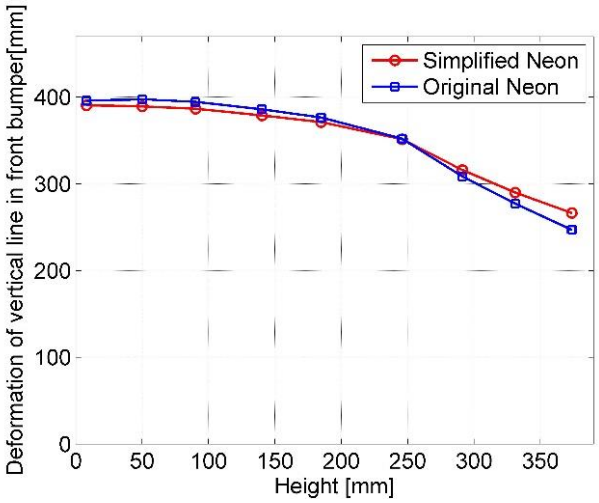

Figure 11.34. Maximum deformation of the vertical line of the front bumper in side fender impact (30 km/h).

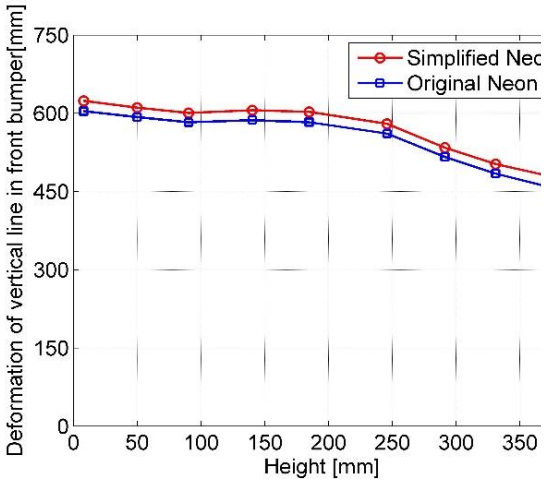

Figure 11.35. Maximum deformation of the vertical line of the front bumper in side fender impact (50 km/h).

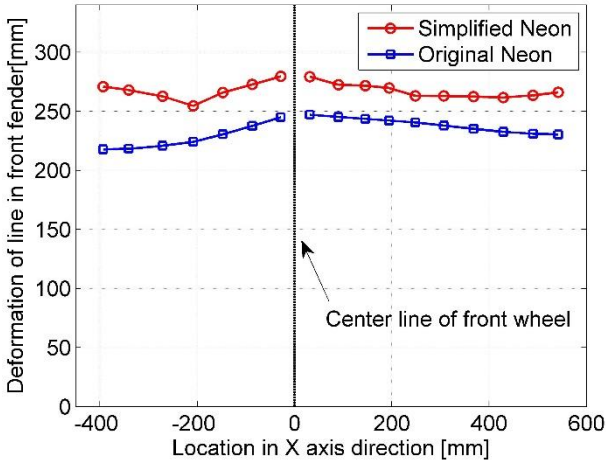

Figure 11.36. Maximum deformation of fender line at height of 394.171 mm in side-impact (30km/h).

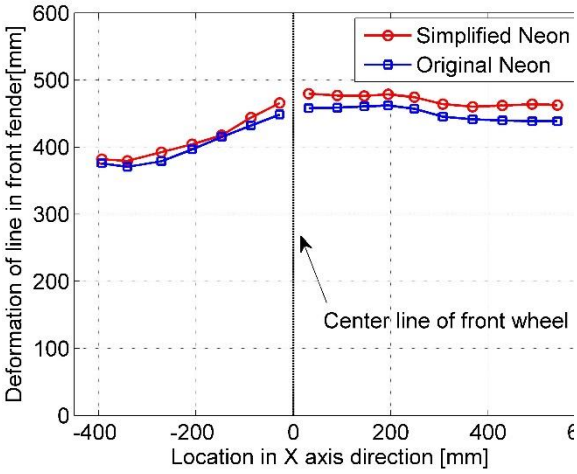

Figure 11.37. Maximum deformation of fender line at height of 394.171 mm in side-impact (50 km/h).

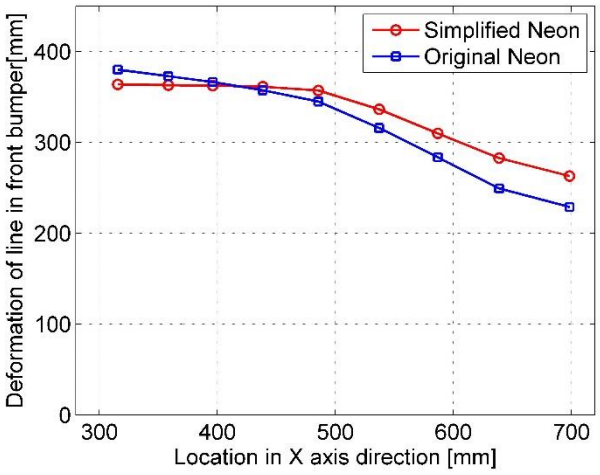

Figure 11.38. Maximum deformation of the line of the front bumper at height of 215.6 mm side fender impact (30 km/h).

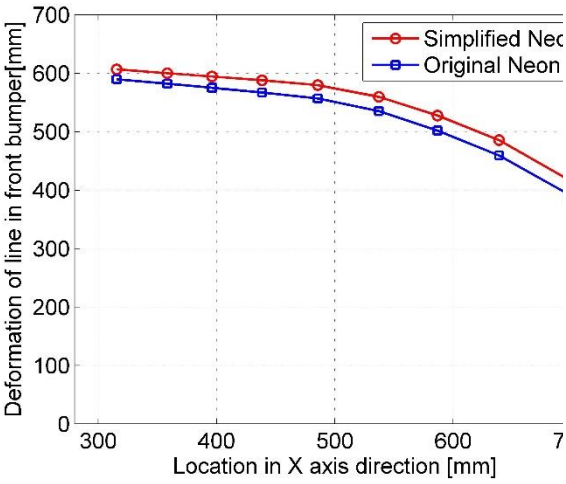

Figure 11.39. Maximum deformation of the line of the front bumper at height of 215.6 mm side fender impact (50 km/h).

11.4 Rear impact model

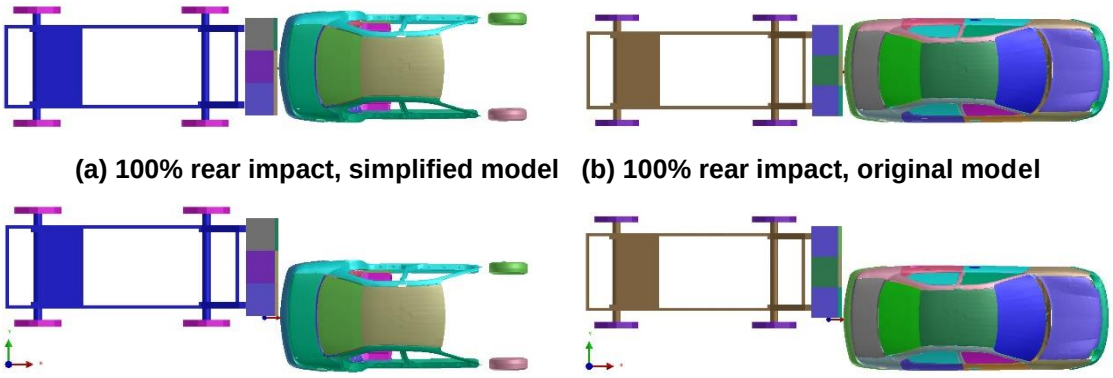

(a) 100% rear impact, simplified model **(b) 100% rear impact, original model**

(c) 50% rear impact, simplified model **(d) 50% rear impact, original model**

Figure 11.40 Simulation setup for rear impact

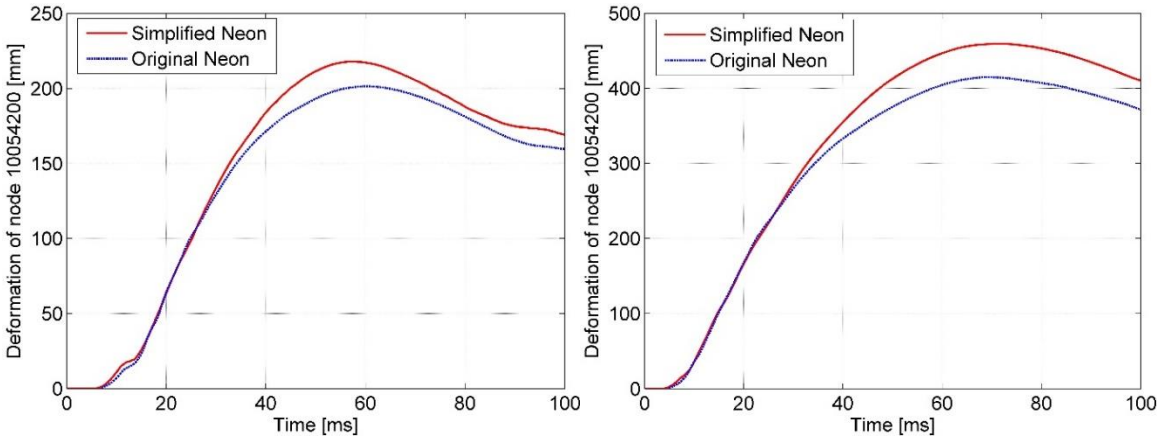

(a) 100%, 30km/h **(b) 100%, 50km/h**

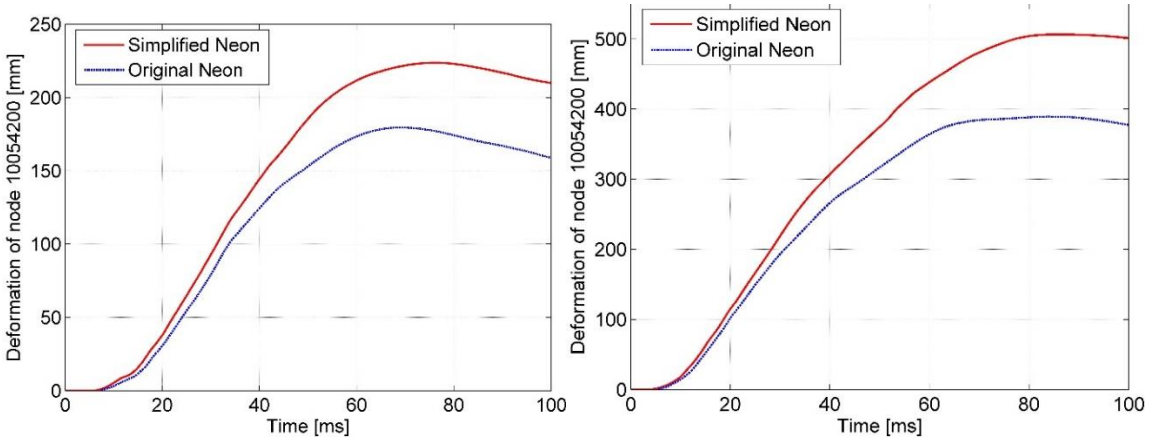

(c) 50% offset, 30km/h **(d) 50% offset, 50km/h**

Figure 11.41 The defomation vs time curves of node 10054200 of rear bumper at height of 239.6 mm in simulations of 100% and 50% offset rear impact.

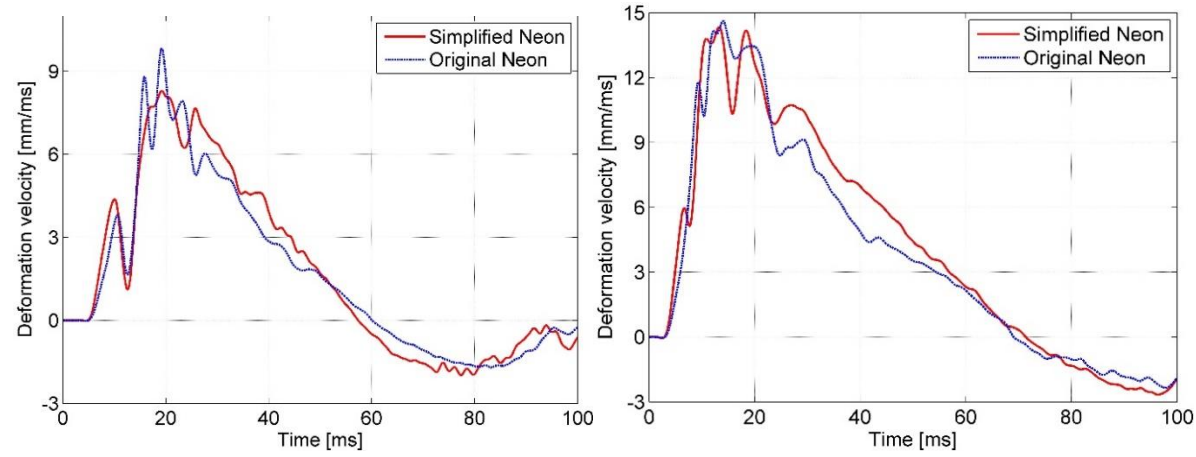

(a) 100%, 30km/h **(b) 100%, 50km/h**

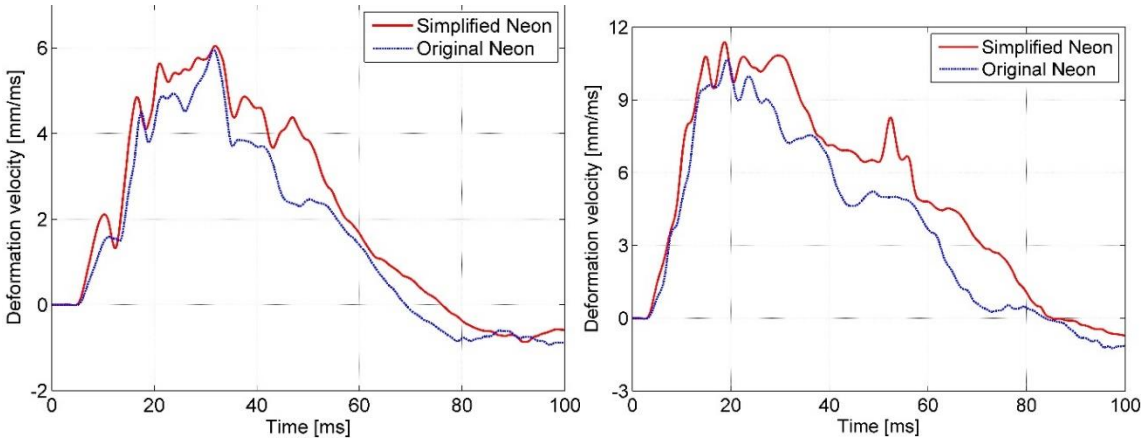

(c) 50% offset, 30km/h **(d) 50% offset, 50km/h**

Figure 11.42 Deformation velocity of node 10054200 of rear bumper at height of 239.6 mm in simulations of 100% and 50% offset rear impact.

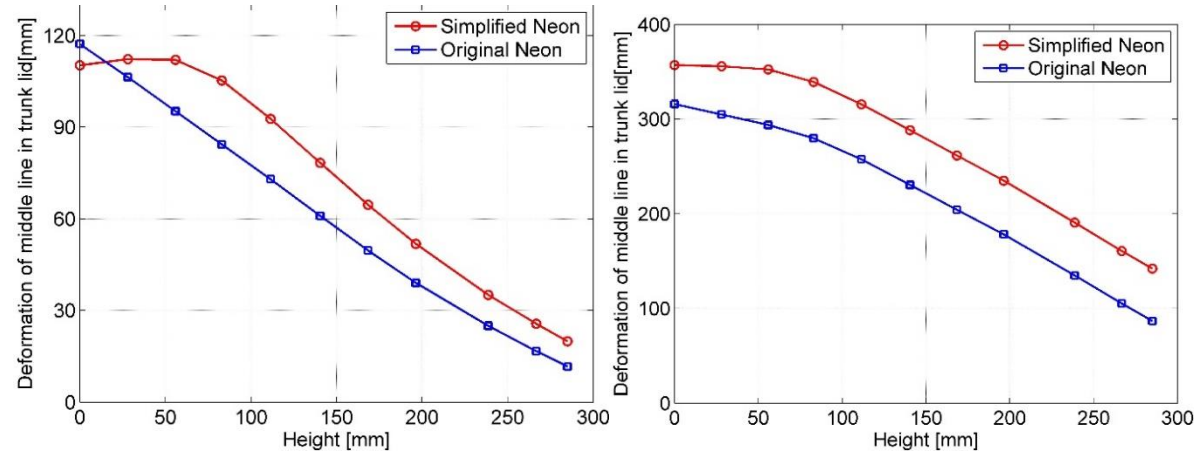

(a) 100%, 30km/h **(b) 100%, 50km/h**

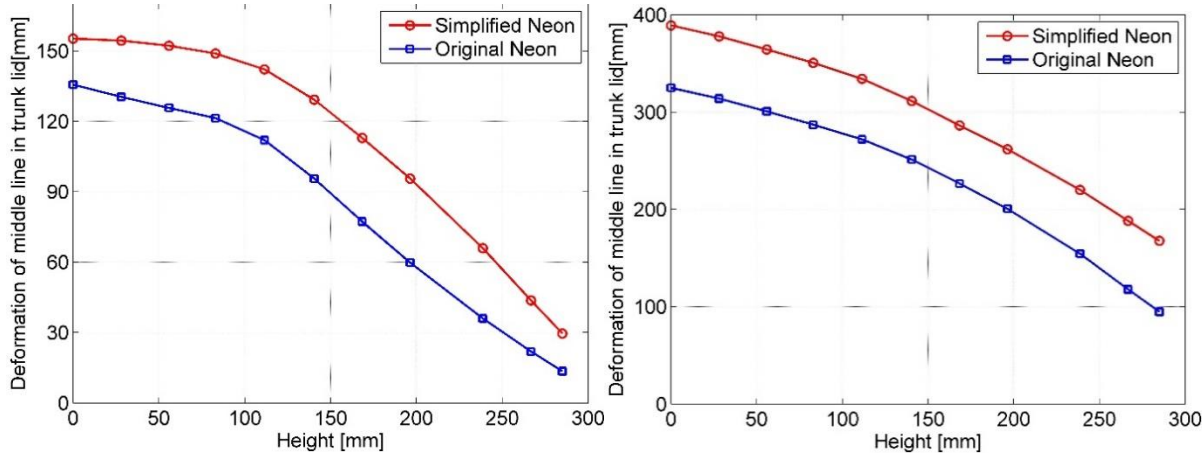

(c) 50% offset, 30km/h **(d) 50% offset, 50km/h**

Figure 11.43 Deformation of middle line of trunk lid in simulations of 100% and 50% offset rear impact.

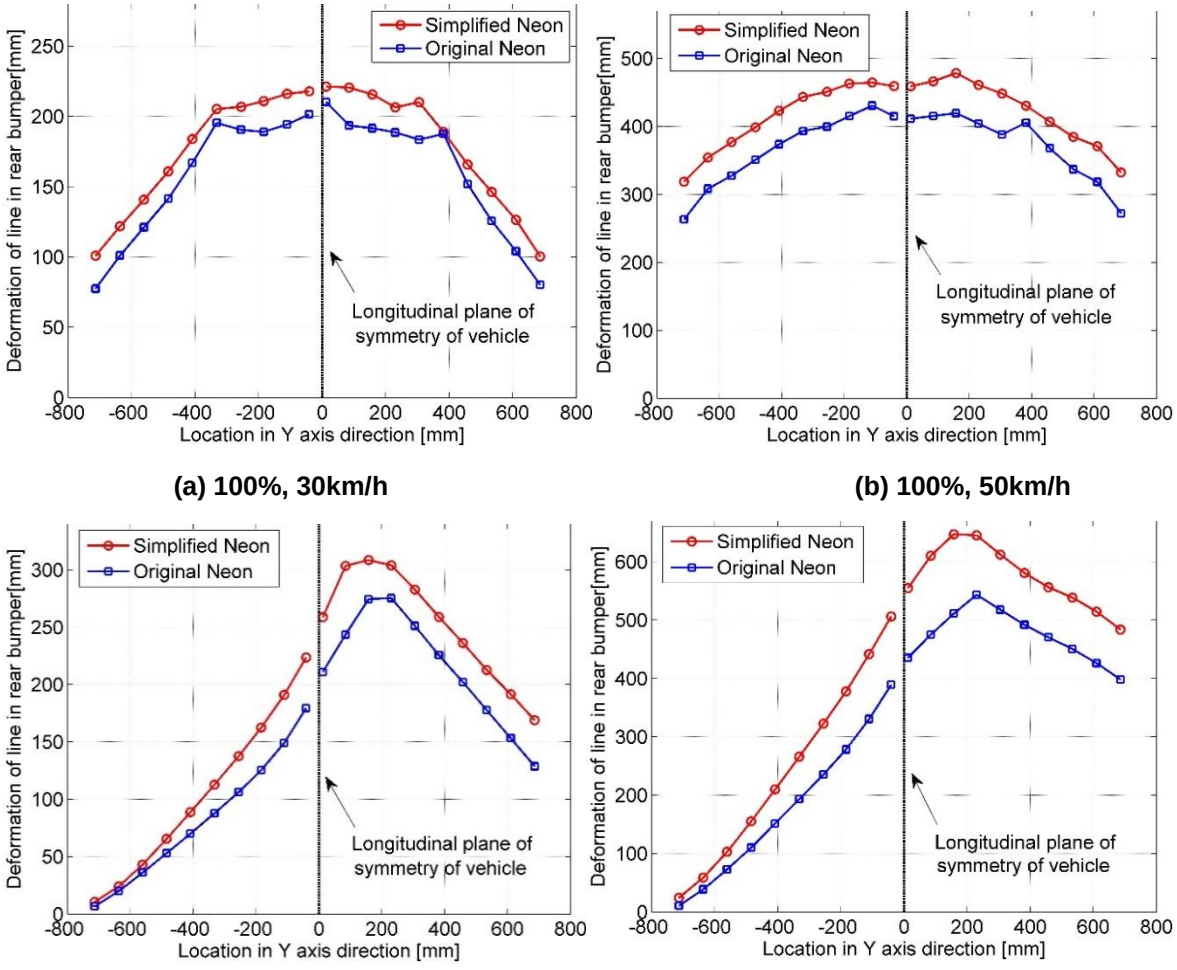

(a) 100%, 30km/h **(b) 100%, 50km/h**

(c) 50% offset, 30km/h **(d) 50% offset, 50km/h**

Figure 11.44 Deformation of horizontal line of rear bumper at height of 239.6mm in simulations of 50% offset rear impact.

L

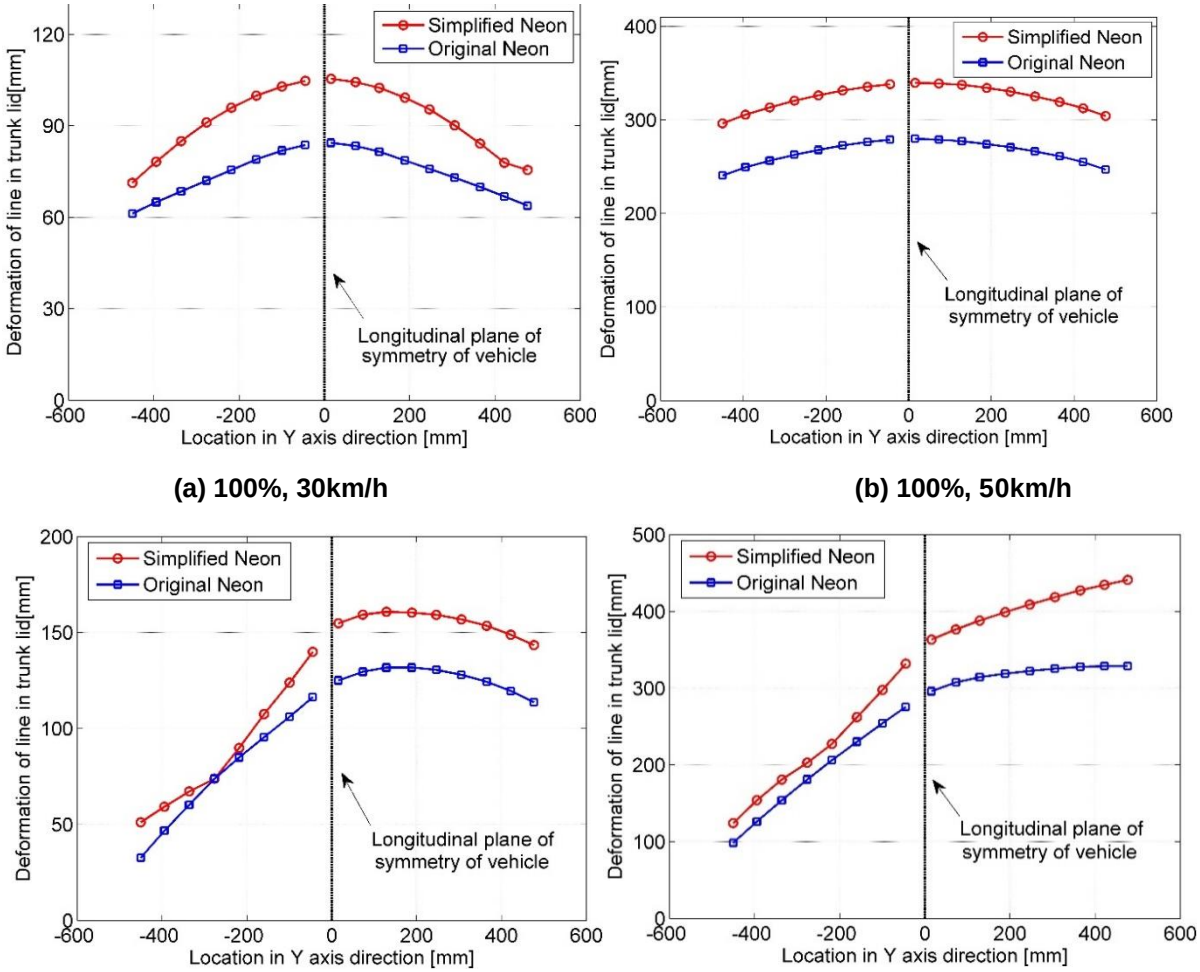

(a) 100%, 30km/h

(b) 100%, 50km/h

(c) 50% offset, 30km/h

(d) 50% offset, 50km/h

Figure 11.45 Deformation of horizontal line of trunk lid at height of 83.21mm in simulations of 50% offset rear impact.

11.5 Side impact model

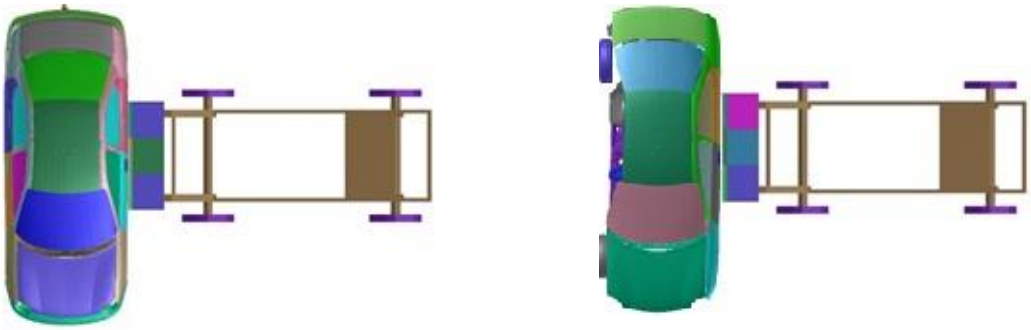

Figure 11.46. Setup for validation in a side impact.

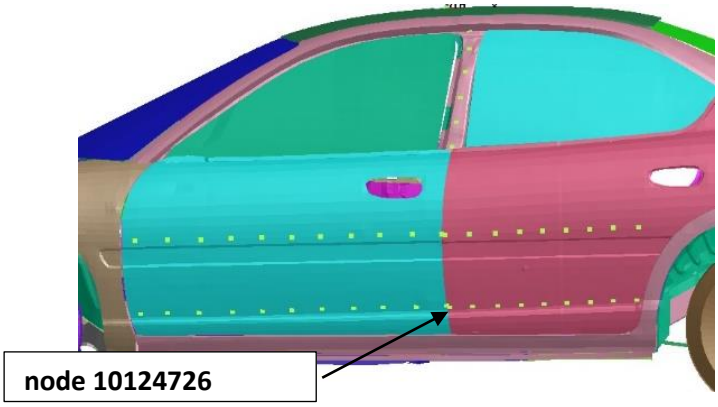

Figure 11.47. Nodes evaluated in side impact validation.

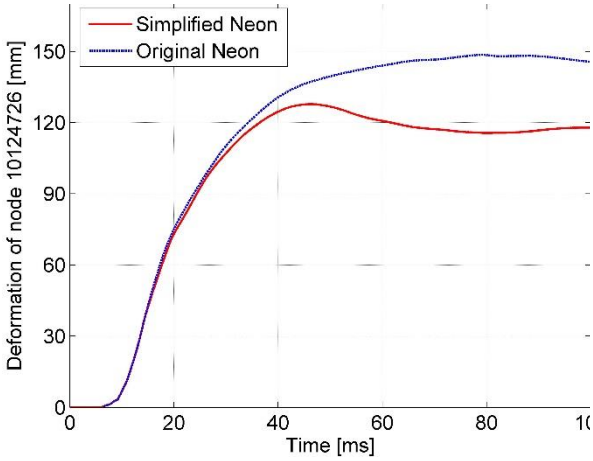

Figure 11.48. Deformation in time of node 10124726 of B pillar (side-impact, 30km/h).

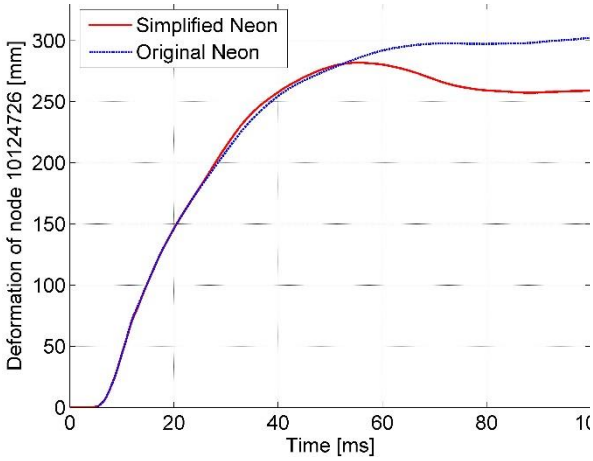

Figure 11.49. Deformation in time of node 10124726 of B pillar (side-impact, 50km/h).

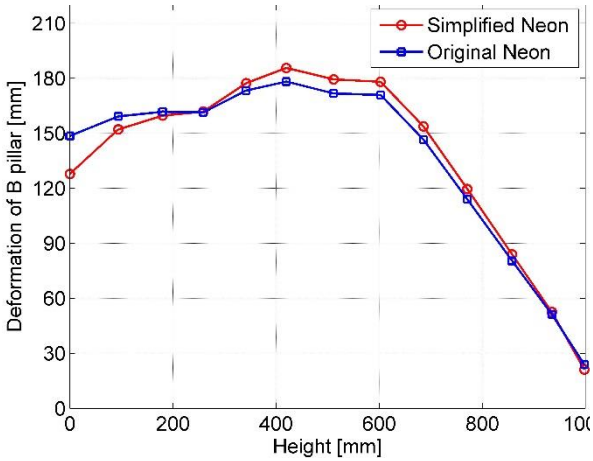

Figure 11.50. Maximum deformation of B pillar in a side impact (30 km/h).

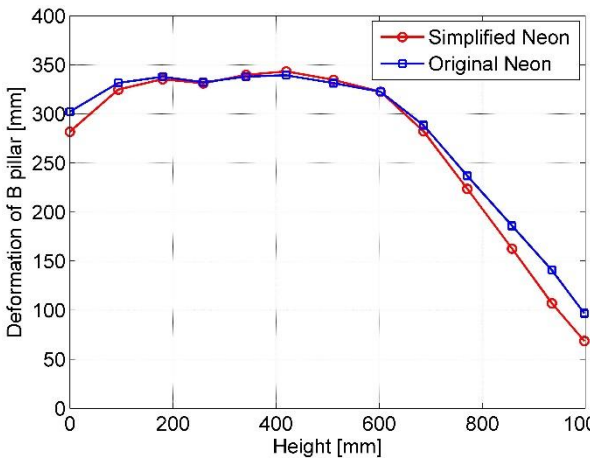

Figure 11.51. Maximum deformation of B pillar in a side impact (50 km/h).

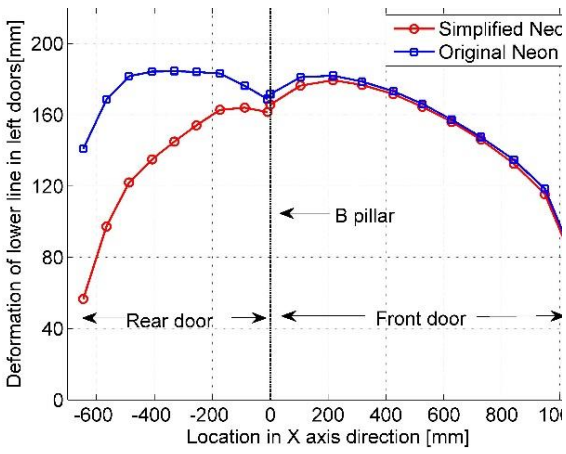

Figure 11.52. Maximum deformation of the lower line on side doors (30 km/h).

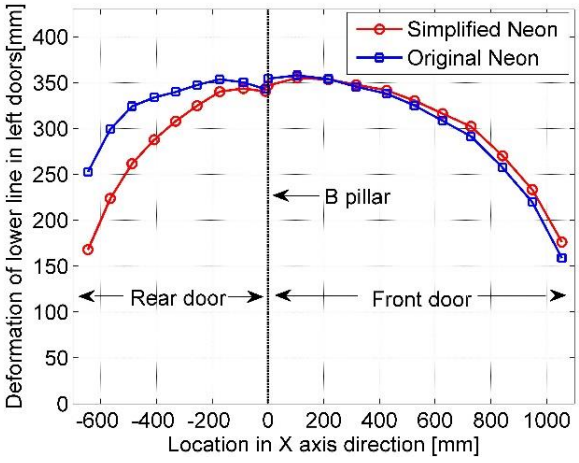

Figure 11.53. Maximum deformation of the lower line on side doors (50 km/h).

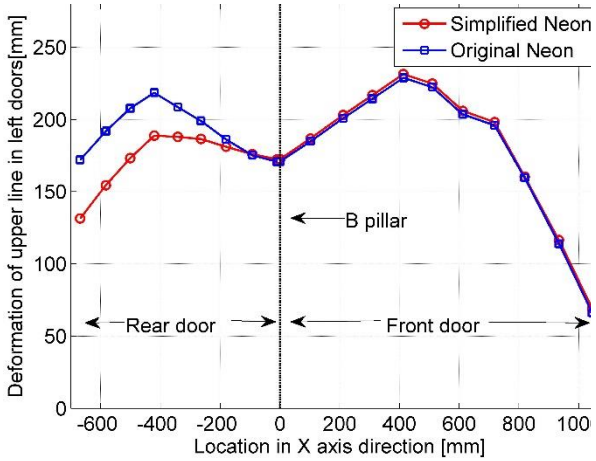

Figure 11.54. Maximum deformation of the upper line on side doors (30 km/h).

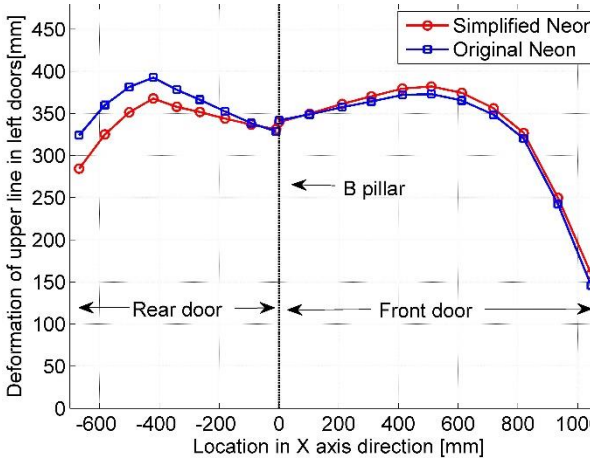

Figure 11.55. Maximum deformation of the lower line on side doors (50 km/h).